THE POTENTIAL APPLICATION OF IMPREGNATED CARBONACEOUS ADSORBENTS IN THE REMOVAL OF SELECTED ORGANOSULFUR COMPOUNDS FROM SYNTHETIC FUEL

BY

Mazen Khaled Hamed Nazal

A Dissertation Presented to the

DEANSHIP OF GRADUATE STUDIES

KING FAHD UNIVERSITY OF PETROLEUM & MINERALS

DHAHRAN, SAUDI ARABIA

In Partial Fulfillment of the
Requirements for the Degree of

DOCTOR OF PHILOSOPHY

In

CHEMISTRY

NOVEMBER 2015

KING FAHD UNIVERSITY OF PETROLEUM & MINERALS

DHAHRAN- 31261, SAUDI ARABIA

DEANSHIP OF GRADUATE STUDIES

This thesis, written by **Mazen Khaled Nazal** under the direction his thesis advisor and approved by his thesis committee, has been presented and accepted by the Dean of Graduate Studies, in partial fulfillment of the requirements for the degree of **DOCTOR OF PHILOSOPHY IN CHEMISTRY.**

Dr. Mazen Khaled
Thesis Advisor

12/11/2015

Dr.Abdulaziz Al-Saadi
Department Chairman

Dr. Muataz Ali Atieh
Co-Advisor

Dr. Salam A. Zummo
Dean of Graduate Studies

Dr. Abdalla Abulkibash
Member

1/12/15
Date

Dr. Ghassan A. Oweimreen
Member

Dr. Isam Al-Jundi
Member

DEDICATION

To my Beloved Mother,

Father,

Brothers and Sisters

ACKNOWLEDGMENTS

My great thanks to Allah who gave me the strength and patient to complete the requirements of this scientific degree. My high appreciation to King Fahd University for providing me the opportunity to pursue my graduate study and research. I am indebted with a sincere gratitude to committee chairman, Dr. Mazen Khaled and Dr. Muataz Ateih who have taught me a lot, motivated, encouraged me and supervised this work. I am also grateful to the committee members,Prof. Abdalla Mahmoud Abulkibash, Prof. Ghassan Oweimreen and Dr. Isam Al-Jundi.

Beside my committee advisor and members, I would like to thank the Chemistry Department chairman Dr. Abdulaziz Al-Saadi and the graduate students' coordinator Prof. Bassam El-Ali. My deep appreciation to all chemistry faculty members who taught me, as well as to all chemistry department stuff. Special thank to Dr. Abdullah Al-Hamdan the ex-chairman of Chemistry Department for his guidance through the past years

I gratefully acknowledgeDr. Abdullah Sultan the Director of Center of Petroleum & Minerals (CPM) and the chairman of petroleum engineering department for his support inpursuing myPh.Ddegree.

I would like to thank all my friends and colleagues here in the KFUPM in Saudi Arabia and there in Jordanian University in Jordan.

I am grateful to my family who encouraged me to complete my Ph.Ddegree. Their love, patience and support were very essentials to complete this thesis.

TABLE OF CONTENTS

ACKNOWLEDGMENTS ..... **V**

TABLE OF CONTENTS ..... **VI**

LIST OF TABLES ..... **XI**

LIST OF FIGURES ..... **XIII**

LIST OF ABBREVIATIONS ..... **XVIII**

ABSTRACT ..... **XXI**

ملخصالرسالة ..... **XXIII**

CHAPTER 1 ..... **1**

1. INTRODUCTION **1**

1.1 Motivation **2**

1.2 Research Objectives **3**

1.3 Dissertation Outline **4**

CHAPTER 2 ..... **6**

2. LITERATURE REVIEW **6**

2.1 Activated Carbon **6**

2.1.1 Types of activated carbons 6

2.1.2 Properties of activated carbon 7

2.1.3 Production of activated carbons 8

2.2 Carbon Nanotubes **9**

2.2.1 Properties of carbon nanotubes **11**

2.2.2 Production of carbon nanotube **12**

2.3 Graphene 15
2.3.1 Types of graphene 16
2.3.2 Applications of graphene based materials 17

2.4 Removing of sulfur compounds 18
2.4.1 Hydrodesulfurization process 20
2.4.2 Oxidative desulfurization 24
2.4.3 Extractive desulfurization 27
2.4.4 Adsorptive desulfurization 30

CHAPTER 3 34

3. EXPERIMENTAL WORK 34

3.1 Materials 34

3.2 Instrumentations 35

3.3 Adsorbents Preparation 36
3.3.1 Graphene oxide (GO) preparation 36
3.3.2 Impregnation of AC, CNT and GO with aluminum oxide 36
3.3.3 Impregnation of AC and CNT with nickel oxide nanoparticles 37
3.3.4 Impregnation of CNT and GO with silver sulfide nanoparticles 38
3.3.5 Impregnation of AC and CNT with uranium oxide 40

3.4 Characterization of Adsorbents 40
3.4.1 Thermal gravimetric analysis (TGA) 40
3.4.2 Adsorbents' surface pH measurements 41
3.4.3 Texture and morphology 41
3.4.4 Characterization of adsorbents surface area and porosity 42

3.5 Thiophene, dibenzothiophene and naphthalene method of analysis 42

3.6 Batch mode adsorption experiment 48
3.6.1 Adsorption isotherms models 48

3.6.2 Adsorption kinetics..... 51

CHAPTER 4.....53

4. RESULTS AND DISCUSSION.....53

4.1 Adsorption Performance of Multiwall Carbon Nanotubes and Graphene Oxide for Removal of Thiophene and Dibenzothiophene from Model Diesel Fuel.....53

4.1.1 The AC, CNT and GO's surface area and porosity..... 53

4.1.2 Effect of shaking speed on the adsorption..... 58

4.1.3 Effect of AC, CNT and GO's mass loaded on the adsorption 60

4.1.4 Effect of the contact time and the adsorption kinetics 62

4.1.5 Effect of initial organosulfur compounds concentration and the adsorption isotherms 66

4.1.6 Conclusion 76

4.2 The Nature and Kinetics of the Adsorption of Dibenzothiophene and Thiophene in Model Diesel Fuel on Carbonaceous Materials Loaded with Aluminum Oxide Particles.....77

4.2.1 Adsorbents thermal gravimetric analysis..... 78

4.2.2 Adsorbent texture and morphology..... 81

4.2.3 Adsorption of thiophene and dibenzothiophene 89

4.2.4 Adsorption kinetics of thiophene and dibenzothiophene..... 94

4.2.5 Effect of adsorbent dosage..... 100

4.2.6 Adsorbents' selectivity 102

4.2.7 Regeneration of adsorbents..... 105

4.2.8 Removal of DBT from a real diesel sample..... 107

4.2.9 Conclusion 108

4.3 Synthesis and Characterization of Modified Carbon Nanotube and Graphene Oxide with Silver Sulfide Nanocomposites for Adsorptive Removal of Dibenzothiophene..... .109

4.3.1 Thermal gravimetric analysis (TGA) 110
4.3.2 Adsorbents' texture and morphology 112
4.3.3 Adsorption kinetics of dibenzothiophene 116
4.3.4 Adsorption isotherms of dibenzothiophene (DBT) 118
4.3.5 Linear and non-linear of dibenzothiophene adsorption modeling 123
4.3.6 Dibenzothiophene adsorption mechanism..... 129
4.3.7 Conclusion 131

4.4 Adsorption Isotherms and Kinetics for Dibenzothiophene on Activated Carbon and Carbon Nanotube Loaded with Nickel Oxide Nanoparticles.....132
4.4.1 Thermal gravimetric analysis of adsorbents..... 133
4.4.2 Surface morphology and texture of adsorbents..... 135
4.4.3 Adsorption isotherms of dibenzothiophene and thiophene 144
4.4.4 Adsorption kinetics of dibezothiophene and thiophene 151
4.4.5 Adsorbent mass loading effect..... 156
4.4.6 Selectivity of the adsorbents..... 158
4.4.7 Effect of Aromatics..... 160
4.4.8 Regeneration of the adsorbents 162
4.4.9 Conclusion 163

4.5 Adsorptive Removal of Dibenzothiophene and Thiophene Using Carbon Nanotube and Activated Carbon Modified with Uranyl Oxide Nanoparticles 164
4.5.1 Thermal gravimetric analysis of adsorbents..... 165
4.5.2 Texture and morphology of adsorbents 167
4.5.3 Adsorption isotherms of thiophene and dibenzothiophene 171
4.5.4 Adsorption kinetics of thiophene and DBT 176
4.5.5 Effect of adsorbent dosage..... 182
4.5.6 Selectivity of the adsorbents..... 184
4.5.7 Conclusion 186

CHAPTER 5 ..... **187**

5. COMPARATIVE ANALYSIS **187**

5.1 Comparative Analysis of the Prepared Adsorbents for DBT and Thiophene Removal **187**

CHAPTER 6 ..... **193**

6. CONCLUSION AND RECOMMENDATION **193**

REFERENCES **196**

VITAE **207**

LIST OF TABLES

Table 2-1: Mechanical properties of some materials **11**
Table 3-1: Chromatographic conditions used in the analysis of thiophene and DBT. **43**
Table 3-2: Method precision and accuracy of thiphene, DBT and naphthalene determination. **47**
Table 4-1: Carbonaceous materials surface area and the microporousity analysis parameters **57**
Table 4-2: Pseudo-first order and pseudo-second order kinetics' parameters and correlation coefficients for the adsorption of Thiophene and DBT on AC, CNT and GO. **65**
Table 4-3: The adsorption capacities of AC, MWCNT and GO compared with some of reported adsorption capacities in the literatures. **72**
Table 4-4: Freundlich and Langmuir parameters and correlation coefficients for the adsorption of Thiophene and DBT on AC, CNT and GO. **73**
Table 4-5: Temkin parameters and correlation coefficients for the adsorption of Thiophene and DBT on AC, MWCNT and GO. **75**
Table 4-6: Weight percent of aluminum in the doped carbon materials adsorbents compared to the theoretical percentages of aluminum (5 % and 10.9 % Al for adsorbents ending with 5 and 10 respectively). **84**
Table 4-7: Surface area, total pore volume and surface pH of AC, CNTs and GO before and after their impregnation with 5 % and 10.9 % Al in the form of Al_2O_3. ..... **88**
Table 4-8: Freundlich and Langmuir parameters and correlation coefficient for thiophene and DBT adsorption on carbonaceous materials before and after doping with Al_2O_3 ..... **93**
Table 4-9: Pseudo-Second order kinetic parameters for thiophene and DBT adsorption on the carbonaceous materials doped with Al_2O_3 ..... **97**
Table 4-10: Intra-particle diffusion parameters for DBT on different adsorbents. **99**
Table 4-11: Adsorption selectivity of ACAL5 and CNTAL5. ..... **104**
Table 4-12: EDX analysis of raw and modified CNT and GO. **114**
Table 4-13: The (PFOM).and (PSOM)parameters with the correlation coefficients for DBT adsorption on AC and CNT before and after modification with silver sulfide 10 % **117**
Table 4-14: List of mathematical equations (original and linear forms) for three isotherm models **119**
Table 4-15: Freundlich, Langmuir and Temkin's parameters for DBT adsorption over raw and modified CNT and GO calculated by the original and linearized forms. **124**
Table 4-16: Adsorption capacity of DBT on different adsorbents from different model fuel media. **125**

Table 4-17: The calculated squared correlation coefficient (R^2) and HYBRID error function for different isotherm models presenting the DBT adsorption over modified and unmodified CNT and GO with silver sulfide nanoparticles.....**128**
Table 4-18: Weight percent of nickel in the doped carbon materials adsorbents compared to the theoretical percentage of nickel. **137**
Table 4-19: Surface area, micropore's surface area and volume and surface pH of AC and CNT at different loading percentage of nickel oxide.....**143**
Table 4-20: Freundlich and Langmuir parameters correlation coefficient for thiophene and DBT adsorption on pristine MWCNT and MWCNT impregnated with nickel oxide **149**
Table 4-21: Pseudo First order and Pseudo-Second order Parameters for thiophene and DBT adsorption on doped AC and CNT with nickel oxide. **153**
Table 4-22: Intra-particles diffusion parameters.....**155**
Table 4-23: Adsorption selectivity of ACNI5 and CNTNI5.....**159**
Table 4-24: EDX results for weight percent of uranium in the doped carbon materials adsorbents compared to the theoretical percentage of uranium. **168**
Table 4-25: Surface area, micropore surface area and its volume and surface pH of unmodified and modified AC and CNT with 5 % U in the form of UO_3. ...**170**
Table 4-26: Freundlich and Langmuir parameters and correlation coefficient for thiophene and DBT adsorption on carbonaceous materials before and after modification with UO_3 .....**175**
Table 4-27: Pseudo-First order and Pseudo-Second order parameters for thiophene and DBT adsorption on the carbonaceous materials doped by UO_3 .....**178**
Table 4-28: Intra-particle diffusion parameters for DBT and thiophene on the modified adsorbents with uranium. **181**
Table 4-29: Adsorption selectivity of ACU5 and CNTU5 for DBT.....**185**
Table 5-1: Comparison between the Freundlich and Langmuir parameters for all the prepared adsorbents. **188**
Table 5-2: Summary of selectivity factor for unmodified and modified AC and CNT with different metals oxide.....**190**
Table 5-3: Comparison of various carbon based adsorbents for DBT removal.....**191**

LIST OF FIGURES

Figure 2-1: (a) CNT made of graphene sheet of C atoms to give (b) armchair or (c) Zigzag conformation **10**

Figure 2-2: Arc discharge apparatus **13**

Figure 2-3: Schematic drawing of a laser ablation apparatus [55] **14**

Figure 2-4: A schematic diagram of a plasma CVD apparatus [57] **15**

Figure 2-5: Desulfurization process classified based on the sulfur compounds transformation. **18**

Figure 2-6: Classification of desulfurization process based on the nature of the process to eliminate sulfur compounds. **20**

Figure 2-7: The effect of size of organosulf compounds on the their reactivity in the HDS process [75]. **21**

Figure 2-8: Two pathways for desulfurization of dibenzothiophene sulfur compound in the HDS process **23**

Figure 2-9: Diagram illustrates Petro Star Inc. technology of desulfurization [81]. **25**

Figure 2-10: Scheme illustrates the extractive desulfurization steps [84] **28**

Figure 2-11: Scheme illustrates the adsorptive desulfurization steps [92] **30**

Figure 3-1: CVD experimental setup for modification of carbon materials with silver sulfide nanoparticles. **39**

Figure 3-2: The calibration curve points overlaid chromatograms for mixture solutions containing A) thiophene, B) naphthalene and C) DBT **45**

Figure 3-3: The calibration curves for thiophene, DBT and naphthalene. The bars are standard deviations obtained from three runs **46**

Figure 4-1: The N_2 adsorption isotherm at 77 K on (a) AC, (b) CNT and (c) GO. **55**

Figure 4-2: Pore width distrubution based on DR method for (a) AC, (b) CNT and (c) GO. **56**

Figure 4-3: The effect of shaking speed for adsorption of a) Thiophene and b) Dibenzothiophene (DBT), by AC, MWCNT and GO at room temperature (25 ºC), and the amount of adsorbent is 100 mg and initial concentration of organosulfur compound is 250 mg/L. **59**

Figure 4-4: The effect of adsorbent loaded on the removal efficiency of a) Thiophene and b) Dibenzothiophene (DBT), by AC, CNT and GO at room temperature (25 ºC), the shaking speed is 200 rpm and the initial concentration of organosulfur compound is 250 mg/L. **61**

Figure 4-5: The effect of contact time on the removal efficiency of a) Thiophene and b) Dibenzothiophene (DBT), by AC, CNT and GO at room temperature (25 ºC), the shaking speed is 200 rpm, the adsorbent amount is 300 mg and the initial concentration of organosulfur compound is 250 mg/L **63**

Figure 4-6: The pseudo-second order for adsorption of a) Thiophene and b) Dibenzothiophene (DBT), by AC, CNT and GO at room temperature (25 ºC), the shaking speed is 200 rpm, the adsorbent amount is 300 mg and the initial concentration of organosulfur compound is 250 mg/L.....**64**

Figure 4-7: Removal efficiency comparison between AC, CNT and GO at different organosulfur compound concentration a) Thiophene and b) Dibenzothiophene (DBT), at room temperature (25 ºC), shaking speed is 200 rpm and the adsorbent amount is 300 mg. **68**

Figure 4-8: The adsorption isotherm of a) Thiophene and b) Dibenzothiophene (DBT) on AC, CNT and GO at room temperature (25 ºC), the shaking speed is 200 rpm and the adsorbent amount is 300 mg. **69**

Figure 4-9: The Freundlich adsorption model linearization for adsorption of A) Thiophene and B) Dibenzothiophene (DBT), by AC, CNT and GO at room temperature (25 ºC), the shaking speed is 200 rpm and the adsorbent amount is 300 mg. **70**

Figure 4-10: The Langmuir adsorption model linearization for adsorption dibenzothiophene (DBT) on AC, CNT and GO at room temperature (25 ºC), the shaking speed is 200 rpm and the adsorbent amount is 300 mg.....**71**

Figure 4-11: The Temkin adsorption model linearization for adsorption of a) Thiophene and b) dibenzothiophene (DBT) on AC, MWCNT and GO at room temperature (25 ºC), the shaking speed is 200 rpm and the adsorbent amount is 300 mg. **74**

Figure 4-12: TGA under air atmosphere with a flow rate of 100 mL/min for (a) AC, (b) CNT and (c) GO impregnated with $Al(NO_3)_3.9H_2O$. **79**

Figure 4-13: TGA under nitrogen atmosphere with a flow rate of 100 mL/min for (a) AC, (b) CNT and (c) GO impregnated with $Al(NO_3)_3.9H_2O$. **80**

Figure 4-14: SEM images of (a) AC, (b) CNT and (c) GO before impregnation with Al_2O_3 .....**82**

Figure 4-15: SEM images of (a) AC, (b) CNTs and (c) GO after impregnation with Al_2O_3. .....**83**

Figure 4-16: EF-TEM image for CNT (a) before and (b) after impregnation with Al_2O_3 .....**85**

Figure 4-17: EF-TEM image for GO (a) before and (b) after impregnation with Al_2O_3. The insets are diffraction patterns for the GO surface (a) before and (b) after impregnation with Al_2O_3.....**86**

Figure 4-18: (a) XPS survey spectrum of CNT-Al_2O_3 (b) O 1s XPS spectrum of CNT-Al_2O_3 and (c) Al 2p XPS spectrum of CNT-Al_2O_3. .....**87**

Figure 4-19: Adsorption isotherms at 25 ºC for (a) DBT on AC, ACAL5 and ACAL10, (b) DBT on CNT, CNTAL5 and CNTAL10, (c) DBT on GO, GOAL5 and GOAL10 and (d) thiophene on different adsorbents. Solid lines are fits to the Langmuir model. **91**

Figure 4-20: Adsorption isotherms at 25 ºC for (a) DBT on AC, ACAL5 and ACAL10, (b) DBT on CNT, CNTAL5 and CNTAL10, (c) DBT on GO, GOAL5 and GOAL10 and (d) thiophene on different adsorbents. Solid lines are fits to the Freundlich model. **92**

Figure 4-21: The effect of agitation time on the adsorption capacity of (a) thiophene and (b) dibenzothiophene (DBT), using different adsorbents impregnated with different percentages of Al_2O_3 at 25 ºC where, the shaking speed is 200 rpm, the adsorbent amount is 150 mg and the initial concentration of the organic sulfur compound is 250 mg/L. The Inset figures show the effect of agitation time up to 60 min. **96**

Figure 4-22: Plots of q_t versus $t^{0.5}$ showing the two diffusion stages predicted by the diffusion model for DBT adsorption on (a) ACAL10, (b) CNTAL10 and (c) GOAL10. ..... **99**

Figure 4-23: Comparison between the removal efficiency of (a) dibenzothiophene (DBT) and (b) thiophene, on AC, CNT and GO impregnated by Al_2O_3, at 25 ºC, a shaking speed of 200 rpm and a sulfur compound concentration of 250 mg/L. **101**

Figure 4-24: The adsorption capacities with error bars after each of 5 adsorbent regeneration cycles for (a) DBT and thiophene on the ACAL5 adsorbent and (b) DBT on the CNTAL5 adsorbent. **106**

Figure 4-25: TGA under (a) air, (b) nitrogen atmosphere with flow rate 100 mL min^{-1}, for carbonaceous materials impregnated by $AgNO_3$ before and after calcinations. **111**

Figure 4-26: SEM images before impregnation of (a) CNT, (b) GO, and after impregnation (c) $CNTAg_2S$ and (d) $GOAg_2S$ **113**

Figure 4-27: TEM images of raw (a) CNT, (b) GO, and modified (c) CNT and (d) GO. Inset figure is the modified CNT with imaging scale of 50 nm. **114**

Figure 4-28: (a) XPS survey spectra of $CNTAg_2S$ (b) Ag3d XPS spectra of $CNTAg_2S$ and (c) S2p XPS spectra of $CNTAg_2S$ **115**

Figure 4-29: The effect of contact time on the adsorption capacity (q_t) of AC and CNT before and after modification with silver sulfide 10 % for DBT. Temperature (25 ºC), shaking speed (200 rpm), adsorbent mass (150 mg) and C_o (250 mg/L). The solid lines are the predicted q_t values. **117**

Figure 4-30: Adsorption isotherms of DBT on unmodified and modified CNT and GO. Solid lines are the predicted Q_e values using (a) Freundlich isotherm, (b) Langmuir-1, (c) Langmuir-2, (d) Langmuir-3, (e) Langmuir-4, and (f) Temkin isotherm. Adsorption temperature 25 ºC, mass of adsorbent 150 mg and shaking time 2 hours at speed 200 rpm. Solid lines are the q_e predicted from the corresponding linear form of the corresponding model **120**

Figure 4-31: Linear least squares fit for (a) Linearized Freundlich model, (b) Langmuir-1, (c) Langmuir-2, (d) Langmuir-3, (e) Langmuir-4 and (f) Temkin linear form. For DBT adsorption on unmodified and modified CNT and GO. **122**

Figure 4-32: FT-IR spectra of raw a) GO and b) CNT. Inset figure is IR spectrum of standard solid DBT **130**

Figure 4-33: FT-IR spectra of DBT adsorbed on a) GO-Ag_2S and b) CNT-Ag_2S **130**

Figure 4-34: Schematic illustrates adsorption state of DBT (lie on flat) on the surface of GO-Ag_2S **131**

Figure 4-35: TGA under atmospheric air with 100mL/min flow rate, before and after $Ni(NO_3)_2$ calcinations on (a) AC and (b) CNT. **134**

Figure 4-36: SEM photograph for AC (a) before, (b) after and for CNT (c) before and (d) after impregnation with nickel oxide. **136**

Figure 4-37: EF-TEM image for CNT (a) before and (b) after impregnation by 1% (c) 5% and (d) 10 % NiO. **138**

Figure 4-38: XRD for CNT before and after impregnation **139**

Figure 4-39: (a) XPS survey spectra of CNTNI10 (b) Ni2p high resolution XPS spectra of CNTNI10. ..... **140**

Figure 4-40: The N_2 adsorption isotherm at 77 K on unmodified and modeified (a) AC and (b) CNT with nickel oxide **142**

Figure 4-41: Adsorption isotherms of (a) DBT on AC, ACNI1, ACNI5 and ACNI10, (b) DBT on CNT, CNTNI1, CNTNI5 and CNTNI10, (c) Thiophene on AC, ACNI1, ACNI5 and ACNI10 and (d) thiophene on CNT, CNTNI1, CNTNI5 and CNTNI10 at 25 ºC. The solid lines are fits to the Freundlich model **147**

Figure 4-42: Adsorption isotherms of (a) DBT on AC, ACNI1, ACNI5 and ACNI10, (b) DBT on CNT, CNTNI1, CNTNI5 and CNTNI10, (c) Thiophene on AC, ACNI1, ACNI5 and ACNI10 and (d) Thiophene on CNT, CNTNI1, CNTNI5 and CNTNI10 at 25 ºC. The solid lines are fits to the Langmuir model **148**

Figure 4-43: Effect of nickel oxide loading percentage on the adsorption capacities of AC and CNT **150**

Figure 4-44: The effect of contact time on the adsorption capacity (q_t) of AC and CNT with different nickel oxide loading percentage for (a) Thiophene and (b) DBT. At room temperature 25 ºC, shaking speed 200 rpm, adsorbent amount 150 mg and initial concentration of organosulfur compound 250 mg/L. The solid lines are the predicted $\boldsymbol{qe}$ values and the inset figures are the effect of contact time in the first 2 hours. **152**

Figure 4-45: Intra-particles diffusion model for (a) DBT adsorption and (b) Thiophene adsorption on ACNI10, ACNI5 and ACNI1. ..... **155**

Figure 4-46: Effect of adsorbent loading on the removal efficiency of (a) dibenzothiophene (DBT) and (b) thiophene, on AC and CNT impregnated with different loading percentage of nickel oxide, at adsorption temperature 25 ºC, shaking speed 200 rpm and the C_o 250 mg/L. **157**

Figure 4-47: Effect of aromatics on the ACNI5 and CNTNI5 adsorbents' adsorption capacity **161**

Figure 4-48: The adsorption capacities comparison with error bars after 5 adsorbent regeneration cycles for dibenzothiophene (DBT) on (a) ACNI5 and (b) CNTNI5 adsorbent. **162**

Figure 4-49: TGA for unmodified and modified adsorbent with UO_3 under a) air and b) nitrogen with flow rate of 100 mL/min. **166**

Figure 4-50: SEM image for a) AC and CNT before and b) AC and CNT after impregnation with UO_3 ..... **168**

Figure 4-51: EF-TEM image for CNT a) before and b) after doping with 5 % UO_3. The insets show the carbon nanotubes before and after the modification at higher magnification (100 nm image scale). **169**

Figure 4-52: The adsorption isotherms of a) DBT and b) Thiophene, on raw and modified AC and c) DBT and d) Thiophene, on raw and modified CNT with 5 % UO_3. Contact time 2 hours, adsorption temperature 25 ºC and shaking speed 200 rpm. Solid lines are fits to the Freundlich model. **173**

Figure 4-53: The adsorption isotherms of a) DBT and b) Thiophene, on raw and modified AC and c) DBT and d) Thiophene, on raw and modified CNT with 5 % UO_3. Contact time 2 hours, at adsorption temperature 25 ºC and shaking speed 200 rpm. The solid line fits to the Langmuir model. ... **174**

Figure 4-54: The effect of adsorption time on the adsorption capacity of a) thiophene and b) dibenzothiophene (DBT), using different adsorbents modified with UO_3. Solid line is second order kinetics fit. Temperature is 25 ºC, the shaking speed is 200 rpm, the adsorbent amount is 75 mg and C_o is 250 mg/L. **177**

Figure 4-55: Plots of $\boldsymbol{qt}$ versus $t^{0.5}$ showing the multi steps diffusion predicted by the diffusion model for DBT adsorption on a) ACU5 and b) CNTU5, and thiophene adsorption on c) ACU5 and d) CNTU5. ..... **180**

Figure 4-56: Effect of the adsorbents mass on the adsorption capacity and removal efficiency of a) dibenzothiophene (DBT) and b) thiophene, on AC and CNT modified with UO_3. The adsorption time is 2 hours at 25 ºC, the shaking speed 200 rpm and the initial sulfur compound concentration is 250 mg. **183**

Figure 5-1: The histogram comparison between the adsorption capacity of the prepared adsorbents **189**

LIST OF ABBREVIATIONS

CNT : Multiwall Carbon Nanotube

GO : Graphene Oxide

AC : Activated Carbon

DBT : Dibenzothiophene

(QC/QA): Quality Control / Quality Assurance

RSD %: Relative standard deviation

RE % : Relative Error

QcL : Quality control levels at low concentration

QcM : Quality control levels at medium concentration

QcH : Quality control levels at high concentration

TGA : Thermal Gravimetric Analysis

SEM : Scanning Electron Microscopy

EDX : Energetic Dispersive X-ray diffractogram

FE-TEM: Field Emission Transmittance Electron Microscope

XPS : X-ray Photoelectron Spectrometer

ACAL5: Activated carbon modified with 5 % Aluminum in the form of Aluminum Oxide

ACAL10: Activated carbon modified with 10.9 % Aluminum in the form of Aluminum Oxide

CNTAL5: Carbon Nanotube modified with 5 % Aluminum in the form of Aluminum Oxide

CNTAL10: Carbon Nanotube modified with 10.9 % Aluminum in the form of Aluminum Oxide

GOAL5: Graphene Oxide modified with 5 % Aluminum in the form of Aluminum Oxide

GOAL10: Graphene Oxide modified with 10.9 % Aluminum in the form of Aluminum Oxide

$CNTAg_2S$: Carbon Nanotube modified with 10 % silver in the form of Silver Sulfide

$GOAg_2S$: Graphene Oxide modified with 10 % silver in the form of Silver Sulfide

ACNI1: Activated Carbon modified with 1 % Nickel in the form of Nickel Oxide

ACNI5: Activated Carbon modified with 5 % Nickel in the form of Nickel Oxide

ACAL10: Activated Carbon modified with 10 % Nickel in the form of Nickel Oxide

CNTNI1: Carbon Nanotube modified with 1 % Nickel in the form of Nickel Oxide

CNTNI5: Carbon Nanotube modified with 5 % Nickel in the form of Nickel Oxide

CNTAL10: Carbon Nanotube modified with 10 % Nickel in the form of Nickel Oxide

ACU5: Activated carbon modified with 5 % Uranium in the form of Uranyl Oxide

CNTU5: Carbon Nanotube modified with 5 % Uranium in the form of Uranyl Oxide

R^2: Squared correlation coefficient

HYBRID: Hybrid fractional error function

Q_{max}: Langmuir maximumadsorption capacity (mg/g)

B : Langmuir constant**(**dm^3/mg**)**

n: Heterogeneity constant

K_F: Freundlich Constant

R: The ideal gas constant (J K^{-1} mol^{-1})

T: The temperature in Kelvin (K),

b_T: The Temkin constant

A_T: Temkin isotherm equilibrium binding constant(L g^{-1})

C_e: The concentration of the sulfur compound in the solution at equilibrium(mg/L)

q_e: The adsorption capacity at equilibrium (mg/g)

q_t: The adsorption capacity at a time t (min),(mg/g)

k_1: The pseudo-first order rate constant (min^{-1})

k_2: The pseudo-second order rate constant(g mg^{-1} min^{-1})

k_{id}: Intra-particle diffusion rate constant ($mg/gmin^{0.5}$)

C: Constant related to the thickness of the boundary layer (mg/g)

K: The adsorption selectivity

K_d: The distribution coefficient

PAH: Polyaromatic Hydrocarbon

BDDT: Brunauer, Deming and Teller Classification

BET: Brunauer–Emmett–Teller

SA: Surface Area

NLDFT: Nonlinear Density Functional Theory

K: Kelvin

V: Pore Volume

OD: Outer Diameter

SSA: Specific Surface Area

ABSTRACT

Full Name : **Mazen Khaled Nazal**

Thesis Title : **The Potential Applications of Impregnated Carbonaceous Adsorbents in the Removal of Selected Organosulfur Compounds from Synthetic Diesel Fuel**

Major Field : **Analytical Chemistry**

Date of Degree : **November, 2015**

The scientific and industrial societies are seeking continually alternatives to the present adsorbents with new ones that have better properties such as, lower mass to volume ratio with high adsorption capacity to remove the organic sulfur compounds from fuel to nearly zero level. Therefore, a set of adsorbents' composite based on carbonaceous materials (activated carbon, carbon nanotube and graphene oxide) modified with different loading percentage of aluminum, nickel or uranium oxide or silver sulfide were prepared using a wetness impregnation and chemical vapor deposition (CVD) methods. These adsorbents were characterized using sophisticated characterization techniques (TGA, N_2 adsorption-desorption surface area analyzer, SEM, EDX, FE-TEM,XRD and XPS). The potential application of these adsorbents for selective removal of dibenzothiophene was studied. The adsorption isotherm of dibenzothiophene and thiophene in *n*-hexane as model fuel were obtained and desulfurization kinetics were carried out. The high DBT removal efficiency (98 %) was achieved within 2 hours using low ration of ACU5 adsorbent's mass to volume of 250 mg/L model fuel. The efficiencies with which the otherprepared adsorbents remove DBT and thiophene from their solutions are reported. The adsorption isotherms fitted both the Langmuir and Freundlich models. The highest adsorption capacity (Q_{max}) of DBT was 108.95mg/g on the ACU5 adsorbent. The

adsorption rates for DBT and thiophene follow pseudo-second order kinetics using all prepared adsorbents in this study, with correlation coefficients close to 1.00. The good removal selectivity by these adsorbents of DBT relative to thiophene and naphthalene is also reported. The ACAL5, CNTAL5, ACNINI5 and CNTNI5 adsorbents showed good reusability for at least 5 adsorption cycles without significant loss in their adsorption capacities. It has been also found that ACAL5 is capable of removing 30 % of the DBT in diesel fuel.

ملخص الرسالة

الاسم الكامل:مازن خالد نزال

عنوان الرسالة: التطبيقات المحتملة للممتزات الكربونية المشربة لإزالة مركبات كبريت عضوية محددة من نموذج لوقود الديزل

التخصص: الكيمياء التحليلة

تاريخ الدرجة العلمية:صفر 1437هـ (الموافق تشرين الثاني 2015)

المجتمعات العلمية والصناعية تبحث باستمرارعن بدائل للممتزات الحالية بأخرى جديدة ذات خصائص أفضل مثل، انخفاض نسبة الكتلة إلى الحجم، مع قدرة امتصاص عالية لإزالة مركبات الكبريت العضوية من الوقود بشكل كامل. لذلك، تم تحضير مجموعة من الممتزات المكونة من المواد الكربونية (الكربون المنشط، أنابيب الكربون النانوية وأكسيد الجرافين) والمشربة بنسب مختلفة من أكسيد الألومنيوم، أكسيد النيكل أو أكسيد اليورانيوم أو كبريتيد الفضة باستخدام طريقة التشريب المبلل وترسيب الأبخرة الكيميائية (CVD). تم توصيف هذه الممتزات باستخدام تقنيات التوصيف الأكثر تطورا (التحليل الحراري الوزني(TGA) ، تحديد المساحة السطحية، المجهر الإلكتروني الماسح (SEM)، وحيوية متبدد الأشعة السينية(EDX)، مجهر حقل الانبعاثات الكترون(TEM)، والأشعة X أداة ديفراكتوميتر (XRD) و مطياف الأشعة السينية الضوئية (XPS).تمت دراسة إمكانية تطبيق هذه الممتزات لإزالة مركبات الكبريت العضوية (الثيوفين و الثيوفين ثنائي البنزين) إزالة انتقائية. وقد تم الحصول على متساوي حرارةإمتزاز الثيوفين و الثيوفين ثنائي البنزين الموجود في محلول الهكسان العضوي كنمزذج للوقود وتمت دراسة حركية إزالة الكبريت لهذه المركبات.تم الحصول علىأعلىكفاءة إزالة(% 98) لمركب DBT في غضون ساعتين باستخدام كمية قليلة من الممتز(ACU5)في 25ملممن نموذج الوقود. كذلك تم حساب كفاءاتالممتزات الأخرى لإزالةمركبات الثيوفين و الثيوفين ثنائي البنزين من الهكسان. متساوي حرارةالإمتزاز للممتزات عينت بنماذج لانجمير وفروندليتش. وكانت أعلى سعة إمتزاز (Q_{max})لمركب الثيوفين ثنائي البنزين 108.95ملغ/غ على المادة الممتزةACU5.سرعات الامتزازللثيوفين ثنائي البنزين والثيوفين تتبع حركية التفاعل شبه الثنائي مع معاملات إرتباطقريبة من 1.00. قد تم التوصللإزالة إنتقائية جيدة بإستخدام هذه الممتزات للثيوفين ثنائي البنزينبسبة إلى ثيوفين والنفثالين من محلول نموذج الوقود. أظهرت الممتزاتACAL5، CNTAL5، ACNINI5وCNTNI5إعادة

استخدام جيدة لا تقل عن 5 دورات إمتزاز من دون خسارة كبيرة في سعة الامتصاص الخاصة بهم. كما تم الكشف عن أن ACAL5 قادر على إزالة % 30 منالثيوفين ثنائي البنزين الموجودفي وقود الديزل الحقيقي.

CHAPTER 1

1. INTRODUCTION

Serious environmental and industrial hazards result from the naturally occurring dibenzothiophene (DBT), and its derivatives, present in diesel fuel. These include catalytic poisoning, corrosion in pipes and emission of SO_x gases that contribute to acid rain **[1]**.These hazards resulted in increasingly restrictive regulations on the contents of these compounds in diesel fuel. The European regulation lowered the specification for the sulfur content in diesel fuel from 2000 ppmw in 1991 to 50 ppmw in 2005 then to 10 ppmw in 2009 **[2-4].** By 2006 the U.S. Environmental Protection Agency (USEPA) restricted sulfur content to 15 ppmw and 30 ppmw in diesel and gasoline fuels respectively **[5, 6]**. Such restriction led to greater interest in research on the removal of sulfur compounds from fuels.

The removal of DBT and its derivatives is challenging due to steric hindrance of their structures **[7, 8]**. The conventional hydrodesulfurization (HDS) process used in the refining industries can bring the sulfur compound level to around 500ppm; a value well above the requirements in the new regulations. To reach lower sulfur levels in the fuel using hydrodesulfurization, higher pressures and temperatures have to be used which make the process costly and lowers the octane level of the fuel **[9]**. To obtain ultra clean diesel fuels chemical oxidation **[10-12]**, photooxidation **[7, 13, 14]** and adsorption **[1, 15-40]**techniques were used.

The adsorption technique is promising as an alternative or complementary technique because it is simple, relatively cost effective and has the potential to remove the aromatic

organic sulfur compounds from fuels to nearly zero level. Zeolites **[15]**, activated alumina **[1, 16-18]** and different carbon materials such as activated carbon, graphite oxide, graphene and single wall carbon nanotube **[1, 20-40]**have been explored and used for removal of organic sulfur compounds from various model fuels and oil types.

There should be a transition here to convince the reader as why you are investigating those. This study investigates the potential use of CNT, GO and AC, doped with different percentage of metal oxide and sulfide as adsorbents for removal of DBT and thiophene. These adsorbents were characterized using thermal gravimetric analysis (TGA), an N_2 adsorption-desorption surface area analyzer, scanning electron microscopy (SEM), energetic dispersive X-ray diffractogram (EDX), Field Emission Electron Microscope (FE-TEM) and X-ray photoelectron spectrometer (XPS), then the nature and kinetics of the adsorption of DBT and thiophene, from their solutions in *n*-hexane as model diesel were studied. To decide on the best adsorption isotherm and the model for the adsorption kinetics the resulting data were fitted to equations for different adsorption isotherms. Additionally, the adsorbents' reusability and their selective adsorption of DBT relative to thiophene and naphthalene were studied.

1.1 Motivation

The removal of organosulfur compounds from crude oil is of utmost importance to the Kingdom of Saudi Arabia due to the severe corrosion of oil refinery industrial setups and because they deactivate the catalysts used in them. In the conventional hydrodesulfurization (HDS), it is hard to remove all of these organosulfur compounds such as dibenzothiophene (DBT). The adsorptive desulfurization is promising technique since it is relatively cheap and may bring the sulfur compounds nearly to zero level at

ambient conditions. Many carbon based materials have been investigated to remove the DBT as selected organic sulfur compound from model and real fuel. That led us to synthesize low cost materialscompositesby employingmetal oxides and sulfides nanoparticles modified carbonaceous micro and nano materials as adsorbents for the efficient removal of organosulfur compounds in general and DBT in particular at trace level.

1.2 Research Objectives

The main purpose of this work to develop a modified activated carbon, carbon nanotube and graphene oxide with metals oxide or sulfide as adsorbents that can remove efficiently and selectively the DBT from model fuel in presence of other compounds (i.e. thiophene and naphthalene). The following objectives were considered in this research to achieve its main goal.

Part one: Develop a quantitative HPLC method of analysis for thiophene,dibenzothiophene and naphthalene in *n*-hexane organic media

Part two: Impregnate, where possible, the surfaces of carbonaceous materials (activated carbon (AC), multi-wall carbon nanotubes (CNT) and graphene oxide (GO)) with one or more of the Ni, Ag, U or Al nanoparticles in oxide or sulfide form as adsorbents.

Part three: Characterize the carbonaceous adsorbents (activated carbon (AC), multi-wall carbon nanotubes (CNT) and graphene oxide (GO)) and the impregnated systems mentioned in part two by SEM, EDX, TEM, TGA,XPS and XRD.

Part four: Study the effect of raw carbonaceous materials with and without impregnation by metals (oxides and sulfides) nanoparticles on the removal of organic sulfur compounds from model fuel.

Part five: Study the removal efficiency by varying the removal parameters such as dosage of adsorbents, contact time, concentration of the organic sulfur compounds, and loading of metal nanoparticles.

Part six: Study the kinetics of the thiophene and DBT adsorption and their isotherms.

Part seven: Carry out the comparison between the existent removal materials with those developed in this thesis.

1.3 Dissertation Outline

This dissertation consist 6 chapters and is structured as following:

Chapter 1 is an introduction for this work, the motivation behind it and the research's objectives.

Chapter 2 presents a background on three different carbon based materials (i.e. activated carbon, carbon nanotube and graphene oxide) their preparation, types and properties. This chapter also provides a background on different desulfurization techniques.

Chapter 3 presents the research methodology including the materials used, adsorbents impregnation with different metals oxide or sulfide, adsorbents characterization and adsorption experiments set-up.

Chapter 4 presents the results and discussion for the following:

- Adsorption performance of multiwall carbon nanotubes and graphene oxide for removal of thiophene and dibenzothiophene from model diesel fuel.
- The nature and kinetics of the adsorption of dibenzothiophene and thiophene in model diesel fuel on carbonaceous materials doped with aluminum oxide particles. Covering the selectivity and reusability of the adsorbents.
- Synthesis and characterization of modified carbon nanotube and graphene oxide with silver sulfide nanocomposites for adsorptive removal of dibenzothiophene: adsorption isotherm modeling
- Adsorption isotherms and kinetics for dibenzothiophene on activated carbon and carbon nanotube doped with nickel oxide nanoparticles. Covering the selectivity and reusability of the adsorbents
- Adsorptive removal of dibenzothiophene and thiophene using carbon nanotube and activated carbon modified with uranyl oxide nanoparticles.

Chapter 6 presents a comparative analysis among the prepared adsorbents in this thesis and with other existing materials in literature.

Chapter 5 provides the conclusion of this thesis and recommendations for the future works.

CHAPTER 2

2. LITERATURE REVIEW

2.1 Activated Carbon

Activated carbon is an allotrope of the carbon family. It is a pure carbon in graphite form with amorphous and highly porous structure. Activated carbons contain wide range of different pore sizes starting from visible cracks to slits of molecular dimensions **[41]**. The powdered activated carbon was first produced commercially from wood, as a raw material, in the early 19th century. The use of activated carbon for water taste and odor control was first reported in 1930 **[42]**. Today, activated carbon is produced from many different raw materials including: coconut shells, wood, refineries coke, carbon black, rice hulls, sugar, and from almost all organic materials. The high surface area is the major feature of activated carbons that makes theses material good for adsorption processes. as shown in figure 5 other factors that give activated carbons the adsorptive properties are their micro-porous structure and the fact that activated carbons have high degree of surface reactivity.

2.1.1 Types of activated carbons

Activated carbon can be classified based on their properties which are obtained during the activation process. Therefore, we may classify activated carbon based on the activation process to the following two main categories:

- Physical or thermal activation: this activation process involves carbonization at raw materials at temperature of 500°C to 600°C **[43]**.
- Chemical activation: this type of activation involves the addition of some inorganic additives, such as metallic chlorides to activated carbons surfaces **[44]**.

Mattson**[45]** suggested another classification, which classify activated carbon as acidic and basic activated carbons. According to Mattson:

- Carbon activated at low temperature range of 200 °C to 400 °C develops acidic surface oxides that lower pH value of the solution. These types of activated carbons are usually adsorbing basic or hydrophilic species and exhibit a negative zeta potential.
- In contrast, carbons activated at high temperature range of 800 ° to 1000 °C develop basic surface oxides and they increase the pH value of the solution. In this case, these activated carbons adsorb acids and exhibit a positive zeta potential.

2.1.2 Properties of activated carbon

Activated carbon is another form of graphene sheets connected together through numerous networks of benzene rings. Therefore, the existing of π-orbital in carbons rings enable activated carbon to accept many modifications.

For instances, the positive zeta potential for the basic activated carbons can be altered to negative value by cooling the activated carbons in presence of oxygen due to the formation of acidic surface oxides.

Activated carbon is used widely in adsorption processes. Today, it is hard to find an industrial processthat is not using activated carbon in the filtration and purification treatment. In water treatment for instances, activated carbon is used to control taste and odor and to adsorb undesired suspended metals **[42]**.

In general, the activated carbon properties can be determined by the starting material used for the activation process and the activation method used. Such properties include the determination of the surface functional groups. Therefore, the activated carbon surface chemistry, and hence the adsorption behavior, depends upon the activation conditions and temperatures employed. Activation also play major role in refining the pore structure that can yield large surface areas up to about 1900 m^2/g **[43, 46]**.

2.1.3 Production of activated carbons

As stated earlier, active carbon is produced from many different raw materials rich with hydrocarbons, such coconut shells, wood, refineries coke, carbon black, rice hulls, sugar, and many almost from all organic materials. Activation carbons are produced by one of the following methods:

- Physical or thermal activation: This activation process involves carbonization at raw materials at temperature of 500°C to 600°C to eliminate all volatile content of the raw materials. The carbonized material is partially processed in gasification process to develop the desired porosity and surface area. For gasification to take place, an oxidizing gas such as CO2, steam or fuel gas at temperature of 800 °C to1000ºC, is required **[43]**.

- Chemical activation: this type of activation involves the addition of some inorganic additives, such as metallic chlorides, before the carbonization process. This process can help improving microporous structure of the activated carbon produced **[44]**.

2.2 Carbon Nanotubes

Carbon exists in many molecular forms, known as allotropes of carbon. These allotropes can be considered as different structural modifications of carbon element **[47]**. Carbon nanotubes (CNTs) are allotropes of carbon described as a rolled-up tubular shell of graphene sheets. These graphene sheets are made of benzene-type hexagonal rings of carbon atoms. Figure 2-1 shows a graphene sheet made of C atoms (a) placed at the corners of hexagons forming the lattice with arrows a and b denoting the rolling direction of the sheet to make (b) a armchair nanotube and (c) a zigzag nanotube **[48]**.

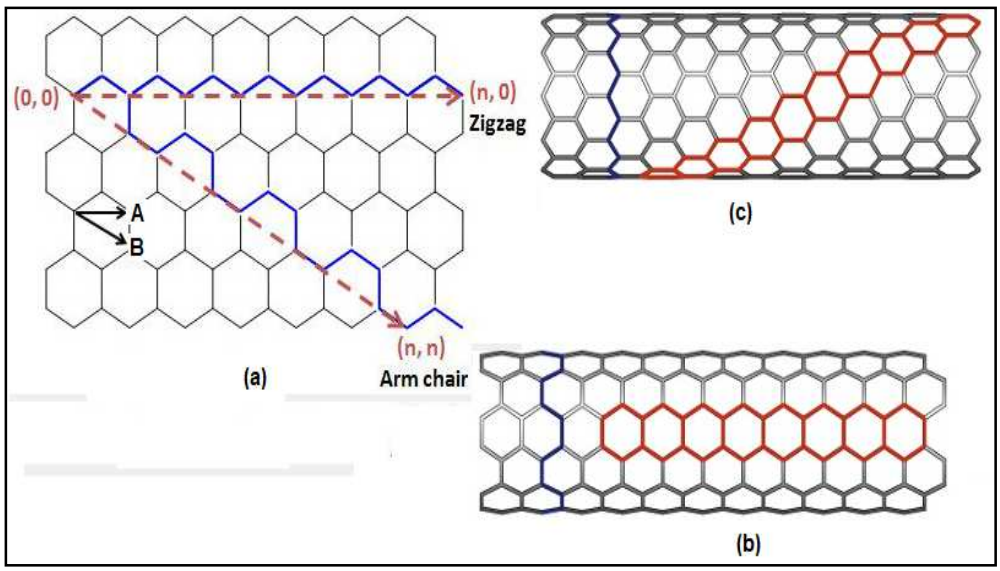

Figure 2-1:(a)CNT made of graphene sheet of C atoms to give (b) armchair or (c) Zigzag conformation

CNT were discovered in 1991 by Sumio Ijima of NEC Laboratory in Tsukuba, Japan, using arc-discharge method and they were characterized by High-Resolution Transmission Electron Microscope (HRTEM) **[49]** Chemical bonding in nanotubes is best described by Applied quantum chemistry, specifically, orbital hybridization. "The chemical bonding of nanotubes is composed entirely of sp^2 bonds, similar to those of graphite. These bonds, which are stronger than the sp^3 bonds found in alkanes, provide nanotubes of a unique strength. Moreover, nanotubes naturally align themselves into "ropes" held together by Van Der Waals forces" **[50].**The reported nanostructure cylindrical shape was found to have length-to-diameter ratio of up to 132,000,000:1, significantly larger than any other material **[48]**.

2.2.1 Properties of carbon nanotubes

The main distinct properties of the carbon nanotubes can be classified under two categories:

- **Mechanical Properties:** Due to the covalent sp^2 bonds formed between the individual carbon atoms, CNT are considered the strongest and stiffest materials on earth, in terms of tensile strength and elastic modulus respectively. Experimental and theoretical results have shown that CNT has an elastic modulus of greater than 1 Tpa, which is 10–100 times higher than the steel at a fraction of the weight **[44]**. Table 2-1 shows a comparison between CNT and some materials that are known to have strong elastic modulus:

- **Thermal properties:** carbon nanotubes are reported to have good thermal conductivity measured from 4 to 300 K **[45]**, similar to that of graphite. Similar behavior was also observed in the measurements of the temperature-dependent thermal conductivity of bundles of SWCNTs from 8 to 350 K **[46]**.

Table 2-1: Mechanical properties of some materials

Material Name	Tensile strength (GPa)	Density (g/cm3)	Young's modulus (GPa)
Wood	0.008	0.6	16
Epoxy	0.005	1.25	3.5
MWCNT	150	2.6	1200
SWCNT	150	2.6	1054
Steel	0.4	7.8	208

- **Electrical properties:**The CNT can be metallic or semiconducting. When they are produced as electrically conductive, they exhibit superior and unique electrical

properties. Conductive CNTs are found to carry electric current 1000 times higher than copper wires **[51]**. For a given (n,m) nanotube, if the difference between n and m is a multiple of 3, then the nanotube is metallic, otherwise the nanotube is a semiconductor. As explained above, all armchair (n=m) nanotubes are metallic, and nanotubes with n-m greater than 3 are semi-conducting.

- **Chemical reactivity:** Carbon nanotubes can undergo chemical reactions that make them more soluble in inorganic, organic, and biological solutions. CNTs reactivity is directly related to the π-orbital mismatch caused by an increased curvature. Therefore, a distinction must be made between the sidewall and the end caps of a nanotube. For the same reason, a smaller nanotube diameter results in increased reactivity. Covalent chemical modification of either sidewalls or end caps has shown to be possible **[52]**.

Based on the above discussed properties, CNT and modified CNT are extremely promising for future applications including environment protection, materials science, medicinal chemistry, and many others.

2.2.2 Production of carbon nanotube

There are many techniques to produce carbon nanotubes; however, the three widely used today are:

1- Arc Discharge Method

Arc Discharge method produces CNT in low pressure of helium gas or any other neutral atmosphere [53]. This method is the method in which carbon nanotubes were first discovered by Ijima in 1991. Figure 2-2 illustrates the Arc Discharge apparatus. This is the most common, simplest, and perhaps easiest way to produce carbon nanotube. However, it produces a mixture of nanotube, soot and the catalytic metals present in the crude product and requires purification to obtain clean CNT. Arc Discharge method produces nanotube through arc-vaporization of two carbon rods separated by approximately 1 mm in an enclosure that is usually filled with inert gas, such as helium or argon, at pressure range of 50 to 700 mbar [54].

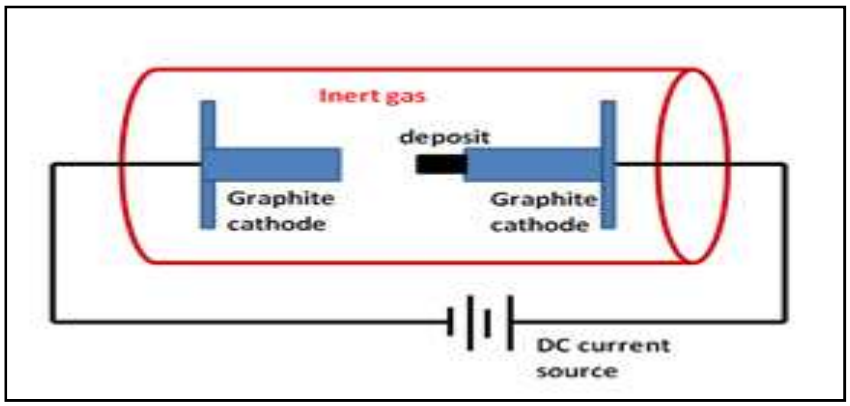

Figure 2-2: Arc discharge apparatus

2- Laser Ablation Method

In 1995, Richard Smalley and co-workers at Rice University reported the synthesis of carbon nanotubes by lasers group vaporisation. Richard used laser beams to vaporise a graphite target in an oven at 1200 ºC [55]. Currently there are two types of laser method: continuous and pulse. The main difference between the two methods is that

the pulsed laser demands a much higher light intensity of 100 kW/cm^2 compared to 12 kW/cm^2 for the continuous laser method.

The nanotube produced by Laser Ablation Method is collected on the cooler surfaces of the reactor as the vaporized carbon condenses. This method produces MWCNTs when pure graphite electrodes are used. However, when nanoparticals catalyst, such as Co, Ni, Fe, are added SWNT are formed **[56]**. An illustration for this method is shown in Figure 2-3

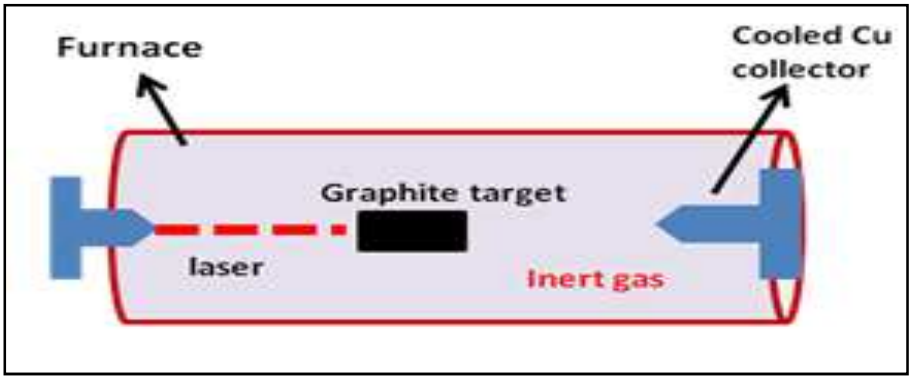

Figure 2-3: Schematic drawing of a laser ablation apparatus**[55]**

3- Chemical Vapor Deposition (CVD)

Chemical Vapor Deposition method is a simple process and is believed to be the easiest method to scale up to industrial production. It has many variables that provide the producer with enough controlling parameters to produce the desired CNT quality. CVD is essentially a two-step process consisting of a catalyst preparation step followed by the actual synthesis of the carbon nanotube. A carbon source in gaseous phase, such as methane and carbon monoxide, passes over an energy source to crack the molecule into reactive atomic carbons. Then, these active carbon atoms diffuse over substrate, which is

heated and coated with a catalyst, to produce the CNTs. The process takes place at high temperature range of 500 to 1000 ºC. Therefore, this process involves dissociation of hydrocarbon molecules to form active carbon atoms, and then these active atoms are catalyzed by the transition metal to achieve the required saturation of carbon atoms in the metal nanoparticle **[57]**. Figure 2-4 shows the CVD process.

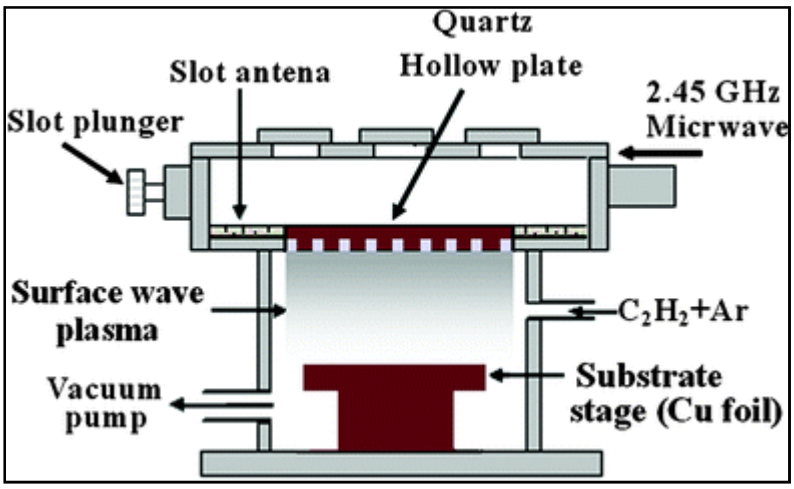

Figure 2-4: A schematic diagram of a plasma CVD apparatus**[57]**

2.3 Graphene

Graphene is defined to be two dimensional nanomaterials has a layer of one sp^2 hybridized carbon atom thick.The unique properties of this material like high specific surface area around 2600m^2**[58]**, great thermal conductivity of 5000 $Wm^{-1}K^{-1}$**[59]**, high speed electron mobility of 200000 $cm^2V^{-1}s^{-1}$ at ambient temperature **[60]**, high stiffness and strength with Young's modulus around 1000GPa and break strength 130 GPa **[61]**, amazing high electrocatalytic activity **[62]** as well as optical properties **[63]**. All of these extraordinary physicochemical properties introduce it for potential applications in many research fields so this material attracted great interest of scientists.

2.3.1 Types of graphene

1- Single layer graphene:A one thick hexagonally arranged sp2 hybridized bonded carbon atoms. Its dimensions vary from nano scale to micro scale. It is available as an adhered layer on a substrate or suspended in a aqueous or organic solution.

2- Multi-layer graphene:A sheet-like carbon material, containing of few flaks of single layer graphene. The number of these 2D layers varies from two to ten layers. Dispersed graphene in solution can have defined thickness distribution. This type of graphene is useful in composite materials preparation and a mechanical strengthening.

3- Graphene oxide (GO):A few layers of graphene with high oxygen content, prepared by chemical oxidation and exfoliation of graphene.

4- Reduced graphene oxide (rGO):A few layers of graphene with high oxygen content, prepared by chemical, thermal or microbial reduction of graphene graphene oxide.

5- Graphite oxide: A bulk solid prepared by oxidation of graphite. It is consider a precursor to single or multi-layer graphene oxide preparation through processes that modify the graphite planes which lead to increase the interlayer spacing.

6- Graphite nanoplatelets, graphite nanosheets, graphite nanoflakes

A graphite with dimensions less than hundred nanometers is different from conventional crushed finely graphite powder whose thickness is more than hundreds nanometers. It is good for preparation high electrically conductive materials composites **[64]**.

2.3.2 Applications of graphene based materials

Graphene based carbon materials can be useful for many applications. There are many adsorbents **[65]** and photocatalysts **[66]** were developed for removal or for photocatalytic degradation of toxic compounds based on the high adsorption capacity, high surface area and catalytic activity of graphene or graphene oxide. In other hand, considering the great electrical conductivity and optical properties of this material many high sensitive electrochemical **[67]** and fluorescent sensors **[68]** were also fabricated to detect of these toxic compounds.

The aggregation of graphene is considered an important factor which leads to the reduction of its effective surface area and as a result decrease its adsorption capacity, in contrast modification of graphene with certain functional groups or metals will prevent its aggregation as well as will lead to increase its water solubility and its affinity toward target pollutants as a result enhance the selectivity of its adsorption process or detection techniques. For example graphene and graphene coated with silica were used for removal some pesticides **[69, 70]** or some phenolic compounds **[71, 72]**, also Liu and others **[70]** synthesized a silica coated with graphene and they could use it as adsorbents to remove eleven organophosphorus pesticides with more efficiency than the other adsorbents (i.e. graphite carbon, activated carbon, C_{18}-silica and silica). Other researchers used the graphene as adsorbent for removal of bisphenol A with an adsorption capacity around 0.182 g g^{-1} **[71]**.

2.4 Removing of sulfur compounds.

There is no universal classification for removing of sulfur compounds (desulfurization) processes. The desulfurization processes can be classified in different approaches, on the basis of the chemical and/or physical nature of the process, the destiny of the sulfur compounds during the desulfurization process, the way in which the sulfur compounds are transformed or the processes that based on the catalytic hydrodesulfurization (HDS). The process can be categorized depending on whether the organosulfur compounds are separated without decomposition from the fuel fractions, decomposed by certain catalytic reaction or by both processes separated and then decomposed as illustrated in figure 2-5.

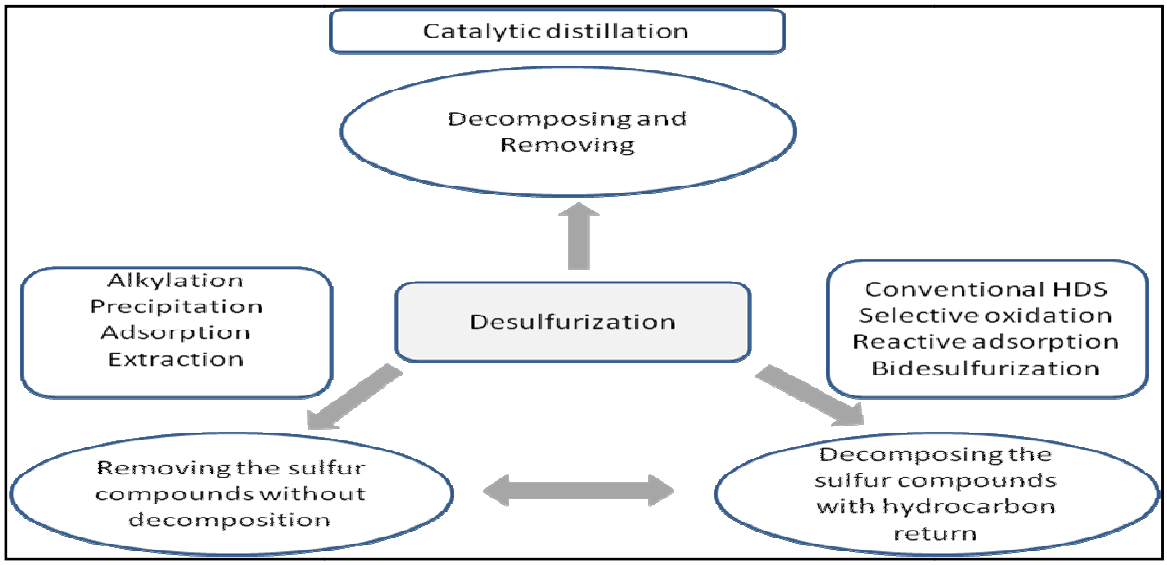

Figure 2-5: Desulfurization process classified based on the sulfur compounds transformation.

The conventional hydrodesulfurization process is the typical example of the process involving decomposition of the sulfur compounds. In removing the sulfur

compounds without decomposition class, simply the organosulfur compounds are separated from the fuel stream. In some cases of this class the organosulfur compounds firstly are converted to other compounds forms that can be separated easier from the streams.

As shown in figure 2-6, the second classification of desulfurization processes depend on the nature of the technique used for removing the sulfur compounds from the fuel fractions. The most know and commercialized methods are based on the catalytic conversion of sulfur compounds and the others are based on the physico-chemical processes to separate and eliminate the sulfur compounds from the fuel fractions without using hydrogen gas. Some of these catalytic methods are the conventional hydrodesulfurization which include advance catalysts, advance reactor design or a combination of hydrotreatment with some chemical processes to maintain the fuel specifications. Some of these processes will not be discussed deeply because they are not our concern in this work. The most common four desulfurization techniques will be mentioned and discussed in this literature review chapter.

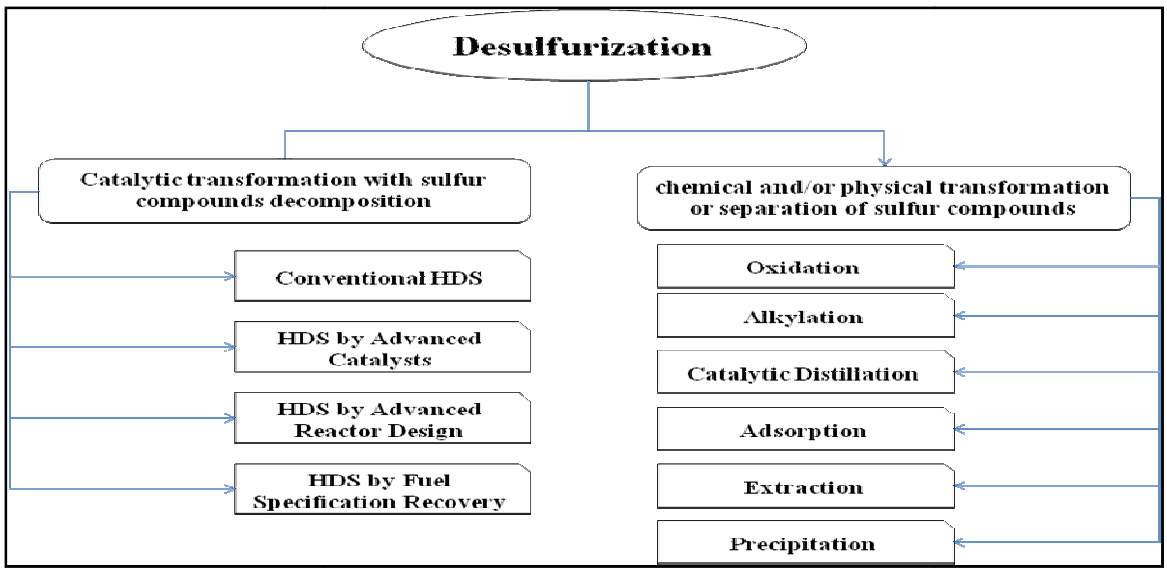

Figure 2-6: Classification of desulfurization process based on the nature of the process to eliminate sulfur compounds.

2.4.1 Hydrodesulfurization process

In the hydrodesulfurization (HDS) process the organosulfur compounds are converted to hydrogen sulfide and hydrocarbon using a catalyst at high temperature and high hydrogen pressure. The HDS process details are mentioned in literatures **[73, 74]**. The HDS process is usually carried out over a nickel and cobalt molybdenum (NiMo and CoMo) catalysts supported on alumina (Al_2O_3) material surface. The efficiency of the HDS process in term of the selectivity and activity depends on many factors such as;

1- The type of the catalyst used

2- The hydrotreating conditions (temperature and relative pressure of hydrogen and hydrogen sulfide gases).

3- The concentration and structure of the organosulfur compounds in the refinery stream.

4- The hydrotreating process and reactor design.

Usually all the fuel fractions contain some of the organosulfur compounds. Higher molecular weight organosulfur compounds are less reactive in the HDS process. These compounds are present in higher boiling point oil fraction. So the reactivity of sulfur-containing compounds should be considered in the HDS process. As illustrated in figure 2-7, the reactivity of the organosulfur compounds depends on their structure and the position of sulfur atom in the structure.

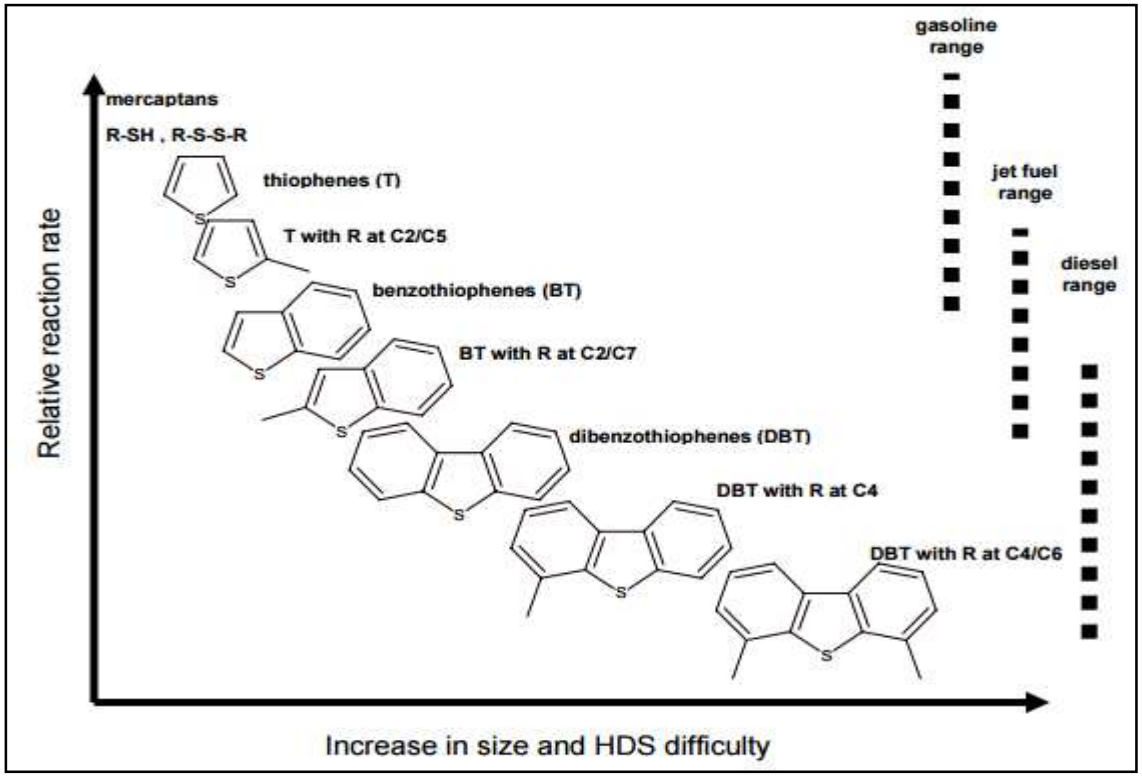

Figure 2-7: The effect of size of organosulf compounds on the their reactivity in the HDS process [75].

The organosulfur compounds can be categorized in four main groups based on their reactivity in the HDS process; 1) Mercaptan, sulfide and disulfide compounds group, 2) thiophene and substituted thiophene compounds, 3) benzothiophene and it substituted compounds, 4) dibenzothiophene and its substituted compounds. The first group has the highest activity and it can be removed easily and completely using the HDS process **[76]**. The chemical equations below present the hydrotreating chemical reaction for those compounds.

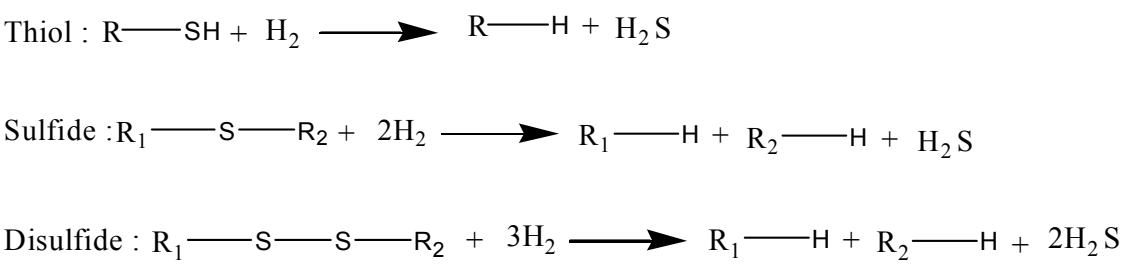

The fourth group has the lowest reactivity and it is the most difficult to be eliminated using the HDS process **[8]**. For example, figure 2-8 shows the two path ways for desulfurization of dibenzothiphene through hydrogenation and hydrogenolysis reactions.

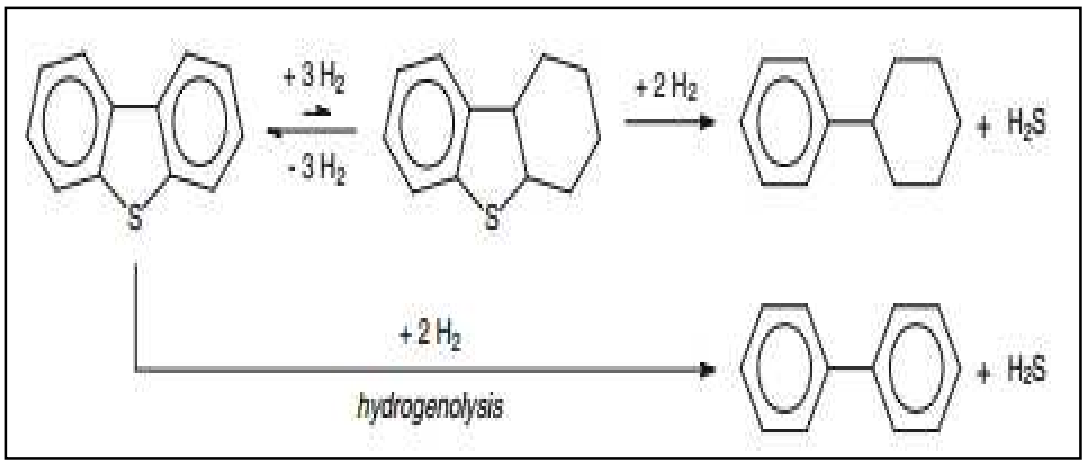

Figure 2-8: Two pathways for desulfurization of dibenzothiophene sulfur compound in the HDS process.

To obtain deep HDS and eliminating the dibenzothiophene and its alkylated compounds, severe conditions should be employed which will not lead only to eliminate the dibenzothiophenes compounds but also produce undesired products and low quality fuel. The reported reactivity and the selectivity value for the catalyst widely differ from study to study depending on the HDS conditions and parameters. For example, the NiMo catalyst is more active for eliminating the 4,6 dimethyldibenzothiophene in a continuous-flow HDS reactor **[77]**, while in a batch reactor the CoMo catalyst is more active for eliminating the same organosulfur compound **[78]**. The main drawbacks in the HDS are mentioned below

1) Requires high purity and high pressure of hydrogen
2) Not feasible for fuel cells.

3) Ultra deep desulfurization with advanced catalysts requires a 7-fold increase in reactor size
4) Hydrogen consumption also increases very sharply at very low product sulfur levels

2.4.2 Oxidative desulfurization

The methods that do not use hydrogen gas for catalytic elimination of sulfur compounds from refineries stream are called Non-HDS techniques. The oxidative desulfurization is a good example for these Non-HDS methods. The oxidative desulfurization involves two key steps, converting the organosulfur compounds to sulfones and sulfoxide followed by removing these products using physical or chemical methods such as thermal decomposition, extraction to polar liquid phase, distillation, precipitation or pyrolysis to SO_2. There is many oxidizing agents can be used for the oxidation step, such as an air, oxygen, ozone, nitric acid, nitrogen oxide, peracides and peroxides.Some of examples in the literature for desulfurization using this method were summarized below.

In 1964 Ford et. al.**[79]** could remove only 40 % from the sulfur contents of petroleum fraction boiling at 250 ºC by oxidizing the sulfur compounds using peroxides with a nickel vanadium catalyst then the organosulfur oxidized products were thermally decomposed at 90 ºC. Other researchers developed an oxidative method to remove sulfur compounds from heavy arabian crude oil using butyl hydroperoxide with Mo catalyst followed by cooling. This method could remove about 40 % of sulfur compounds **[80]**.

In 1996 Petro Star Inc. developed a desulfurization method based on oxidative organosulfur removal. This method starts by mixing diesel fuel with a mixture from hydrogen peroxide/acetic acid as an oxidant, an oxidation reaction take place at atmospheric pressure under 100 ºC. Subsequently, a low sulfur fuel is produced by extraction the oxidized sulfur compounds using liquid/liquid extraction combined with solid phase adsorption to decrease the sulfur level from 4720 **μ**g/g to 70 **μ**g/g **[81]** as illustrated in figure 2-9.

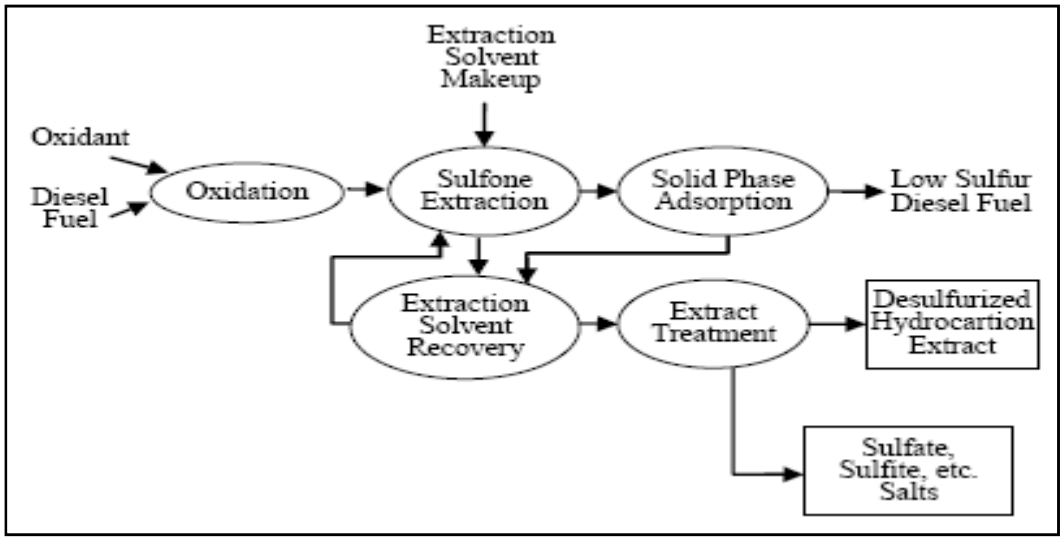

Figure 2-9: Diagram illustrates Petro Star Inc. technology of desulfurization**[81]**.

In 2014 Arellano U. *et. al.***[82]** prepared a series of catalysts based on graphite carbon modified with copper oxide. The catalytic activity of these catalysts in presence of acetic acid and H_2O_2 was tested for dibenzothiophene oxidation in the oxidative desulfurization. The high surface acidity resulted from reaction the H_2O_2 with acetic acid molecules and forming peroxyacetic which coordinated with the impregnated copper

cations on the surface of the copper/graphite carbon catalysts to promote the catalytic activity toward oxidation of dibenzothiophene sulfur compounds in hexadecane as model oil. 80 % conversion of DBT 300 ppm in 100 mL model oil was achieved at 30 ºC using 0.1 g graphite carbon modified with 15 % copper oxide.

Simultaneous extractive and oxidative desulfurization method was developed in 2014 by Jianlong Wang and co-researchers **[83]**. This method based on using N-hydroxyphthalimide (NHPI) catalyst in [Bmin]BF_4 ionic liquid and molecular oxygen as an oxidant. Using this method at 120 C and 0.3 Mpa oxygen pressure was able to remove 100 % of 500 ppm DBT in *n*-octane model fuel compared to only about 33 % removal efficiency using the same method without NHPI catalyst.

Using oxygen or air as an oxidant for organosulfur compounds oxidative removal is more attractive than using hydrogen gas in the hydrodesulfurization, because of low cost of these gases and their availability. However, the main disadvantages of the oxidative desulfurization **[84]** are:

1) Inappropriate for all oil fractions particularly FCC gasoline.
2) Low removal efficiency for organosulfur compounds.
3) Most of the oxidizing agents (peroxides, paracides, etc.) are expensive
4) Formation of CO_x gases as by-products.

2.4.3 Extractive desulfurization

The principle of the extractive desulfurization technique is based on the organosulfur compounds have better solubility than other components of fuel (hydrocarbons) in suitable single solvent or solvent mixtures**[84]**. Figure 2-10 illustrates the general process scheme for the extractive desulfurization. The fuel oil is pumped in a mixing tank with an appropriate extraction solvent to transfer the sulfur compounds from the fuel to the solvent followed by a separation step to obtain desulfurized fuel and consumed solvent. In another unite the consumed solvent is regenerated by distillation process to separate the organosulfur compounds and reuse the extractive solvent again. The main advantages of the extractive desulfurization process are as following:

1- The extractive desulfurization does not change the structure of the fuel oil.

2- It can be easily integrated into the oil refineries.

3- It does not need special equipments.

4- It works at ambient temperature and atmospheric pressure.

The process is not highly efficient for removal all of the organosulfur compounds from all fuel fractions. Therefore, the extractive desulfurization should be repeated on the same fuel portion more than one time using different extractive solvent to insure removing most of the sulfur compounds and obtain deep desulfurized fuel. The selection of the extractive solvent is the crucial step for the extractive desulfurization. Since the solvent should be immiscible with the fuel, inexpensive, available, has low viscosity to improve his mixing with the fuel, has a capability to dissolve as much as possible the sulfur

compounds selectively and has a boiling point different from the boiling point of the organosulfur compounds. Some of organic solvents have been tested and they showed reasonable efficiency ranging from 50 % to 90 % sulfur removal, depending on the number of extractive desulfurization process repetition. Among of these solvent are polyethylene glycol **[85]**, aceton **[86]** and organic solvent containing nitrogen **[87]**.

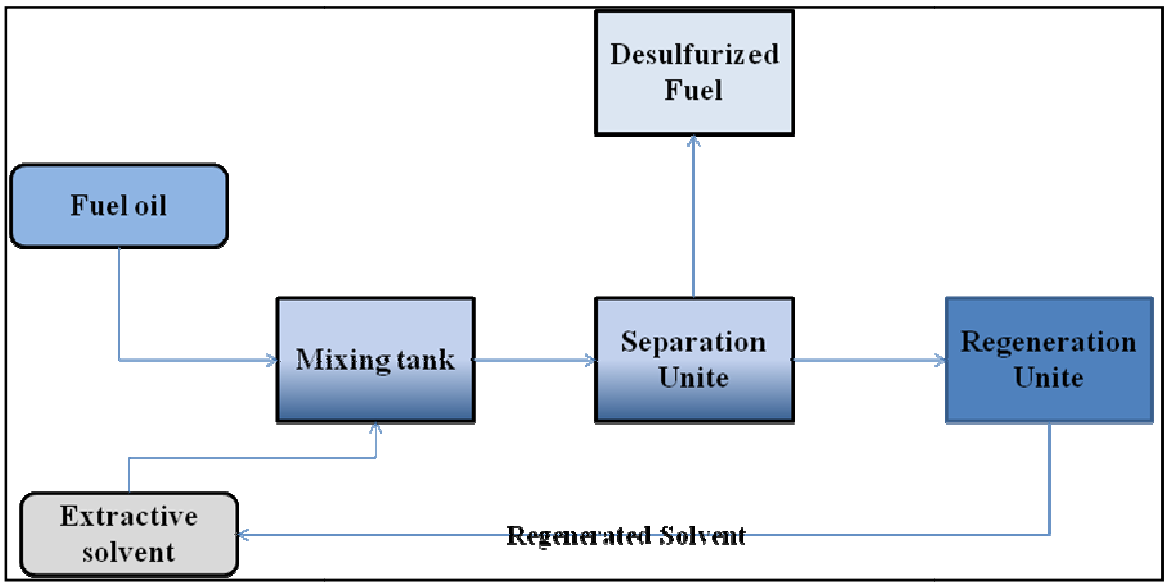

Figure 2-10: Scheme illustrates the extractive desulfurization steps**[84]**

Many processes based on the extractive desulfurization have been reported in the literature. Herein, some of these processes based on using ionic liquid as an extractive solvent were mentioned.

The ionic liquid solvents have many advantageous over the organic solvents. It has low viscosity, high distribution coefficient for organosulfur compounds, fast phase separation with fuel and different boiling point from sulfur compounds.

Different ionic liquid based on 1-butyl-3-methylimidazolium (Bmim) cation and different anions were tested in removing dibenzothiophene from n-dodecan model fuel [88]. Because of the low viscosity of [Bmim]Cl and its ability to provide stronger Lewis acid,it showed the highest removal efficiency (77.1 %) compared with [Bmim]Br, [Bmim]BF_4, [Bmim]BF_6, [Bmim]PF_4, [Bmim]$AlCl_4$, [Bmim]OSO_4. In 2014 a new set of ionic liquids (N-methylpiperazinium lactate ([C_1pi][Lac]), N-ethylpiperazinium lactate ([C_2pi][Lac]), and N,N′-dimethylpiperazinium dilactate ([C_1C_1pi][$Lac]_2$)) were synthesized and used as novel extractive solvent for removing some of organosulfur compounds (thiophene, benzothiophene, dibenzothiophene and 1-methylbenzothiophene) **[89]**. The selectivity of these ionic liquids was high due to their non-aromatic properties which could not provide stronger π-π interaction between the sulfur compounds and the ionic liquid solvent. The good distribution coefficient of organosulfur compounds was explained by the ion-dipole and dipole-dipole interactions between the polar property of ionic liquid and sulfur compounds.

The π- complexation interaction between thiophene in gasoline and Cu^+ in CuCl based ionic liquid [HMim]Cl/CuCl) was the reason behind improving the extraction ability of that ionic liquid to reach about 41 % desulfurization after 5 time successive extraction **[90]**. It has been concluded by Rashad Javadli and Arno de Klerk **[91]**, although of the distribution coefficient of model sulfur compounds like dibenzothiophene in ionic liquid, the performance of real ionic liquid in real straight run distillate is not efficient

2.4.4 Adsorptive desulfurization

Removing of organosulfur compounds by adsorption is based on using solid adsorbents have ability to interact with these sulfur compounds and remove them selectively from refineries stream.

As shown in figure 2-11, the desulfurization by adsorption technique is promising and efficient as an alternative or complementary technique because it is simple, relatively cost effective and has the potential to remove the aromatic organic sulfur compounds from fuels to nearly zero level[92]. The adsorbents can be regenerated using certain gas or solvent to re-dissolve the adsorbed sulfur and hydrocarbon compounds.

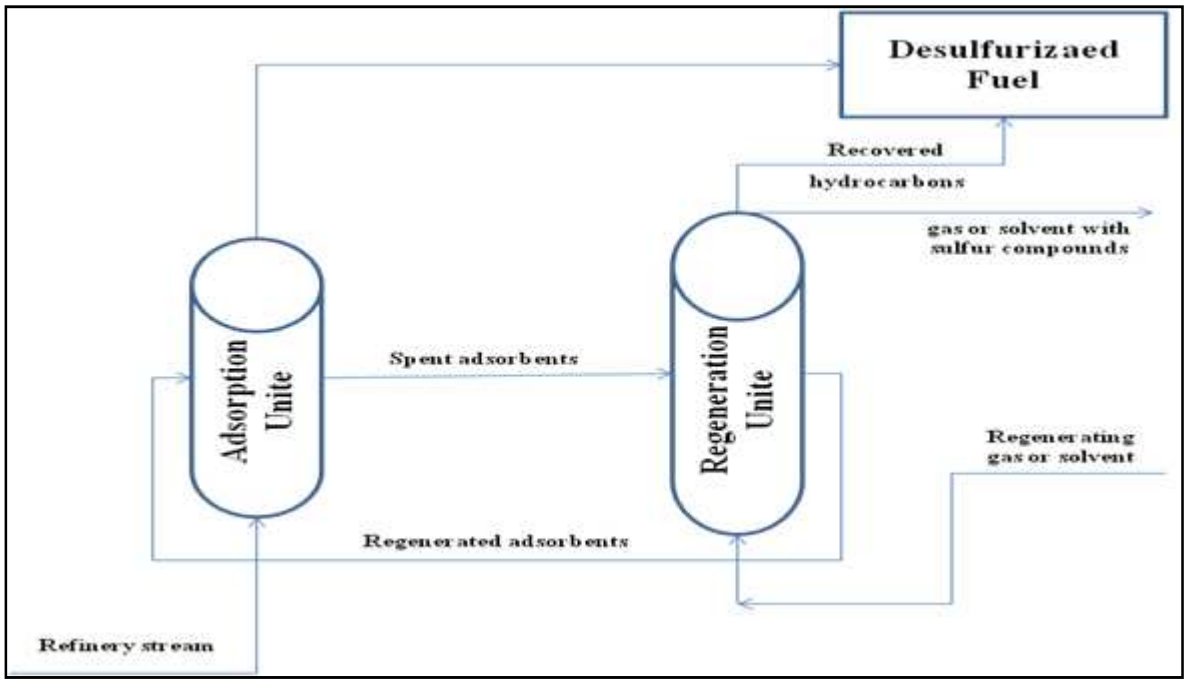

Figure 2-11: Scheme illustrates the adsorptive desulfurization steps[92]

Zeolites **[15]**, activated alumina **[1, 16-18]** and different carbon materials such as activated carbon, graphite oxide, graphene and single wall carbon nanotube **[1, 20-40]**have been explored and used for removal of organic sulfur compounds from various model fuels and oil types. The efficient adsorbent should have good properties such as, high adsorption capacity, their selectivity to remove sulfur compounds, inexpensive, able to be reusable and has fast kinetics. Some of the reported adsorbents used in the adsorptive desulfurization for removing dibenzothiophene and/or thiophene were discussed below.

Among of the carbonaceous materials, the activated carbon with high surface area and high average pore volume is known as an excellent adsorbent for organic molecules such as DBT. Recently, Kumagai and co-worker**[20]**studied the adsorption behavior of DBT from *n*-hexane model diesel on coconut shell activated carbon and compare it with activated carbon fiber and found that, at low DBT concentration the adsorption capacity of activated carbon is higher than of activated carbon fiber in spite of the activated carbon fiber has higher surface area.

Graphite oxide has received high attention to be adopted for many applications due to their distinct properties. Possessing the graphite oxide oxygenated functional group makes it able to be modified with different metals oxide or other functional groups to improve its surface chemistry and anchoring additional active sites **[23]**. Graphene and graphene oxide based materials are known to be useful for the removal of toxic gases and for water purification **[23, 24].**Hoon et. al. **[22]** studied the adsorption of DBT on graphene and graphite oxide adsorbents prepared with phosphoric acid and compared their adsorption capacity with graphene and graphite oxide prepared by the conventional

Hummers's method and reported that, graphite oxide and graphene which prepared using phosphoric acid have higher surface area and adsorption capacity for DBT.

Hiyang Chen **[25]** investigated the effect of DBT's adsorption on modified carbon nanotube, activated carbon and alumina with different CoMo catalysts on the HDS process efficiency and found that, the ratio between the adsorbed DBT surface area and the catalysts total surface area is the highest is case of CoMoS/CNT. Consequently, the CoMoS/CNT has the highest catalytic activity due to nano size effect of CNT; in spite of the AC has higher surface area and higher loading ability than the CNT. On other hand, Lilin Wang et. al. **[26]** explored the potential use of single wall carbon nanotube (SWCNT) as a drug carrier and adsorbent for N and S-heterocyclic aromatic compounds including thiophene compound as a model S-heterocyclic aromatic compound. They found that the O-functional group on the oxidized CNT could enhance the adsorption of these compounds based on two main enhancement adsorption mechanisms which are electron donor-acceptor interaction and Lewis acid-base interaction with the CNT.

Dennis and Ralph**[34]**investigated the adsorption properties of two different single wall carbon nanotube (SWCNTs) diameters (12 Å and 16.8 Å) for three different compounds (benzene, thiophene and cyclohexane) as well as the potential use of SWCNTs for fuel desulfurization. They found that, the adsorption isotherm in gas phase and the isosteric heat of adsorption are followed the order thiophene > benzene > cyclohexane. It was reported also that, the 16.8 Å SWCNTs treated with nitric acid contains higher oxygenated group and it has better adsorption capacity for thiophene molecules (0.86 mg thiophene/ g adsorbent) from 99.9 % benzene as model fuel.

The removal efficiencies of thiophenes compounds by metal oxide alone as adsorbents (i.e PbO, BaO, CdO, CoO, ZnO and CuO) were very low **[93]**.

The chemistry of adsorbents' surfaces was investigated for DBT adsorption, where the acidic groups **[33]**, oxygen-containing functional groups **[94]**and transition metals type (Ag^{+}, Cu^{+2}, Ni^{+2} and Zn^{+2}) **[95]** play a major role in improving the adsorbents surface and in turn enhancing adsorption of DBT from model fuel. Acidic functional groups on the adsorbent's surface are classified into two main types; Lewis or Bronsted. Lewis acid is unsaturated adsorption site that is electron acceptor. Sulfur compounds removal has been generally attributed to the interaction of empty d orbitals in transition metals as electrons acceptor with π electrons on sulfur aromatic as electron donor.

The modified carbon based materials showed significant enhancement in the adsorption capacity of the adsorbents. Elham et. al. reported that, modifying the hydrogen-treated activated carbon and the activated carbon fiber with Ni, NiO, Cu, Cu_2O, or CuO led to enhance the adsorption capacity for the thiophenic compounds from model fuel due to provide more specific interaction between these compounds and the Ni and Cu cationic species including π-complexation interaction**[96]**. Same result was shown by Nazmul Abedin Khan et. al.**[97]**, good enhancement was achieved in the removal of DBT after modifying the granular activated carbon with different loading of Cu^{+} cation.

Clearly by introducing other transition metals oxide as an additional active adsorption site on the carbonaceous materials (AC, CNT and GO) that have hydrophobic nature and π electrons in their structures rather than using each of them individually is expecting to improve the adsorption efficiency and capacity for them.

CHAPTER 3

3. Experimental Work

3.1 Materials

Multi-wall carbon nanotubes (CNT) was purchased from Timesnano company with purity 95%, outer diameter (OD) 10-20nm, length 10-30μm and a specific surface area (SSA) of 200 m^2/g. A coconut activated carbon (AC) was purchased from Cenapro Chemical Corporation, Mandaue City, Philippine. They were usedas received without further purification. Graphene oxide (GO) was prepared using Hummers's method **[98].**Thiophene > 99 %, dibenzothiophene > 99 %, analytical grade ethanol, sulfuric acid, graphite powder > 99 %, nickel nitrate hexahydrate ($Ni(NO_3)_2.6H_2O$),99.9 % silver nitrate ($AgNO_3$), uranyl nitrate hexahydrate ($UO_2(NO_3)_2.6H_2O$), sulfur powder, potassium permanganate ($KMnO_4$), hydrogen peroxide, hydrochloric acid, *n*-heptane, benzene, toluene, xylene and anhydrous HPLC grade *n*-hexane were obtained from Sigma-Aldrich. Naphthalene > 98% was obtained from Fluka and 99.9 % aluminum nitrate nonahydrate $Al(NO_3)_3.9H_2O$ was obtained from Researchlab. The diesel sample was purchased from a local Sahel gas station in Dhahran, Saudi Arabia.

3.2 Instrumentations

An analytical balance (Shimadzu Japan) was used for weighing. An ultrasonic vibrator (UP400S Hielscher-Ultrasound Technology) was used for homogenizing the metals precursors' solution with the carbonaceous materials. An oven (Precision from Thermo Scientific) was used for adsorbents drying. The calcination process was carried out using a furnace (Lindberg blue M Thermo scientific). The pH of solutions was measured using a pH meter (Thermo Scientific CyberScan pH 1500).The samples in the adsorption experiments were shaken using a shaker (Lab. Campanion Shaker SK-600). The adsorbents oxidation under air and their degradation under nitrogen atmosphere were studied using thermal gravimetric analysis (TGA)from TA Instrument Q Series Q600 SDT. An automated gas sorption analyzer (Autosorb iQ Quantachrome USA) was used for adsorbents surface area and porosity analysis. The adsorbents' textures and morphologies were studied using scanning electron microscope (SEM) (TESCAN LYRA3) coupled with energy-dispersive X-ray spectroscopy (EDX) Oxford detector model X-Max. A JOEL-2100F field emission transmittance electron microscope (FE-TEM) was used for particle size measurement. A wide angle X-ray diffractometer instrument (XRD) from Rigaku MiniFlexII Desktop Company with αCuK source was used in range 10 to 90 2θ. The oxidation state of metal doped on the adsorbents surface was determined using an X-ray photoelectron spectrometer (XPS) (Thermo scientific ESCALAB 250Xi).The DBT concentration in real diesel samples was determined using gas chromatography (Agilent 7890 A) coupled with a sulfur chemiluminescence detector (GC-SCD) (Dual Plasma Technology 355) using hydrophobic Agilent DB-1 GC capillary column (30m x 0.32mm x 1μm). The concentration of thiophene, DBT and

naphthaleneinthe model fuel were measured before and after the adsorption using HPLC-UV system (Agilent Technology 1260 Infinity series).

3.3 Adsorbents Preparation

3.3.1 Graphene oxide (GO) preparation

The graphene oxide was prepared using Hummers's method, the procedure described elsewhere **[98].**Briefly,200mL H_2SO_4 (Sigma-Aldrich) was added to 5g graphite powder in ice bath then gradually 2 g $KMnO_4$was added with stirring and was kept at 50 ºC for 4 hours, when the oxidation reaction was completed 200mL of deionized water was added gradually with stirring for 15minutes. A suspended solution was produced when hydrogen peroxide 100mL was added. The suspended material was filtrated then washed by HCl 36 wt%and distilled water respectively until achieving a neutral solution. The washed filtrated solid was dried at 100 ºC for 48 hours.

3.3.2 Impregnation of AC, CNT and GO with aluminum oxide

AC, CNT and GO were doped with both 5 % and 10.9 % Al in the form of aluminum oxide (Al_2O_3) using the incipient wetness impregnation method.These percentages are denoted by the endings AL5 and AL10 and the resulting adsorbents are denoted by ACAL5, ACAL10, CNTAL5, CNTAL10, GOAL5, and GOAL10. Accurately weighed 15.3 g of $Al(NO_3)_3.9H_2O$ were dissolved in 400 mL 1 % deionized water in ethanol solution which was added slowly with stirring to 9.0 g of AC, CNT or GO to obtain carbon materials doped with 10.9 % Al (18.8 % Al_2O_3). The resulting

mixtures were homogenized using an ultrasonic vibrator for 2 hours to obtain a uniform loading of aluminum oxide on the surface of the carbon materials. Next they were dried in an oven at 80°C for 48 hours. The resulting solid materials were ground and calcinated in a furnace at 350 °C for 2 hours. The produced impregnated adsorbents were stored in tightly closed vials before using them in the experiments. In case of doping with 5.0 % Al (9.0 % Al_2O_3) the same procedure was followed by mixing 6.95 g $Al(NO_3)_3.9H_2O$ with 9.5 g AC, CNT or GO.

3.3.3 Impregnation of AC and CNT with nickel oxide nanoparticles

A 6 g of activated carbon (AC) and carbon nanotubes (CNT) with different loading percentage (1, 5 and 10%) of nickel oxide nanoparticles (NI) adsorbents were prepared by weighting 0.30, 1.49 and 2.97g nickel nitrate hexahydrate for 1, 5 and 10% Ni loading percentage respectively. They were dissolved in 400mL solution 1% deionized water in ethanol which was added slowly with stirring to 5.94, 5.70 and 5.40g CNT or AC respectively. The resulted solutions were kept under stirring for 10 minutes then for 2 hours under sonication. Next they were dried in oven at 70 ºC for 72 hours.The produced powder was ground then was calcinated at 300 ºC for two hours. The formed doped adsorbents were stored in tightly closed vials and were denoted ACNI1, ACNI5, ACNI10, CNTNI1, CNTNI5 and CNT10.

3.3.4 Impregnation of CNT and GO with silver sulfide nanoparticles

The wetness impregnation method and the chemical vapor deposition (CVD) method were used to modify the CNT and GO with 10 % silver sulfide (Ag_2S)nanoparticles. A 1.57 g $AgNO_3$ was weighted accurately and dissolved in 400 mL of 1% deionized water in ethanol solution which was added slowly with stirring to 9.0 g of CNT or GO. The mixtures were kept under ultrasound vibration for 2 hours to obtain homogeneous distribution of loaded silver salt on the surface of the carbon materials. Then, the mixture was dried in an oven at 70 ºC for 48 hours. The dried materials were ground well and around 3.0 g was transferred to a 1.0 m long quartz tube in the CVD furnace system. One gram of sulfur powder was dried at 120ºC in an oven for 1 hour then was inserted inside the quartz tube of the CVD furnace system as shown in figure 3-1. The systemwas flushed by Argon (Ar) gas for 15min before start heating the first furnaceat 200 ºC to evaporate the sulfur. After 15 min the second CVD furnace which contains the impregnated carbonaceous materialswas heatedto 800 ºC withheating rateof 50 ºC/min. The reaction was kept for 3 hours under Ar atmosphere with flow rate of 200 mL/min. Upon completing the reaction, the reactors were cooled down to 25 ºC under Ar atmosphere. The prepared impregnated adsorbents were stored tightly in closed vials.

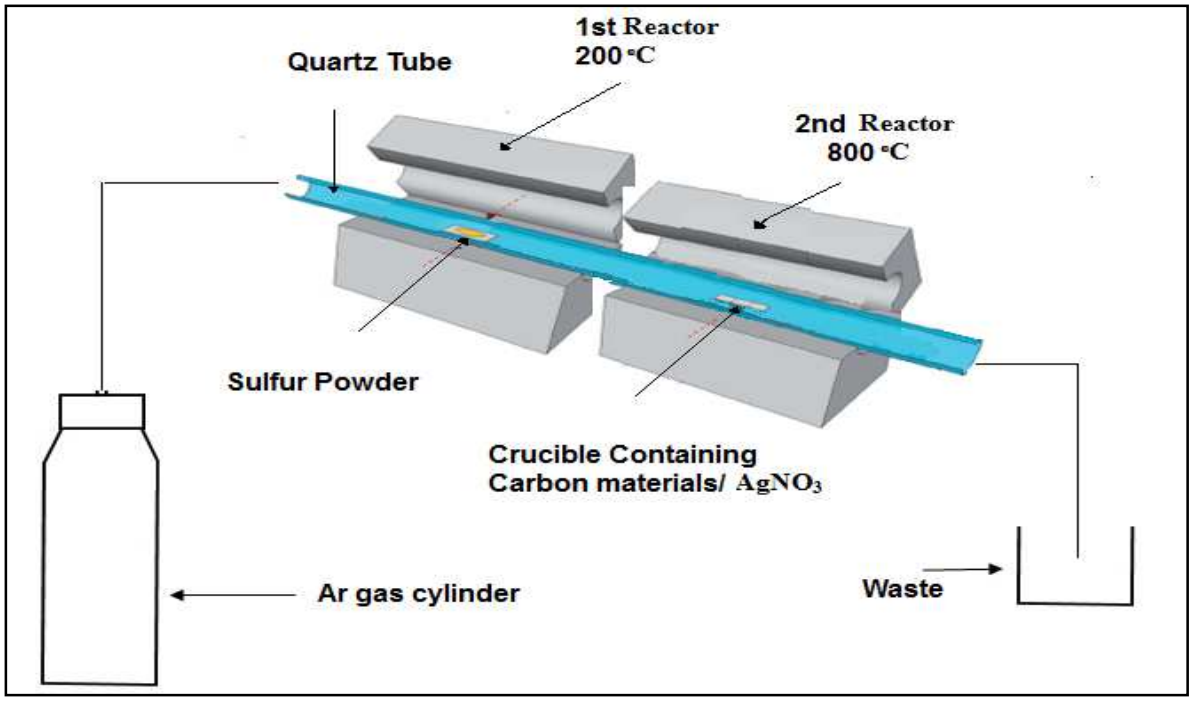

Figure 3-1: CVD experimental setup for modification of carbon materials with silver sulfide nanoparticles.

3.3.5 Impregnation of AC and CNT with uranium oxide

The incipient wetness impregnation method was followed to modify the AC and CNT with 5 % uranium (U) in the form of uranyl oxide (UO_3). A 1.05 g $UO_2(NO_3)_2.6H_2O$ was weighted accurately and dissolved in 400 mL solution(1% deionized water in ethanol). The resulted solution was added slowly with stirring to 9.5 g of AC or CNT. The produced mixtures were kept for 2 hours under ultrasound vibration to obtain homogeneous distribution of loaded uranyl oxide on the surface of the carbon materials. The resulted mixtures were dried in oven at 80 ºC for 48 hours. The resulting solid materials were ground and calcinated at 350 ºC in furnace for 2 hours. The produced impregnated adsorbents were stored in tightly closed vials.

3.4 Characterization of Adsorbents

3.4.1 Thermal gravimetric analysis (TGA)

The thermal oxidation of raw and doped AC, CNT and GO was investigated using TGA instrument. The oxidation parameters were fixed at 10 mg of sample with heating rate of 10 ºC/min and oxidation temperature from 25 to 800 ºC. For each measurement of thermal oxidation of unmodified adsorbent, a specified weight of 10 mg sample was heated under atmospheric air or nitrogen with a flow rate of 100 mL/min.

3.4.2 Adsorbents' surface pH measurements

A 0.20 g sample of the well dried adsorbent was suspended in 10 mL distilled water then kept under ultrasonic vibration for 2 hours. The suspension was filtered and the pH of the filtrated solution was measured using a pH meter (Thermo Scientific CyberScan pH 1500).

3.4.3 Texture and morphology

The adsorbents' texture and morphology were studied using scanning electron microscope (SEM) coupled with energy-dispersive X-ray spectroscopy (EDX) Oxford detector model X-Max. The samples were prepared for SEM and EDX analysis by smearing a trace amount of each adsorbent on the surface of SEM aluminum plate and then coated with 5 nm thickness of gold nanoparticles to enhance their conductivity. A JOEL-2100F field emission transmittance electron microscope (FE-TEM) was used for particle size measurement. High diluted adsorbent solutions were prepared by suspending few milligrams of adsorbents in ethanol. Few milliliters from the resulted solution was dropped on the surface of TEM H2 200 grid then dried under vacuum for 30 minutes before carrying out the TEM imaging. A wide angle X-ray diffractometer instrument (XRD) with αCuK source was used in range 10 to 90 2θ. A trace amount of each modified carbon nanotube adsorbent was smeared on a carbon adhesive fixed on the X-ray photoelectron spectrometer (XPS) sample holder to apply the XPS measuring then verifying the metal oxide or metal sulfide formation and knowing their oxidation state on the adsorbents surface.

3.4.4 Characterizationof adsorbents surface area and porosity

The surface area and porosity of the adsorbents were analyzed for about 0.2 g sample using an automated gas sorption analyzer at relative pressuresfrom0.01 to 1.00. The liquid nitrogen adsorption-desorption isotherms were measured at 77 K after degassing all the adsorbents at 473 Kto a pressure of 6.5 x 10^{-5} Torr. The Brunauer-Emmett-Teller (BET) and the nonlinear density functional theory (NLDFT) methods were used to calculate the surface area (SA), the total pore volume (V) was calculated from the NLDFT method only and the adsorbents micropore volume and surface area were calculated using the V-t method **[99-101].**

3.5 Thiophene, dibenzothiophene and naphthalene method of analysis

Several analytical methods have been reported for the determination of DBT and thiophene compounds in model diesel fuel, some are quite complex, expensivetime consuming or suffer from lack of selectivity or required expensive procedures (i. e. GC-MS, GC FID and gradient HPLC-UV).The present method is a simple, rapid, accurate and precise method able to detect thiophene, DBT and naphthalene simultaneously with isocratic normal phase HPLC coupled with UV detector.In the adsorption experiments the thiophene, DBT and naphthalene concentrations were measured before and after the adsorption using HPLC-UV system.The chromatographic parameters are summarized in table 3-1.

Table 3-1: Chromatographic conditions used in the analysis of thiophene and DBT.

Parameters	Description
Mobile Phase	100 % *n*-Hexane
Analytical column	Silica, 5 µm (200 x 4.6 mm i.d.)
Guard column	C18, 5 µm (10 x 4.6 mm i.d.)
Auto-sampler temperature	24 °C
Flow rate	1.0mL/min
Back pressure	29 -30 bar
Column temperature	24 °C
Injection volume	5 µL
Wave length	In first 3.5 min the λ is 235 nm for thiophene and from 3.5 to 5.0 min the λ is 280 for DBT and naphthalene detection.
Total run time	5.5 min.

Stock solutions were prepared by dissolving each of accurately weighed of 25.0 mg thiophene, 25.0 mg DBT and 100 mg naphthalene in *n*-hexane and the solutions made up in volumetric flasks to 100 mL.By appropriate dilutions, solutions containing between 2.5 and 250 mg/L from each of thiophene and DBT and between 10 and 1000 mg/L of naphthalene were used to obtain calibration curves. These calibration curves were highly linear (with correlation coefficients in excess of 0.999). Ternary standard mixtures were prepared from these analytes at concentrations identical to those used in the previous concentration ranges to study their linearity simultaneously and to examine their effect on each other. Furthermore each of these stock solutions(ternary mixtures) was separately prepared three more times and used to obtain three sets of calibration curves(three replicates for each calibration point). Three quality control levels at low, medium and high concentration (QcL, QcM and QcM) were prepared for thiophene and DBT (7.5, 125 and 225 mg/L) and (30, 500 and 900 mg/L) of naphthalene to study the precision and accuracy of the method over the entire linear working ranges and to check the system precision during the analysis stage.

Overlaid chromatograms for the calibration curve points are shown in figure 3-2. The linear working range for both thiophene and DBT (shown in figure 3-3) was from 2.5 to 250 mg/L with squared correlation coefficients (R^2) of 0.9997 and 0.9998 for thiophene and DBT respectively. For naphthalene the linear working range was from 10 to 1000 mg/L with an R^2 value of 0.9996. As shown in table 3-2. The precision and accuracy were evaluated based on the calculated concentration from average of three replicates of each quality control level containing the three compounds.The relative standard deviation (RSD %) for these three measurements varied from 0.58 to 2.64 %, 0.70 to 3.22 % and from 0.71 to 5.19 % for thiophene, DBT and naphthalene respectively with a relative error (RE %) ranging from –0.52 to 2.80 %, –1.33 to 1.34 % and –-0.17 to 1.38 % for thiophene, DBT and naphthalene respectively.

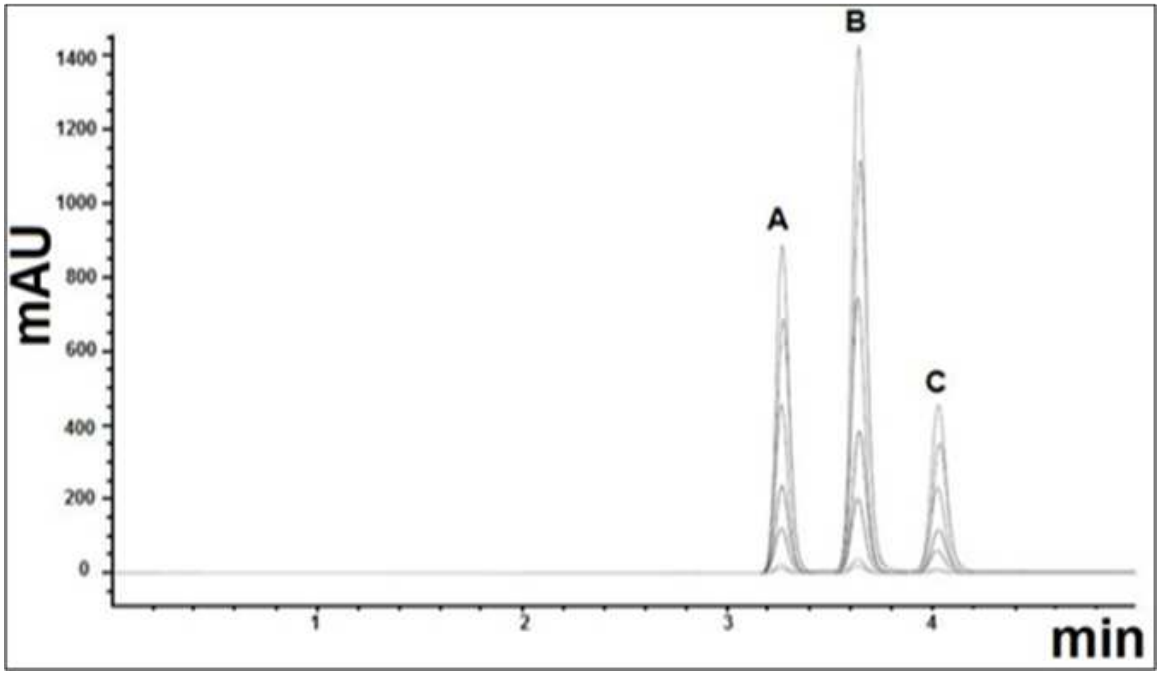

Figure 3-2: The calibration curve points overlaid chromatograms for mixture solutions containing A) thiophene, B) naphthalene and C) DBT

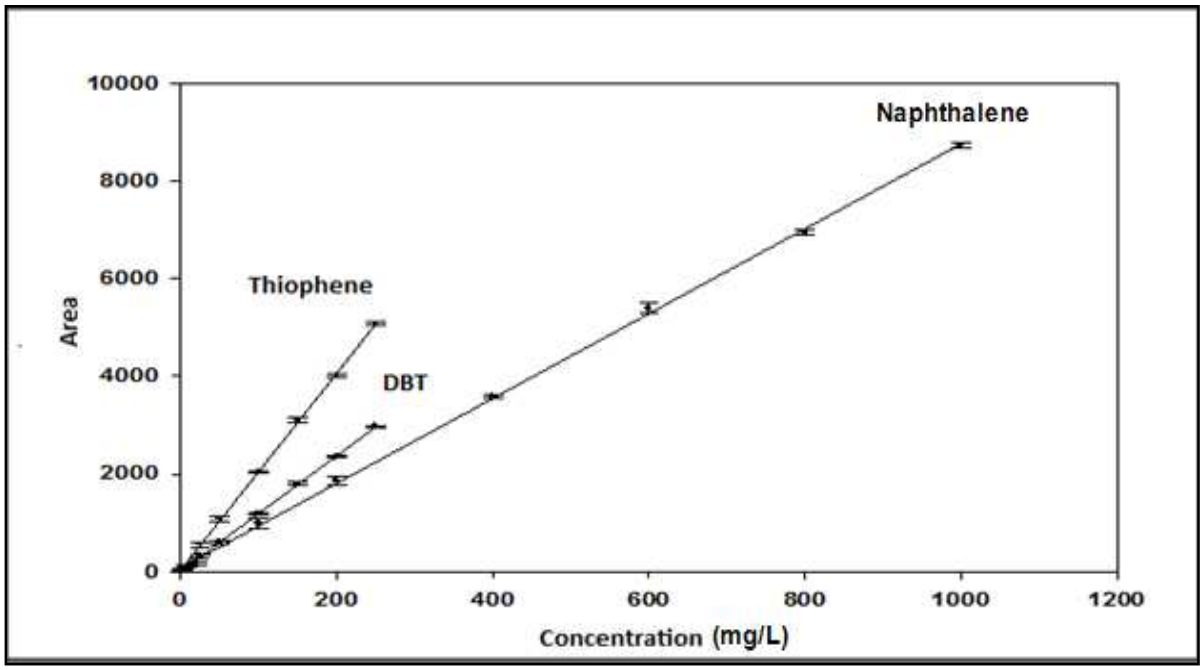

Figure 3-3: The calibration curves for thiophene, DBT and naphthalene. The bars are standard deviations obtained from three runs

Table 3-2: Method precision and accuracy of thiphene, DBT and naphthalene determination.

	Thiophene			DBT			Napthalene		
Replicate	**QcL (7.5 mg/L)**	**QcM (125 mg/L)**	**QcH (225 mg/L)**	**QcL (7.5 mg/L)**	**QcM (125 mg/L)**	**QcH (225 mg/L)**	**QcL (30 mg/L)**	**QcL (500 mg/L)**	**QcL (900 mg/L)**
1	7.71	126.88	226.10	7.22	126.16	222.18	29.64	511.03	854.06
2	7.90	128.15	228.25	7.67	127.71	224.86	30.39	504.75	941.44
3	7.51	126.86	217.10	7.31	126.18	219.22	29.81	504.93	928.34
Precision									
Average	**7.71**	**127.30**	**223.82**	**7.40**	**126.68**	**222.09**	**29.95**	**506.90**	**907.95**
SD	**0.20**	**0.74**	**5.915**	**0.24**	**0.89**	**2.82**	**0.39**	**3.58**	**47.13**
RSD (%)	**2.53**	**0.58**	**2.64**	**3.22**	**0.70**	**1.27**	**1.31**	**0.71**	**5.19**
Accuracy									
Error	**0.21**	**2.30**	**-1.18**	**-0.10**	**1.68**	**-2.91**	**-0.05**	**6.90**	**7.95**
RE %	**2.80**	**1.84**	**-0.52**	**-1.33**	**1.34**	**-1.29**	**-0.17**	**1.38**	**0.88**

3.6 Batch mode adsorption experiment

The adsorption isotherms of thiophene and DBT on pristine and impregnated AC, CNT and GO were studied. A desired amount of adsorbents varying from 100 to 1500 mg were added to a 25 mL *n*-hexane solventas model fuel with certain concentrations of thiophene or DBT analytes (i.e. 25, 50, 100, 125, 150, 200, and 250 mg/L), then mixed thoroughly in capped-type conical flasks. A mechanical shaker was used to shake these conical flasks at a wanted speed. The effect of shaking speed on the adsorption performance of DBT and thiophene on the unmodified adsorbents was studied also in the rage of speeds (50, 75, 100, 150, 200 and 250 rpm). Five (5.0) mL samples were then collected from the flask at certain time intervals of 10, 20, 30, 40, 60 120, 240 and 1560 minutes and tested for residual concentrations of analytes. The analysis of analytes in model fuel samples was carried out using High Performance Liquid Chromatography instrument coupled with UV detector. The system already installed in Center of Petroleum and Minerals (CPM) lab at Research Institute (RI). Then, the effect of the dosage of carbon materials, the initial concentration of analytes, the contact time and the agitation speed were studied. Quality control / quality assurance (QA/QC) measures were followed in performing the analysis work.

3.6.1 Adsorption isotherms models

The most frequently used adsorption isotherm models (i.e. Freundlich, Langmuir and Tempkin) **[102-104]**were tested to fit the adsorption experimental data. The Langmuir model assumes adsorption on a homogeneous adsorbent surface with identical

adsorption sites and no interaction between molecules on neighboring sites. According to this model the adsorption capacity at equilibrium, q_e is given by,

$$q_e = \frac{(Q_{max}\mathrm{bC_e})}{(1+\mathrm{bC_e})} \quad \textbf{(1)}$$

where Q_{max} in mg/g is the maximum adsorption capacity, b is Langmuir constant and $C_e$in mg/L is the concentration of the sulfur compound in the solution at equilibrium. q_e is also given by,

$$q_e = \frac{\mathrm{Vs(C_o - C_e)}}{(m)} \quad \textbf{(2)}$$

where V in mL is the volume of solution in the adsorption experiment, $C_o$in mg/L is the initial concentration of the sulfur compound in the solution and *m* in mg is the mass of adsorbent. Equation 1 can be rearranged to the linear form:

$$\frac{\mathrm{C}_e}{q_e} = \frac{1}{\mathrm{b}Q_{max}} + \frac{\mathrm{C}_e}{Q_{max}} \quad \textbf{(3)}$$

The Freundlich model assumes that the adsorbent surface is heterogeneous with a multi-layer adsorption capacity **[105]**. According to this model,

$$q_e = K_F \mathrm{Ce}^{1/n} \quad \textbf{(4)}$$

where K_F is the Freundlich constant and the parameter n is a measure of the heterogeneity of the surface of the adsorbent. The linear form of equation 4 is:

$$\ln(q_e) = \ln(K_F) + \frac{1}{\mathrm{n}}\ln(C_e) \quad \textbf{(5)}$$

The maximum adsorption capacity (Q_{max}) for each adsorbent can be obtained from the slope of a linear least squares fit of $\frac{C_e}{q_e}$ versus C_e (equation. 3). The n value for each adsorbent can be obtained from the slope of a linear least square fit of ln (q_e) versus $\ln(C_e)$ (equation 5) while the K_F value can be calculated from the intercept of equation 5. n and K_F give an idea about the degree of surface heterogeneity and the adsorption capacity respectively. Larger n and K_F values correspond respectively to greater heterogeneity on the adsorbent's surface and a higher adsorption capacity **[106]**.

Temkin isotherm equation (6) is the earlier isotherm that includes a factor that clearly taking into the account the interaction between the adsorbate and adsorbent**[104]**

$$q_e = \frac{RT}{b_T}\ln A_T C_e \quad \textbf{(6)}$$

R is the ideal gas constant in J K^{-1} mol^{-1}, T is the temperature in Kelvin (K), b_T is the Temkin constant and A_T is the Temkin isotherm equilibrium binding constantin L g^{-1}. The linear form of equation (6) gives an equation (7):

$$q_e = \frac{RT}{b_T}\ln A_T + \frac{RT}{b_T}\ln C_e \quad \textbf{(7)}$$

The b_T value gives an idea about the heat of adsorption of adsorbate on each adsorbent. It can be obtained from the slope of a linear least square fit of q_e versus $\ln(C_e)$ while the A_T value can be calculated from the intercept of equation (7).

3.6.2 Adsorption kinetics

Studying the adsorption kinetics in the batch mode is essential to design the adsorption columns for further study and for industrial applications **[107]**. To study the DBT and thiophene adsorption kinetics on carbonaceous adsorbents modified with aluminum oxide, a 25 mL *n*-hexane solution with an initial concentration of 250 mg/L from each sulfur compound was added to 150 mg of the adsorbent in a vial that was capped then shaken continuously for a fixed time intervals. The adsorbent was then allowed to settle and quickly a 5 mL sample was removed and filtered, 5 µL from the filtered solution were analyzed using HPLC-UV (described in section 2.5). The same procedure was carried out for shaking time intervals of 10, 20, 30, 40, 60, 120, 240 and 1560 minutes.

The adsorption results were fitted using the kinetic models reported by Lagergren **[108]** and Ho **[108]** that led to linear formof pseudo-first order adsorption rate equation (8)

$$\ln (q_e - q_t) = \ln (q_e) - k_1 t \tag{8}$$

andlinear form of pseudo-second order adsorption rate equation (9)

$$\frac{t}{q_t} = \frac{1}{q_e^2 k_2} + \frac{t}{q_e} \tag{9}$$

Where q_e (mg/g) is the adsorption capacity at equilibrium, q_t in (mg/g) is the adsorption capacity at a time t (min), k_1 (min^{-1}) is the pseudo-first order rate constant and k_2 (g mg^{-1} min^{-1}) is the pseudo-second order rate constant.

The selection of best kinetic model for the adsorption of DBT and thiophene on each adsorbent was based on calculating the squared correlation coefficient (R^2) which reflects the degree of good of fitness.

The linear form of pseudo-first order equation (8) is derived by integrating equation (10) for the boundary conditions t = 0 to t = t and q_t = 0 to q_t = q_e then rearranging the resulted equation.

$$\frac{dq_t}{dt} = k_1 (q_e - q_t) \tag{10}$$

The linear form of pseudo-second order equation (9) is derived by integrating equation (11) for the boundary conditions t = 0 to t = t and q_t= 0 to q_t= q_e then rearranging the resulted equation.

$$\frac{dq_t}{(q_e - q_t)^2} = k_2 dt \tag{11}$$

CHAPTER 4

4. Results and Discussion

4.1 Adsorption Performance of Multiwall Carbon Nanotubes and Graphene Oxide for Removal of Thiophene and Dibenzothiophene from Model Diesel Fuel

The adsorption performance of multiwall carbon nanotube (CNT) and graphene oxide (GO) has not been investigated before for Dibenzothiophene (DBT) and thiophene sulfur organic compounds in model fuel. To attain this investigation, the surface area and porosity of CNT and GO were characterized. The adsorption isotherm and kinetics of DBT and thiophene adsorption on CNT and GO were investigated and compared with activated carbon (AC) adsorbent. In addition, many experimental parameters such shaking speed, adsorbent dosage amount and organic sulfur concentration were studied for their effect on the adsorption performance of DBT and thiophene in organic phase.

4.1.1 The AC, CNT and GO's surface area and porosity

On the basis of Brunauer, Deming and Teller (BDDT) classification **[109]**, the AC, CNT and GO adsorbents exhibit type IV, III and V N_2 adsorption isotherm

respectively as shown in figure 4.1. In case of AC and GO, a hysteresis loop is observed. That indicates presence of mesopores in their structure. As shown in figure 4.2 the highest micropore volume was in AC adsorbent. The surface area and microporosity results given in table 4.1 show that, the adsorbents's BET surface area and micropore volume follow the order AC > CNT > GO while the trend in the average of micropore width is CNT > GO > AC. Table 4.1 also shows that the highest N_2 adsorption energy (17.99 kJ/mol) was on AC adsorbent. However, the adsorption energy on GO was little bit higher than the adsorption energy on CNT.

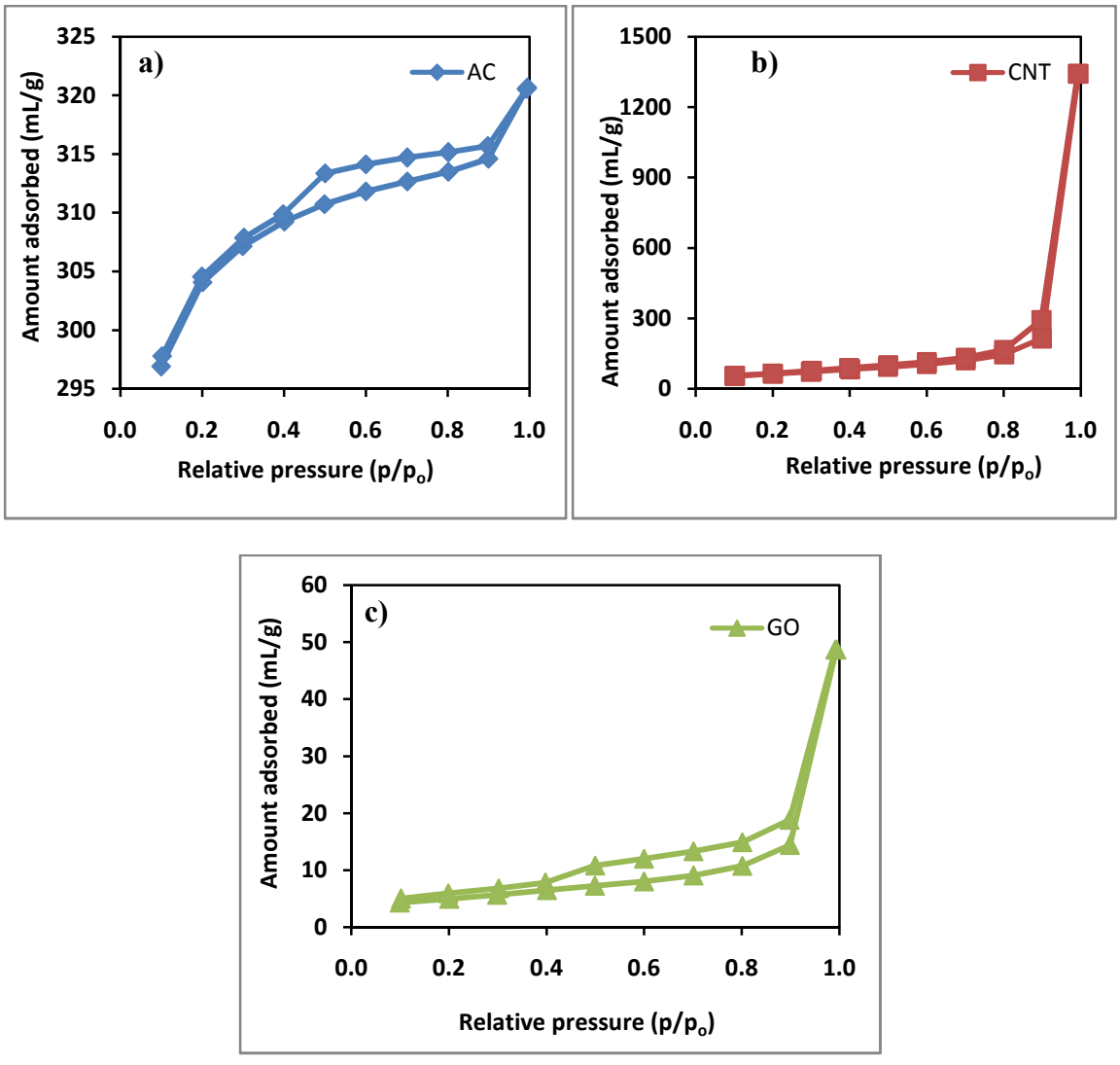

Figure 4-1: The N_2 adsorption isotherm at 77K on (a) AC, (b) CNT and (c) GO.

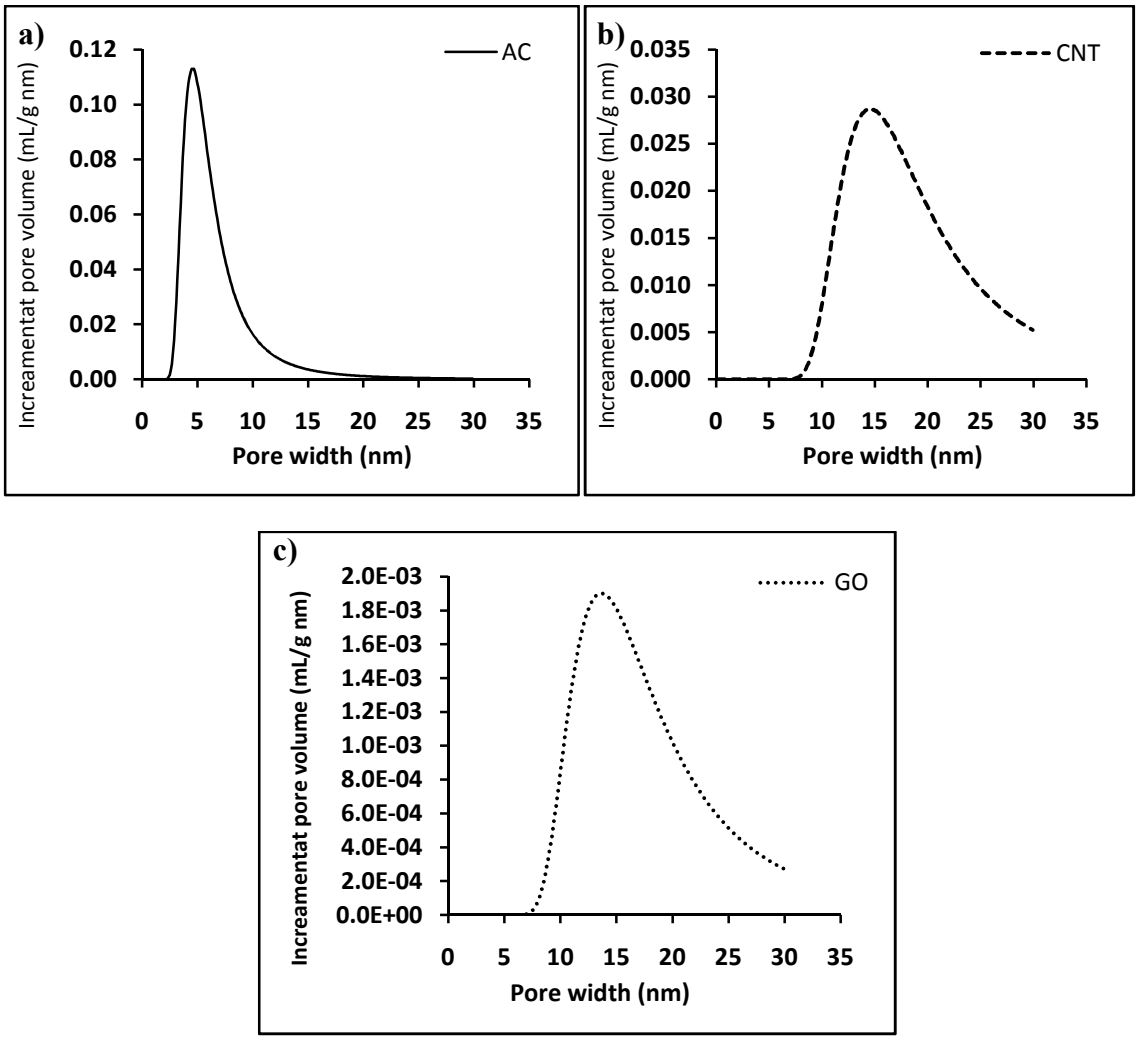

Figure 4-2: Pore width distrubution based on DR method for (a) AC, (b) CNT and (c) GO.

Table 4-1: Carbonaceous materials surface area and the microporousity analysis parameters

	BET	DR Method		
Adsorbent	**Surface Area (m^2/g)**	**Average pore width (Å)**	**Adsorption energy (kJ/mol)**	**Micropore volume (mL/g)**
AC	882	14.5	17.99	0.487
CNT	217	73.8	3.52	0.286
GO	11	68.5	3.80	0.021

4.1.2 Effect of shaking speed on the adsorption

The mechanical shaker was used to test the effect of shaking speed on the adsorption of 250 mg/L thiophene and 250 mg/L dibenzothiophene as initial concentration using 100 mg of AC, CNT and GO adsorbents individually at different speeds (50, 75, 100, 150, 200 and 250 rpm), as shown in figure 4.3at fixed contact time 1 hour and room temperature 25 ºC, the maximum adsorption on the three adsorbents types was obtained at 200rpm and mostly there was no significant change in the removal efficiency at higher shaking speed.

The shaking facilitates suitable contact between the organic sulfur compounds (dibenzothiophene and thiophene) in the model fuel and the adsorbents and thereby leads to effective transfer of dibenzothiophene or thiophene to the active adsorption sites on the AC, CNT or GO. That is due to the fact of increase of shaking speed increases the mass transfer of organic sulfur compounds towards the surface of the AC, CNT or GO.

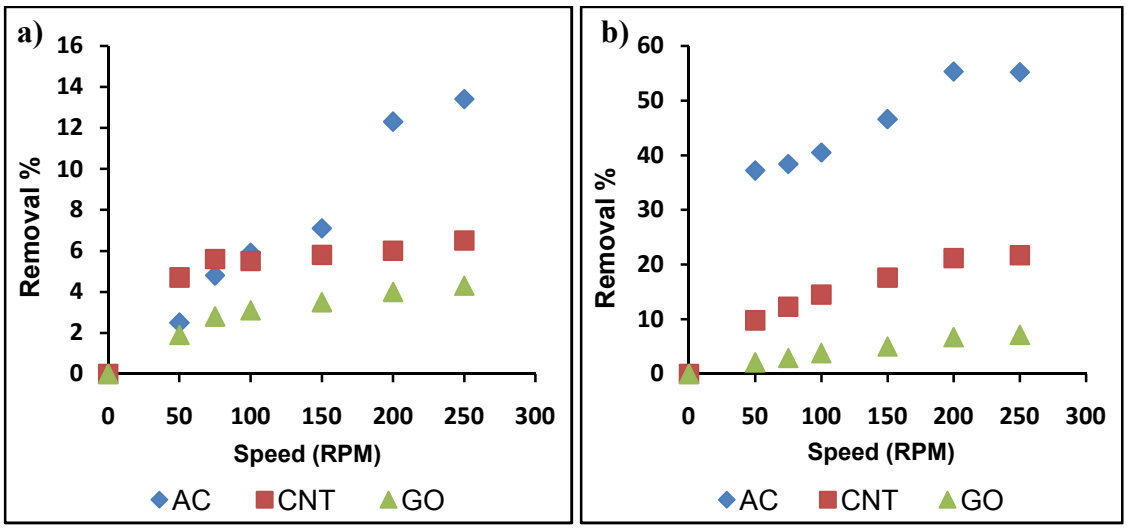

Figure 4-3: The effect of shaking speed for adsorption of a) Thiophene and b) Dibenzothiophene (DBT), by AC, MWCNT and GO at room temperature (25 ºC), and the amount of adsorbent is 100 mg and initial concentration of organosulfur compound is 250 mg/L.

4.1.3 Effect of AC, CNT and GO's mass loaded on the adsorption

Different amount of CNT, GO and AC were used to test the effect of adsorbent quantities on the thiophene and DBT removal efficiency. The initial concentration of each sulfur compound was 250 mg/L. As depicted in figure 4.4, the maximum removal efficiency using 1500 mg AC was 32.12 % and 96.10 % for thiophene and DBT respectively. In case of MWCNT and GO the removal efficiency of thiophene and DBT slightly increased with increasing the adsorbent loaded amount. However, the maximum removal efficiencies using 1500mg MWCNT adsorbent are 86.91% and 9.00 % for DBT and thiophene respectively. While they were 46.70 % for DBT and 6.70 % thiophene using 1500mg GO adsorbent. The higher adsorption capacity for AC is explained by the larger surface area and volume of microporous compared to the surface area and the volume of microporous of CNT and GO adsorbent. The adsorption of DBT and thiophene on these adsorbents can be achieved through engagement of S heterocyclic aromatic molecules in π–π electron donor-acceptor or π–π coupling interactions and the lone-pair electrons of the S heteroatoms is n-electron donors and can enable n–π electron donor-acceptor interactions with the π-electron deficient regions of the adsorbents's surface or the oxygenated functional groups on their surfaces **[26]**. The higher removal of DBT by these adsorbents compared to thiophene is explained by three factors; first one is that, DBT has bigger molecular size and higher dipole moment than thiophene molecules which allow it to be trapped in the adsorbents' microporous easier than thiophene and engaged with stronger van der Waals and π–π interactions. Second factor, The DBT is stronger Lewis base than thiophene which provides stronger acid-base

interaction between the lone-pair electrons of S atoms and the sp2 orbitals in the adsorbents structure.

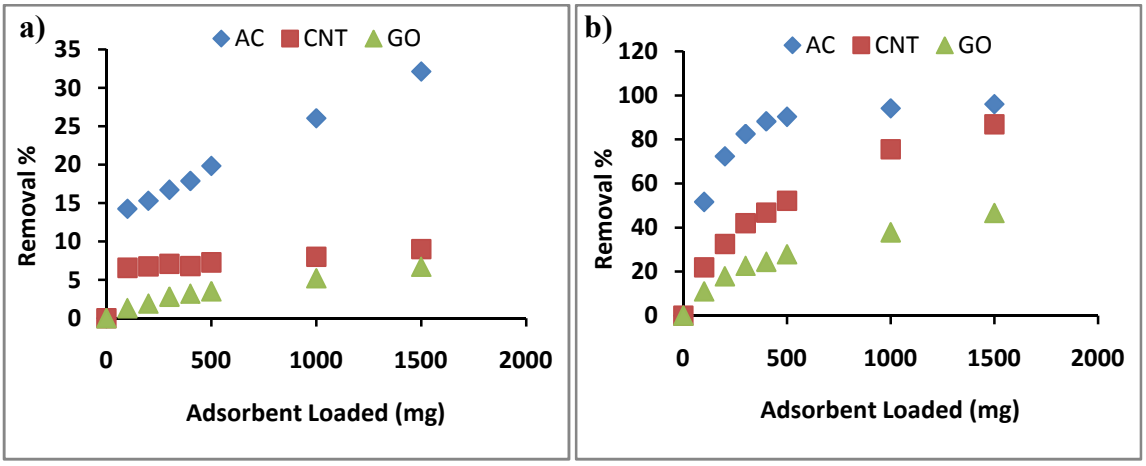

Figure 4-4: The effect of adsorbent loaded on the removal efficiency of a) Thiophene and b) Dibenzothiophene (DBT), by AC, CNT and GO at room temperature (25 ºC), the shaking speed is 200 rpm and the initial concentration of organosulfur compound is 250 mg/L.

4.1.4 Effect of the contact time and the adsorption kinetics

The effect of contact time between 300mg adsorbent and 250 mg/L initial concentration of thiophene and DBT was studied at room temperature (25 ºC)and 200rpm shaking speed by varying the contact time from 10 minutes to4 hours. As shown in figure 4.5 the adsorption equilibrium using AC, CNT and GO adsorbents was achieved mainly after 40 minutes for both thiophene and DBT. The uptake rate of thiophene and DBT was evaluated using different kinetics' models (i.e. pseudo-first order and pseudo-second order) rate equations. It has been found that, the uptake rate follows the pseudo-second order kinetic with excellent correlation coefficient for both thiophene and DBT on all types of adsorbents where straight lines were obtained by plotting t vs t/q_t as shown in figure 4.6 and table 4.2. Table 4.2 also shows the low R^2values of pseudo-first order. The initial adsorption rate (k_2) (mg/g.min)for thiophene is the highest on AC which may be due to the high porosity of the AC and the small size of thiophene which make the diffusion of these molecules in the AC's pores easier and faster than DBT. $k_2$of DBT on CNT and GO was higher than the adsorption rate on AC which may be correlated with the size of DBT and the low porosity of both MWCNT and GO compared to the AC porosity thereby the DBT molecules diffusion from bulk solution to the AC adsorption sites is limited by the diffusion through the pores.

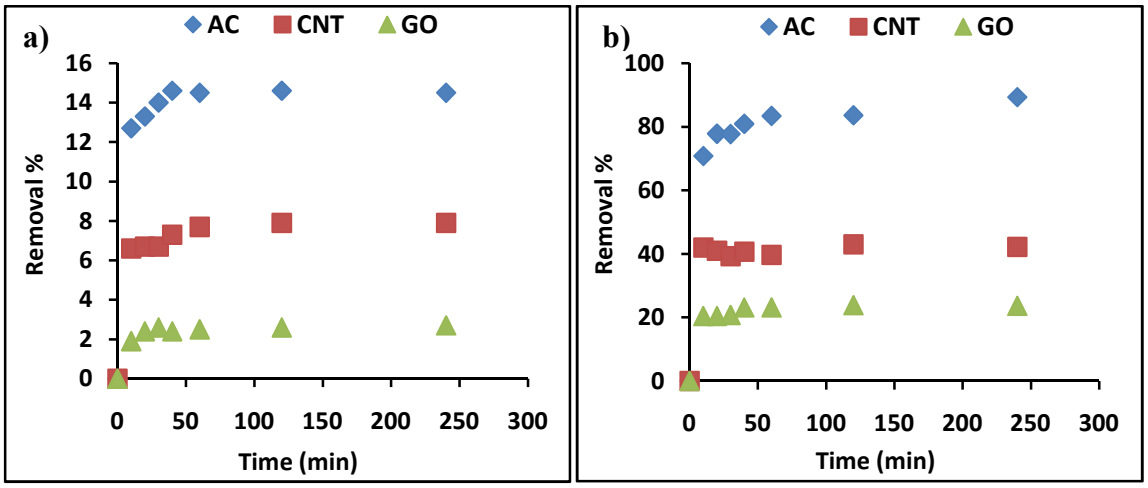

Figure 4-5: The effect of contact time on the removal efficiency of a) Thiophene and b) Dibenzothiophene (DBT), by AC, CNT and GO at room temperature (25 ºC), the shaking speed is 200 rpm, the adsorbent amount is 300 mg and the initial concentration of organosulfur compound is 250 mg/L

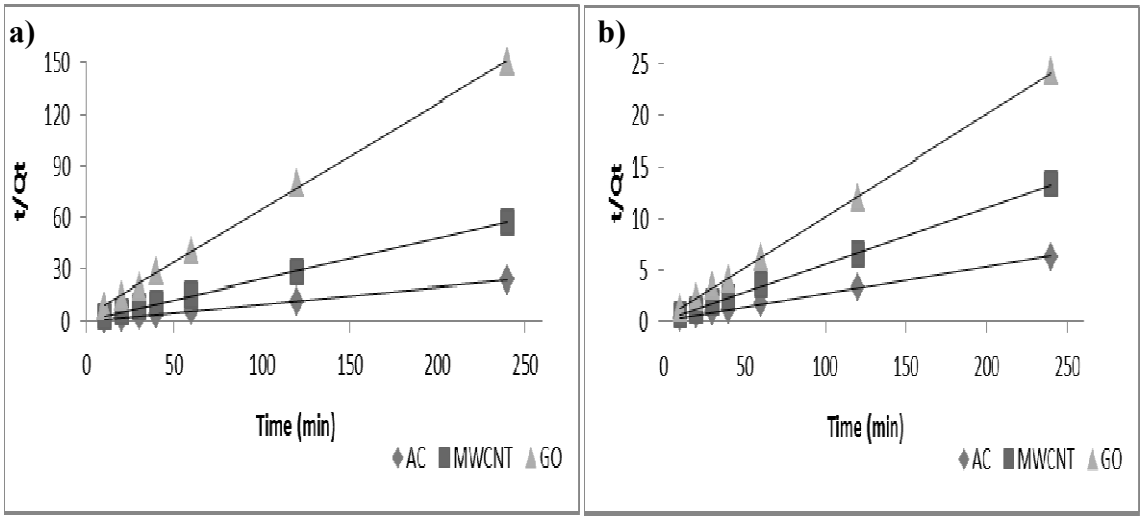

Figure 4-6: The pseudo-second order for adsorption of a) Thiophene and b) Dibenzothiophene (DBT), by AC, CNT and GO at room temperature (25 ºC), the shaking speed is 200 rpm, the adsorbent amount is 300 mg and the initial concentration of organosulfur compound is 250 mg/L.

Table 4-2: Pseudo-first order and pseudo-second order kinetics' parameters and correlation coefficients for the adsorption of Thiophene and DBT on AC, CNT and GO.

Adsorbent	Pseudo-First order Parameters			
	Thiophene		DBT	
	k_1 (min^{-1})	R^2	k_1 (min^{-1})	R^2
AC	1.01×10^{-2}	0.5265	9.70×10^{-3}	0.7133
CNT	1.89×10^{-2}	0.8688	1.18×10^{-2}	0.4787
GO	7.20×10^{-3}	0.6576	4.10×10^{-3}	0.7505
	Pseudo-Second order Parameters			
	Thiophene		**DBT**	
	k_2 (mg/g.min)	R^2	k_2 (mg/g.min)	R^2
AC	1.72×10^{-1}	0.9999	5.80×10^{-3}	0.9992
CNT	6.87×10^{-2}	0.9998	4.00×10^{-2}	0.9996
GO	1.29×10^{-1}	0.9989	3.95×10^{-2}	0.9997

4.1.5 Effect of initial organosulfur compounds concentration and the adsorption isotherms

The initial thiophene and DBT concentration effect has been evaluated by varying their concentrations from 25 to 250 mg/L using 300mg adsorbents in the batch adsorption method at room temperature, optimum shaking speed of 200rpm and contact time for 1 hour. As shown in figure 4.7 the highest removal efficiency (18.4 %) for thiophene by AC was achieved at 50mg/L then remained constant. In contrast, by using CNT and GO the removal efficiency kept increasing with increasing the thiophene concentration to reach 8.0 % and 4.5 % removal efficiency respectively. In the three cases of removal of DBT by AC, MWCNT and GO the maximum removal efficiency was achieved at 25 mg/L DBT concentration then decreased as the concentration of the DBT increased. This can be explained by the fact that at higher concentrations the competition between of DBT molecules increases at the available adsorption sites on the carbonaceous surface and hence result in increasing the repulsion between the adsorbed and free molecules over the saturated adsorbents surface. At the lowest DBT concentration of 25 mg/L the removal efficiency was 96.4, 68.8 and 30.4 % for AC, MWCNT and GO respectively. Figure 4.8 shows the adsorption isotherm of thiophene and DBT on the three carbonaceous materials. The Langmuir, Freundlich and Temkin models have been applied to evaluate the adsorption isotherm for thiophene and DBT. The Freundlich empirical constants *n* and K_f for thiophene and DBT adsorptions on AC, MWCNT and GO were calculated from the slope and the intercept of the straight lines in figure 4.9 which were obtained from the linearization of Freundlich equation. The R^2 was > 0.97 and n values were higher than 1 for DBT which indicate its favorable adsorption on the

three types of carbonaceous adsorbents. On contrary, the adsorption of thiophene on all adsorbents was not favorable with n values less than 1. That can be explained by the small dipole moment of the thiophene molecule (0.55D) compared to the DBT (0.95) which results in a weaker dipole-dipole interaction.The DBT maximum adsorption capacity (Q_{max}) on AC, MWCNT and GO, and Langmuir constant (b) were calculated from the slope and intercept of the Langmuir linear form respectively as shown in figure 4.10. The Q_{max} of the adsorbents are compared with some of the adsorption capacities that reported in the literature as presented in table 4.3. All of Freundlich and Langmuir parameters in addition to the degree of fitness R^2 were summarized in table 4.4. Temkin linear form was used to get an idea about the heat of thiophene and DBT adsorption on the adsorbents. Figure 4.11 shows a comparison between the Temkin model linearization for the thiophene and DBT adsorption on AC, MWCNT and GO adsorbents. Temkin parameters were presented in table 4.5, where $B = \frac{RT}{b_T}$ in J/molis correlated to heat of adsorption. It has been found that, the AC has the highest *B* value (2.53 and 8.40 J/mol) for thiophene and DBT respectively. However, the MWCNT has higher *B* than GO for both adsorbate. This trend agrees with the adsorption capacity's trend for the carbonaceous materials. It is clear from squared correlation coefficient (R^2) values, generally Freundlich model fit the experimental data better than Langmuir or Temkin models which means the multi layers physisorption is predominant through π-π interaction between the DBT and the thiophene with the benzene rings of the adsorbents and the Q_{max}values for DBT decrease in orderAC>CNT > GO which correlate with the respective decrease in their surface area and micropore volume.

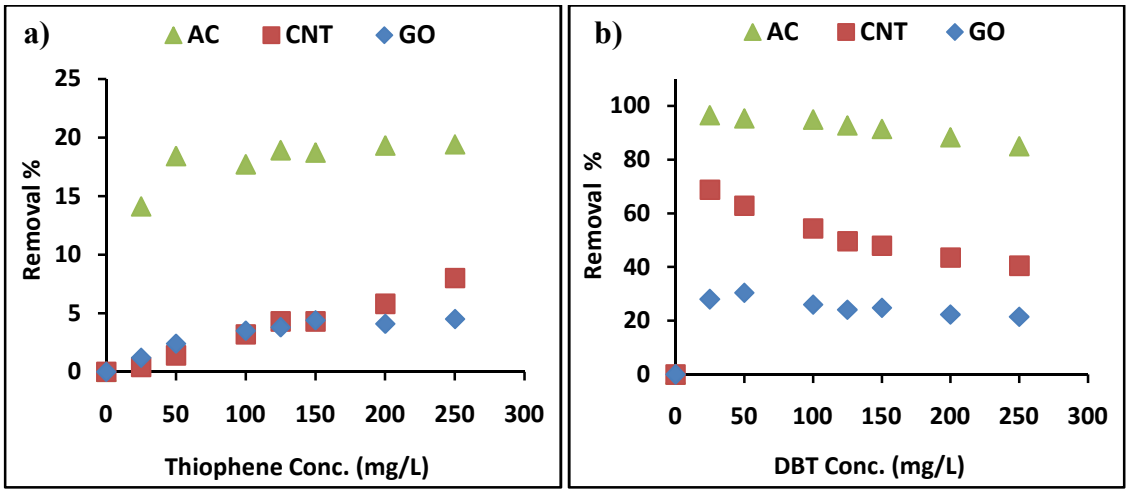

Figure 4-7: Removal efficiency comparison between AC, CNT and GO at different organosulfur compound concentration a) Thiophene and b) Dibenzothiophene (DBT), at room temperature (25 ºC), shaking speed is 200 rpm and the adsorbent amount is 300 mg.

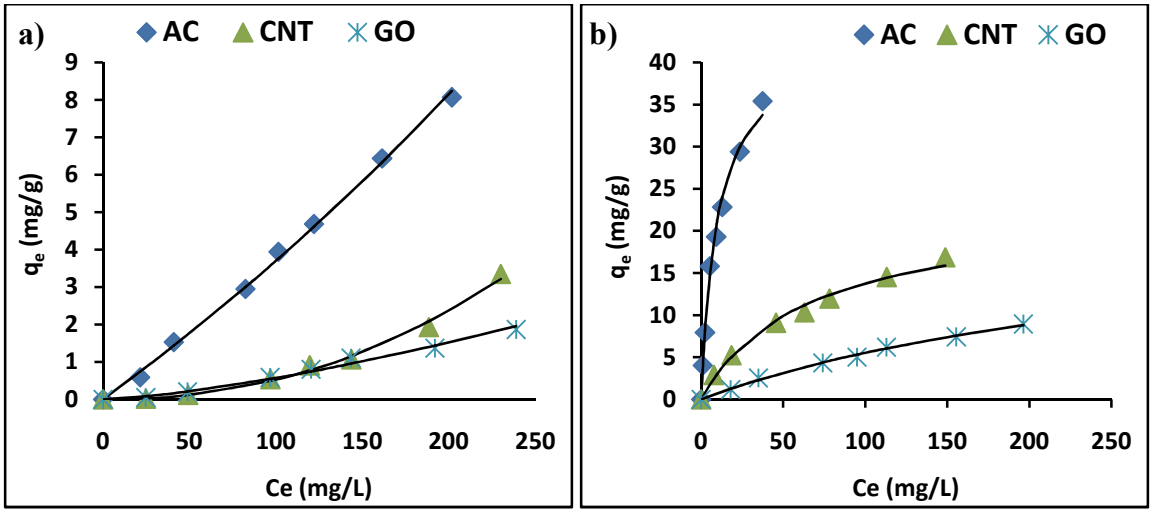

Figure 4-8: The adsorption isotherm of a) Thiophene and b) Dibenzothiophene (DBT) on AC, CNT and GO at room temperature (25 ºC), the shaking speed is 200 rpm and the adsorbent amount is 300 mg.

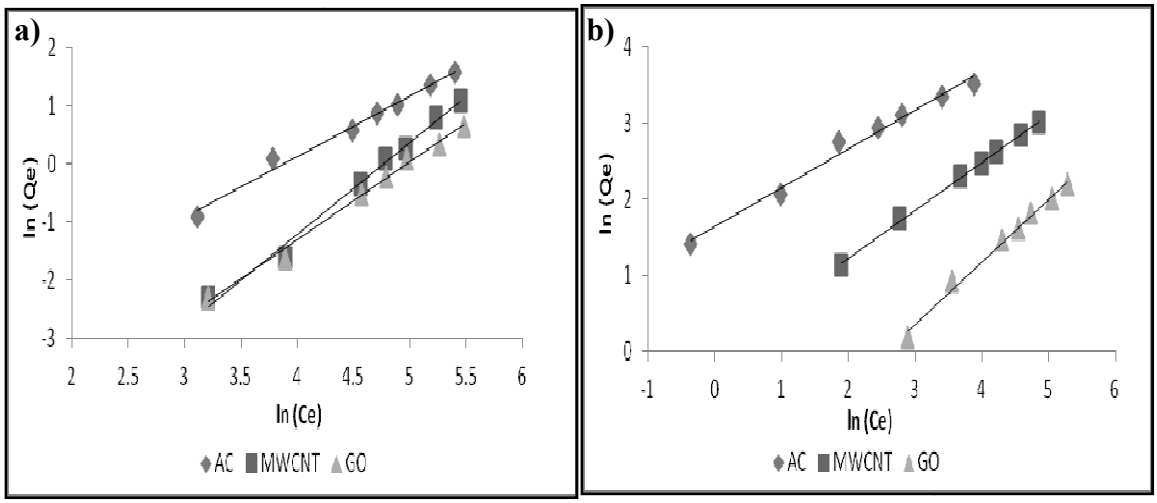

Figure 4-9: The Freundlich adsorption model linearization for adsorption of A) Thiophene and B) Dibenzothiophene (DBT), by AC, CNT and GO at room temperature (25 ºC), the shaking speed is 200 rpm and the adsorbent amount is 300 mg.

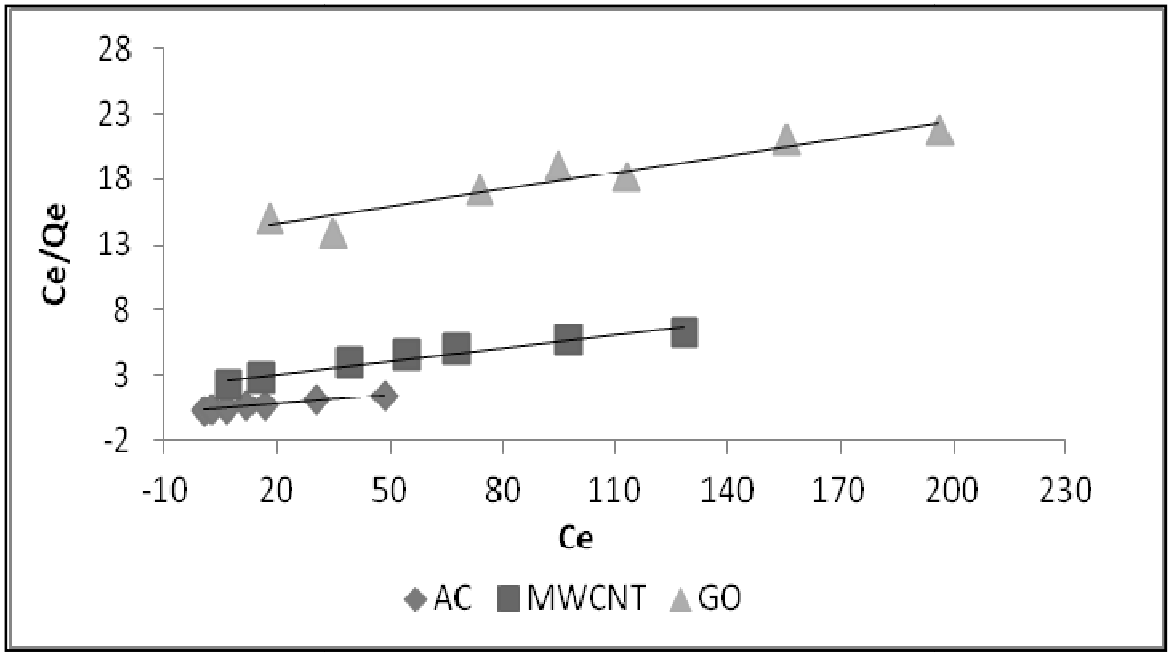

Figure 4-10: The Langmuir adsorption model linearization for adsorption dibenzothiophene (DBT) on AC, CNT and GO at room temperature (25 ºC), the shaking speed is 200 rpm and the adsorbent amount is 300 mg.

Table 4-3: The adsorption capacities of AC, MWCNT and GO compared with some of reported adsorption capacities in the literatures.

Adsorbent	Sulfur Compound	Model Diesel	Adsorption Capacity	Reference
Cu-Al_2O_3	Thiophene	*n*-pentane	1.79 *	[110]
Nanocrystalline NaY Zeolite	DBT	*n*-nonane	6.7 **	[111]
GPP [1]	DBT	*n*-tetradecane	10.6 **	[22]
GPH [2]	DBT	*n*-tetradecane	5.5 **	
AC [3]	DBT	*n*-heptane	10.9 *	[32]
ACws [4]	DBT	*n*-heptane	47.1 *	
Alumina	DBT	*n*-hexane	21.02 *	[17]
AC	DBT	*n*-hexane	41.49 *	This work
MWCTN	DBT	*n*-hexane	23.42 *	This work
GO	DBT	*n*-hexane	22.73 *	This work

(1) Graphene prepared using phosphoric acid

(2) Graphene prepared using Hummers's method

(3) Activated carbon, (4) Activated carbon treated with steam at 900°C then washed by H_2SO_4 and

(*) The adsorption capacity unit is mg (DBT)/g (adsorbent)

(**) mg (S) / g (adsorbent).

Table 4-4: Freundlich and Langmuir parameters and correlation coefficients for the adsorption of Thiophene and DBT on AC, CNT and GO.

Adsorbent	Freundlich						Langmuir		
	Thiophene			DBT			DBT		
	n	K_f ((mg/g)(L/mg)$^{1/n}$)	R^2	n	K_f ((mg/g)(L/mg)$^{1/n}$)	R^2	Q_{max} (mg/g)	b (L/mg)	R^2
AC	0.83	1.07 X 10^{-2}	0.9898	1.71	4.87	0.9747	41.49	1.06 X 10^{-1}	0.9795
CNT	0.45	1.80 X 10^{-5}	0.9934	1.69	1.12	0.9968	23.42	1.48 X 10^{-2}	0.9702
GO	0.75	1.30 X 10^{-3}	0.9935	1.22	0.12	0.9912	22.73	3.20 X 10^{-3}	0.9201

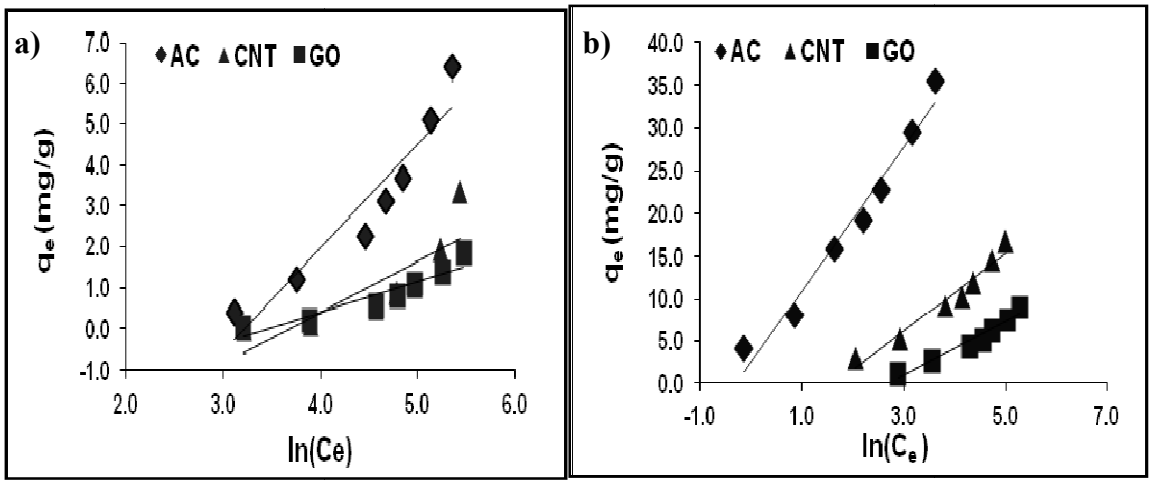

Figure 4-11: The Temkin adsorption model linearization for adsorption of a) Thiophene and b) dibenzothiophene (DBT) on AC, MWCNT and GO at room temperature (25ºC), the shaking speed is 200 rpm and the adsorbent amount is 300 mg.

Table 4-5: Temkin parameters and correlation coefficients for the adsorption of Thiophene and DBT on AC, MWCNT and GO.

Adsorbent	Temkin					
	Thiophene			DBT		
	A_T (L/g)	*B* (J/mol)	R^2	A_T (L/g)	*B* (J/mol)	R^2
AC	0.9915	2.53	0.8949	1.0089	8.40	0.9712
MWCNT	0.9977	1.24	0.6880	0.9853	4.63	0.9590
GO	0.9992	0.76	0.8801	0.9892	3.12	0.9498

4.1.6 Conclusion

The MWCNT and GO were investigated for adsorptive desulfurization (ADS) as nano carbonaceous materials. The results show that these adsorbents exhibit lower adsorption capacity (Q_{max})for thiophene and DBT compared to AC.The adsorption of DBT compound on the MWCNT and GO adsorbents was represented by Langmuir and Temkin with better fitting by Freundlich isotherm model. The heterogeneity (n) values of adsorbents for DBT were more than 1, which indicates favorable adsorption using these adsorbents. The adsorption capacity has been calculated to be 23.4 mg/g and 22.7 mg/g using CNT and GO respectively. However, the adsorption experimental data of thiophene compound on MWCNT and GO represented by Freundlich and Temkin model isotherms only with n values lower than 1 and B values lower than those for DBT which mean unfavorable adsorption. The DBT adsorb faster on CNT and GO compared to the adsorption on the AC. Although the adsorption capacity for DBT on CNT and GO was lower than adsorption capacity on AC, their low volume to mass ratio makes them compressible materials therefore theycan be used as mobile filters in vehicles and in fuel cells for deep desulfurization process.

4.2 The Nature and Kinetics of the Adsorption of Dibenzothiophene and Thiophene in Model Diesel Fuel on Carbonaceous Materials Loaded with Aluminum Oxide Particles

The aluminum oxide unsaturated surface ability can provide a strong electron acceptor site (Lewis acid) and the carbonaceous nanomaterials such as CNT and GO have distinct properties. Therefore, this section discusses the potential use of CNT, GO and AC, loaded with both 5 % and 10.9 % aluminum in form of the aluminum oxide as adsorbents for DBT and thiophene. These percentages are denoted by the endings AL5 and AL10 in the notations ACAL5, ACAL10, CNTAL5, CNTAL10, GOAL5, and GOAL10. The adsorbents were characterized using thermal gravimetric analysis (TGA), an N_2 adsorption-desorption surface area analyzer, scanning electron microscopy (SEM), energetic dispersive X-ray diffractogram (EDX), Field Emission Electron Microscope (FE-TEM) and X-ray photoelectron spectrometer (XPS), then the nature and kinetics of the adsorption of DBT and thiophene, from their solutions in *n*-hexane as model diesel were studied. To decide on the best adsorption isotherm and the model for the adsorption kinetics the resulting data were fitted to equations for different adsorption isotherms. Additionally, the adsorbents' reusability and their selective adsorption of DBT relative to thiophene and naphthalene were studied.

4.2.1 Adsorbents thermal gravimetric analysis

The thermal oxidation of raw and loaded AC, CNT and GO was investigated using TGA. The oxidation parameters were fixed at 10 mg of sample with heating rate of 10 °C/min and oxidation temperature from 25 to 800 ºC. For each measurement of thermal oxidation of unmodified adsorbent, a specified weight of 10 mg sample was heated under atmospheric air with a flow rate of 100 mL/min. As shown in figure 4-12, the residual solvents evaporated below 100 ºC while the initial oxidation temperature of raw AC, CNT and GO starts approximately at 400 ºC, 550 ºC and 500 ºC respectively. However the final oxidation temperature for AC, CNT and GO was at 600 °C, 650 ºC and 700 ºC respectively. AC, CNT and GO doped with 10.9 % Al in the form of Al_2O_3 show the same results as raw carbon materials thus the formation of aluminum oxide particles does not accelerate their oxidation. The same experiment also shows that, aluminum nitrate nonahydrate starts dehydrating at around 110 ºC while the calcination temperature of aluminum nitrate starts at 200 ºC and is complete at around 400 ºC. The dehydration of aluminum nitrate nonahydrate and its conversion to aluminum oxide on different carbon materials was also confirmed under nitrogen gas which gave the same trend of results as under air as shown in figure 4-13.

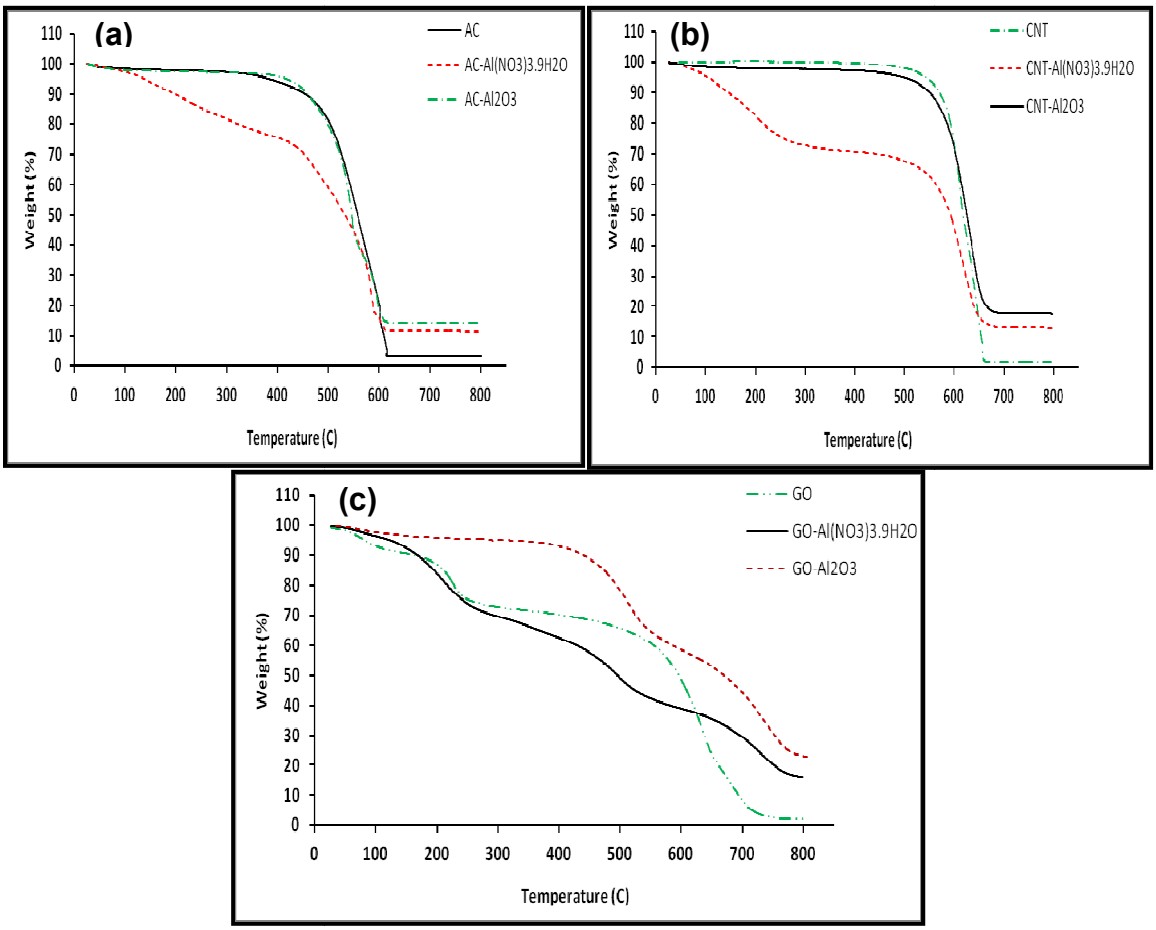

Figure 4-12: TGA under air atmosphere with a flow rate of 100 mL/min for (a) AC, (b) CNT and (c) GO impregnated with $Al(NO_3)_3.9H_2O$.

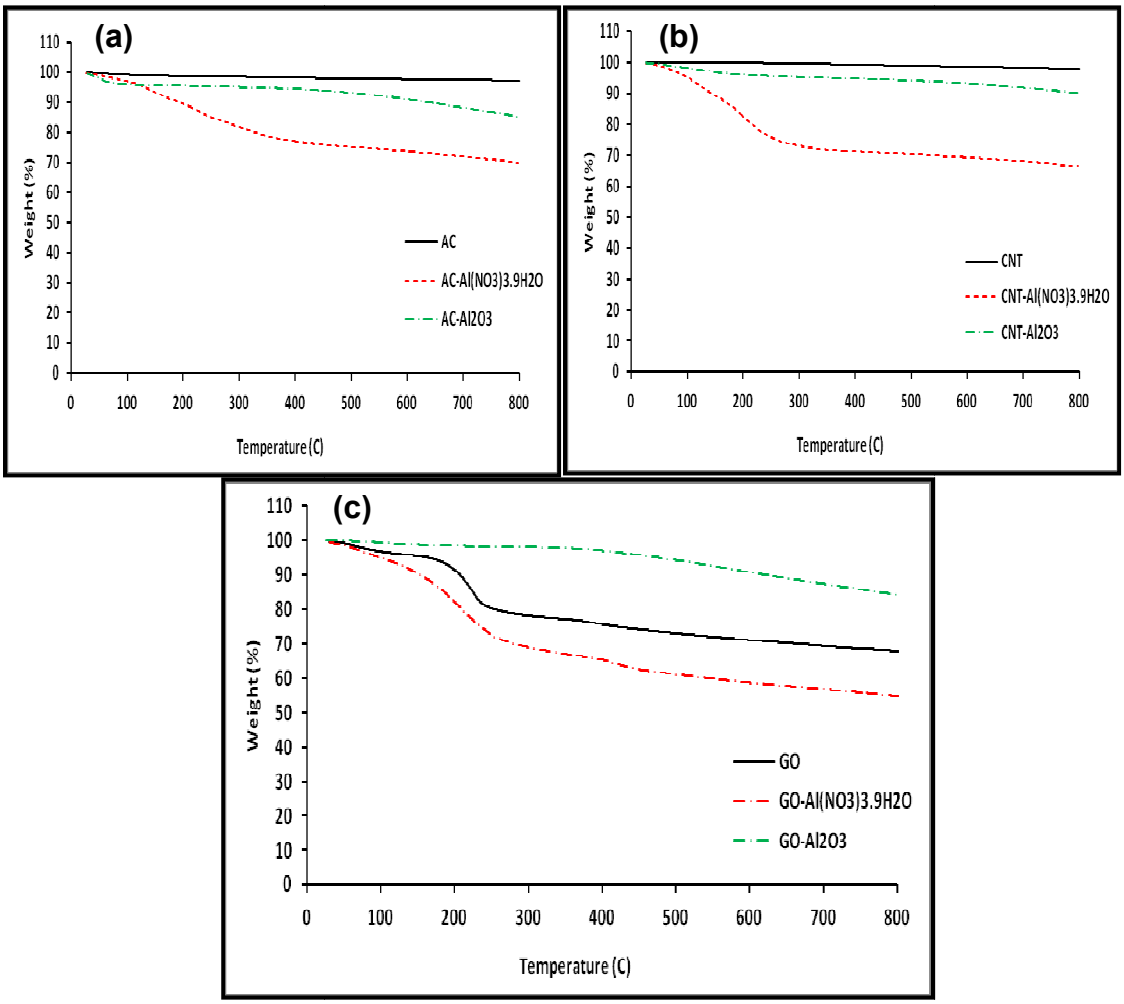

Figure 4-13:TGA under nitrogen atmosphere with a flow rate of 100 mL/min for (a) AC, (b) CNT and (c) GO impregnated with $Al(NO_3)_3.9H_2O$.

4.2.2 Adsorbent texture and morphology

The adsorbents' morphologies were characterized using a scanning electron microscope (SEM) and a field emission electron microscope (FE-TEM). The SEM images of AC, CNT and GO respectively are given before impregnation with Al_2O_3 particles in figure 4-14 and after impregnation with Al_2O_3 particles in figure 4-15. The diameter of the AC particles varied from 300 to 500 microns with an average around 450 microns and the diameter of GO particles varied from 0.5 to 10.0 microns seen at a lower magnification than that shown in figure 4-14. The CNT had diameters between 10 and 30 nm with lengths, seen at a lower magnification, in the range of 10-30 microns. As figure 4-15 shows a layer of Al_2O_3 particles covers the surface of the AC and GO sheets, while spherical particles cover the surface of the CNT. The elemental composition of the Al_2O_3-impregnated carbon based adsorbents was obtained by energy dispersive X-ray analysis (EDX) which is summarized in table 4-6. It was found that the GO has higher oxygen content compared to AC and CNT due to the availability of oxygenated functional groups on the GO surface. In addition the oxygen percentage increased after impregnation with aluminum oxide particles and the percentages of aluminum in the adsorbents are close to the theoretical percentages (5 % and 10.9 %). TEM images for raw and doped CNT and GO are shown in figures 4-16 and 4-17. The images show that all the nanotubes are hollow with many deflection sites, while the graphene oxide looks like multilayered flakes. As the TEM image in figure 4-16(b) shows the aluminum oxide nanoparticles coated on CNT were spherical with diametersbetween 30 and 80 nm. For loaded GO the nature of the aluminum oxide particles was difficult to predict so the

diffraction pattern was obtained from the TEM for both GO and GO doped with aluminum oxide to confirm that the GO layers were covered by Al_2O_3 after the impregnation as shown in figure 4-17(b).

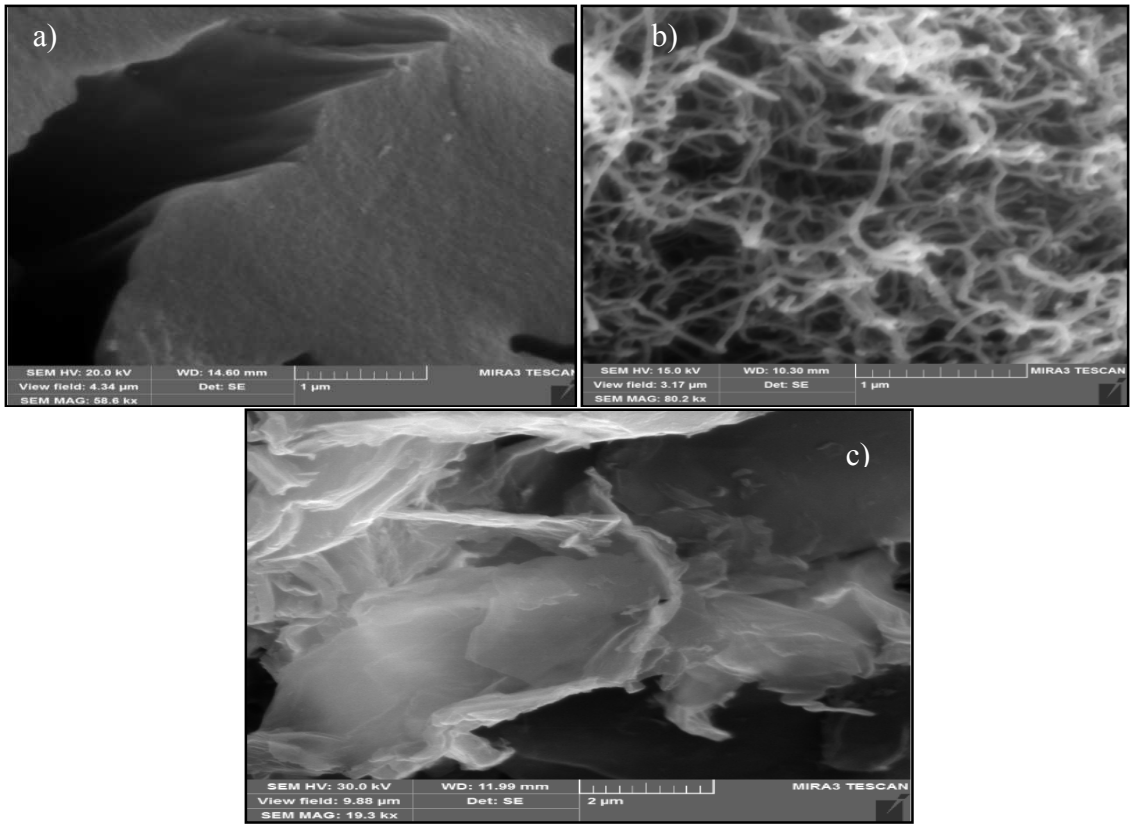

Figure 4-14:SEM images of (a) AC, (b) CNT and (c) GO before impregnation with Al_2O_3

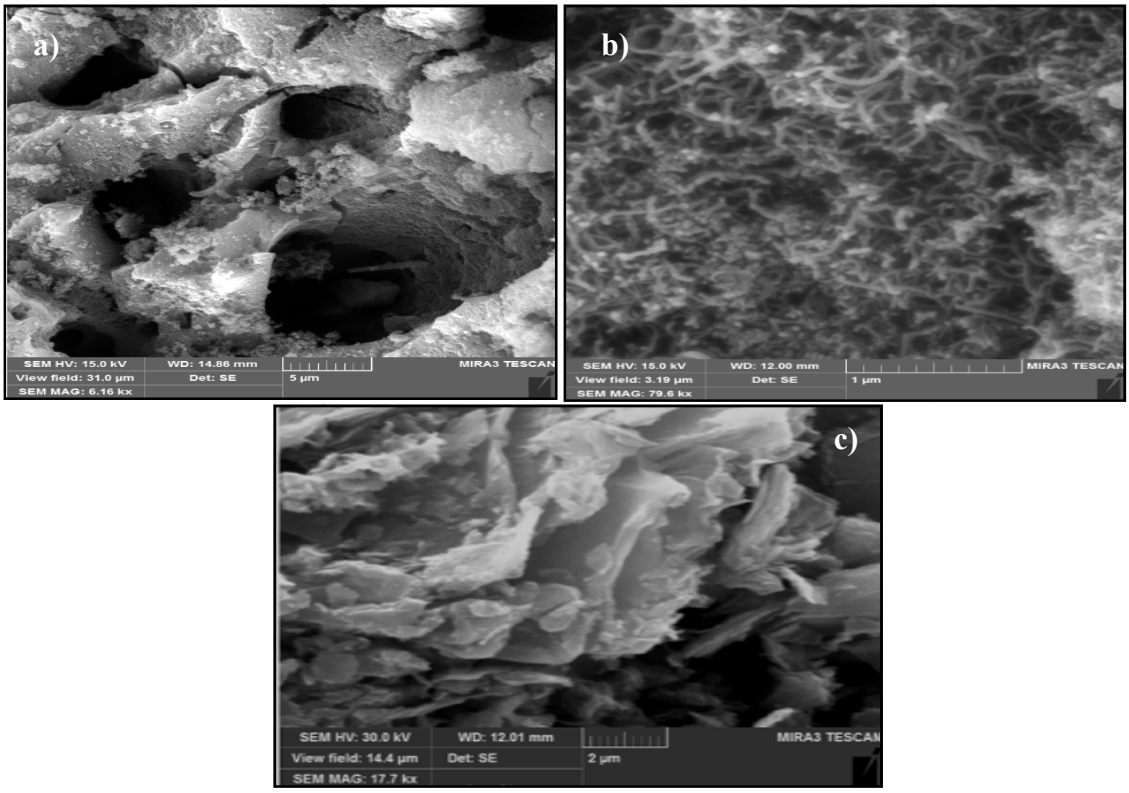

Figure 4-15:SEM images of (a) AC, (b) CNTs and (c) GO after impregnation with Al_2O_3.

Table 4-6: Weight percent of aluminum in the doped carbon materials adsorbents compared to the theoretical percentages of aluminum (5 % and 10.9 % Al for adsorbents ending with 5 and 10 respectively).

Adsorbent	Element	Weight %
AC	C	92.01
	O	7.99
ACAL10	C	62.11
	O	23.05
	Al	12.95
ACAL5	C	63.39
	O	29.17
	Al	6.44
CNT	C	96.48
	O	3.52
CNTAL10	C	68.96
	O	18.86
	Al	11.18
CNTAL5	C	86.53
	O	10.07
	Al	3.40
GO	C	79.07
	O	15.65
GOAL10	C	68.08
	O	23.80
	Al	9.12
GOAl5	C	69.40
	O	26.31
	Al	4.30

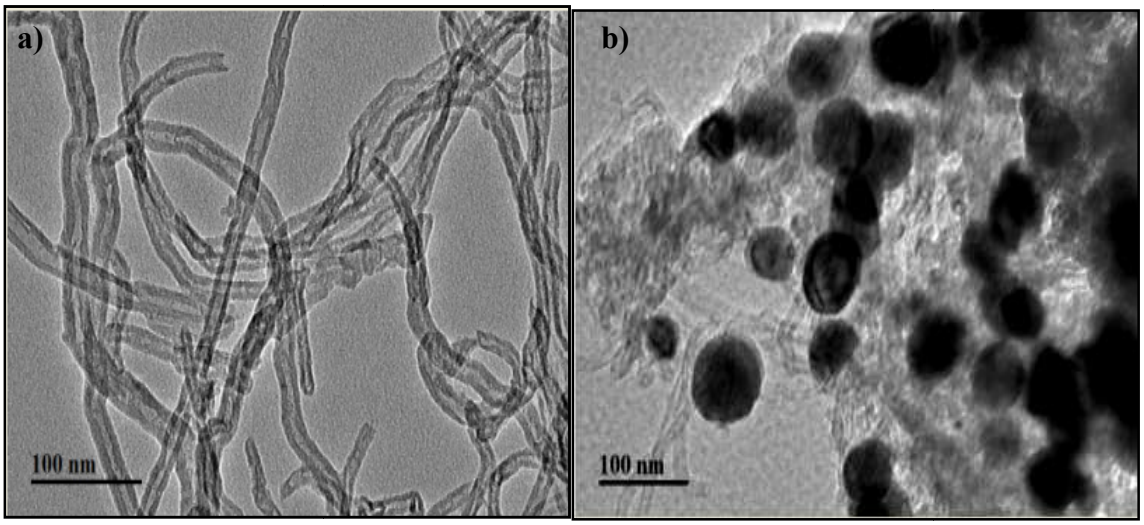

Figure 4-16: EF-TEM image for CNT (a) before and (b) after impregnation with Al_2O_3

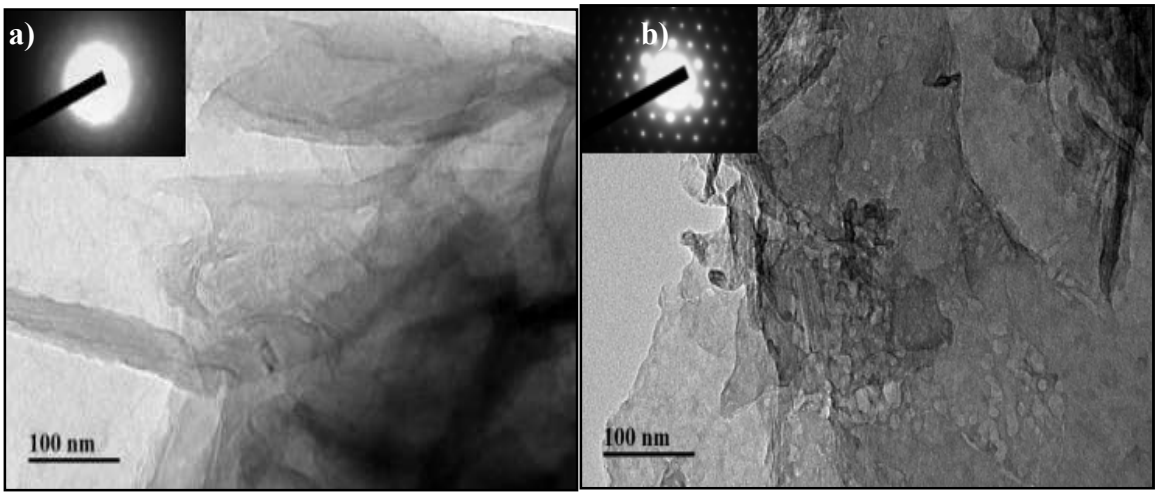

Figure 4-17: EF-TEM image for GO (a) before and (b) after impregnation with Al_2O_3. The insets are diffraction patterns for the GO surface (a) before and (b) after impregnation with Al_2O_3.

For further evidence the X-ray photoelectron spectrometer (XPS) (Thermo scientific ESCALAB 250Xi) was used to confirm the availability of aluminum oxide (Al_2O_3). The XPS survey spectrum and single element scan in figure 4-18 show binding energies of 74.6 and 531.4 eV which match the XPS fitting online library **[112]** values for the Al 2p electron and the O 1s electron in Al_2O_3.

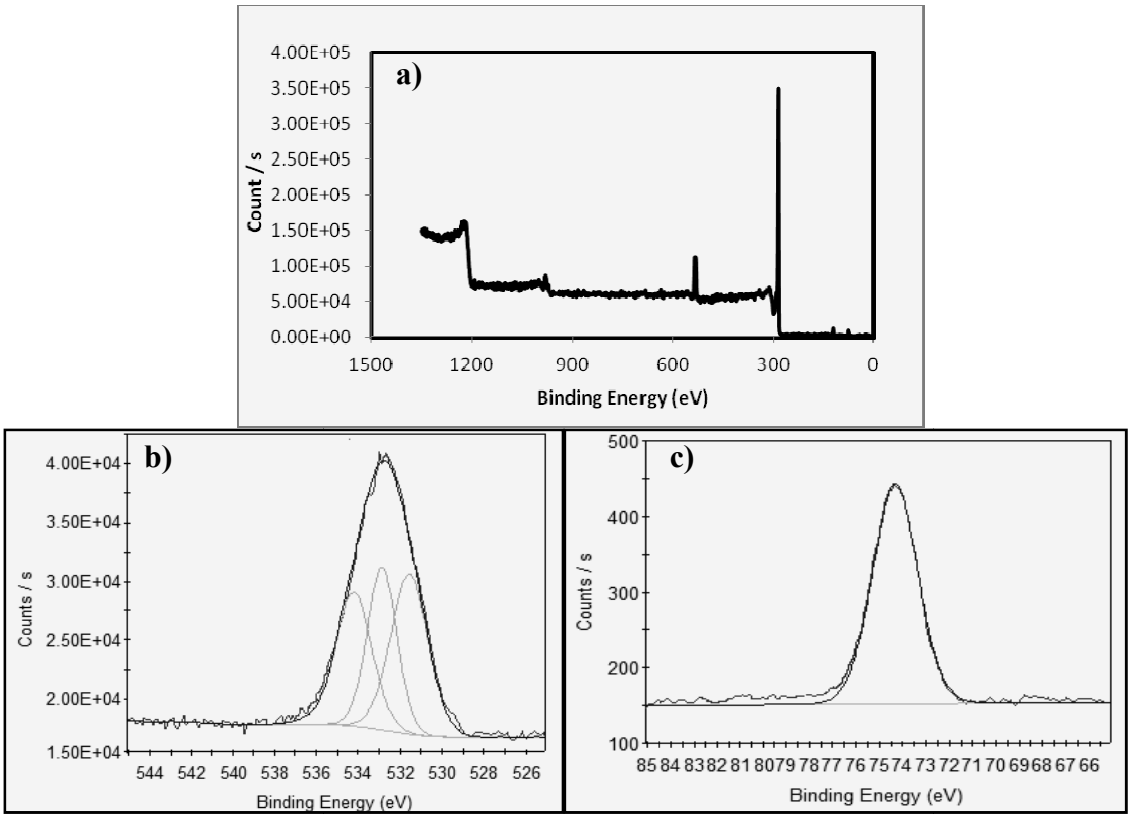

Figure 4-18:(a) XPS survey spectrum of CNT-Al_2O_3 (b) O 1s XPS spectrum of CNT-Al_2O_3 and (c) Al 2p XPS spectrum of CNT-Al_2O_3.

The surface area and porosity characterization results given in table 4.7 show that for the pristine adsorbents the trend in surface area is AC > CNT > GO while the trend in total pore volume is CNTs > AC > GO. Table 3 also shows that all impregnated adsorbents have lower surface areas, porosities and surface pH values relative to their corresponding pristine adsorbents. Both effects are accounted for by the accumulation of the amphoteric Al_2O_3 particles on the surfaces of the pristine adsorbents **[28, 31, 113].**

Table 4-7: Surface area, total pore volume and surface pH of AC, CNT and GO before and after their impregnation with 5 % and 10.9 % Al in the form of Al_2O_3.

	BET	DFT		pH
Adsorbent	**SA (m^2/g)**	**SA (m^2/g)**	**V (cm^3/g)**	
AC	882	1415	0.449	9.35
ACAL10	799	950	0.407	8.94
ACAL5	825	778	0.391	8.45
CNT	217	173	1.513	5.81
CNTAL10	184	138	0.716	5.73
CNTAL5	118	150	0.550	5.52
GO	11	15	0.059	2.23
GOAL10	12	11	0.082	3.03
GOAL5	10	9	0.048	2.63

4.2.3 Adsorption of thiophene and dibenzothiophene

The adsorption of thiophene and DBT on pristine and impregnated AC, CNT and GO with 5 and 10.9 wt% Al in the form of Al_2O_3 was investigated at 25 ºC. Solutions of thiophene and DBT at concentrations of 25, 50, 100, 125, 150, 200, and 250 mg/L in 25 mL *n*-hexane as a model fuel were each used with 150 mg of adsorbent. The concentration of thiophene and DBT before and after the adsorption study was measured using an HPLC method coupled with a UV detector. However, for the selectivity study the wavelength switching mode was used to measure the concentrations of thiophene, naphthalene and DBT simultaneously in the model diesel fuel. Figures 4-19 and 4-20 present the respective Langmuir and Freundlich adsorption isotherms at 25 °C for DBT and thiophene on ACAL5, ACAL10, CNTAL5, CNTAL10, GOAL5, and GOAL10. As shown in table 4-8 the n and K_F values for thiophene on adsorbents impregnated with Al_2O_3 particles are larger than those of thiophene on unmodified carbon adsorbents, indicating that the modification increased the adsorbents surface heterogeneity and adsorption capacity. However for DBT there is no significant change in the n values of modified adsorbents. These n values fall between 1.2 and 1.9 which indicate DBT tendency for adsorption. While K_F increased for modified adsorbents which represent higher adsorption capacity for DBT molecules compared to unmodified adsorbents.For thiophene and DBT the goodness of fit values (R^2; the squares of the correlation coefficients) of ln (q_e) versus ln(C_e) (for thelinearized form of Freundlich's equation) were better than those of $\frac{C_e}{q_e}$ versus C_e (for the linearized formof Langmuir's equation). On the other hand the experimental data for thiophene adsorption on AC, CNT, GO,

CNTAL5, GOAL10 and GOAL5 did not fit the Langmuir adsorption isotherm. They, on the other hand, fitted the Freundlich isotherm which indicates that thiophene and DBT form multi-layers on the adsorbents.

It was found that the maximum adsorption capacity (Q_{max}) for DBT on AC, ACAL10 and ACAL5 follows the trend ACAL5 > ACAL10 > AC. In a similar manner Q_{max} for CNT, CNTAL10 and CNTAL5 follows the trend CNTAL5 > CNTAL10 > CNT. On the other hand Q_{max} for GO, GOAL0 and GOAL5 follows the different trend GOAL5 > GO > GOA10. As groups the Q_{max} values for AC, ACAL10 and ACAL5 are higher than those for CNT, CNTAL10 and CNTAL5 which are in turn higher than those for GO, GOAL10 and GOAL5. AC and CNT impregnated with 5 % Al and 10.9 % Al in the form of Al_2O_3 had, respectively Q_{max} values nearly double and 1.5 times those of their un-impregnated forms. Within the uncertainties in the Q_{max} values for GO, GOAL10 and GOAL5 it can be safely stated that there is no significant change in the Q_{max} value of GO after impregnation with either 5 % Al or with 10.9 % Al. This may be explained by agglomeration of the graphene oxide layers after their impregnation with Al in the form of Al_2O_3. The highest adsorption capacity (85 ± *1*mg/g) was by ACAL5 and the others follow the order ACAL10 > AC > CNTAL5 > CNTAL10 > GOAL5 > CNT > GO > GOAL10. The increase in the adsorption of DBT from model diesel using carbon adsorbents doped with Al in the form of Al_2O_3 is a consequence of the introduction of additional acidic adsorption sites rather than an increase in the surface area and pore volume. In other words the amphoteric Al_2O_3 acts as a Lewis acid in the environment of the soft base DBT.

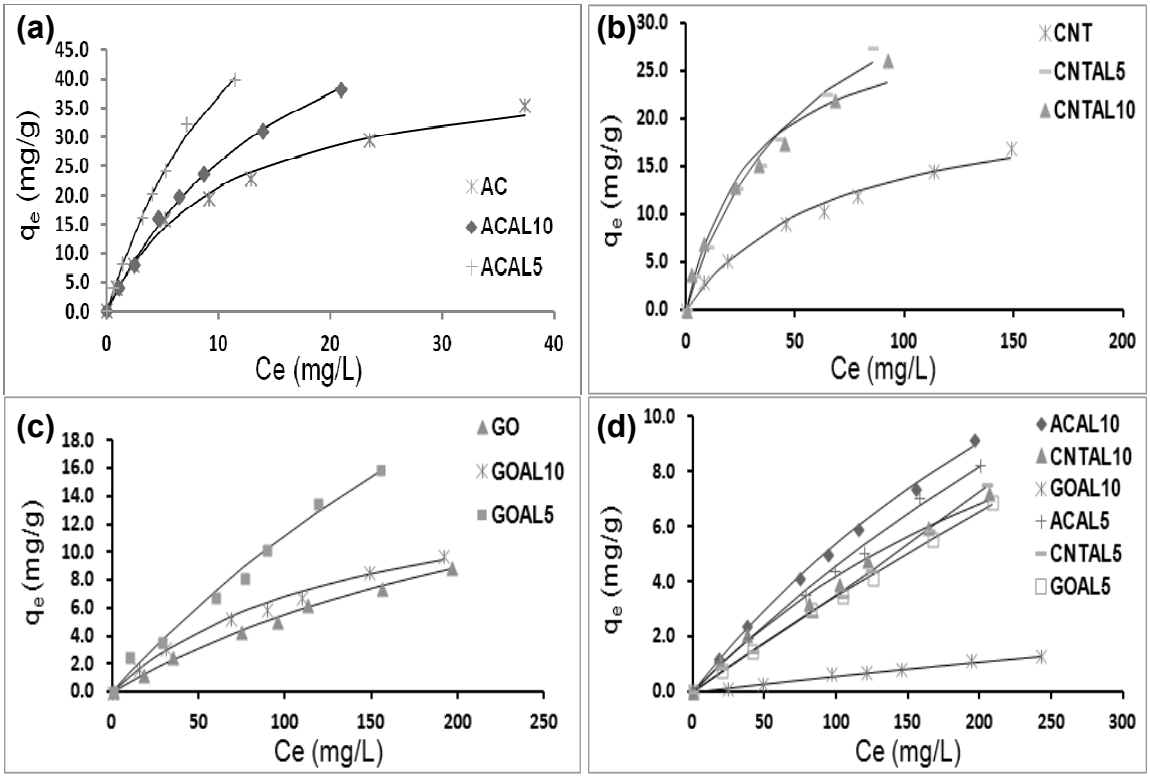

Figure 4-19: Adsorption isotherms at 25 ºC for (a) DBT on AC, ACAL5 and ACAL10, (b) DBT on CNT, CNTAL5 and CNTAL10, (c) DBT on GO, GOAL5 and GOAL10 and (d) thiophene on different adsorbents. Solid lines are fits to the Langmuir model.

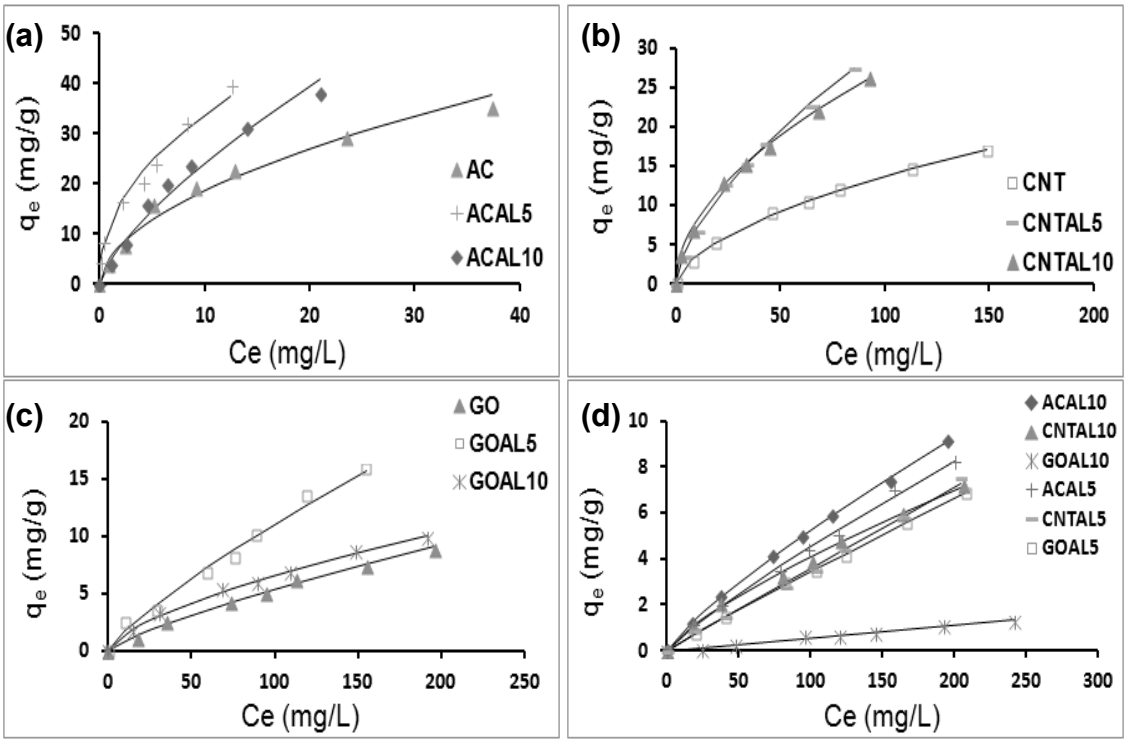

Figure 4-20: Adsorption isotherms at 25 ºC for (a) DBT on AC, ACAL5 and ACAL10, (b) DBT on CNT, CNTAL5 and CNTAL10, (c) DBT on GO, GOAL5 and GOAL10 and (d) thiophene on different adsorbents. Solid lines are fits to the Freundlich model.

Table 4-8: Freundlich and Langmuir parameters and correlation coefficient for thiophene and DBT adsorption on carbonaceous materials before and after doping with Al_2O_3

Adsorbent	Freundlich					
	Thiophene			DBT		
	n [a]	K_f [b] ($mg^{(1-1/n)}\ mg^{-1}\ L^{1/n}$)	R^2	n [a]	K_f [b] ($mg^{(1-1/n)}\ mg^{-1}\ L^{1/n}$)	R^2
AC	0.83 ±*0.04*	(1.1± *0.3*) x 10^{-2}	0.9898	1.7 ±*0.1*	4.9 ± *0.5*	0.9747
CNT	0.45 ±*0.02*	(2.0 ± *0.8*) x 10^{-5}	0.9934	1.69 ±*0.04*	(8.9 ± *0.5*) x 10^{-1}	0.9968
GO	0.75 ±*0.03*	(1.3 ± *0.3*) x 10^{-3}	0.9935	1.22 ±*0.05*	(1.2 ± *0.2*) x 10^{-1}	0.9912
ACAL10	1.20 ±*0.02*	(1.1 ± *0.1*) x 10^{-1}	0.9987	1.29 ±*0.08*	4.94 ± *0.04*	0.9821
ACAL5	1.18 ±*0.03*	(9.1 ± *0.8*) x 10^{-2}	0.9971	1.26 ±*0.04*	6.3± *0.2*	0.9953
CNTAL10	1.32 ±*0.04*	(1.3 ± *0.1*) x 10^{-1}	0.9943	1.93 ±*0.04*	2.5± *0.1*	0.9982
CNTAl5	1.10 ±*0.05*	(6 ± *1*) x 10^{-2}	0.9901	1.55 ±*0.04*	1.6 ± *0.1*	0.9973
GOAL10	0.93 ±*0.07*	(4 ±2) x 10^{-3}	0.9692	1.49 ±*0.05*	(3.0 ± *0.3*) x 10^{-1}	0.9935
GOAL5	1.08 ±*0.01*	(4.9 ± *0.3*) x 10^{-2}	0.9991	1.4 ±*0.1*	(4 ± *1*) x 10^{-1}	0.9562
Adsorbent	**Langmuir**					
	Thiophene			**DBT**		
	Q_{max} [c] (mg/g)	**b** [d] (dm^3/mg)	R^2	Q_{max} [c] (mg/g)	**b** [d] (dm^3/mg)	R^2
AC	---	---	---	42 ± *3*	(1.1 ± *0.1*) x 10^{-1}	0.9795
CNT	---	---	---	24 ± *2*	(1.5 ± *0.1*) x 10^{-2}	0.9702
GO	---	---	---	23 ± *3*	(3 ± *1*) x 10^{-3}	0.9201
ACAL10	26 ± *3*	(3 ± *1*) x 10^{-3}	0.9414	70 ± *3*	(4.7 ± *0.2*) x 10^{-2}	0.8503
ACAL5	29 ± *1*	(1.94 ± *0.04*) x 10^{-3}	0.7401	85 ± *1*	(7.8 ± *0.3*) x 10^{-2}	0.9603
CNTAL10	17 ± *3*	(4 ± *1*) x 10^{-3}	0.8729	33 ± *4*	(3.4 ± *0.2*) x 10^{-2}	0.9395
CNTAl5	---	---	---	41 ± *4*	(2.10 ± *0.01*) x 10^{-2}	0.9450
GOAL10	---	---	---	16 ± *2*	(7.3 ± *0.1*) x 10^{-3}	0.9571
GOAL5	---	---	---	29 ± *9*	(6.1 ± *0.9*) x 10^{-3}	0.5310

[a] The uncertainty was calculated on the basis of the uncertainty in the slope of the Freundlich linearized equation.
[b] The uncertainty was calculated on the basis of the uncertainty in the intercept of the Freundlich linearized equation.
[c] The uncertainty was calculated on the basis of the uncertainty in the slope of the Langmuir linearized equation.
[d] The uncertainty was calculated on the basis of the uncertainty in the intercept of the Langmuir linearized equation

4.2.4 Adsorption kinetics of thiophene and dibenzothiophene

Studying the adsorption kinetics in the batch mode is essential to design the adsorption columns for further study and for industrial applications **[107]**. To study the DBT and thiophene adsorption kinetics on carbonaceous adsorbents modified with aluminum oxide, a 25 mL *n*-hexane solution with an initial concentration of 250 mg/L from each sulfur compound was added to 150 mg of the adsorbent in a vial that was capped then shaken continuously for a fixed time intervals. The adsorbent was then allowed to settle and quickly a 5 mL sample was removed and filtered, 5 μL from the filtered solution were analyzed using HPLC-UV (described in section 3.5). The same procedure was carried out for shaking time intervals of 10, 20, 30, 40, 60 120, 240 and 1560 minutes. The results presented in figures 4-21a and 4.21b show that, for all the adsorbents in this study, the adsorption rates of thiophene and DBT reach equilibrium within 1 hour. The experimental adsorption capacities ($q_{e,exp}$) for thiophene and DBT on the carbonaceous adsorbents modified with aluminum oxide are given in table 4-9. As the insets in figures 4-21a and 4-21b show most of the thiophene and DBT are adsorbed in the first 30 minutes and slowly reach a maximum value after 1 hour. The initial fast adsorption is attributed to the large number of available active adsorption sites while the slowness at which maximum adsorption is reached is due to the then few adsorption sites and the repulsive forces between adsorbate molecules in solution and adsorbate molecules on the adsorbents. The adsorption results were fitted using the kinetic models reported by Lagergren**[99]** and Ho**[108]** (shown in the experimental section).

Linear least squares fits of ln $(q_e - q_t)$versus t for the adsorption data of thiophene and DBT yielded low correlation coefficients (R). On the other hand linear least squares fits of $\frac{t}{q_t}$ versus $t$yielded correlation coefficients equal or very close to 1 (see table 4-9). Clearly the adsorption process follows pseudo second order kinetics.

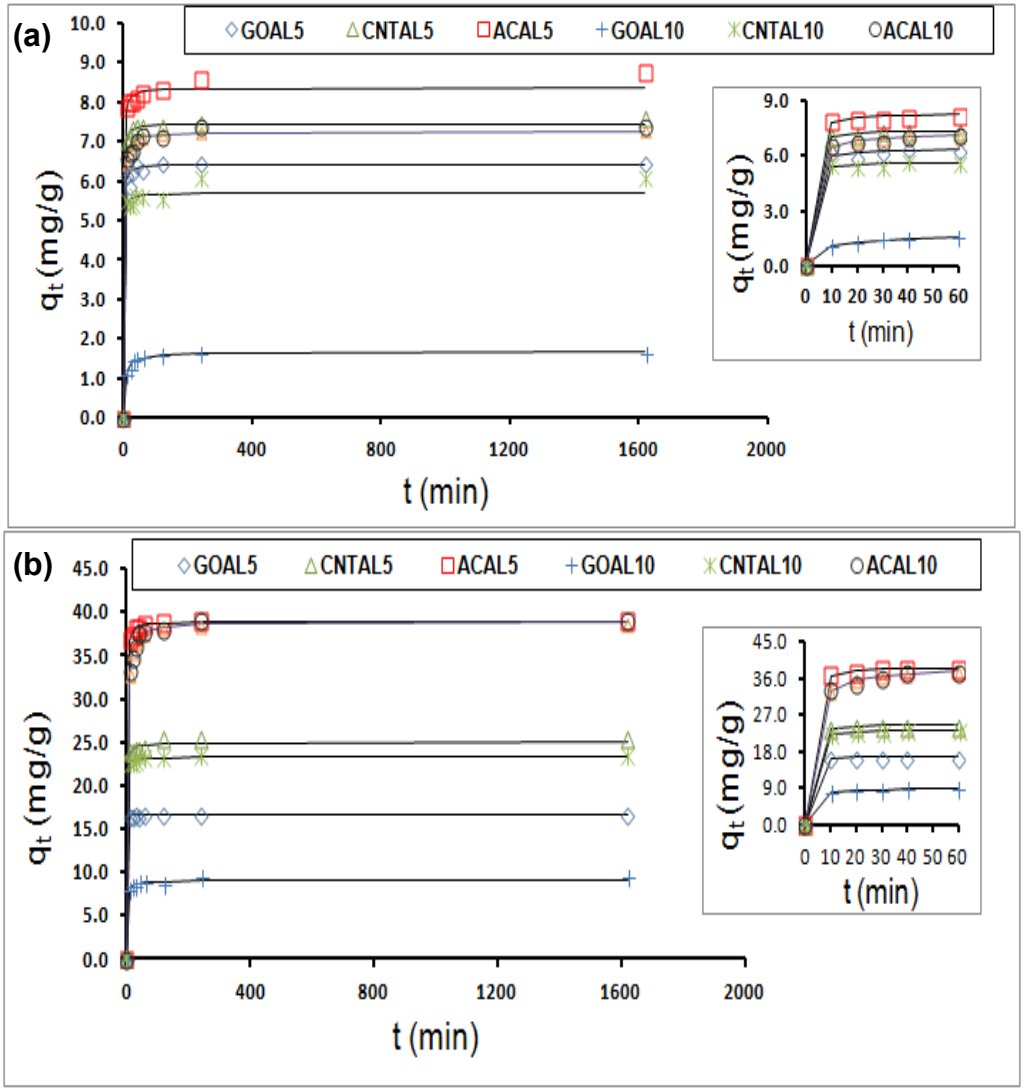

Figure 4-21: The effect of agitation time on the adsorption capacity of (a) thiophene and (b) dibenzothiophene (DBT), using different adsorbents impregnated with different percentages of Al_2O_3 at 25ºC where, the shaking speed is 200 rpm, the adsorbent amount is 150 mg and the initial concentration of the organic sulfur compound is 250 mg/L. The Inset figures show the effect of agitation time up to 60min.

Table 4-9: Pseudo-Second order kinetic parameters for thiophene and DBT adsorption on the carbonaceous materials doped with Al_2O_3

Adsorbent	Pseudo-First order Parameters							
	Thiophene (250 mg/L)				DBT (250 mg/L)			
	$q_{e,exp}$ (mg/g)	$q_{e\ pred.}$ (mg/g)	k_1 (min^{-1})	R^2	$q_{e,exp}$ (mg/g)	$q_{e\ pred.}$ (mg/g)	k_1 (min^{-1})	R^2
ACAL10	7.4	1.5	0.004	0.6218	39.3	6.3	0.012	0.7021
CNTAL10	6.1	0.1	0.002	0.2246	23.4	0.8	0.019	0.8235
GOAL10	1.6	0.4	0.019	0.8053	9.4	1.2	0.005	0.3315
ACAL5	8.8	0.9	0.006	0.9852	39.2	1.7	0.011	0.8829
CNTAL5	7.6	0.9	0.005	0.6742	25.4	2.6	0.016	0.8922
GOAL5	6.5	2.2	0.024	0.1994	16.8	0.4	0.007	0.3113
Adsorbent	Pseudo-Second order Parameters							
	Thiophene (250 mg/L)				DBT (250 mg/L)			
	$q_{e,exp}$ (mg/g)	$q_{e,pred.}$[e] (mg/g)	k_2[f] (g/mg min)	R^2	$q_{e,exp}$ (mg/g)	$q_{e,pred.}$[e] (mg/g)	k_2[f] (g/mg min)	R^2
ACAL10	7.4	7.2 ± 0.1	0.13 ± 0.04	0.9998	39.3	38.7 ± 0.2	0.015 ± 0.002	0.9999
CNTAL10	6.1	6.1 ± 0.1	0.06 ± 0.03	0.9980	23.4	23.4 ± 0.1	0.09 ± 0.02	1.0000
GOAL10	1.6	1.64 ± 0.02	0.13 ± 0.02	0.9992	9.4	9.5 ± 0.2	0.035 ± 0.02	0.9981
ACAL5	8.8	8.38 ± 0.03	0.12 ± 0.02	1.0000	39.2	39.1 ± 0.1	0.033 ± 0.004	1.0000
CNTAL5	7.6	7.42 ± 0.02	0.3 ± 0.1	1.0000	25.4	25.7 ± 0.3	0.02 ± 0.01	0.9993
GOAL5	6.5	6.5 ± 0.1	0.13 ± 0.06	0.9996	16.8	16.8 ± 0.1	0.15 ± 0.07	0.9999

[e] The uncertainty was calculated from the uncertainty in the slope of the linearized equation.

[f] The uncertainty was calculated from on the uncertainty in the intercept of the linearized equation.

The mechanism of adsorption can be explored by studying the adsorption kinetics. Bearing in mind that the kinetic results fit perfectly into the pseudo second order kinetic model for DBT and thiophene in all adsorbents, the influence of mass transfer resistance on their binding on the adsorbents was verified using Weber and Morris intra-particle diffusion model which allows exploring the intra-particle diffusion resistance **[114]:**

Figure 4-22 shows plots of q_t versus $t^{0.5}$ for DBT on ACAL10, CNTAL10 and GOAL10. These results imply that the adsorption processes involve more than a single kinetic stage or sorption rate **[114]**. All adsorbents exhibited two stages, which can be attributed to two linear parts. The first linear part can be attributed to intra-particle diffusion, which produces a delay in the adsorption process. The second stage may be regarded as the diffusion through smaller pores, which is followed by the establishment of equilibrium. The presence of micropores on the adsorbents is in line with this stage. Table 4-10 shows the calculated values of the diffusion constants for DBT on ACAL10, CNTAL10 and GOAL10. Higher values of k_{id} represent a faster net rate of adsorption as a result of slow desorption because of the improved bonding between DBT and the adsorbent.

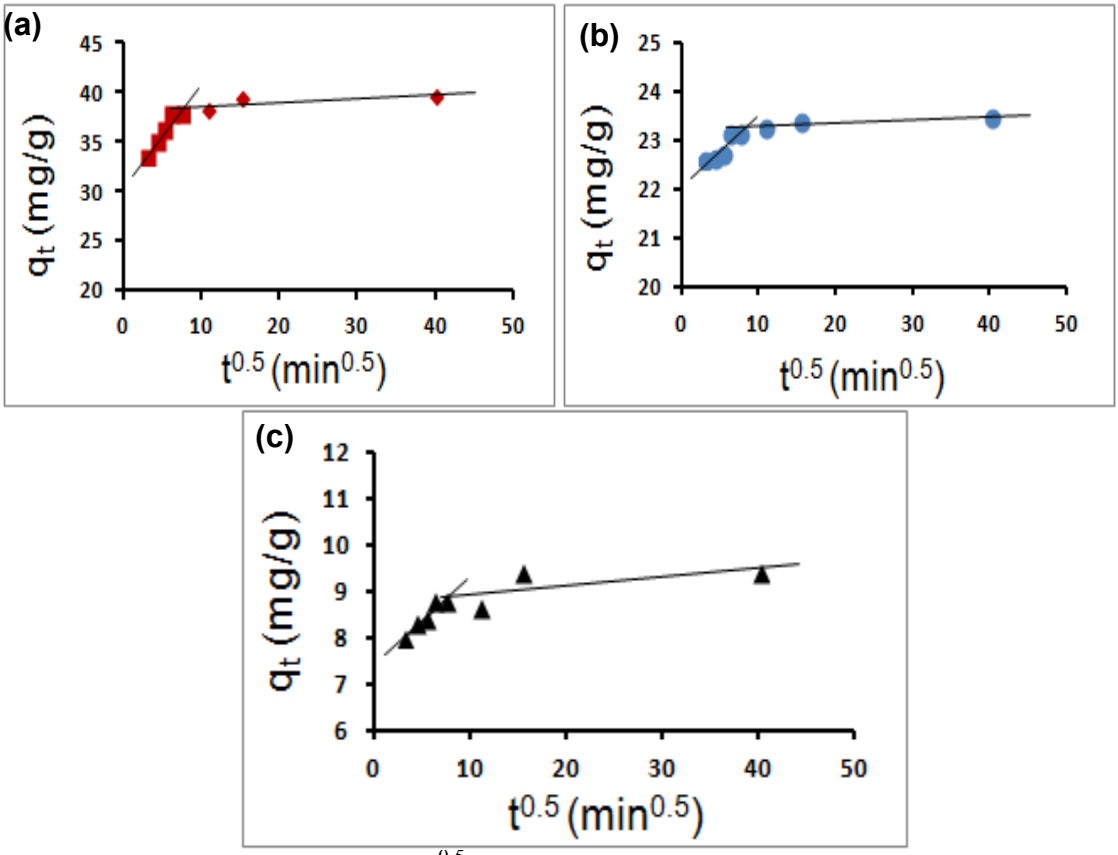

Figure 4-22: Plots of q_t versus $t^{0.5}$ showing the two diffusion stages predicted by the diffusion model for DBT adsorption on (a) ACAL10, (b) CNTAL10 and (c) GOAL10.

Table 4-10: Intra-particle diffusion parameters for DBT on different adsorbents.

Adsorbents	Intra-particle Diffusion Parameters		
	K_{id} ($mg/gmin^{0.5}$)	C (mg/g)	R^2
ACAL10	1.04	30.30	0.9338
CNTAL10	0.14	22.09	0.8046
GOAL10	0.19	7.41	0.9089

4.2.5 Effect of adsorbent dosage

The effect of the adsorbent dose on the removal of DBT and thiophene was studied by varying it from 100 to 1500 mg at 25 ºC, a shaking speed of 200 rpm and an initial concentration (C_o) of 250 mg/g for the sulfur containing compound (see figure 4-23). It has been observed that, the percentage removal of DBT and thiophene increased with the increase in the dose of AC doped with Al_2O_3. High removal percentage of DBT (around 98 %) was found at an adsorbent dosage of 500 mg for ACAL5 and ACAL10, while the maximum adsorption of DBT (100 % removal) was found at an adsorbent dosage 1500 mg. The same trend of adsorption was observed when AC doped with Al_2O_3 was used to remove thiophene from model diesel. Only 30 % removal of thiophene was achieved when 1500 mg of ACAL10 was used, while 40 % removal was achieved with ACAL5. 80 % removal of DBT was obtained when CNTAL5 and CNTAL10 were used, while 20 % removal of thiophene was observed when same materials were used. Low removal of DBT and thiophene compounds was noticed when GO doped with Al_2O_3 was used, due to its low surface area and fewer adsorption sites compared to the impregnated AC and CNT. The high removal efficiency and good adsorption capacities of DBT by ACAL5 and CNTAL5 led us to study the selectivity which is covered in the next section.

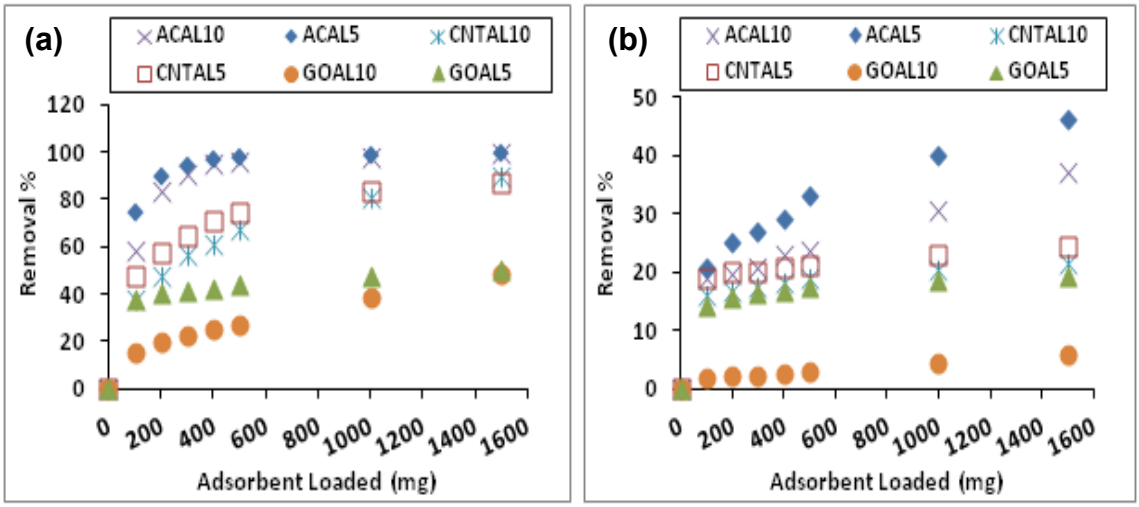

Figure 4-23: Comparison between the removal efficiency of (a) dibenzothiophene (DBT) and (b) thiophene, on AC, CNT and GO impregnated by Al_2O_3, at 25 ºC, a shaking speed of 200 rpm and a sulfur compound concentration of 250 mg/L.

4.2.6 Adsorbents' selectivity

The selectivity of ACAL5 and CNTAL5 for DBT removal from *n*-hexane has been studied relative to thiophene as model molecule for small heterocyclic aromatic sulfur containing compounds, as well as relative to naphthalene which represents the availability of polyaromatic hydrocarbons (PAH) with molecular structures close to that of DBT. The stock solution for the ternary mixture from these three compounds thiophene/DBT/naphthalene in *n*-hexane was prepared with concentrations of 250 mg/L for both thiophene and DBT and 1000 mg/L for naphthalene to simulate the actual availability of PAH in real diesel. A 150 mg adsorbent was used in 25 mL of model diesel solution and the batch adsorption experiments were performed over a wide range of adsorbate concentrations at 200 rpm shaking speed and a 120 min adsorption time at room temperature. The concentrations of these three compounds were measured simultaneously before and after the adsorption equilibrium was achieved. The distribution coefficient K_d (L/g) was calculated for each analyte based on the following equation,

$$K_d = \frac{Q_e}{C_e} \tag{12}$$

where Q_e is the adsorption capacity (mg/g) and C_e (mg/L)is the equilibrium concentration of one of the sulfur compounds or naphthalene. The distribution coefficient is used to calculate the selectivity factor for DBT with respect to thiophene and naphthalene according to following equation.

$$k = \frac{\mathrm{K}_{d\,(DBT)}}{\mathrm{K}_{d\,(C)}} \tag{13}$$

Where k expresses the adsorption selectivity factor using ACAL5 and CNTAL5, K_d is the distribution coefficient and the subscript (c) is the competing molecule (i.e thiophene or naphthalene).

As shown in table 4-11, the ACAL5 and CNTAL5 exhibit high adsorption capacities for DBT which are around 54 and 34 mg/g respectively. Using these adsorbents the removal efficiency was around 4 times the removal efficiencyof naphthalene. However, the selectivity factors of DBT to naphthalene were about 25 by ACAL5 and 7 by CNTAL5. On the other hand the selectivity factor of DBT to thiophene was around 255 using ACAL5 and 127 using CNTAL5. The selectivity factor of DBT to thiophene and naphthalene can be explained by three main factors. First, the size of the DBT molecule is closer to the size of the adsorbents' pores which allows them to be preferably trapped into the adsorbent. The second factor is the higher dipole moment, molar mass and aromaticity of DBT which lead to stronger van der Waals and π-π interactions with the adsorbents surface. The third factor is the higher basicity of DBT relative to thiophene and in turn its stronger acid-base interaction with the Al_2O_3 (Lewis acid) on the adsorbent surface.

Table 4-11: Adsorption selectivity of ACAL5 and CNTAL5.

Adsorbate	Adsorbent							
	ACAL5				CNTAL5			
	q_e(mg/g)	K_d	$k_{(\text{DBT/Naphthalene})}$	$k_{(\text{DBT/Thiophene})}$	q_e(mg/g)	K_d	$k_{(\text{DBT/Naphthalene})}$	$k_{(\text{DBT/Thiophene})}$
DBT	54.35	1.531			34.01	0.253		
Thiophene	1.50	0.006	25.10	255.17	0.44	0.002	6.49	126.50
Naphthalene	46.73	0.061			33.78	0.039		

4.2.7 Regeneration of adsorbents

Since the cost effectiveness and regeneration of the adsorbents are significant factors for actual diesel desulfurization their reusability has been considered. The regeneration procedure for ACAL5 and CNTAL5 was very simple. Upon the completion of adsorption experiments, the ACAL5 and CNTAL5 loaded with DBT were filtrated and collected in crucibles that were then heated at 350 ºC for 2 hours in air to remove the adsorbed DBT molecules. The regenerated ACAL5 and CNTAL5 were reused for the next adsorption, and the successive adsorption–desorption cycles were repeated five times. As shown in figure 4-24, ACAL5 and CNTAL5 remained, within experimental error, nearly unchanged in their ability for DBT adsorption for at least five cycles. However, the adsorption ability for thiophene (measured in ACAL5) decreased by about 30 % relative to the fresh adsorbent after the fifth cycle. The thiophene-CNTAL5 system is excluded from figure 4-24b since, as the reader may recall, it gave very poor correlation coefficients in the fits used for the calculation of Q_{max}.

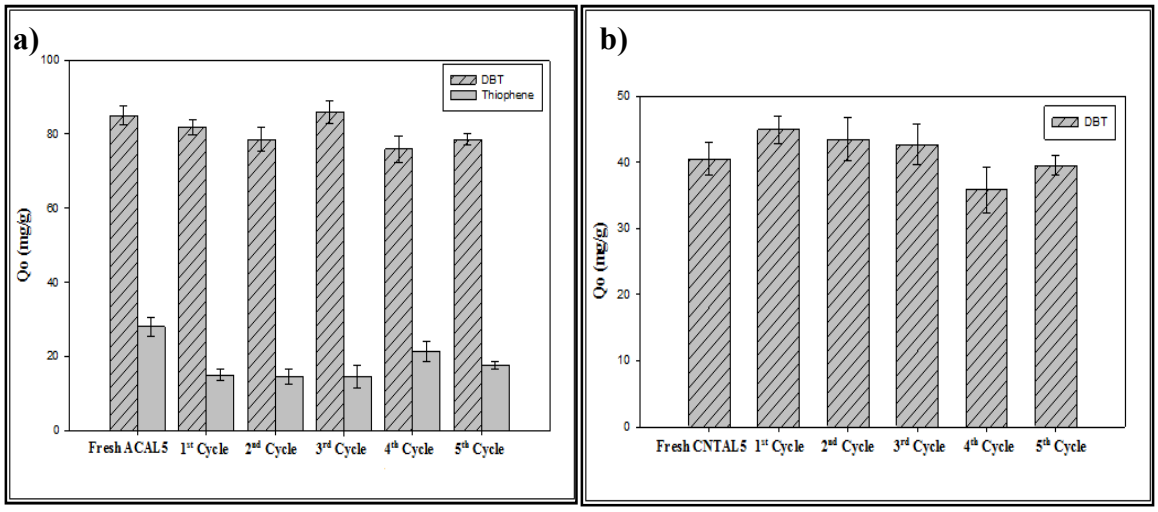

Figure 4-24: The adsorption capacities with error bars after each of 5 adsorbent regeneration cycles for (a) DBT and thiophene on the ACAL5 adsorbent and (b) DBT on the CNTAL5 adsorbent.

4.2.8 Removal of DBT from a real diesel sample

The potential application of using ACAL5 which has the best adsorption capacity and selectivity among the prepared adsorbents was evaluated for DBT removal from real diesel by measuring the DBT concentration before and after the adsorption based on the standard addition method. The original DBT was around 43 mg/L and was reduced by about 30 %. Furthermore to check the effectiveness of this adsorbent for DBT removal at higher concentration, a real diesel sample was spiked with DBT to increase its concentration in the original diesel sample to 153 mg/L. The adsorption results show that the DBT concentration was reduced to 102 mg/L with removal percentage about 33 %. This relatively low removal efficiency is attributable to the severe medium of a real diesel which contains other competing aliphatic and aromatic sulfur compounds. In addition, the solubility of DBT in these components is much higher and its diffusion to the adsorbent surface is very low compared with its diffusion in the model diesel used in this study. Never-the-less this adsorbents proved its ability to remove about 30 % of the DBT in real diesel.

4.2.9 Conclusion

Three different types of carbonaceous adsorbents namely AC, CNT and GO loaded with two loadings of Al (5% and 10.9 %) in the form of Al_2O_3 were used for the removal of DBT and thiophene from *n*-hexane as a simulant of diesel fuel. The Al_2O_3 was impregnated on the surface of carbon materials using the wetness impregnation technique. The raw and modified carbonaceous materials were characterized using TGA, SEM, EDX, TEM and XPS. The highest removal efficiency of DBT and thiophene was achieved using the ACAL5 adsorbent. The adsorption capacities were 84.5 mg/g and 29.0 mg/g for DBT and thiophene respectively. The selectivity study of DBT relative to thiophene and DBT relative to naphthalene was carried out using ACAL5 and CNTAL5. It has been found that in ACAL5 the selectivity factor of DBT/thiophene was 255 and of DBT/naphthalene was 25, while in CNTAL5 the selectivity of DBT/thiophene was 127 and of DBT/naphthalene was 6.5. These adsorbents showed good reusability for at least 5 adsorption cycles without significant loss in their adsorption capacity. It has also been found that ACAL5 is capable of removing 30 % of the DBT in diesel fuel.

4.3 Synthesis and Characterization of Modified Carbon Nanotube and Graphene Oxide with Silver Sulfide Nanocomposites for Adsorptive Removal of Dibenzothiophene

Multi-wall carbon nanotube (CNT) and graphene oxide (GO) were modified with silver sulfide using chemical vapor deposition. The new nanocomposite materials ($CNTAg_2S$ and $GOAg_2S$) were characterized using the most sophisticated characterization techniques; thermal gravimetric analysis (TGA), scanning electron microscope (SEM), energetic dispersive X-ray diffractogram (EDX), Field Emission Electron Microscope (FE-TEM) and X-ray photoelectron spectrometer (XPS). The raw and modified materials were tested for the removal of Dibenzothiophene (DBT) from model diesel in batch mode adsorption experiments. The removal efficiencies of DBT were 61.48 %, 56.7 %, 41.8 % and 22.7 % for $CNTAg_2S$,$GOAg_2S$, CNT and GO respectively. The adsorption rate for DBT follows pseudo-second order kinetics. The adsorption isotherm was modeled using Freundlich, Langmuir and Temkin models using linear and non-linear regression. The squared correlation coefficient (R^2) and HYBRIDerror function were used to determine the best adsorption model. It was found that Freundlich model was the best to describe the experimental data of DBT adsorption on CNTAg2S, GOAg2S and CNT while for GO, the best model was Langmuir. The IR spectroscopy was used to study the DBT adsorption mechanism and found that the DBT molecules lie flat on the surface of the developed adsorbents. Significant improvement was achieved in the adsorption of DBT using CNT-Ag2S and GO-Ag_2S where the maximum adsorption capacity increased by 127% and 117% respectively, indicates stronger interaction between DBT and modified adsorbents.

4.3.1 Thermal gravimetric analysis (TGA)

The thermal oxidation of raw and modified CNT and GO was investigated using the TGA. The oxidation parameters were fixed at 10 mg of sample with heating rate of 10 ºC/min and oxidation temperature ranging from 25 to 800 ºC. For the measurement of thermal oxidation of unmodified adsorbent, the sample was heated under atmospheric air with a flow rate of 100 mL min^{-1}. As shown in figure 4-25a, the residual solvents evaporated below 100 ºC while the initial oxidation temperature of raw CNT and GO starts approximately at 550 ºC and 500 ºC; respectively. While the GO thermally exfoliated at around 200 ºC. However the final oxidation temperature for the same materials was at 650 ºC and 700 ºC respectively. The modified CNT and GO start oxidation at around 500 ºC and 400 ºC; respectively. This behavior shows evidence that the presence of silver sulfide nanoparticles accelerates the oxidation of the modified carbon materials. Another experiment was carried out to study the oxidation of silver nitrate and formation of silver oxide under atmospheric air. The results showed that the silver nitrate loaded on the CNT starts oxidizing at around 200 ºC while in the case of GO, oxidation starts at 350 ºC and it completes at around 400 ºC in both cases. The thermal degradation of silver nitrate and its conversion to silver oxide on different carbon materials was also confirmed under nitrogen gas, which gave the same trend of results as shown in figure 4-25b.

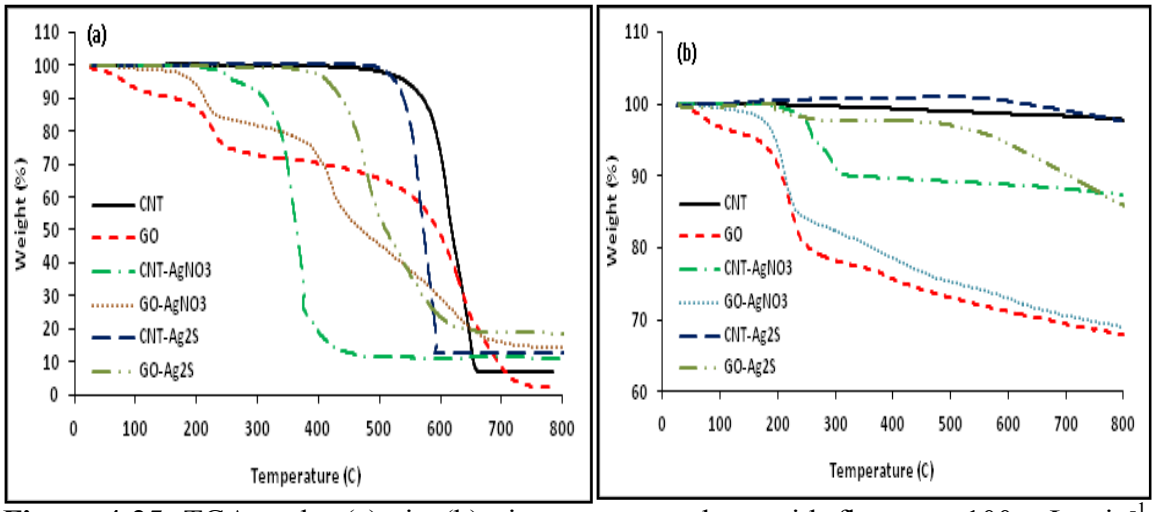

Figure 4-25: TGA under (a) air, (b) nitrogen atmosphere with flow rate 100 mL min^{-1}, for carbonaceous materials impregnated by $AgNO_3$ before and after calcinations.

4.3.2 Adsorbents' texture and morphology

The adsorbent's morphology was characterized using the scanning electron microscope (SEM) and field emission electron microscope (FE-TEM). Figure 4-26a and 4-26b show the SEM images of CNT and GO before modification with silver sulfide nanoparticles, respectively. Figure 4-26c and 4-26d reveals that -after modification- Ag_2S nanoparticles are dispersed homogeneously on the surface of the CNT and the GO sheets.The elemental composition of the Ag_2S-modified CNT and GO adsorbents was obtained by energy dispersive X-ray analysis (EDX) which is summarized in table 4-12. It was found that the GO has higher oxygen content compared to the CNT due to the availability of oxygenated functional groups on the GO surface. In addition, the percent of silver element in the adsorbents is close to the theoretical percentage (10 %) which was considered in the preparation steps.

TEM images for raw and modified CNT and GO are shown in figure 4-27. The TEM was used to characterize the structure of graphene oxide/nanotubes and to observe the silver sulfide particles on their surfaces. It is clear from figure 4-27a that all the nanotubes are hollow and tubular in shape with many deflection sites, while the graphene oxide looks like multilayered flaks as shown in figure 4-27b. Figure 4-27c shows the TEM image of CNT modified with spherical and crystalline silver sulfide nanoparticles with sizes varied from 30 to 80 nm. However, figure 4-27d shows modified GO with silver sulfide nanoparticles with sizes of 10 to 65 nm.

The measured surface areas of the CNT and GO before the impregnation based on the BET method was 217.24 and 10.83 $m^2\ g^{-1}$ respectively, while the pore volumes were

calculated 1.51 and 0.06 mL g^{-1} respectively using the density functional theory (DFT) methods.

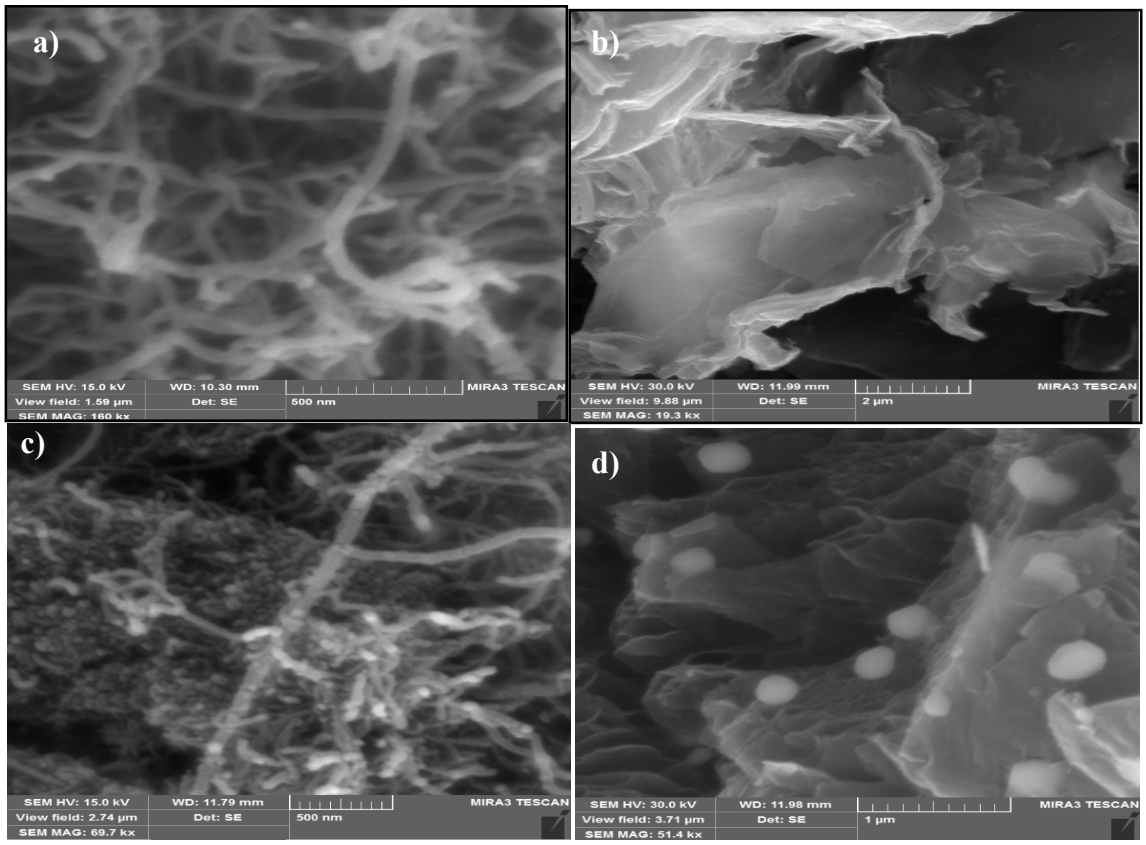

Figure 4-26: SEM images before impregnation of (a) CNT, (b) GO, and after impregnation (c) CNTAg_2S and (d) GOAg_2S

Table 4-12: EDX analysis of raw and modified CNT and GO.

Adsorbents	elements	Weight %
CNT	C	96.48
	O	3.52
CNTAg2S	C	85.31
	O	2.34
	S	2.91
	Ag	9.44
GO	C	79.07
	O	15.65
GOAg2S	C	72.42
	O	13.41
	S	4.03
	Ag	10.14

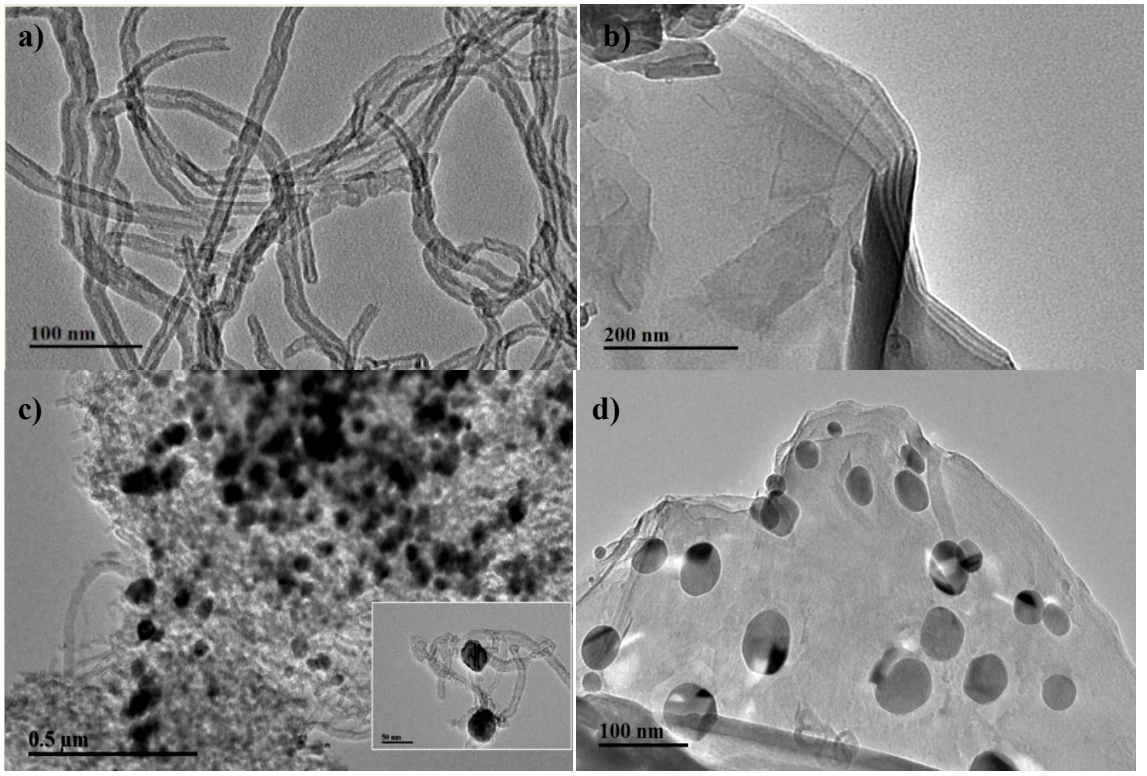

Figure 4-27: TEM images of raw (a) CNT, (b) GO, and modified (c) CNT and (d) GO.

Inset figure is the modified CNT with imaging scale of 50 nm.

For further qualitative evidence the X-ray photoelectron spectrometer (XPS)(Thermo scientific ESCALAB 250Xi) was used to confirm forming of Ag_2S. Figure 4-28 shows the XPS survey spectrum and single element scan for Ag 3d and S 2p respectively. The obtained binding energies are matching the reported XPS fitting values **[112]** for Ag $3d_{5/2}$ and S $2p_{3/2}$ in the Ag_2S at 368.8 and 161.8 eV respectively. The XPS spectrum shows forming some of silver sulfate (S $2p_{3/2}$ around ~168.6 eV) and thiol bonds (S $2p_{3/2}$ ~ 164 eV) in the adsorbents after the modification.

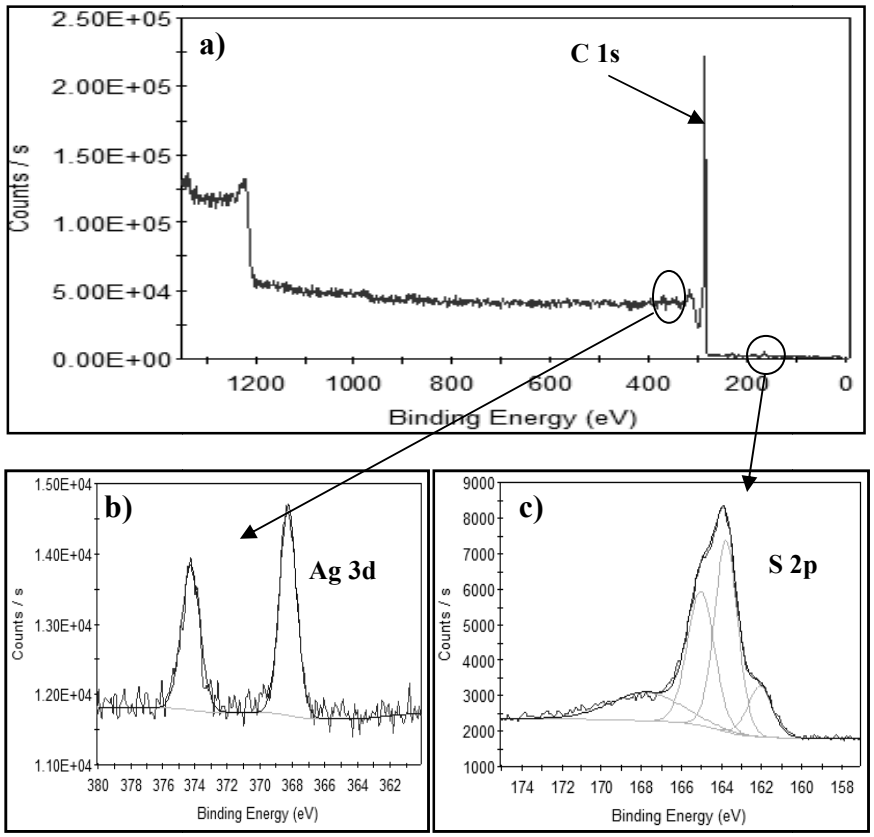

Figure 4-28: (a) XPS survey spectra of $CNTAg_2S$ (b) Ag3d XPS spectra of $CNTAg_2S$ and (c) S2p XPS spectra of $CNTAg_2S$

4.3.3 Adsorption kinetics of dibenzothiophene

The results presented in figure 4-29 show that for all adsorbents a fast adsorption-desorption equilibrium for DBT is reached within 40 minutes of contact time. This can be attributed to the maximum availability of unoccupied active sites on the adsorbents. The adsorption kinetic data for DBT on the prepared adsorbents were fitted using the most frequently used kinetic models reported by Lagergren**[115]** and Ho**[108]**(shown in the experimental section).

The low correlation coefficients and the large difference between the calculated and experimental values of q_e given in table 4-13 show the DBT data do not fit the pseudo-first order kinetic model (PFOM). The correlation coefficients close to or equal to 1 obtained for fits of $\frac{t}{q_t}$ versus t and the closeness of the calculated and experimental values of q_e given in table 3 show the DBT data fit the pseudo-second order kinetic model (PSOM).

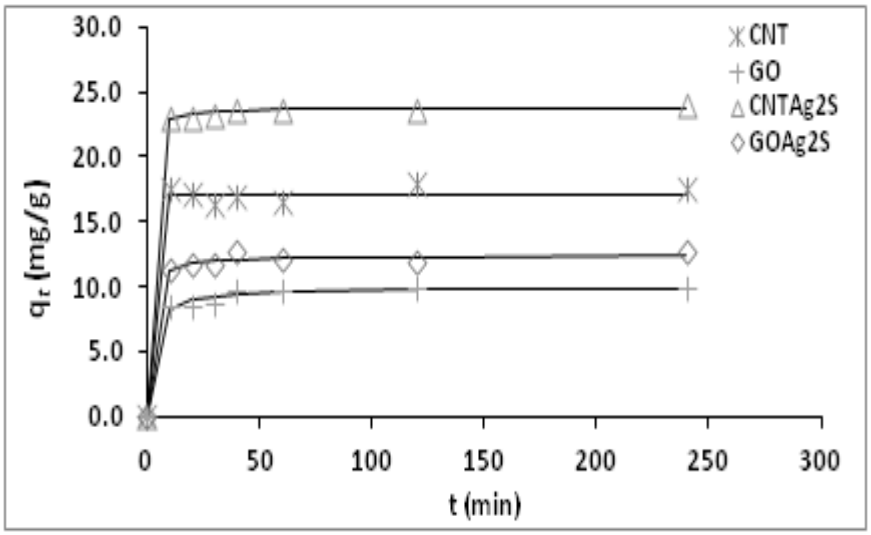

Figure 4-29: The effect of contact time on the adsorption capacity (q_t) of AC and CNT before and after modification with silver sulfide 10 % for DBT. Temperature (25 ºC), shaking speed (200 rpm), adsorbent mass (150 mg) and C_o (250 mg/L). The solid lines are the predicted q_t values.

Table 4-13: The (PFOM).and (PSOM)parameters with the correlation coefficients for DBT adsorption on AC and CNT before and after modification with silver sulfide 10 %

Adsorbent	Pseudo-First order Parameters				Pseudo-Second order Parameters		
	$q_{e\ exp}$	$q_{e\ pred}$	k_1	R^2	$q_{e\ pred}$	k_2	R^2
CNT	17.60	0.72	0.0118	0.4787	17.99	0.0270	0.9978
GO	9.90	2.54	0.0041	0.7505	10.24	0.0281	0.9990
CNTAg2S	24.19	1.13	0.0078	0.7246	23.81	0.0813	1.0000
GOAg2S	12.63	1.13	0.0051	0.4953	11.96	2.2545	0.9992

4.3.4 Adsorption isotherms of dibenzothiophene (DBT)

The adsorption of DBT by raw and modified CNT and GO with 10 wt% $Ag_2S$was investigated in a batch mode at room temperature (25 ºC). Different concentrations of DBT (i. e. 25, 50, 100, 125, 150, 200 and 250 mg L^{-1}) were dissolved in 25 mL of *n*-hexane model diesel while the amount of adsorbent was fixed at 150 mg and the adsorption time for 2 hours. The concentration of DBT before and after the adsorption study was measured using HPLC method coupled with UV detector.

Frequently, the linearized form of the adsorption model is used to determine the isotherm parameters. Freundlich and Temkin isotherms have a specific linear form for each one of them **[102, 104]**. However, the Langmuir isotherm has four different linear forms **[116]**. The original equations for these three isotherm models and their linear forms are summarized in table 4-14. The first and second Langmuir linear forms are the most commonly used forms, since they give the best error distribution as a result of minimal deviation from the experimental data **[116]**. In these models (Freundlich, Langmuir and Temkin), $q_e$is the adsorption capacity at equilibrium in mg g^{-1}, C_e is the concentration of DBT in the solution at equilibrium in mg L^{-1}, $Q_{max}$is the maximum adsorption capacity in mgg^{-1}, and b is Langmuir constant in the Langmuir model. $K_F((mgg^{-1})(Lmg^{-1}))^{1/n}$and n(dimensionless) are the Freundlich parameters where n is a measure of the heterogeneity of the surface of the adsorbent. In Temkin isotherm equation, R is the ideal gas constant in J K^{-1} mol^{-1}, T is the temperature in Kelvin (K), $b_T$is the Temkin constant and A_T is the Temkin isotherm equilibrium binding constantin L g^{-1}.

Table 4-14: List of mathematical equations (original and linear forms) for three isotherm models

Isotherm	Non-linear form	Linear form	Plot	Ref.
Freundlich	$q_e = K_F C_e^{1/n}$	$\ln(q_e) = \ln(K_F) + \frac{1}{n}\ln(C_e)$	$\ln(q_e)\ vs\ \ln(C_e)$	**[102]**
Langmuir	$q_e = \frac{(Q_{max} b C_e)}{(1 + bC_e)}$	$\frac{C_e}{q_e} = \frac{1}{bQ_{max}} + \frac{C_e}{Q_{max}}$	$\frac{C_e}{q_e}\ vs\ C_e$	**[103]**
		$\frac{1}{q_e} = \frac{1}{Q_{max}} + \frac{1}{bQ_{max}C_e}$	$\frac{1}{q_e}\ vs\ \frac{1}{C_e}$	
		$q_e = Q_{max} - \frac{q_e}{bC_e}$	$q_e\ vs\ \frac{q_e}{C_e}$	
		$\frac{q_e}{C_e} = bQ_{max} - bq_e$	$\frac{q_e}{C_e}\ vs\ q_e$	
Temkin	$q_e = \frac{RT}{b_T}\ln A_T C_e$	$q_e = \frac{RT}{b_T}\ln A_T + \frac{RT}{b_T}\ln C_e$	$q_e vs\ \ln C_e$	**[104]**

Figure 4-30 presents the adsorption isotherm of DBT on CNT, GO, $CNTAg_2S$ and $GOAg_2S$ fitted by Langmuir, Freundlich and Temkin isotherm models.

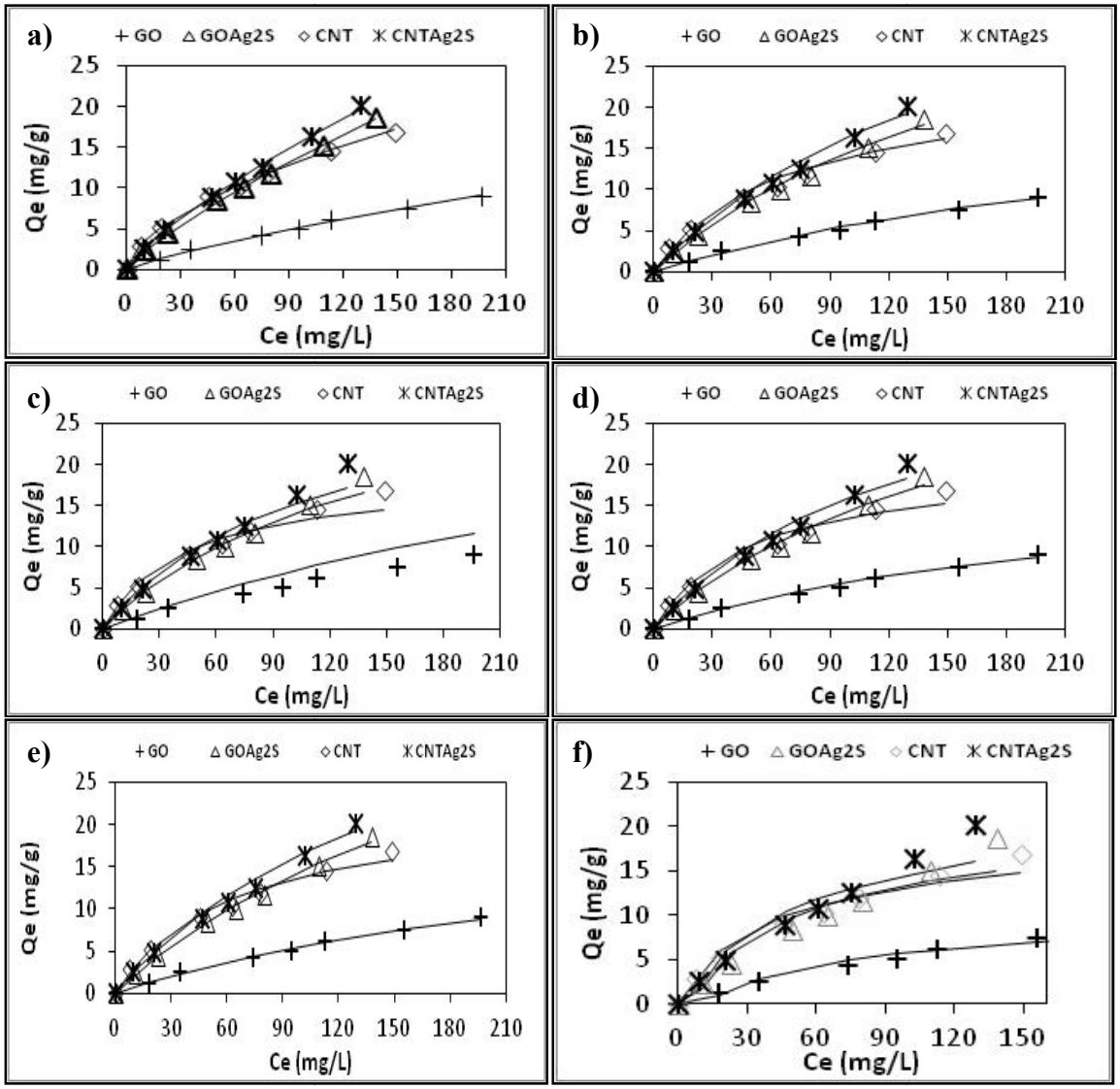

Figure 4-30: Adsorption isotherms of DBT on unmodified and modified CNT and GO. Solid lines are the predicted Q_e values using (a) Freundlich isotherm, (b) Langmuir-1, (c) Langmuir-2, (d) Langmuir-3, (e) Langmuir-4, and (f) Temkin isotherm. Adsorption temperature 25 ºC, mass of adsorbent 150 mg and shaking time 2 hours at speed 200 rpm. Solid linesare the q_e predicted from the corresponding linear form of the corresponding model

The Langmuir model assumes adsorption on a homogeneous adsorbent surface with identical adsorption sites and no interaction between molecules on neighboring sites. Freundlich model is an empirical model describing the multilayer adsorption. This model is the earliest model assumes reversible adsorption on non-uniform distribution of active adsorption site, heat and affinities over a heterogeneous adsorption surface **[105]**. However the earlier isotherm that includes a factor that clearly taking into the account the interaction between the adsorbate and adsorbent, that is Temkin isotherm **[104]** which described the adsorption of hydrogen gas on the platinum surface in acidic media.

In Freundlich isotherm, the n and K_F values give an idea about the degree of surface heterogeneity and the adsorption capacity respectively. Larger n and K_F values correspond respectively to greater heterogeneity on the adsorbent surface and a higher adsorption capacity **[106]**.The model parameters can be calculated from the slope and intercept of an appropriate plot of the linear form as shown in figure 4.31.

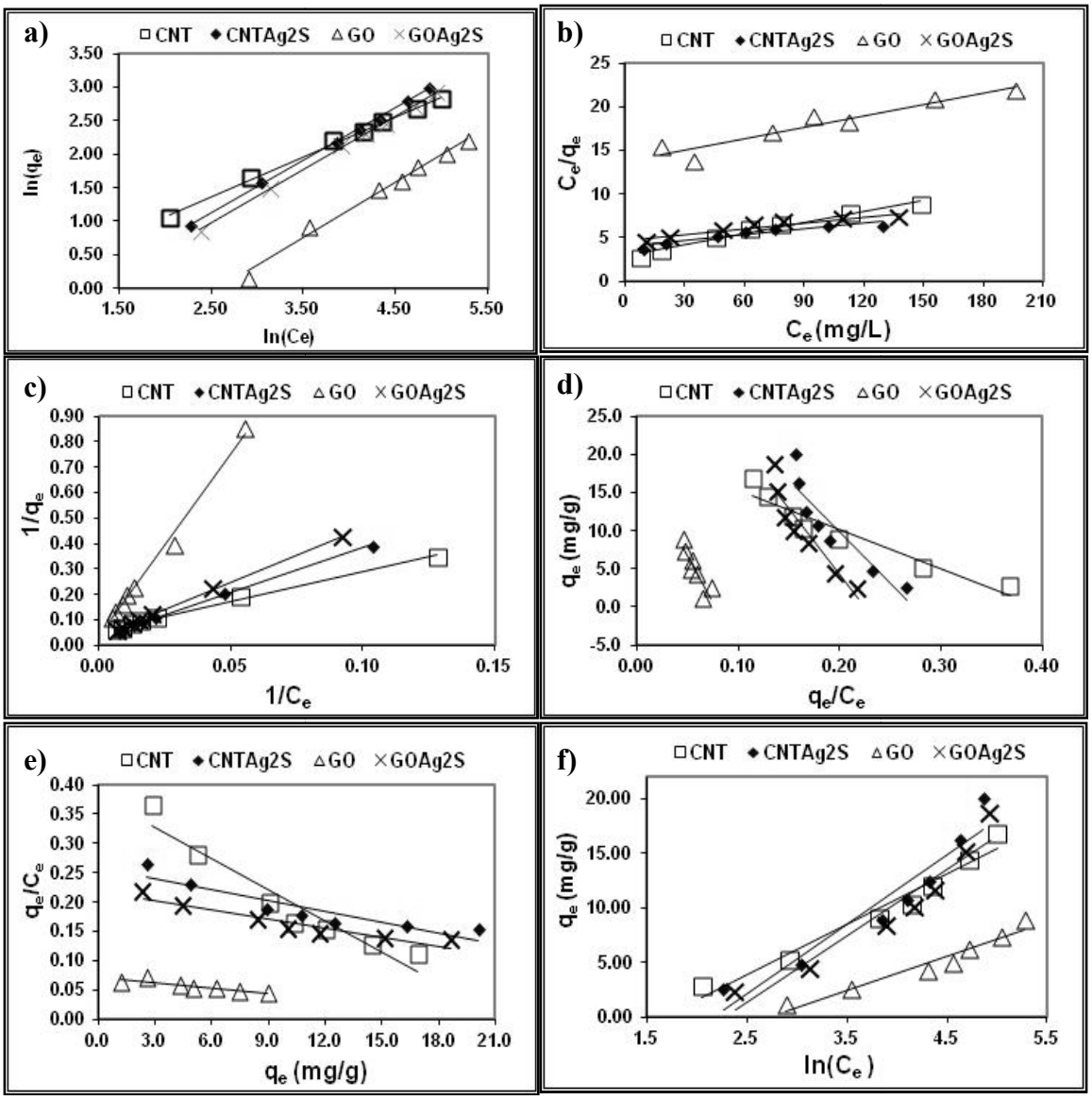

Figure 4-31: Linear least squares fit for (a) Linearized Freundlich model, (b) Langmuir-1, (c) Langmuir-2, (d) Langmuir-3, (e) Langmuir-4 and (f) Temkin linear form. For DBT adsorption on unmodified and modified CNT and GO.

4.3.5 Linear and non-linear of dibenzothiophene adsorption modeling

In the non-linear form, however, the least square method was used in addition to the Solver option in the Microsoft Excel to calculate the isotherm parameters. As summarized in table 4.15, the n and K_F values for DBT on the raw and modified CNT are larger than those of DBT on raw and modified GO, indicating that the surface heterogeneity and adsorption capacity of the CNT before and after the modification are higher than those for GO and $GOAg_2S$. In addition, the modification increased the GO adsorbent surface heterogeneity and adsorption capacity. In contrast, the n valuesfor CNT that were calculated from the non-linear form decreased from 1.7 to 1.3 and K_F decreased from 0.94 to 0.43 after the modification.

Table 4-15: Freundlich, Langmuir and Temkin's parameters for DBT adsorption over raw and modified CNT and GO calculated by the original and linearized forms.

	Linear Form		Original Form			Linear form		Original form	
CNT	**Freundlich**				**GO**	**Freundlich**			
	n [a]	K_F [b]	n	K_F		n [a]	K_F [b]	n	K_F
	1.68 ± 0.04	(8.9 ± *0.5*) X 10^{-1}	1.72	0.9391		1.21 ± 0.06	(1.2 ± *0.2*) X 10^{-1}	1.26	0.1370
	Langmuir-1					**Langmuir-1**			
	Q_{max} [c] mg/g	b [d]	Q_{max} mg/g	B		Q_{max} [c] mg/g	b [d]	Q_{max} mg/g	b
	24 ± *2*	(1.49 ± *0.03*) X 10^{-2}	23	1.50 X 10^{-2}		23 ± *3*	(3.2 ± *0.3*) X 10^{-3}	23	3.18 X 10^{-3}
	Langmuir-2					**Langmuir-2**			
	19 ± *1*	(2.3 ± *0.1*) X 10^{-2}	23	1.50 X 10^{-2}		38 ± *17*	(2 ± *1*) X 10^{-3}	23	3.18 X 10^{-3}
	Langmuir-3					**Langmuir-3**			
	20 ± *2*	(2.0 ± *0.3*) X 10^{-2}	23	1.50 X 10^{-2}		20 ± *3*	(4.1 ± *0.9*) X 10^{-3}	23	3.18 X 10^{-3}
	Langmuir-4					**Langmuir-4**			
	22 ± *5*	(1.8 ± *0.2*) X 10^{-2}	23	1.50 X 10^{-2}		24 ± *7*	(3.2 ± *0.7*) X 10^{-3}	23	3.18 X 10^{-3}
	Temkin					**Temkin**			
	A_T [e]	b_T [f]	A_T	b_T		A_T [e]	b_T [f]	A_T	b_T
	0.986 ± *0.002*	528 ± *49*	0.2250	573		0.9894 ± 0.0007	785 ± *81*	0.0784	863
CNTAg$_2$S	**Freundlich**				**GOAg$_2$S**	**Freundlich**			
	n [a]	K_F [b]	n	K_F		n [a]	K_F [b]	n	K_F
	1.28 ± 0.02	(4.4 ± *0.2*) X 10^{-1}	1.2706	4.29 X 10^{-1}		1.25 ± 0.02	(3.6 ± *0.2*) X 10^{-1}	1.25	0.3632
	Langmuir-1					**Langmuir-1**			
	Q_{max} [c] mg/g	b [d]	Q_{max} mg/g	B		Q_{max} [c] mg/g	b [d]	Q_{max} mg/g	b
	46 ± *7*	(5.6 ± *0.5*) X 10^{-3}	52	4.50 X 10^{-3}		45 ± *6*	(4.8 ± *0.4*) X 10^{-3}	50	4.10 X 10^{-3}
	Langmuir-2					**Langmuir-2**			
	32 ± *4*	(9.2 ± *0.8*) X 10^{-3}	52	4.50 X 10^{-3}		34 ± *3*	(6.9 ± *0.5*) X 10^{-3}	50	4.10 X 10^{-3}
	Langmuir-3					**Langmuir-3**			
	37 ± *5*	(8 ± *2*) X 10^{-3}	52	4.50 X 10^{-3}		39 ± *4*	(5.9 ± *0.9*) X 10^{-3}	50	4.10 X 10^{-3}
	Langmuir-4					**Langmuir-4**			
	44 ± *11*	(6 ± *1*) X 10^{-3}	52	4.50 X 10^{-3}		44 ± *8*	(5.1 ± *0.8*) X 10^{-3}	50	4.10 X 10^{-3}
	Temkin					**Temkin**			
	A_T [e]	b_T [f]	A_T	b_T		A_T [e]	b_T [f]	A_T	b_T
	0.966 ± *0.004*	388 ± *55*	0.146	445		0.967 ± *0.003*	406 ± *53*	0.128	462

[a] The uncertainty was calculated based on the uncertainty in the slope of the Freundlich linearized equation.
[b] The uncertainty was calculated based on the uncertainty in the intercept of theFreundlich linearized equation.
[c] The uncertainty was calculated based on the uncertainty in the slope of the Langmuir linearized equation.
[d] The uncertainty was calculated based on the uncertainty in the intercept of the Langmuir linearized equation
[e] The uncertainty was calculated based on the uncertainty in the slope of the Temkin linearized equation.
[f] The uncertainty was calculated based on the uncertainty in the intercept of the Temkin linearized equation

The highest adsorption capacity Q_{max} (52 mgg^{-1})for DBT was on $CNTAg_2S$ and the others follow the trend$GOAg_2S>CNT \approx GO$ as shown in tables 4-15. The Q_{max} values for modified adsorbents are nearly double those of the raw adsorbents. Within the uncertainties in the Q_{max} values for GO and CNT, it can be safely stated that there is no significant difference in their maximum adsorption capacity. As shown in table 4-16, these adsorbents provide good DBT adsorption capacity compared with other adsorbents reported in the literature used for DBT desulfurization from different model fuel.

Table 4-16: Adsorption capacity of DBT on different adsorbents from different model fuel media.

Adsorbent	Model Fuel	Adsorption Capacity	Reference
AC [1]	*n*-octane	0.2748 *	**[117]**
AC-HNO_3 [2]	*n*-octane	0.2887 *	**[117]**
Nanocrystalline NaY Zeolite	*n*-nonane	6.70**	**[111]**
ACFH-Cu(I) [3]	*n*-hexane	19.00 **	**[96]**
D-MIP/CMSs [4]	*n*-hexane	86.40 ***	**[118]**
GPP [5]	*n*-tetradecane	10.60**	**[22]**
GPH [6]	*n*-tetradecane	5.50 **	**[22]**
AC [1]	*n*-heptane	10.19 ***	**[32]**
ACWS [7]	*n*-heptane	47.10***	**[32]**
Alumina	*n*-hexane	21.02 ***	**[17]**
$CNTAg_2S$	*n*-hexane	52 ***	This work
$GOAg_2S$	*n*-hexane	50 ***	This work

(1) Activated carbon, (2) Activated carbon modified with nitric acid at 90 ºC, (3) Activated carbon fiber thermally treated and modified with copper cation, (4) Carbon microsphere modified with Double molecularly Imprinted Polymer, (5) Graphene prepared using phosphoric acid, (6) Graphene oxide prepared using Hummers's method and (7) Activated carbon treated with steam at 900 ºC then washed by H_2SO_4
(*) the adsorption capacity unit is mmol/g , (**) mg S / g and (***) mg DBT /g

In the adsorption experiments at 250 mg L^{-1}, the removal efficiencies of DBT using CNTAg_2S, GOAg_2S, CNT and GO were 61.48 %, 56.7 %, 41.8 % and 22.7 %; respectively. The increase in the adsorption of DBT from model diesel using carbon adsorbents modified with Ag_2S is a consequence of the introduction of additional acidic adsorption sites. In other words the Ag_2S acts as a Lewis acid in the environment of the soft base DBT. In addition, there is a possibility to form a sulfur-sulfur bond between the sulfur atom in the DBT molecule and the sulfur atom that was introduced on the adsorbent surface after the modification process.

The error structure, error variance and the standard least squares normality assumptions would be clearly altered and violated by the linearization of isotherm models **[119, 120]**. This can be the reason behind better fitting the experimental data with the linear Freundlich isotherm than Langmuir or Temkin isotherm models. To evaluate and later to determine the best isotherm model fitting with the experimental data, two error functions were used: the hybrid fractional error function (HYPRID) as shown in equation (14) **[121]**and the squared correlation coefficient (R^2) as shown in equation (15) **[122]**.

$$\text{Hybrid} = \frac{100}{n-p}\sum_{i=1}^{n}\left[\frac{(q_{e\,exp}-q_{e\,pre})_i^2}{q_{e\,exp}}\right] \tag{14}$$

$$R^2 = \frac{\sum(q_{e\,exp}-\overline{q_{e\,pre}})^2}{\sum(q_{e\,exp}-\overline{q_{pre}})^2+\sum(q_{e\,exp}-q_{e\,pre})^2} \tag{15}$$

where n is the number of data points in the experiment, p is the number of the parameters in the isotherm model, $q_{e\ exp}$ is the experimental adsorption capacity at equilibriumin mg g^{-1}, $q_{e\ pre}$ is the predicted equilibrium adsorption capacity in mg g^{-1} and $\overline{q_{e\ pre}}$ is the average predicted equilibrium adsorption capacity.

As shown in table 4-17, fitting the experimental data for the DBT adsorption on the CNT, GO, $CNTAg_2S$ and $GOAg_2S$ adsorbents by Temkin model using the non-linear form gave the lowest R^2 and the highest HYBRID value. Freundlich model was the best model to fit the experimental data of CNT, $CNTAg_2S$ and $GOAg_2S$. However, the Langmuir original form was the best to describe and fit the experimental adsorption data of GO with a little difference in R^2 and HYBRID from that of Freundlich.

Among the four linear forms of Langmuir model, the second linear form had always the highest R^2 but not the lowest HYBRID. That can be explained by the simplicity of the mathematical structure of the first linear form which can distribute the errors in the qe and Ce but once the difference between these two variables is considered the error re-appear in the HYBRID error function. In general, the linear form assumes a Gaussian distribution of data points around the line and similar error distribution at every point **[123]**. However, this is rarely true for most of the adsorption-isotherm models and eventually the error distribution will change after linearizing the isotherm model. This change in error depends on the linearized form resulting in different parameters for each linearized form.

Table 4-17: The calculated squared correlation coefficient (R^2) and HYBRID error function for different isotherm models presenting the DBT adsorption over modified and unmodified CNT and GO with silver sulfide nanoparticles

CNT				**GO**			
Linear		**Original Form**		**Linear**		**Original Form**	
R^2	**HYBRID**	**R^2**	**HYBRID**	**R^2**	**HYBRID**	**R^2**	**HYBRID**
Freundlich							
0.9966	**1.1834**	**0.9984**	**0.9986**	0.9886	2.2562	0.9959	1.6750
Langmuir -1							
0.9704	5.1446	0.9905	4.6701	0.9064	**1.3496**	**0.9967**	**1.1143**
Langmuir -2							
0.9944	10.5440	0.9905	4.6701	**0.9913**	58.2227	0.9967	1.1143
Langmuir -3							
0.9152	6.9551	0.9905	4.6701	0.8068	2.0216	0.9967	1.1143
Langmuir -4							
0.9152	7.3737	0.9905	4.6701	0.8068	4.0977	0.9967	1.1143
Temkin							
0.9590	1066.9942	0.9905	12.9436	0.9498	2793.7006	0.9649	8.6351
$CNTAg_2S$				**$GOAg_2S$**			
Linear		**Original Form**		**Linear**		**Original Form**	
R^2	***HYBRID***	***R^2***	***HYBRID***	***R^2***	***HYBRID***	***R^2***	***HYBRID***
Freundlich							
0.9993	**0.56**	**0.9989**	**0.53**	**0.9991**	**0.02**	**0.9992**	**0.02**
Langmuir -1							
0.8877	5.71	0.9942	3.89	0.9243	2.96	0.9959	2.20
Langmuir -2							
0.9974	11.97	0.9942	3.89	0.9988	5.98	0.9959	2.20
Langmuir -3							
0.8390	8.42	0.9942	3.89	0.8949	4.00	0.9959	2.20
Langmuir -4							
0.8390	10.34	0.9942	3.89	0.8949	4.44	0.9959	2.20
Temkin							
0.9085	2897.73	0.9333	38.64	0.9194	3654.23	0.9413	32.21

On the other hand, the non-linear method gave the lowest HYBRID and the highest R^2 values for all adsorbents. Hence, we can conclude that the non-linear method is better to be used to obtain the adsorption isotherm's parameters.

4.3.6 Dibenzothiophene adsorption mechanism

FT-IR spectra were carried out to investigate the DBT molecules adsorption's mechanism on the silver sulfide modified carbon materials. Figure 4.32 shows the FT-IR spectra for raw CNT and GO, and the DBT IR spectrum given as inset in the same figure as reference. Figure 4.33 represents the FT-IR spectra of DBT adsorbed on CNT-Ag_2S or GO-Ag_2S after performing the adsorption experiments. The band at about 3450 cm^{-1} represents the stretching vibration of surface hydroxyl group in the GO **[124]**, whereas the shift from 3458 cm^{-1} to 3433 cm^{-1} after DBT adsorption indicates that some of DBT molecules interact with hydroxyl group via H-bonding **[124]**. The strong peaks at 1565 cm^{-1} and 1726 cm^{-1} are attributed to the presence of Bronsted acid and carbonyl groups respectively on the surface of the raw GO and the decrease in their intensities after DBT adsorption may be attributed to interacting DBT -has basic nature- with these acidic groups. At the low frequency region, the peak shift from 740 cm^{-1} in the DBT FT-IR spectrum -inset of figure 32- to 725 cm^{-1} and 735 cm^{-1} after DBT adsorption on GO-Ag_2S and CNT-Ag_2S respectively indicates that DBT molecules mainly lie flat on their surface **[125]**, as illustrated in figure 4.34.

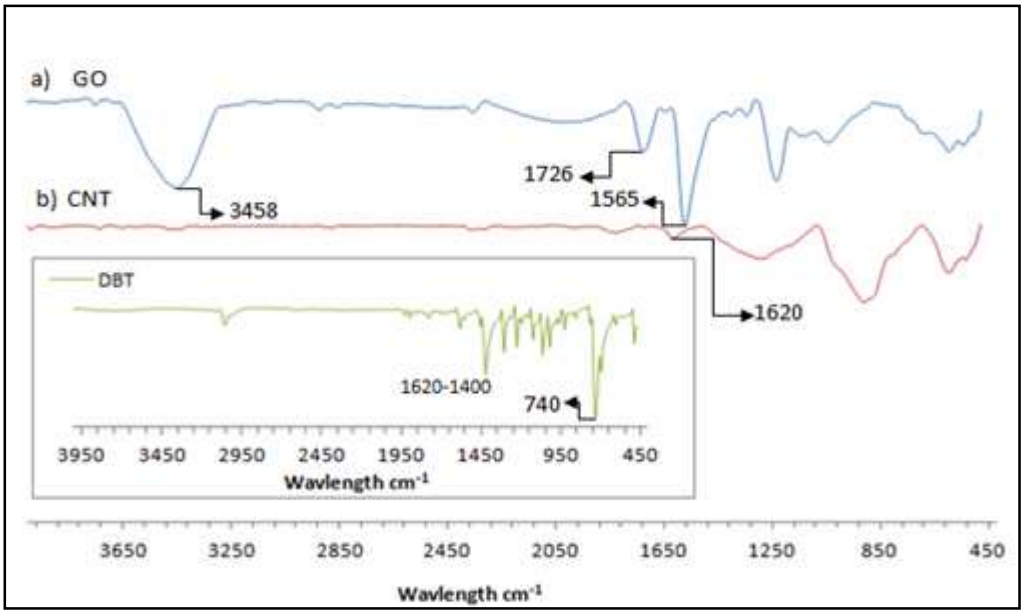

Figure 4-32:FT-IR spectra of raw a) GO and b) CNT. Inset figure is IR spectrum of standard solid DBT

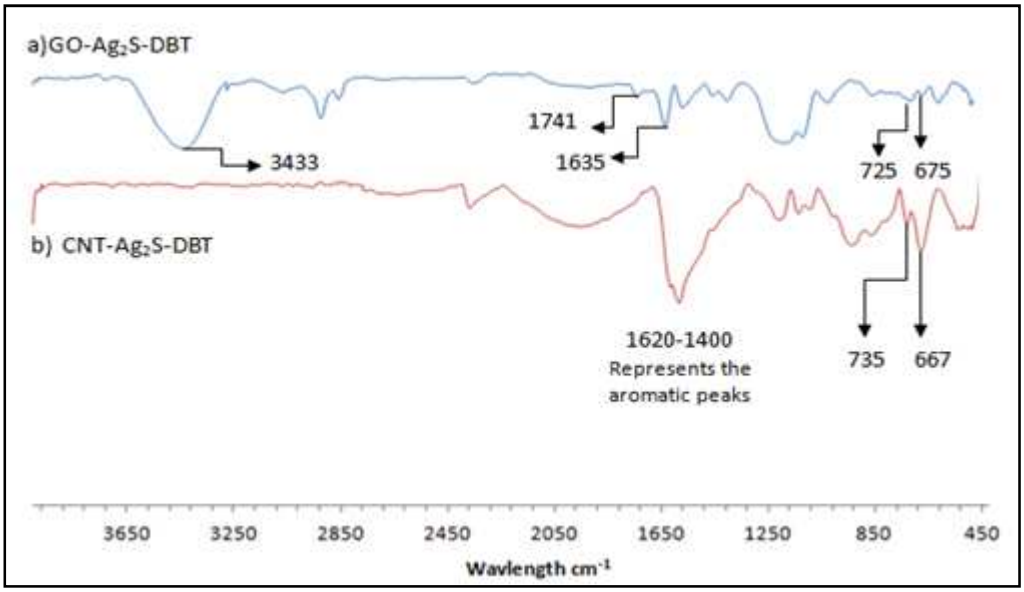

Figure 4-33:FT-IR spectra of DBT adsorbed on a) GO-Ag_2S and b) CNT-Ag_2S

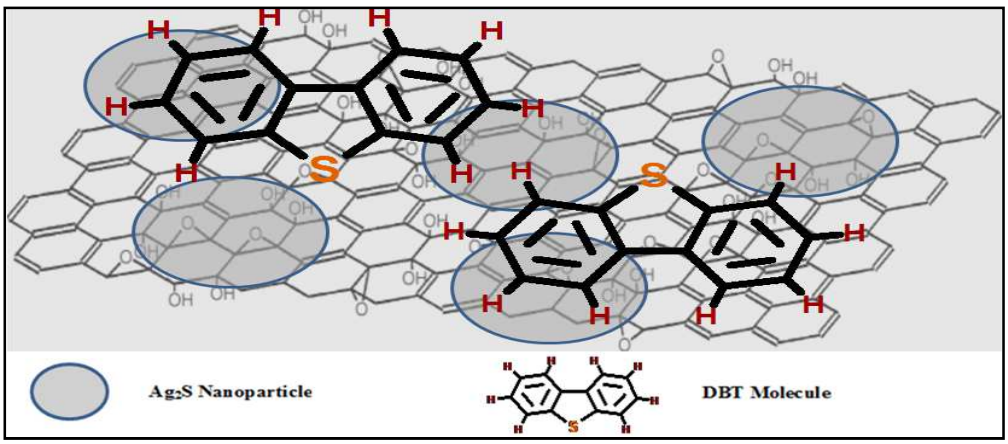

Figure 4-34: Schematic illustrates adsorption state of DBT (lie on flat) on the surface of GO-Ag_2S

4.3.7 Conclusion

Two different types of carbonaceous adsorbents namely CNT and GO modified with Ag_2Swere prepared using the CVD technique. The removal of DBT from *n*-hexane as a simulant of diesel fuel was improved using the modified adsorbents where the maximum adsorption capacity increased 127 % and 117 % for the CNTAg_2S and GOAg_2S; respectively. The adsorption kinetics data of DBT fit the pseudo-second order kinetic model. The highest removal efficiency of DBT was achieved using the CNTAg_2S adsorbent with amaximum adsorption capacity of52.18mg DBT g^{-1}. It was found that Freundlich model was the best to describe the experimental data of DBT adsorption on CNTAg_2S, GOAg_2S and CNT, while the Langmuir model was the best for GO.In addition, the nonlinear form of adsorption models was almost better than the linearized form in fitting the experimental data. The removal of DBT using the new nanocomposite adsorbents compared favorably with that reported in the literature.

4.4 Adsorption Isotherms and Kinetics for Dibenzothiophene on Activated Carbon and Carbon Nanotube Loaded with Nickel Oxide Nanoparticles

Anchoring an additional adsorption site, such as low cost nickel oxide (Lewis acid) nanoparticle on the surface of promising adsorptive material such as carbon nanotube which has distinct properties, is expected to improve the adsorption capability for sulfur compounds such as DBT (Lewis base), thereby providing a new adsorbent. This section discusses the adsorption capacity of CNT modified with different loadings of nickel oxide nanoparticles for the removal of DBT and thiophene from a model fuel. The selectivity of CNT and activated carbon for DBT were compared before and after doping CNT and activated carbon with 5 % nickel oxide nanoparticles; the loading that gave the highest adsorption capacity. The reusability of the adsorbents and the effect of aromatic compounds on their adsorption capacity were also studied. The prepared adsorbents were characterized using a thermal gravimetric analysis (TGA), N_2 adsorption-desorption surface area analyzer, scanning electron microscope (SEM), energetic dispersive X-ray diffractogram (EDX), Field Emission Electron Microscope (FE-TEM),X-ray diffractometer instrument (XRD) and X-ray photoelectron spectrometer (XPS) techniques.

4.4.1 Thermal gravimetric analysis of adsorbents

Thermal gravimetric analysis (TGA) was used to study the degradation of raw and doped AC and CNT under atmospheric air. The experimental results were used toconfirm the conversionof nickel nitrate hexahydrate $Ni(NO_3)_2.6H_2O$ to nickel oxide. For each measurement, approximately a 10 mg sample was heated from room temperature to 800 ºC at a rate of 10 ºC/min under air with a flow rate of 100 mL/min. As shown in figure 4-35, the initial oxidation temperatures of pristine AC and CNT start at 400 ºC and 500 ºC and are complete at 600 ºC and 650 ºC respectively. In the case of impregnated AC and CNT with 10 % Ni in the form $Ni(NO_3)_2.6H_2O$ the $Ni(NO_3)_2.6H_2O$ starts decomposing at around 90 ºC. An approximate 11% decrease in weight was observed at 200 ºC mainly asa result of removing water molecules from $Ni(NO_3)_2.6H_2O$. The formation of nickel oxides starts at about 200 ºC and is complete at about 300 ºC which is in line with the finding of W. Brockner et al.**[126].** Subsequently, the burning of AC and CNT starts at 380 ºC and 400 ºC respectively and is completed at 420 ºC and 560 ºC respectively. Clearly doping AC and CNT with nickel nitrate lowers their oxidation temperatures. The weight loss following the conversion of nickel nitrate hexahydrate to nickel and the oxidation of the carbon materials was around 87 %. The TGA results of doped AC and CNT with nickel oxide show no weight loss in the temperature ranges from 25 ºC to 380 ºC and from 25 ºC to 400 ºC respectively. On the contrary, the loss ofabout 87 % from the original weight of doped AC and CNT at 420 ºC and 560 ºC respectively indicates oxidation of AC and CNT.

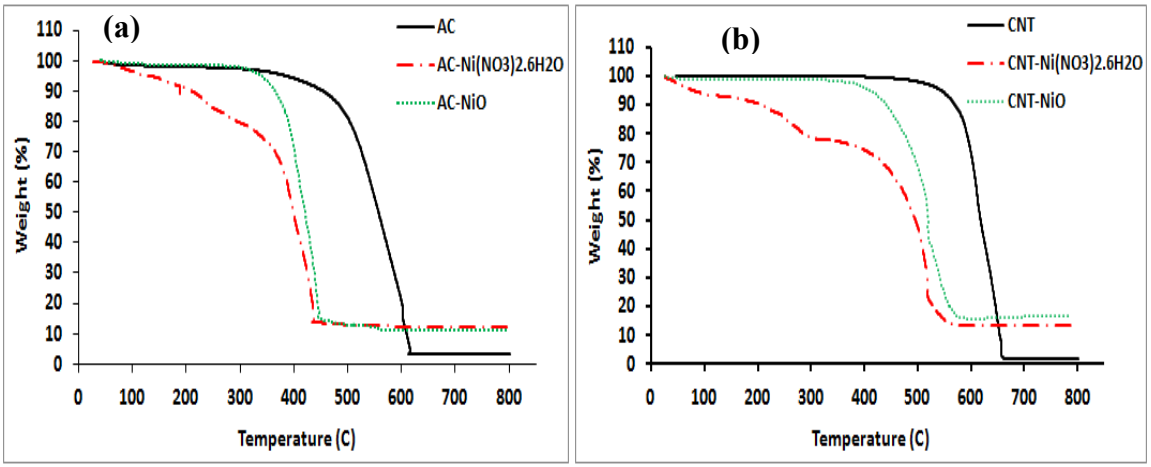

Figure 4-35: TGA under atmospheric air with 100mL/min flow rate, before and after $Ni(NO_3)_2$ calcinations on (a) AC and (b) CNT.

4.4.2 Surface morphology and textureof adsorbents

The adsorbents' morphology was studied using a scanning electron microscope SEM and a Field Emission Electron Microscope (FE-TEM). Figure 4-36 shows the SEM images of AC and CNT before and after doping with 10 % nickel oxide. Needle-like nickel oxide nanoparticles were observed on the surface of AC while spherically shaped nanoparticles of nickel oxide were observed on the surface of CNT. Table 4-18 presents the elemental composition of the doped carbon adsorbents obtained from an energy dispersive X-ray analysis (EDX). It was found that AC has a higher oxygen content compared to CNT due to availability of oxygenated functional groups on its surface. As a result of doping with nickel oxide the oxygen percentage in the adsorbents increased. Table 4-18 also shows that, the weight percentages of nickel obtained from EDX are in good agreement with the experimentally expected values (1 %, 5 % and 10 %). The TEM images shown in figure 4-37 for raw and doped CNT with different nickel oxide percentages were used to characterize the structure of the nanotubes and to observe the distribution of nickel oxide particles on their surfaces. The images show that the nanotubes have many deflection sites. They also show that the nickel oxide nanoparticles on the surface of doped CNT were spherical and varied in diameter from 10 to 60 nm.

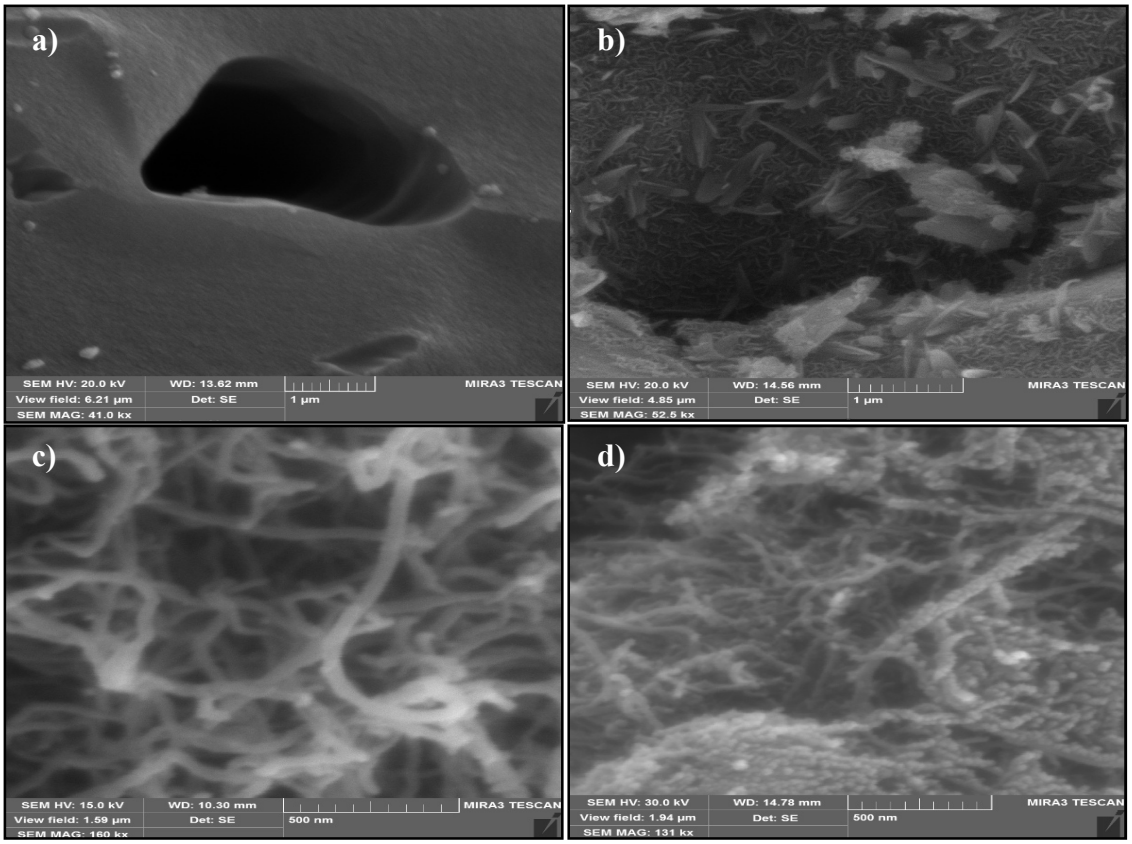

Figure 4-36: SEM photograph for AC (a) before, (b) after and for CNT (c) before and (d) after impregnation with nickel oxide.

Table 4-18: Weight percent of nickel in the loaded carbon materials adsorbents compared to the theoretical percentage of nickel.

Adsorbent	Element	Weight %
AC	C	92.01
	O	7.99
ACNI10	C	75.36
	O	13.36
	Ni	11.28
ACNI5	C	79.48
	O	15.73
	Ni	4.79
ACNI1	C	89.08
	O	9.56
	Ni	1.36
CNT	C	97.33
	O	2.67
CNTNI10	C	84.43
	O	5.83
	Ni	9.74
CNTNI5	C	90.68
	O	4.53
	Ni	4.79
CNTNI1	C	94.97
	O	4.06
	Ni	0.97

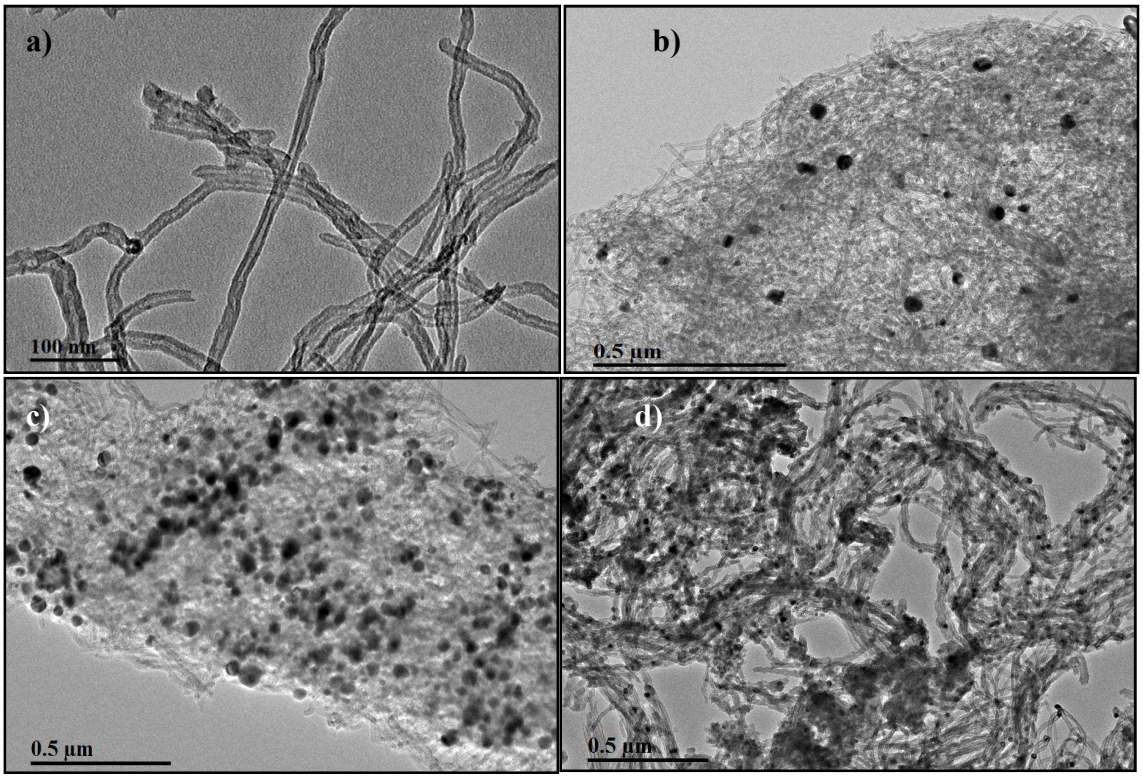

Figure 4-37: EF-TEM image for CNT (a) before and (b) after impregnation by 1% (c) 5% and (d) 10 % NiO.

The XRD spectra were obtained using an X-ray diffractometer with a CuKα source with a 2θ angle in the range 10 º to 100 º. As figure 4-38 shows, there is a distinct carbon peak at 25.89 º in three spectra; one for unmodified CNT and two for modified CNT (before and after calcination). Figure 4 also shows that after calcination the characteristics peaks for nickel nitrate disappear and broad distinct peaks characteristic of NiO appear at 2θ angles of 36.2 º, 43.2 º, 62.07 º,74.7 º and 78.7 º. The low peak intensity and broadening **[127]** indicates that the nickel oxide particles in the doped CNT fall in a low nano size range.

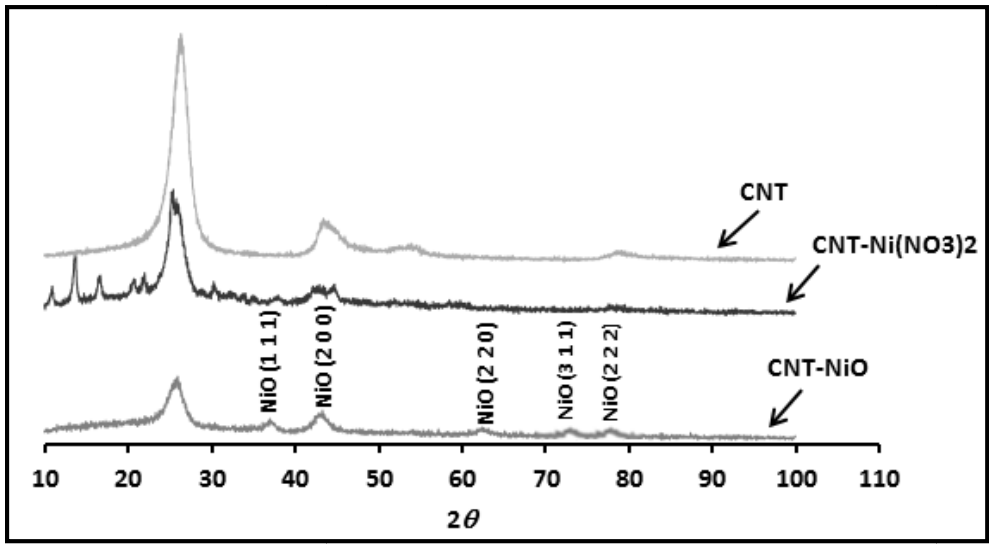

Figure 4-38: XRD for CNT before and after impregnation

Figure 4-39 shows the X-ray photoelectron spectrometry (XPS) survey spectrum and the single element scan for Ni 2p. The survey spectrum confirms the presence of the carbon, oxygen and nickel. The binding energies obtained for Ni $2p_{1/2}$ at 856.0, 861.5 and for Ni $2p_{3/2}$ at 873.8 881.8 eV match the reported binding energy values for NiO in the XPS fitting online library**[112].** The observed small peaks at 853.1 and 870.2 eV for Ni $2p_{1/2}$ and Ni $2p_{3/2}$ respectively match the reported binding energy for Nimetal. This might be attributed to the formation of trace of nickel metals in its zero oxidation state through the preparation process.

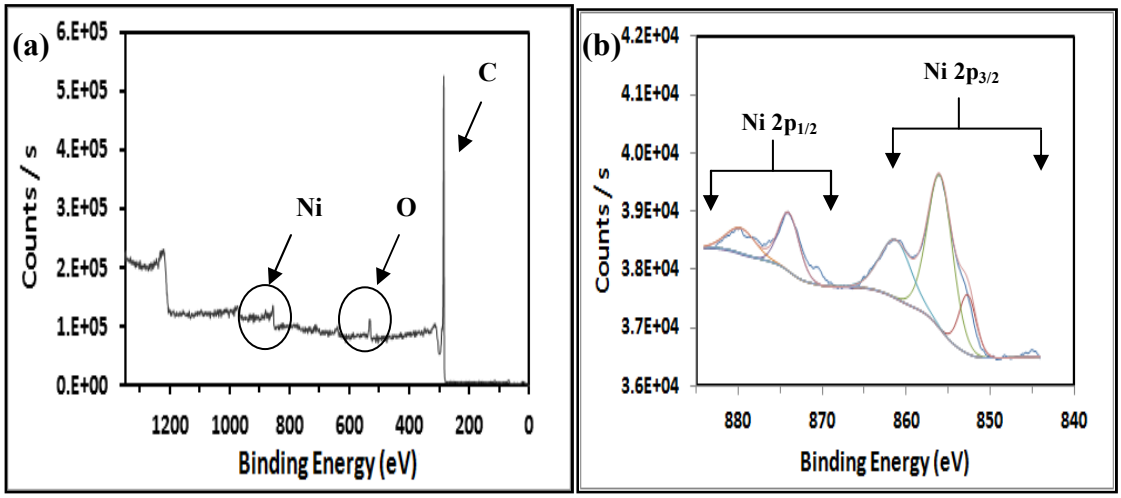

Figure 4-39: (a) XPS survey spectra of CNTNI10 (b) Ni2p high resolution XPS spectra of CNTNI10.

As shown in figure 4.40 the raw and modified AC and CNT exhibit type IV and V N_2 adsorption isotherms respectively on the basis of the Brunauer, Deming and Teller (BDDT) classification **[109]**.In allisotherms a hysteresis loop was either absent or too slight to be discerned,which reflects the near absence of a mesoporous structure, was observed. Table 4-19 presents the surface areas (SA) of and the results of micropore analyses for the adsorbents on the basis of BET and V-t methods of analysis respectively. The V-t method procedure is same as BET surface area measurement, but it extends the pressure range to higher pressures to permit calculation of the external surface area, that is, the non-microporous part of the material. It has been observed that, the highest surface area is for ACNI1 and the other activated carbon based adsorbents follow the order AC > ACNI10 > ACNI5 with a little decrease in the surface area after modification with nickel oxide. However, in case of the carbon nanotube based adsorbents the surface areas follow the trend CNT > CNTNI1 > CNTNI10 > CNTNI5. The same trend was observed in the adsorbents' micropore surface area while the adsorbents' micropore volumes (V) follow the order AC > ACNI1 > ACNI10 > ACNI5 > CNTNI1. On the other hand, microporosity has not been observed in CNT, CNTNI10 and CNTNI5. The decrease in the surface areas and micropore volumes of doped AC and CNT is attributable to the blocking of their pores at high percentages of nickel oxide.

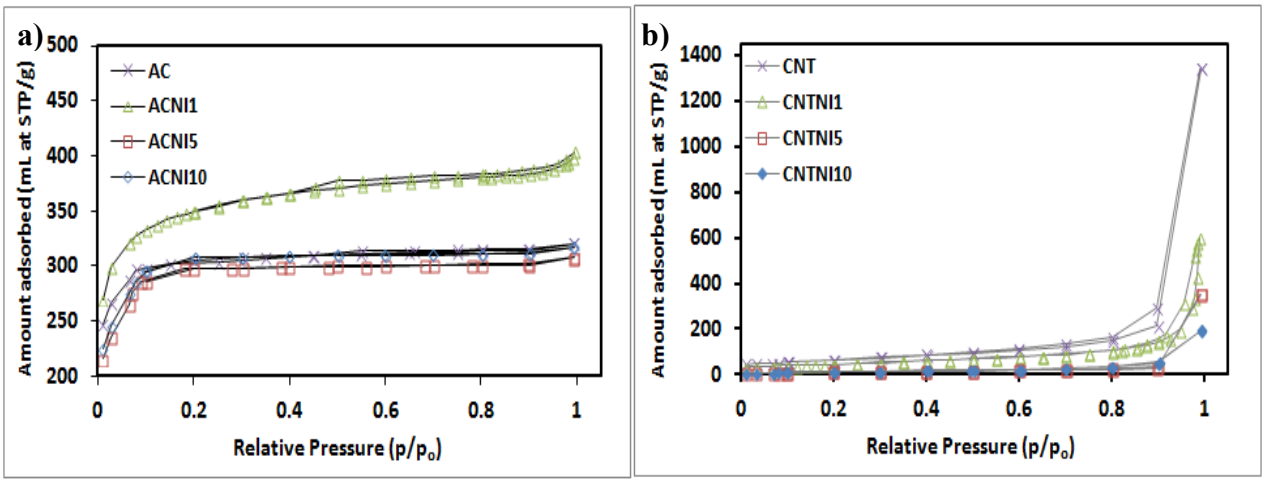

Figure 4-40: The N_2 adsorption isotherm at 77 K on unmodified and modeified (a) AC and (b) CNT with nickel oxide

Table 4-19: Surface area, micropore's surface area and volume and surface pH of AC and CNT at different loading percentage of nickel oxide

		BET	V-t Method	
Adsorbent	**pH**	**SA(m^2/g)**	**Micropore Volume (mL/g)**	**Micropore SA (m^2/g)**
AC	9.35	882	0.466	865
ACNI10	8.97	825	0.379	792
ACNI5	8.21	745	0.377	699
ACNI1	8.44	1080	0.384	921
CNT	5.81	217	-------	195
CNTNI10	5.68	118	-------	99
CNTNI5	5.75	90	-------	69
CNTNI1	5.58	162	0.011	134

4.4.3 Adsorption isotherms ofdibenzothiophene and thiophene

The adsorption isotherms of were obtained at room temperature (25 ºC). The method involves adding a 150 mg sample of adsorbent to a solution of a known concentration of thiophene in *n*-hexane as a model fuel. This system is agitated at 200 rpm for 2 hours then allowed to settle. This system is filtered and the concentration of thiophene in the filtrate is measured using HPLC and the amount of adsorbed thipohene is calculated. This was carried out for different concentrations of thiophene (25, 50, 100, 125, 150, 200 and 250 mg/L) on the adsorbents AC, ACNI10, ACNI5, ACNI1, CNT, CNTNI10, CNTNI5 and CNTNI1. The same procedure was carried out for DBT using the same concentrations and the same adsorbents.

Figures (4-41 & 4-42)respectively show the Feundlich and Langmuir fits for the adsorption of thiophene and DBT on AC, ACNI10, ACNI5, ACNI1, CNT, CNTNI10, CNTNI5 and CNTNI1. The Langmuir model (equation 1) assumes a homogeneous adsorbent surface with the same adsorption energy and with no interaction between molecules adsorbed on neighbor siteswhile The Freundlich model (equation 4) assumes that the adsorption takes place at a heterogeneous adsorbent surface with a multi-layer adsorption capacity**[105].**

The maximum adsorption capacity (Q_{max})for each adsorbent was obtained from the slope of the linearized Langmuir model (equation. 2). The n value for each adsorbent was obtained from the slope of the linear least square fit of ln (q_e) versus ln(C_e) (equation 5) while the intercept was used to calculate the Freundlich constant (K_F). The uncertainties in the parameters of the Langmuir and Freundlich isotherms and of pseudo second order kinetics were calculated using the uncertainties in the slopes and intercepts of the

corresponding linear least squares fits. Each parameter was calculated three times; using the relevant slope (or intercept) and its minimum and maximum values. The standard deviation calculated from those three values was taken as an estimate of the uncertainty in the parameter calculated from the slope (or intercept). *n*and K_F values give an idea about the degree of surface heterogeneity and the adsorption capacity respectively. Larger *n*and K_F values correspond respectively to greater adsorbent surface heterogeneity and higher adsorption capacity.**[106]**. As shown in table 4-20 the *n* and K_F values for thiophene adsorption on modified adsorbents with nickel oxide nanoparticles are larger than those of unmodified carbon adsorbents, indicating the modification increases the adsorbent's surface heterogeneity and adsorption capacity for thiophene. While K_F increased for modified adsorbents reflecting a higher adsorption capacity for thiophene molecules on them relative to unmodified adsorbents. However, the n and K_F values for DBT on unmodified and modified adsorbents did not differ appreciably but were higher than those for thiophene which indicates that DBT has a better tendency for adsorption and in turn a higher adsorption capacity.

For the adsorption of DBT the Freundlich fits had comparable or slightly higher squares of correlation coefficients than the Langmuir fits. This consistency with both models reflects the complexity and non-uniformity of the adsorbents' and the predominance of multilayer adsorption. For thiophene only the Freundlich model fitted the adsorption results well possibly due to the weaker interaction of thiophene, relative to DBT, with the adsorbents.

It was found that, the highest adsorption capacity (74± *5* mg/g)was for ACNI5 and the others follow the trend ACNI1> ACNI10 >AC > CNTNI5> CNTNI1 >CNTNI10

> CNT. Except for ACNI1 impregnation of AC and CNT with nickel oxide generally reduced their surface area and pore volume. Probably the absence of agglomeration of the nickel oxide in ACNI1 and in turn the absence of blocking of pores led to an increase in its surface area. The increase in the overall adsorption of DBT on modified AC and CNT relative to unmodified AC and CNT is in the main attributable to the active nickel oxide sites. The main contribution of carbon materials used in the adsorption process is in enhancing direct adsorption of thiophene and dibenzothiophene compounds through π-π and van der Waals interactions with the surface of unmodified carbon materials. Furthermore, their large surface area assists in improving the dispersion of nickel oxide nanoparticles, which in turn increase the uncovered active nickel oxide sites on the modified carbon materials. The acidic nature of Ni^{+2} makes it play a major role in improving the adsorption of DBT (Lewis base) through the acid-base interaction through direct sulfur metal bond or π-complexation between Ni^{+2} and thiophenic aromatic rings**[96]**.

As depicted in figure 4-43, the maximum enhancement in the AC and CNT adsorption capacities was after modification with 5 % percentage loading of nickel oxide. The Q_{max} of unmodified AC adsorbent for DBT was enhanced by about 78 % after the modification with 5% nickel oxide loading percentage. While the enhancement in Q_{max} of unmodified CNT was approximately 62 % after the modification with 5 % nickel oxide nanoparticles. The slight improvement in the adsorption capacities AC and CNT modified with 10 % nickel oxide may be attributed to the agglomeration of the nanoparticles, which in turn led to a decrease in the active adsorption sites on the adsorbents' surface.

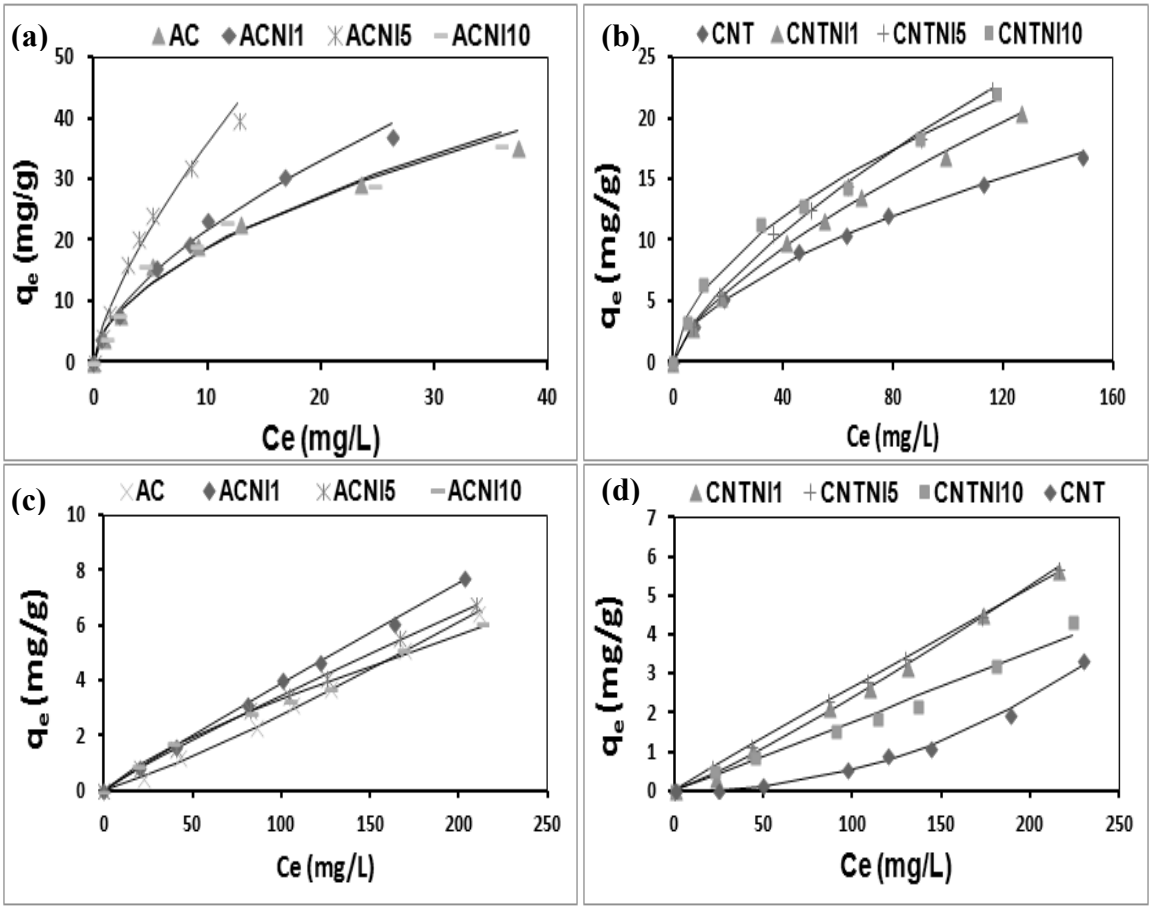

Figure 4-41: Adsorption isotherms of (a) DBT on AC, ACNI1, ACNI5 and ACNI10, (b) DBT on CNT, CNTNI1, CNTNI5 and CNTNI10, (c) Thiophene on AC, ACNI1, ACNI5 and ACNI10 and (d) thiophene on CNT, CNTNI1, CNTNI5 and CNTNI10 at 25 ºC. The solid lines are fits to the Freundlich model

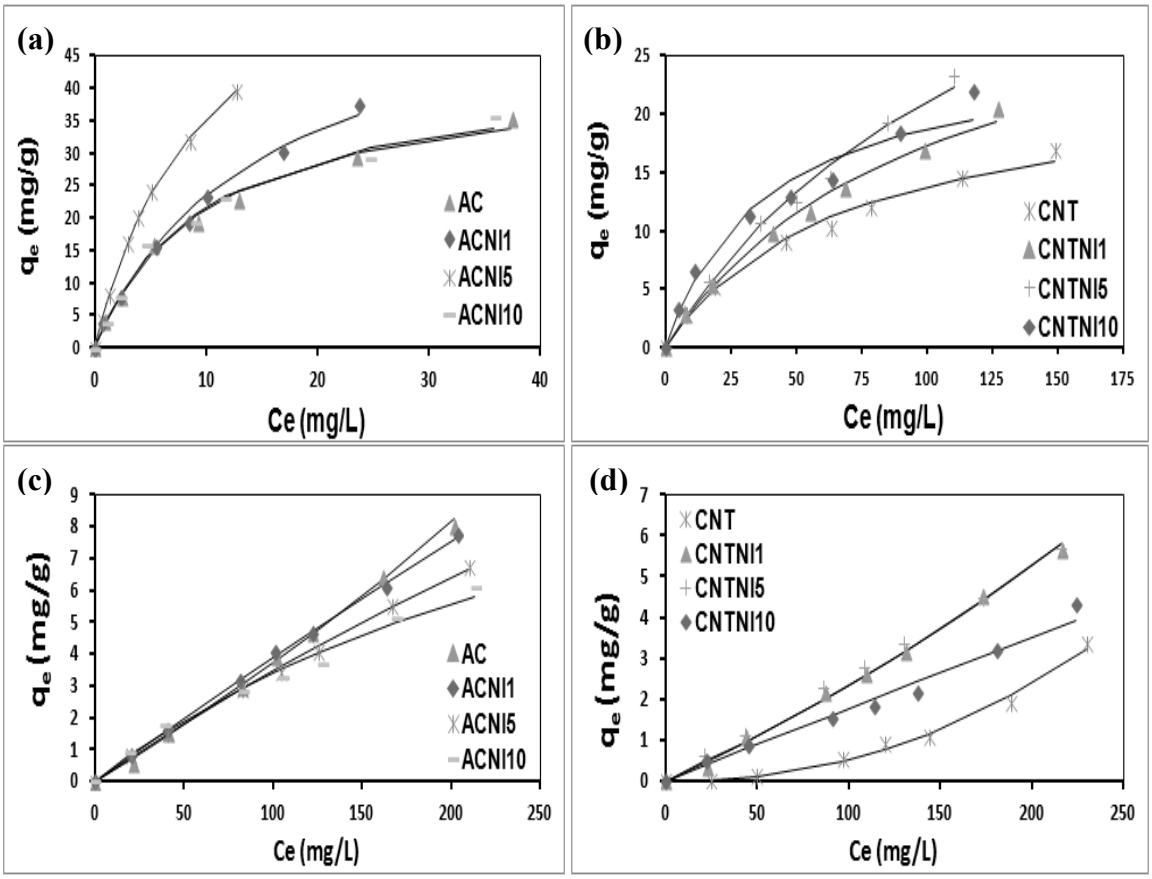

Figure 4-42: Adsorption isotherms of (a) DBT on AC, ACNI1, ACNI5 and ACNI10, (b) DBT on CNT, CNTNI1, CNTNI5 and CNTNI10, (c) Thiophene on AC, ACNI1, ACNI5 and ACNI10 and (d) Thiophene on CNT, CNTNI1, CNTNI5 and CNTNI10 at 25 ºC. The solid lines are fits to the Langmuir model

Table 4-20: Freundlich and Langmuir parameters correlation coefficient for thiophene and DBT adsorption on pristine MWCNT and MWCNT impregnated with nickel oxide

Adsorbent	Freundlich					
	Thiophene			DBT		
	n^a	K_f^b ($mg^{(1-1/n)}$ mg^{-1} $L^{1/n}$)	R^2	n^a	K_f^b ($mg^{(1-1/n)}$ mg^{-1} $L^{1/n}$)	R^2
AC	0.83 ±*0.04*	(1.1± *0.3*) x 10^{-2}	0.9898	1.7 ±*0.1*	4.9 ± *0.5*	0.9747
CNT	0.45 ±*0.02*	(2.0 ± *0.8*) x 10^{-5}	0.9934	1.69 ±*0.04*	(8.9 ± *0.5*) x 10^{-1}	0.9968
ACNI10	1.30 ±*0.06*	(10 ± *2*)x 10^{-2}	0.9897	1.7 ±*0.2*	4.8 ± *0.7*	0.9480
ACNI5	1.12 ±*0.02*	(5.6 ± *0.3*)x 10^{-2}	0.9989	1.29 ±*0.09*	6.4 ± *0.5*	0.9782
ACNI1	1.02 ±*0.01*	(4.3 ± *0.3*)x 10^{-2}	0.9991	1.59 ±*0.05*	5.1 ± *0.2*	0.9948
CNTNI10	1.12 ±*0.06*	(3.0 ± *0.7*)x 10^{-2}	0.9856	1.80 ±*0.09*	1.5 ± *0.2*	0.9880
CNTNI5	1.03 ±*0.02*	(3.0 ± *0.2*)x 10^{-2}	0.9986	1.39 ±*0.03*	(7.5 ± *0.5*)x 10-1	0.9976
CNTNI1	0.88 ±*0.04*	(1.3 ± *0.3*)x 10^{-2}	0.9908	1.45 ±*0.02*	(7.4 ± *0.3*)x 10-1	0.9992
Adsorbent	**Langmuir**					
	Thiophene			**DBT**		
	Q_{max}^c (mg/g)	b ^{d}(dm^3/mg)	R^2	Q_{max}^c (mg/g)	b ^{d}(dm^3/mg)	R^2
AC	-------	-------	0.4657	42 ± *3*	(1.07 ± *0.06*) x 10^{-1}	0.9795
CNT	-------	-------	0.6969	24 ± *2*	(1.5 ± *0.1*) x 10^{-2}	0.9702
ACNI10	14 ± *3*	(3.4 ± *0.4*) x 10^{-3}	0.8110	48 ±*3*	(8.2 ± *0.2*)x 10^{-2}	0.9850
ACNI5	31 ± 7	(1.3 ± *0.2*) x 10^{-3}	0.8208	74 ±*5*	(9.4 ± *0.3*)x 10^{-2}	0.9793
ACNI1	-------	-------	0.4975	53 ±*5*	(8.42 ± *0.08*)x 10^{-2}	0.9556
CNTNI10	-------	-------	0.1792	28 ±*3*	(2.3 ± *0.1*)x 10^{-2}	0.9337
CNTNI5	-------	-------	0.1287	39 ±*3*	(1.05 ± *0.03*)x 10^{-2}	0.9616
CNTNI1	-------	-------	0.4191	34 ±*3*	(1.07 ± *0.03*)x 10^{-2}	0.9542

(a) The uncertainty was calculated based on the uncertainty in the slope of the Freundlich linearized equation.
(b) The uncertainty was calculated based on the uncertainty in the intercept of theFreundlich linearized equation.
(c) The uncertainty was calculated based on the uncertainty in the slope of the Langmuir linearized equation.
(d) The uncertainty was calculated based on the uncertainty in the intercept of the Langmuir linearized equation

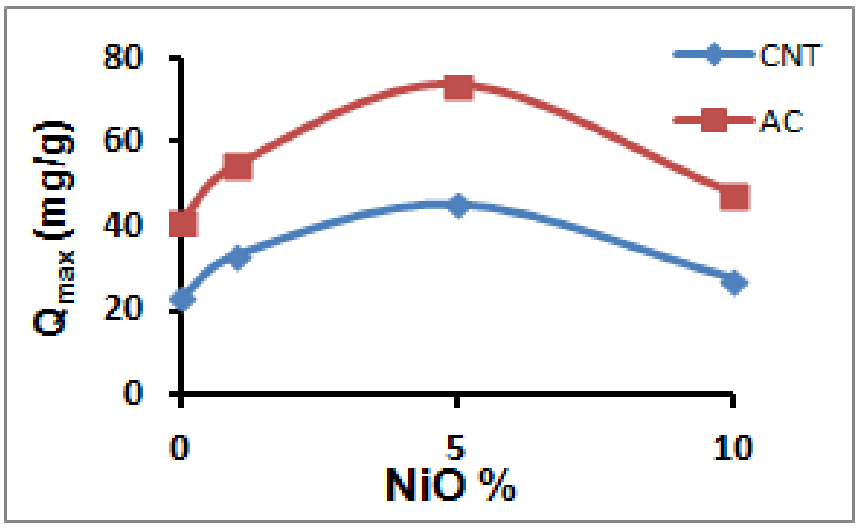

Figure 4-43: Effect of nickel oxide loading percentage on the adsorption capacities of AC and CNT

4.4.4 Adsorption kinetics of dibezothiophene and thiophene

To study the DBT and thiophene adsorption kinetics on the nickel oxide modified carbonaceous adsorbents the following procedure was followed. A 150 mg of adsorbent was added to a 25 mL *n*-hexane solution with an initial concentration of 250 mg/L DBT. The mixture was shaken for 10 minutes then, using the HPLC method described earlier. The residual concentration of DBT was measured. This procedure was repeated for shaking time intervals of 20, 30, 40, 60, 120, 240 and 1560 minutes. The same procedure was followed in studying the adsorption kinetics for thiophene. The results presented in figure 4-44 show that for all adsorbents the adsorption-desorption equilibrium for both thiophene and DBT is reached within 1 hour. Fast adsorption of thiophene and DBT was observed in the first 20 minutes of contact time due to the maximum availability of unoccupied active sites on the adsorbents. While the maximum adsorption of thiophene and DBT was achieved after 1 hour contact time. The adsorption kinetic data for DBT and thiophene on the prepared adsorbents were fitted using the most frequently used kinetic models those are a pseudo-first order adsorption rate (equation 8)and a pseudo-second order adsorption rate (equation 9),

The low correlation coefficients and the large difference between the calculated and experimental values of q_e given in table 4-21 show the DBT and thiophene data do not fit the pseudo-first order kinetic model. The correlation coefficients close to or equal to 1 obtained for fits of $\frac{t}{q_t}$ versus t and the closeness of the calculated and experimental values of q_e given in table 4-21 show the DBT and thiophene data fit the pseudo-second order kinetic model. The uncertainties in the parameters of the pseudo-second order were

calculated on the basis of the uncertainties in the slope and the intercept of the linear $\frac{t}{q_t}$vs t plot.

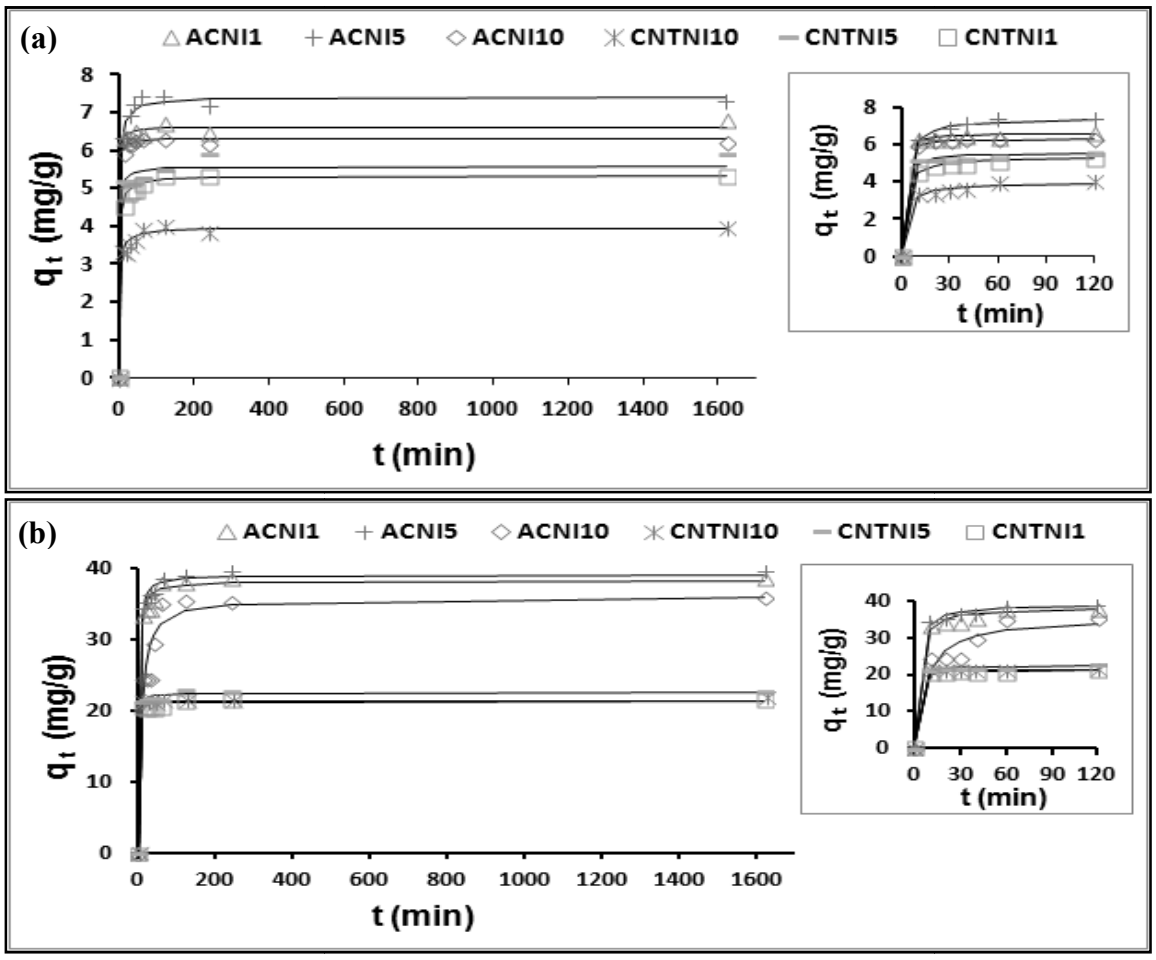

Figure 4-44: The effect of contact time on the adsorption capacity (q_t) of AC and CNT with different nickel oxide loading percentage for (a) Thiophene and (b) DBT. At room temperature 25 ºC, shaking speed 200 rpm, adsorbent amount 150 mg and initial concentration of organosulfur compound 250 mg/L. The solid lines are the predicted q_e values and the inset figures are the effect of contact time in the first 2 hours.

Table 4-21: Pseudo First order and Pseudo-Second order Parameters for thiophene and DBT adsorption on doped AC and CNT with nickel oxide.

Adsorbent	Pseudo-First order Parameters							
	Thiophene				DBT			
	q_e exp	q_e pred	k_1 (min^{-1})	R^2	q_e exp	q_e pred	k_1 (min^{-1})	R^2
ACNI10	6.33	0.43	8.70×10^{-3}	0.4504	35.67	21.37	8.06×10^{-2}	0.7647
CNTNI10	4.02	0.90	2.39×10^{-2}	0.9373	20.63	0.86	4.00×10^{-4}	0.0045
ACNI5	7.43	2.60	5.92×10^{-2}	0.8825	38.95	10.34	5.07×10^{-2}	0.8589
CNTNI5	5.50	2.47	6.30×10^{-3}	0.3875	23.00	1.61	4.10×10^{-3}	0.3168
ACNI1	6.72	0.56	5.06×10^{-2}	0.9001	38.07	38.92	6.22×10^{-2}	0.7882
CNTNI1	5.32	1.53	4.54×10^{-3}	0.8526	21.38	0.23	8.30×10^{-3}	0.0959
Adsorbent	**Pseudo-Second order Parameters**							
	Thiophene				**DBT**			
	q_e exp	q_e pred[e]	k_2[f] (g mg^{-1} min^{-1})	R^2	q_e exp	q_e pred[e]	k_2[f] (g mg^{-1} min^{-1})	R^2
ACNI10	6.33	6.38 ± *0.01*	(2.3± *0.4*) x 10^{-1}	1.0000	35.67	39.1 ±*2.1*	(2.5 ± *0. 5*)x 10^{-3}	0.9884
CNTNI10	4.02	4.16 ± *0.07*	(6 ± *1*) x 10^{-2}	0.9989	20.63	21.53 ±*0.06*	(2.2 ± *0.1*)x 10^{-1}	1.0000
ACNI5	7.43	7.63 ± *0.09*	(5± *1*) x 10^{-2}	0.9994	38.95	39.7 ±*0.5*	(1.1 ±*0.2*) x 10^{-2}	0.9997
CNTNI5	5.50	5.56 ± *0.08*	(10± *4*) x 10^{-2}	0.9993	23.00	23.18 ±*0.4*	(2.7 ±*0.1)*x 10^{-2}	0.9989
ACNI1	6.72	6.77 ± *0.07*	(1.1± *0.4*)x 10^{-1}	0.9995	38.07	39.0 ±*0.5*	(1.0 ± *0.3*)x 10^{-2}	0.9993
CNTNI1	5.32	5.42 ± *0.05*	(7± *1*)x 10^{-2}	0.9996	21.38	21.5 ±*0.2*	(4.6 ± *0.2*)x 10^{-2}	0.9995

(e) The uncertainty was calculated based on the uncertainty in the slope of the linearized equation.
(f) The uncertainty was calculated based on the uncertainty in the intercept of the linearized equation.

The mechanism of adsorption can be explored by studying the adsorption kinetics. Bearing in mind that the kinetic results fit perfectly into the pseudo second order kinetic model for DBT and thiophene using all adsorbents, the influence of mass transfer resistance on binding DBT (or thiophene) on adsorbents was verified using the intra-particle diffusion model represented in equation 16**[114]**.

$$q_t = k_{id} t^{0.5} + C \tag{16}$$

Figure 4-45 shows plots of q_e versus $t^{0.5}$ for DBT on ACNI10, ACNI5 and ACNI1. The linear parts in these plots imply that the adsorption processes involve two kinetic stages or sorption rates**[114].** The first linear part may be attributed to intra-particle diffusion, which produced a delay in the adsorption process. The second stage may be attributed to diffusion through micropores. Table 4-22 shows the calculated values of the diffusion constants.

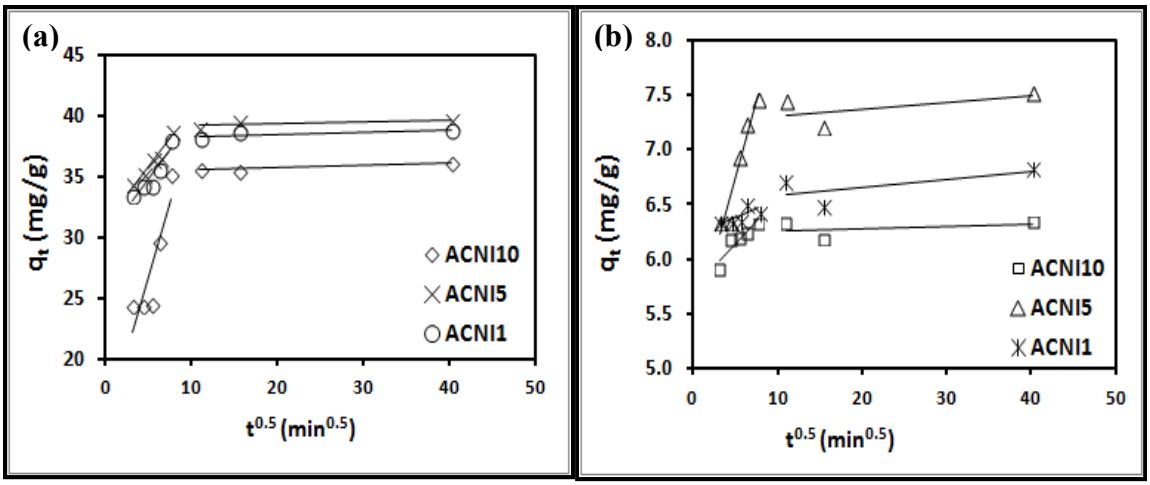

Figure 4-45: Intra-particles diffusion model for (a) DBT adsorption and (b) Thiophene adsorption on ACNI10, ACNI5 and ACNI1.

Table 4-22: Intra-particles diffusion parameters.

Adsorbents	Intra-particles Diffusion Parameters		
	DBT		
	K_{id} ($mg/gmin^{0.5}$)	C (mg/g)	R^2
ACNI10	2.3986	14.617	0.7789
ACNI5	0.8963	31.341	0.9553
ACNI1	0.9425	30.01	0.8634
	Thiophene		
ACNI10	0.0828	5.7263	0.8551
ACNI5	0.2783	5.3436	0.9041
ACNI1	0.0311	6.2212	0.5359

4.4.5 Adsorbent mass loading effect

Using an initial concentration of 250 mg/Lof DBT or thiophene and a shaking speed of 200 rpm for two hours the effect of adsorbent dose on their removal was studied at room temperature (25 °C) by varying the dose of adsorbent from 50 to 750 mg as shown in figure 4-46. It has been observed that the percentage removal of DBT and thiophene increased with the increase in the dose of AC doped with nickel oxide. At an absorbent dosage of 250 mg the percent removal of DBT was much higher for ACNI5 (around 97.5 %) than for AC (90.4 %); these percentages reached their highest values 99.6 % and 96.1 % respectively at a 750 mg loading. The removal efficiencies for thiophene were much lower but followed the same trend. Only 34.3 % removal of thiophene was achieved when 750 mg of ACNI5 was used, while 32.1 % removal was achieved withAC. On using CNTNI5 and CNT at a dosage of 250 mg 68.7 % and 52.1 % of DBT and 11.8 % and 9.0 % of thiophene were removed respectively. The low removal of thiophene is attributable to their weaker interaction with the adsorbent sites.The high removal efficiency and good adsorption capacities of DBT by ACNI5 and CNTNI5 led us to study their selectivity which is covered in the next section.

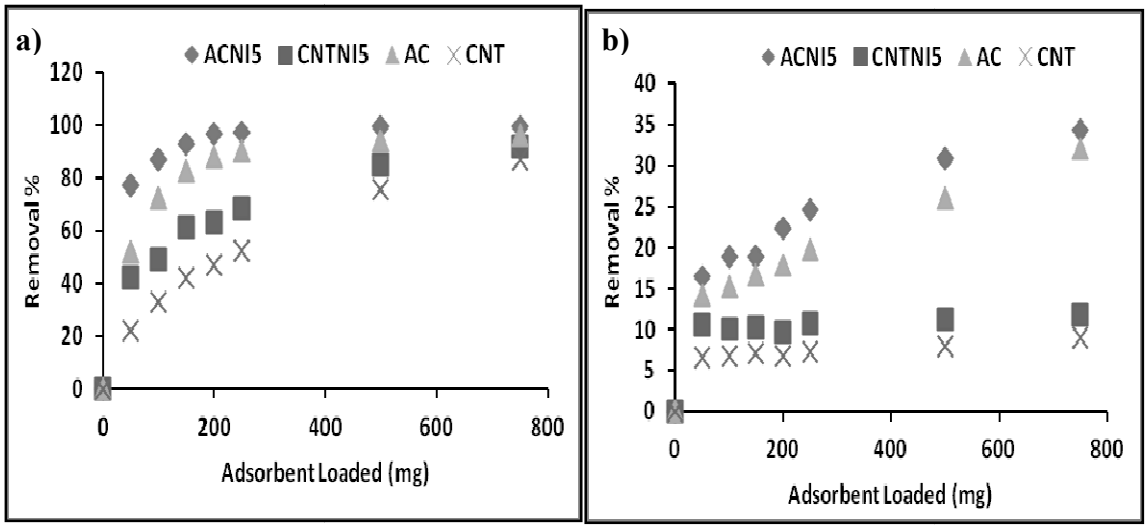

Figure 4-46: Effect of adsorbent loading on the removal efficiency of (a) dibenzothiophene (DBT) and (b) thiophene, on AC and CNT impregnated with different loading percentage of nickel oxide, at adsorption temperature 25 ºC, shaking speed 200 rpm and the C_o 250 mg/L.

4.4.6 Selectivity of the adsorbents

The selective removal of DBT by ACNI5 and CNTNI5 from *n*-hexane solutions, also containing thiophene and naphthalene, was studied. Thiophene was chosen to model small aromatic sulfur containing compounds while naphthalene was selected as a representative of poly aromatic hydrocarbons (PAH) with a structure similar to DBT; all present in diesel fuel. Seven adsorption measurements were carried out at 25 ºC and shaking speed of 200 rpm for two hours using 150 mg adsorbent in 25 mL of model fuel solutions containing thiophene, DBT and naphthalene. In experiments 1 to 7 the concentrations of DBT and thiophene were in the order of 25, 50, 100, 125, 150, 200 and 250 mg/L and those of naphthalene were in the order of 100, 200, 400, 500, 600, 800 and 1000 mg/L. The concentrations of these three compounds were measured simultaneously before and after the adsorption experiment. The distributiosn coefficient K_d (L/g) was calculated for each analyte based on equation 12 shown section 4.2.6.The distribution coefficient is used to calculate the selectivity factor for DBT with respect to thiophene and to naphthalene according to equation 13 shown in section 4.2.6.

As shown in table 4-23, the adsorption capacities for DBT on ACNI5 and CNTNI5 are about 41 and 28 mg/g respectively. The removal efficiencies for DBT using these adsorbents were 76.4 % and 43.4 % respectively, which are about four times the removal efficiencies for naphthalene (22.1 % and 9.6 %). However, the selectivity factor of DBT to naphthalene was about 12 for ACNI5 and 6 for CNTNI5. On the other hand, the higher selectivity factors of DBT to thiophene were about 50 using ACNI5 and about 9 using CNTNI5. The selectivity factors of DBT to thiophene and DBT to naphthalene can be explained by three possible factors. First the size of the DBT molecule may be

closer the size of the adsorbent pores which allows them to be better trapped into the adsorbent. The second factor is related to the higher dipole moment, molar mass and aromaticity values for DBT which lead to stronger van der Waals and π-π interactions with the adsorbents surface. The third factor is the lower basicity of thiophene relative to DBT and in turns its weaker acid-base interaction with nickel oxide (Lewis acid) on the adsorbent surface.

Table 4-23: Adsorption selectivity of ACNI5 and CNTNI5.

Adsorbate	**Adsorbent**							
	ACNI5				**CNTNI5**			
	Q_{max} (mg/g)	K_d	K DBT/Naphthalene	K DBT/Thio	Q_{max} (mg/g)	K_d	K DBT/Naphthalene	K DBT/Thio
DBT	40.98	0.693	11.95	49.5	28.33	0.200	5.71	8.70
Thiophene	3.45	0.014			5.56	0.023		
Naphthalene	45.25	0.058			31.55	0.035		

4.4.7 Effect of Aromatics

Diesel fuel consists of complex mixture containing approximately 65 % aliphatic hydrocarbons and 35 % of aromatics hydrocarbons**[128].**To study the effect of the aromatic hydrocarbon content on DBT adsorption, the benzene percentage was varied from 0 to 20 % in *n*-hexane. In addition, the adsorption capacities of ACNI5 and CNTNI5 for DBT in another model fuel (MDF), consisting of 25 % *n*-hexane, 45 % *n*-heptane, 10 % benzene, 10 % toluene, 10 % xylene and 1000 mg/L naphthalene, were measured. The adsorption capacities of ACNI5 and CNTNI5 for the DBT in a diesel sample purchased from a local Sahel gas station in Dhahran, Saudi Arabia were also measured. 150 mg adsorbents were loaded to aliquots of 25 mL of each of the three preceding solutions and were shaken for 2 hours at a speed of 200 rpm. The concentrations of DBT in the MDF and in the benzene/hexane mixtures after adsorption were determined using the HPLC method (described in section 3.5). Prior to its adsorption the concentration of DBT in these mixtures was 250 mg/L. The commercial diesel (containing 43.4 mg DBT/L) was spiked with DBT to increase its DBT concentration to 243.4 mg/L thereby bringing it close to the value of 250 mg/L that was used in the model fuel. This concentration dropped to 212.2 mg/L and to 221.4 mg/L after adsorption on ACNI5 and CNTNI5 respectively. The DBT concentrations were determined using gas chromatography (Agilent 7890 A) coupled with a sulfur chemiluminescence detector (GC-SCD) (Dual Plasma Technology 355) with hydrophobic Agilent DB-1 GC capillary column (30m x 0.32mm x 1μm). As shown in figure 4-47, theequilibrium adsorption capacities of ACNI5 and CNTNI5 for DBT decreased with the increase in the volume % of the aromatic hydrocarbon.As expected

the lowest adsorption capacities were encountered in the commercial diesel and were 5.2mg/gand 3.7 mg/g for ACNI5 and CNTNI5 respectively. This decrease in adsorption capacities is attributable to the severe medium of a commercial diesel that contains other competing aliphatics and aromatics and aromatic sulfur compounds. In addition it may be inferred that the lower adsorption capacities for DBT in the aromatic containing systems is due to an increase in their solvation in these systems.

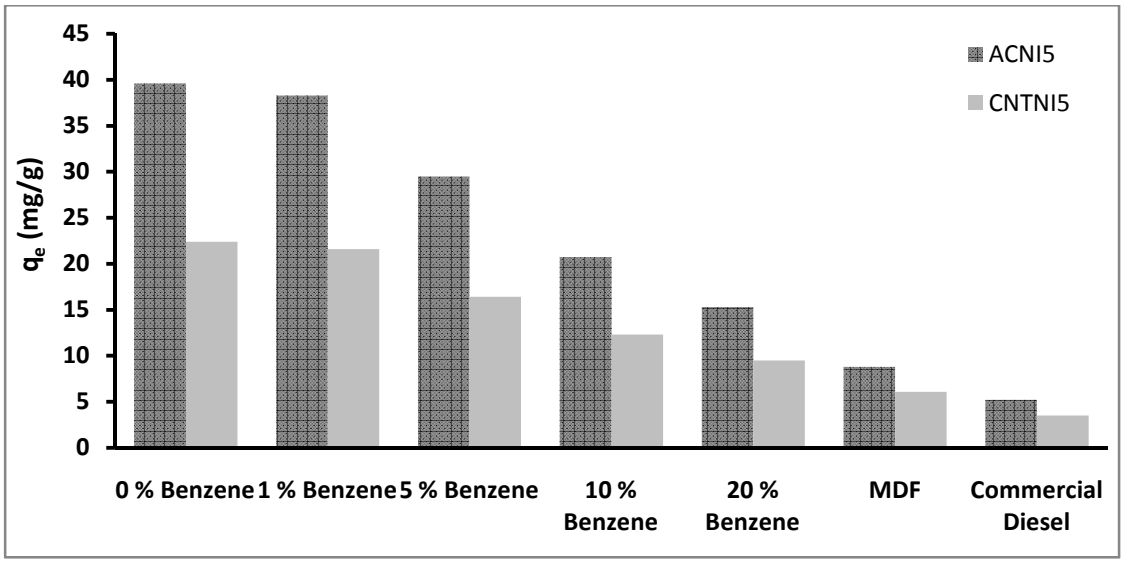

Figure 4-47: Effect of aromatics on the ACNI5 and CNTNI5 adsorbents' adsorption capacity

4.4.8 Regeneration of the adsorbents

The regeneration of adsorbents was studied because it contributes significantly to their cost effectiveness in diesel desulfurization. The regeneration procedure involved the removal of the DBT adsorbed on ACNI5 and CNTNI5 by heating to 300 ºC for 2 hours. The regenerated adsorbents were reused. This adsorption-desorption cycle was repeated five times. As figure 4-48 shows the adsorption capacity of CNTNI5 remained practically unchanged while the adsorption capacity of ACNI5% dropped by about 15 % after the fifth cycle.

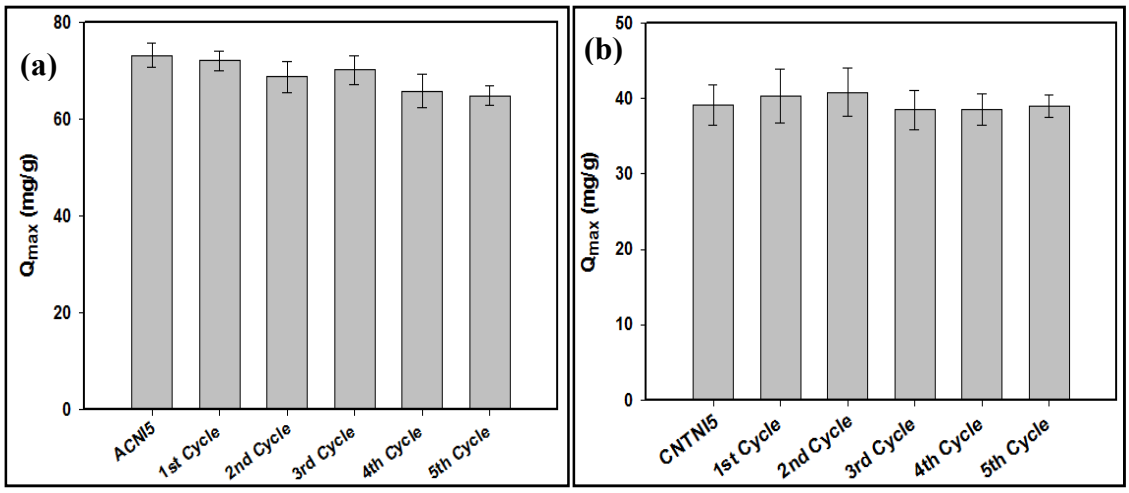

Figure 4-48: The adsorption capacities comparison with error bars after 5 adsorbent regeneration cycles for dibenzothiophene (DBT) on (a) ACNI5 and (b) CNTNI5 adsorbent.

4.4.9 Conclusion

Three different types of carbonaceous adsorbents namely AC, CNT and GO loaded with three different loading of nickel oxide(1 %, 5 % and 10 %) were prepared, characterized and tested for the removal of DBT and thiophene from *n*-hexane as model diesel fuel. The carbon materials were doped with nickel oxideusing the wetness impregnation technique. The raw and modified carbonaceous materials were characterized using TGA, SEM, EDX, TEM and XPS. The highest removal efficiency of DBT and thiophene was achieved using ACNI5 adsorbent. The adsorption capacities were 74mg/g and 31mg/g for DBT and thiophene respectively. The selectivities of ACNI5and CNTNI5 for DBT relative to thiophene and DBT relative to naphthalene were obtained. The selectivities on ACNI5 for DBT relative to thiophene and DBT relative to naphthalene were 50 and 12 respectively, while the selectivitieson CNTNI5 for DBT relative to thiophene and DBT relative to naphthalene were9 and 6 respectively. These adsorbents showed good reusability after five cycles with practically no loss in the adsorption capacity of CNTNI5 and a maximum of 15 % loss in the adsorption capacity of ACNI5. Three aromatics-containing systems were tested for DBT adsorption. They showed a decrease in adsorption with increase in benzene content. The least adsorption capacity was obtained in the commercial diesel. This is attributed to competing molecules. In general, decrease in adsorption with increase in benzene content maybe attributable to greater solvation of DBT.

4.5 Adsorptive Removal of Dibenzothiophene and Thiophene Using Carbon Nanotube and Activated Carbon Modified with Uranyl Oxide Nanoparticles

The natural uranium consists three main isotopes ^{238}U (99.27 %), ^{235}U (0.72 %) and ^{234}U (0.0054 %). The ^{238}U has the highest half life (4.468 billion years) and the lowest is for ^{234}U (246 thousand years). Its chemical compounds found in different chemical forms in seas, rockes even it present in drinking water. Naturally occurred uranium exists in human body (90 μg) from the usual intake of food, air and water, 66 % found in bone, 16 % in liver, 8 % in kidney and 10 % in other tissue **[129]**. The main use of uranium for nuclear reactor in nuclear power plant, whereas the ^{235}U is enriched to about 4 %. However, the high density and availability of depleted uranium make it useful materials in different industrial fields such as aircraft, boat industry and oil and gas exploration and production **[130]**, for many applications such as counterbalance weights and ballast, radiation shielding, dentistry and glassware and ceramics**[131]**. The uranium used also as a catalyst for chemical reactions and in photographic films. The oil and gas industries use depleted uranium in percent 10 to 65 % mixed with nickel as a chemical catalyst **[131]**. The electronic configuration of U is [Rn] $5f^3$ $6d^1.7s^2$. The empty d and f-orbitals in the uranyl oxide provide an excellent electron acceptor for the lone pair electrons on the sulfur atom and the π electrons in the structure of dibenzothiophene and thiophene sulfur compounds.

Merging the uranyl oxide with the high surface area of the activated carbon and carbon nanotube with their distinct surface chemistry offers new adsorbents for

adsorptive desulfurization. In this chapter a new adsorbents composites have been discussed. These adsorbents were prepared by anchoring the activated carbon (AC) and carbon nanotube (CNT) with 5 % U in the form of uranium trioxide as an additional adsorption site on the surface of the carbonaceous materials. The potential use of these adsorbents for the removal of dibenzothiophenewas investigated. The adsorption isotherms and kinetics of DBT and thiophene introduced in model fuel and the selectivity of the adsorbents for removal of DBT was studied.

4.5.1 Thermal gravimetric analysis of adsorbents

As shown in figure 4-49 (a), the residual solvents evaporated below 100 ºC while the initial oxidation temperature of raw AC and CNT starts approximately at 400 ºC and 550 ºC respectively. However the final oxidation temperature for the same materials was at 600 ºC and 650 ºC respectively. While the modified AC and CNTs with UO_3 oxidized completely in air at 520 ºC and 550 ºC respectively. The results show that the formation of uranyl oxide led to accelerate the oxidation of the carbon materials in air. The same experiment was carried out under nitrogen atmosphere to study the degradation of the unmodified and modified adsorbents. The TGA curves in figure 4-49 (b) show that, there is no significant loss in the unmodified adsorbent's weight in the measuring temperature range. That weight loss around 2 % resulted from evaporation the residual solvents. However, the modified adsorbents lost about 5 % from its original weight in the temperature range from 500 to 800 ºC as a result of reduction of the uranyl oxide (UO_3) to uranium dioxide (UO_2) in presence of carbon materials **[132]**.

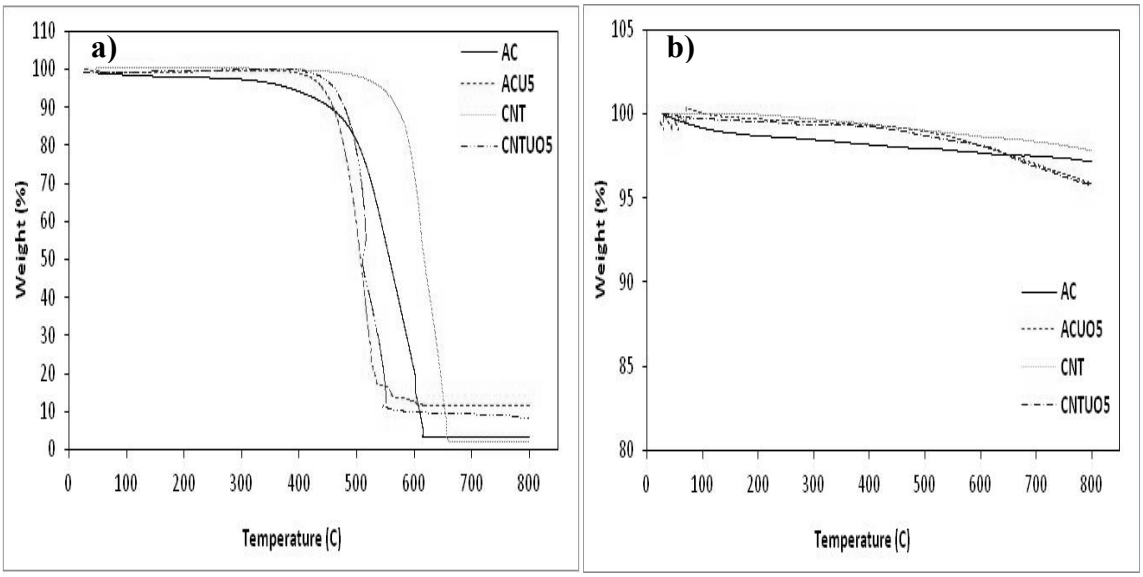

Figure 4-49: TGA for unmodified and modified adsorbent with UO_3 under a) air and b) nitrogen with flow rate of 100 mL/min.

4.5.2 Texture and morphology of adsorbents

The adsorbents' morphologies were characterized using a scanning electron microscope (SEM) and afield emission electron microscope (FE-TEM). The SEM images of AC and CNT respectively are given before impregnation with UO_3 particles in figures 4-50 (a & b) and after impregnation with UO_3 particles in figures 4-50 (c & d). A layer of UO_3 particles coated the surface of the AC and spherical particles coated the surface of the CNT. The elemental composition of the UO_3-impregnated carbon based adsorbents was obtained by energy dispersive X-ray analysis (EDX) which is summarized in table 4-24. The percentages of uranium in the adsorbents are close to the theoretical percentages (5 %). TEM images for raw and doped CNT are shown in figures 4-51 (a & b). The images show that all the nanotubes are hollow with many curvature sites. As the TEM image in figure 4-51 (b) shows the uranium oxide nanoparticles coated on CNT were spherical with diametersbetween 10 and 80 nm.

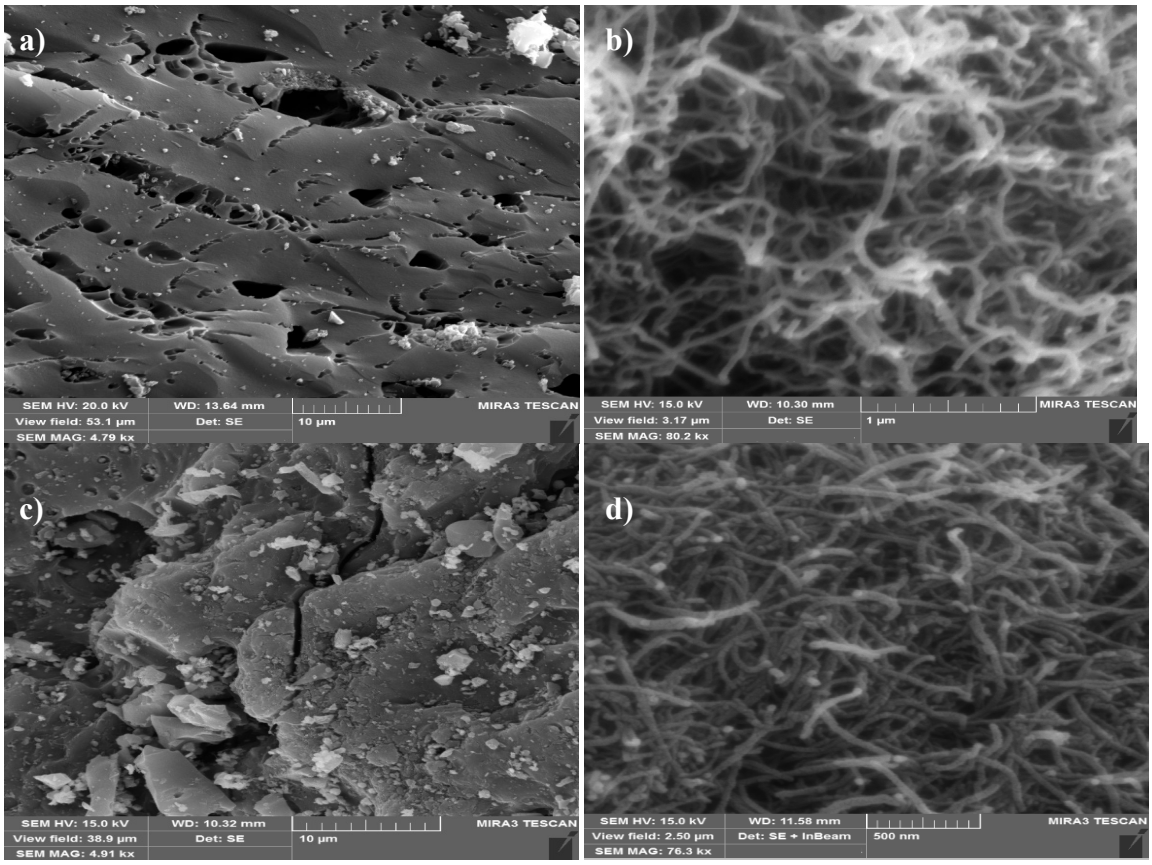

Figure 4-50: SEM image for a)AC and CNT before and b) AC and CNT after impregnation with UO_3

Table 4-24: EDX results for weight percent of uranium in the doped carbon materials adsorbents compared to the theoretical percentage of uranium.

Adsorbent	Element	Weight%
ACU5	C-K	87.44
	O-K	7.21
	U-M	5.35
CNTU5	C-K	80.39
	O-K	12.41
	U-M	6.66

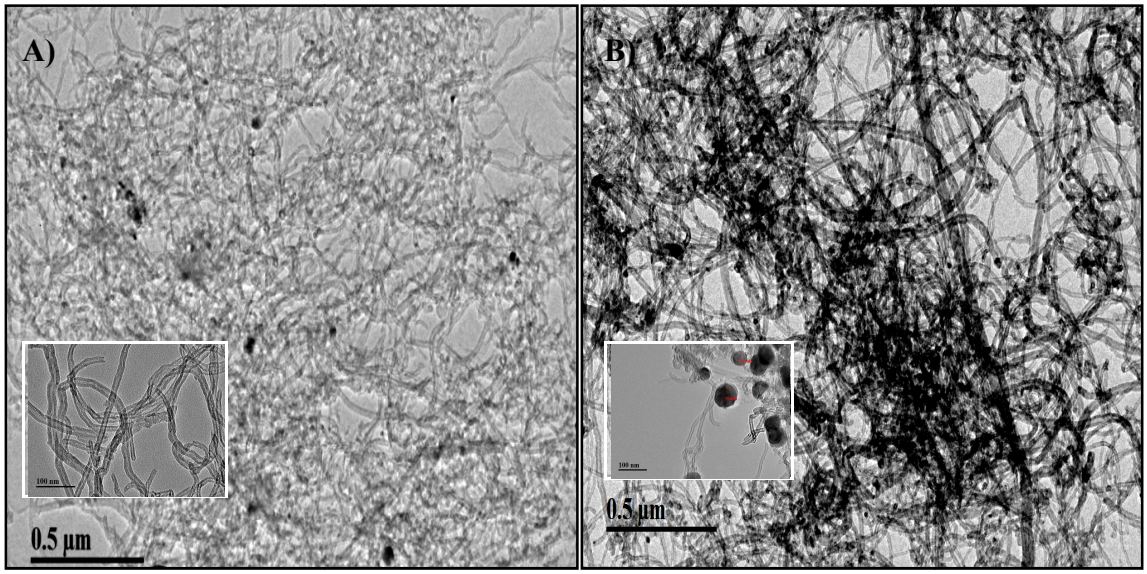

Figure 4-51: EF-TEM image for CNT a) before and b) after doping with 5 % UO_3. The insets show the carbon nanotubes before and after the modification at higher magnification (100 nm image scale).

The surface area and porosity characterization results given in table 4-25reveal that, for the unmodified adsorbents the trend in surface area based on BET method is ACU5>AC >CNT > CNTU5 while the trend in the micropores volume based on the t-plot method is AC > ACU5>CNTU5 >CNT. Modification of AC with uranyl oxide increased the surface area of AC and decreased the micropores volume because of the particle accumulation in the AC's micropores. In contrast, the surface area decreases and micropore volume increases in the modified CNT with uranyl oxide which can be explained by the agglomeration of the modified CNT which led to form micropores structure. Table 4-25 also shows that, all the modified adsorbents have lower pH values compared with the unmodified adsorbents as a result of accumulation the uranyl oxide (Lewis acid) on the virgin adsorbents' surfaces**.**

Table 4-25: Surface area, micropore surface area and its volume and surface pH of unmodified and modified AC and CNT with 5 % U in the form of UO_3.

	BET	**t-Plot Micropore**	**pH**
Adsorbent	**SA (m^2/g)**	**V (cm^3/ g)**	
AC	882	0.466	9.35
ACU5	928	0.373	7.99
CNT	217	--------	5.81
CNTU5	204	0.008	5.40

4.5.3 Adsorption isotherms of thiophene and dibenzothiophene

The adsorption of thiophene and DBT on raw and modified AC and CNT with 5 % $UO_3$was investigated at room temperature (25 ºC). Solutions of thiophene and DBT at concentrations of 25, 50, 100, 125, 150, 200, and 250 mg/L in 25 mL *n*-hexane as a model fuel were each used with 150 mg of adsorbent. The concentration of thiophene and DBT before and after the adsorption study was measured using HPLC method coupled with UV detector as described in previous section. However, for the selectivity study the wavelength switching mode was used to measure the concentrations of thiophene,naphthalene and DBT simultaneously in the model diesel. Figures (4-52 & 4-53) present the adsorption isotherm of DBT and thiophene on unmodified and modified AC and CNT with 5 % UO_3fitted by Freundlich and Langmuir respectively

As shown in table 4-26 the*n* and K_F values for thiophene on adsorbents modified with UO_3 nanoparticles are larger than those of thiophene on unmodified carbon adsorbents, indicating that, the modification increased the adsorbents surface heterogeneity and adsorption capacity. However for DBT the K_F values increased significantly but the *n* values decreased with keeping higher than 1 for modified adsorbents. These *n* values fall between 1.1 and 1.7 which indicate DBT tendency for adsorption. For thiophene and DBT the goodness of fit values (R^2; the squares of the correlation coefficients) of ln (q_e) versus ln(C_e) (for thelinearized form of Freundlich's equation) were better than those of $\frac{C_e}{q_e}$ versus C_e (for the linearized formof Langmuir's equation).

The maximum adsorption capacities (Q_{max}) values of DBT on each adsorbent were obtained from the slope of Langmuir isotherm linear form. However, the Q_{max}value of thiophene was calculated only for the ACU5 because the other adsorbents didnot fit the Langmuir isotherm model. However, their experimental data fitted the Freundlich isotherm which indicates that, adsorption of thiophene form multilayer on the adsorbents.

As shown in table 4-26, the ACU5 has the highest Q_{max} (109 ± *6*) to DBT with improvement in the adsorption capacity of AC by about 150 %. The others adsorbents follow the order CNTU5 > AC > CNT. The increase in adsorption of DBT from model diesel using modified carbonaceous adsorbents resulted from introducing additional adsorption sites represented by the UO_3 Lewis acid which can interact with the sulfur compounds through a π complexation between the π electrons of benzene rings in the organosulfur compound structure or the lone pair electrons on the sulfur atom with the emptyd and f orbitals in the uranium.

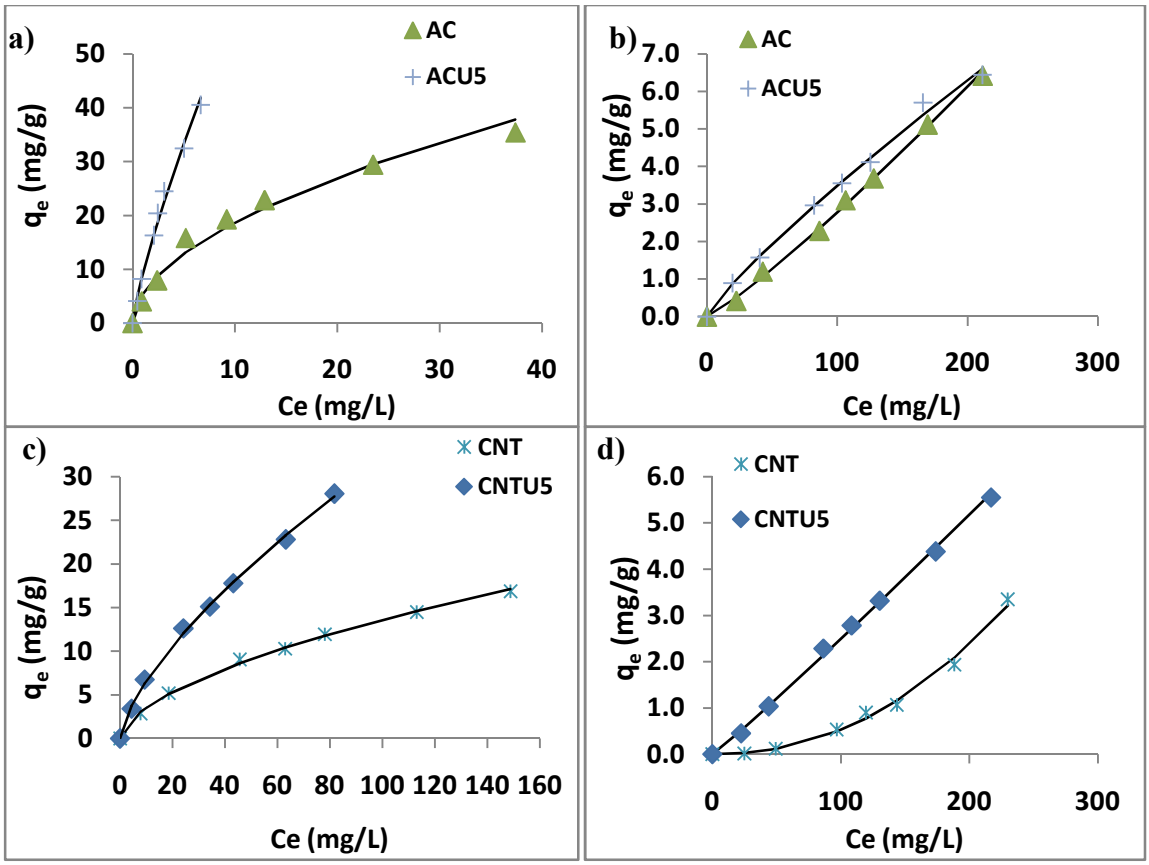

Figure 4-52: The adsorption isotherms of a) DBT and b) Thiophene, on raw and modified AC and c) DBT and d) Thiophene, on raw and modified CNT with 5 % UO_3. Contact time 2 hours, adsorption temperature 25 ºC and shaking speed 200 rpm. Solid lines are fits to the Freundlich model.

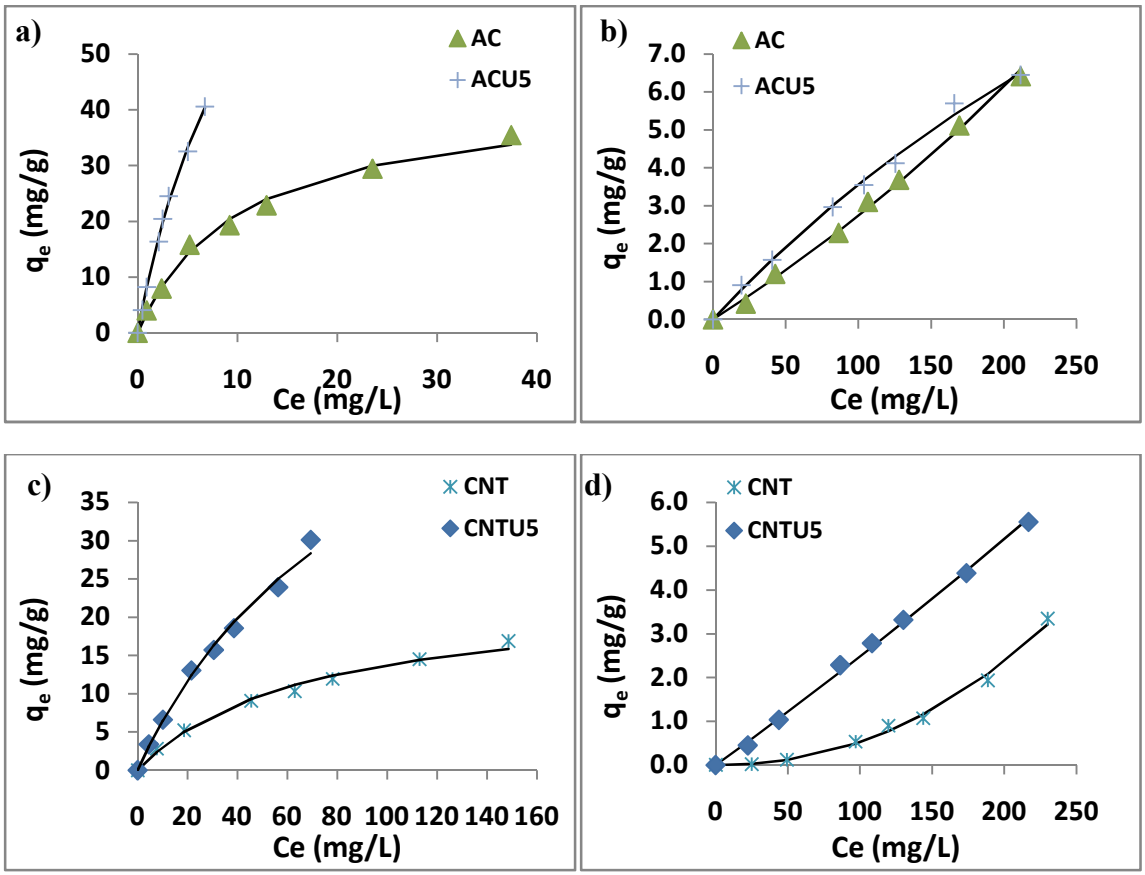

Figure 4-53: The adsorption isotherms of a) DBT and b) Thiophene, on raw and modified AC and c) DBT and d) Thiophene, on raw and modified CNT with 5 % UO_3. Contact time 2 hours, at adsorption temperature25 ºC and shaking speed 200 rpm. The solid line fitsto the Langmuir model.

Table 4-26: Freundlich and Langmuir parameters and correlation coefficient for thiophene and DBT adsorption on carbonaceous materials before and after modification with UO_3

Adsorbent	Freundlich					
	Thiophene			DBT		
	n [1]	K_F [2] ($mg^{(1-1/n)}$ mg^{-1} $L^{1/n}$)	R^2	**n** [1]	K_F [2] ($mg^{(1-1/n)}$ mg^{-1} $L^{1/n}$)	R^2
AC	0.83 ± *0.04*	(1.1± *0.3*) x 10^{-2}	0.9898	1.7 ± *0.1*	4.9 ± *0.5*	0.9747
CNT	0.45 ± *0.02*	(2.0 ± *0.8*) x 10^{-5}	0.9934	1.69 ± *0.04*	(8.9 ± *0.5*) x 10^{-1}	0.9968
ACU5	1.18 ± *0.02*	(7 ± *0.6*) x 10-2	0.9979	1.17 ± 0.05	8.7 ± *0.4*	0.9913
CNTU5	0.91 ± *0.02*	(1.6 ± *0.2*) x 10-2	0.9964	1.27 ± 0.04	1.06 ± *0.08*	0.9961
	Langmuir					
	Thiophene			**DBT**		
	Q_{max} [3] (mg/g)	**b** [4] (dm^3/mg)	R^2	Q_{max} [3] (mg/g)	**b** [4] (dm^3/mg)	R^2
AC	-------	-------	0.4657	42 ± *3*	(1.07 ± *0.06*) x 10^{-1}	0.9795
CNT	-------	-------	0.6969	24 ± *2*	(1.5 ± *0.1*) x 10^{-2}	0.9702
ACU5	21.6 ± *2.5*	(2.0 ± *0.1*) x 10^{-3}	0.8335	109 ± *6*	(8.9 ± *0.2*) x 10^{-2}	0.9374
CNTU5	-------	-------	0.4159	64 ±*2*	(1.15 ± *0.02*) x 10^{-2}	0.9286

[1] The uncertainty was calculated on the basis of the uncertainty in the slope of the Freundlich linearized equation.
[2] The uncertainty was calculated on the basis of the uncertainty in the intercept of the Freundlich linearized equation.
[3]The uncertainty was calculated on the basis of the uncertainty in the slope of the Langmuir linearized equation.
[4]The uncertainty was calculated on the basis of the uncertainty in the intercept of the Langmuir linearized equation

4.5.4 Adsorption kinetics ofthiophene and DBT

To study the DBT and thiophene adsorption kinetics on carbonaceous adsorbents modified with uranyl oxide, a 25 mL *n*-hexane solution with an initial concentration of 250 mg/L from each sulfur compound was added to 75 mg of adsorbent in a vial that was capped then shaken continuously for a fixed time intervals. The shaking time intervals were2, 4, 6, 8, 10, 20, 30, 40, 60, 120, 240 and 1560 minutes. The results presented in figure 4-54 (a & b) show that, for all the adsorbents in this study, the adsorption rates of thiophene reach equilibrium quickly within 10 minutes. However, the adsorption rates of DBT on CNTU5 reach equilibrium within 10 minutes and on ACU5 needed longer time to reach equilibrium within 1 hour. As the inset in figure 4-54b shows most of the DBT is adsorbed in the first 10 minutes and slowly reach a maximum value. The experimental adsorption capacities ($q_{e,\exp}$) for thiophene and DBT on the carbonaceous adsorbents modified with uranyl oxide are given in table 4-27. The initial fast adsorption is attributed to the large number of available active adsorption sites while the slowness at which maximum adsorption is reached is due to the few adsorption sites and the repulsive forces between adsorbate molecules in solution and adsorbate molecules on the adsorbents. The adsorption results were fitted using the kinetic models (i.e. pseudo-first order adsorption rate and pseudo-second order adsorption rate).

Linear least squares fits of $\ln(q_e - q_t)$versus (t) for the adsorption data of thiophene and DBT yielded low squared correlation coefficients (R^2) and high deviation of predicted adsorption capacities from the experimental adsorption capacities.On the other hand the linear least squares fits of $\frac{t}{q_t}$ versus t yielded squared correlation

coefficients equal or very close to 1 (see table 4-26). This indicates clearly the adsorption process follows pseudo second order kinetics.

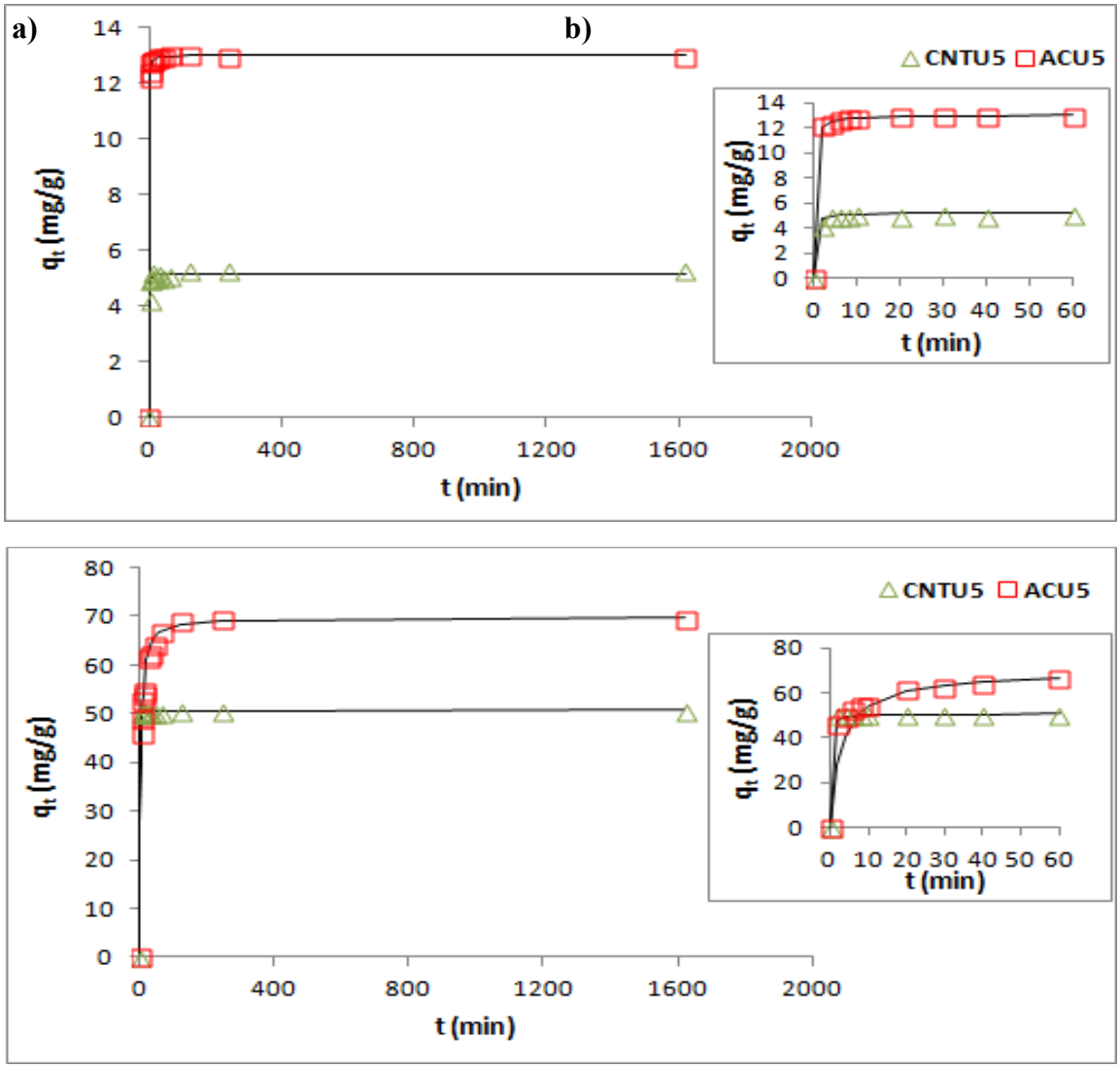

Figure 4-54: The effect of adsorption time on the adsorption capacity of a) thiophene and b) dibenzothiophene (DBT), using different adsorbents modified with UO_3. Solid line is second order kinetics fit. Temperature is 25 ºC, the shaking speed is 200 rpm, the adsorbent amount is 75 mg and $C_o$is 250 mg/L.

Table 4-27: Pseudo-First order and Pseudo-Second order parameters for thiophene and DBT adsorption on the carbonaceous materials doped by UO_3

Adsorbent	Pseudo-First order Parameters							
	Thiophene				DBT			
	$q_{e\,exp}$	$q_{e\ pred}$[1]	k_1[2] (min^{-1})	R^2	$q_{e\ exp}$	$q_{e\ pred}$[1]	k_1[2] (min^{-1})	R^2
ACU5	12.97	0.8 ± *0.2*	(1.3 ± *0.2*) x 10^{-1}	0.9090	69.57	20 ± *1*	(3.10 ± 0.15) x 10^{-2}	0.9828
CNTU5	5.30	0.6 ± 0.2	(2 ± *1*) x 10^{-2}	0.5194	50.87	0.65 ±0.04	(7.32 ± 1.98) x 10^{-3}	0.7742
Adsorbent	**Pseudo-Second order Parameters**							
	Thiophene				**DBT**			
	$q_{e\ exp}$	$q_{e\ pred}$[3]	k_2[4] (g mg^{-1} min^{-1})	R^2	$q_{e\ exp}$	$q_{e\ pred}$[3]	k_2[4] (g mg^{-1} min^{-1})	R^2
ACU5	12.97	13.03 ± 0.01	0.5 ± *0.1*	1.0000	69.57	69.9 ±*0.6*	(6.0 ± *0.9*) x 10^{-3}	0.9994
CNTU5	5.30	5.29 ± 0.04	0.3 ± *0.1*	0.9995	50.87	50.82 ±0.09	0.2 ± *0.1*	1.0000

1- The uncertainty was calculated based on the uncertainty in the slope of the pseudo-first order linearized equation.
2- The uncertainty was calculated based on the uncertainty in the intercept of the pseudo-first order linearized equation.
3- The uncertainty was calculated based on the uncertainty in the slope of the pseudo-second orderlinearized equation.
4- The uncertainty was calculated based on the uncertainty in the intercept of the pseudo-second orderlinearized equation.

The mechanism of adsorption can be explored by studying the adsorption kinetics. Bearing in mind that the kinetic results fit perfectly into the pseudo second order kinetic model for DBT and thiophene in all adsorbents, the influence of mass transfer resistance on their binding on the adsorbents was verified using Weber and Morris intra-particle diffusion model allows exploring the intra-particle diffusion resistance**[114]**. The diffusion constant, k_{id} , can be obtained from the slope of the plot of q_t versus the square root of time. If this plot passes through the origin, then intra-particle diffusion is the rate controlling step.

Figure 4-55 shows plots of q_t versus $t^{0.5}$ for DBT on ACU5 and CNTU5. These results imply that the adsorption processes involve multiple kinetic stage or adsorption rate **[114]**. ACU5 adsorbent exhibited three stages, which can be attributed to three linear parts. The first sharp linear part can be attributed to surface adsorption or faster adsorption step, followed by intra-particle diffusion, which produces a delay in the adsorption process. The third stage may be regarded as the diffusion through smaller pores, the presence of micropores on the adsorbents is in line with this stage which establishedthe adsorption equilibrium. In contrast, CNTU5 exhibited two stages. The first step involves the DBT diffusion from the bulk solution to the surface to be adsorbed, followed by intra-particle diffusion through the adsorbent. The first sharp line was used to calculate the intra-particle diffusion constants k_{id} and C. Table 4-28 shows the calculated values of the diffusion constants for DBT and thiophene on ACU5 and CNTU5. Higher values of k_{id} represent a faster net rate of adsorption as a result of slow desorption because of the improved bonding between DBT and the adsorbent.

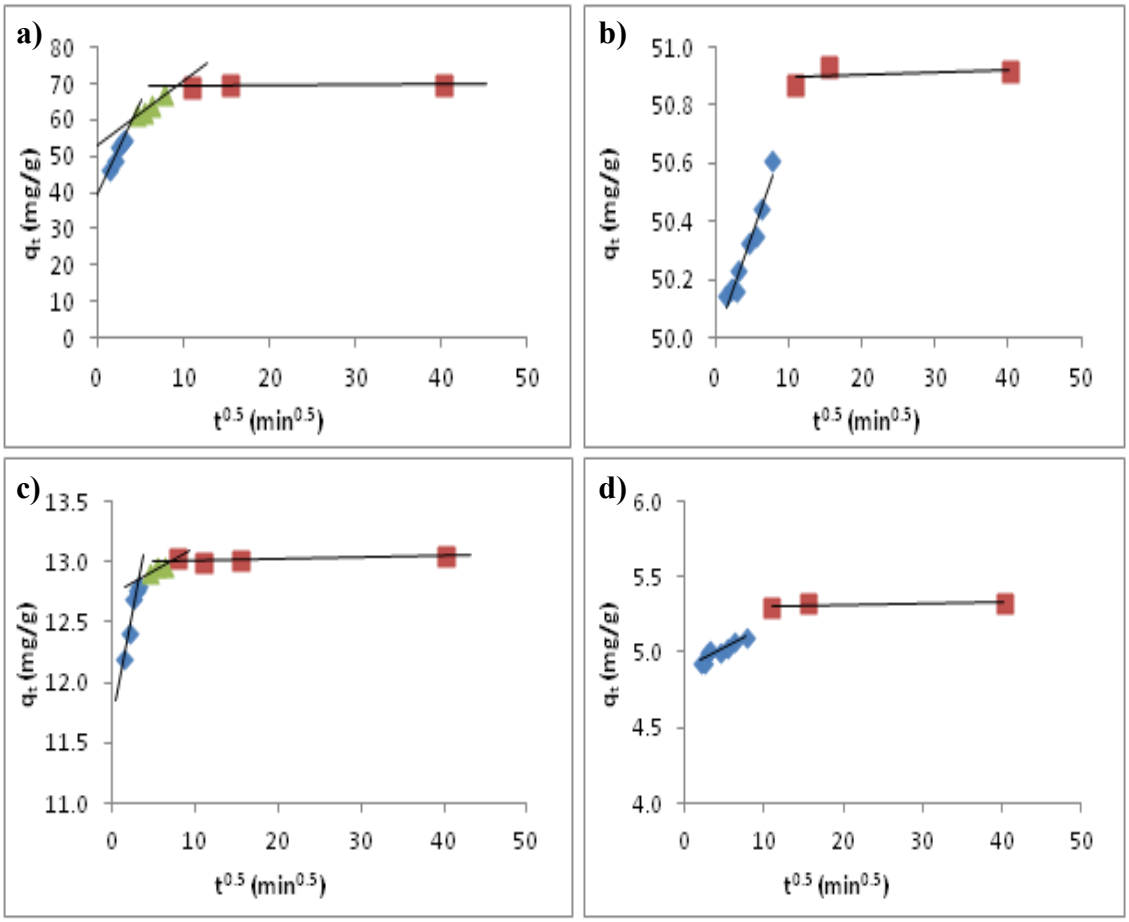

Figure 4-55: Plots of q_t versus $t^{0.5}$ showing the multi steps diffusion predicted by the diffusion model for DBT adsorption on a) ACU5 and b) CNTU5, and thiophene adsorption on c) ACU5 and d) CNTU5.

Table 4-28: Intra-particle diffusion parameters for DBT and thiophene on the modified adsorbents with uranium.

Adsorbents	Intra-particles Diffusion Parameters		
	DBT		
	K_{id} ($mg/gmin^{0.5}$)	C (mg/g)	R^2
ACU5	5.05	39.26	0.9634
CNTU5	0.07	50.00	0.9586
	Thiophene		
	K_{id} ($mg/gmin^{0.5}$)	C (mg/g)	R^2
ACU5	0.37	11.70	0.9411
CNTU5	0.03	4.90	0.8455

4.5.5 Effect of adsorbent dosage

The effect of the adsorbent amount on removal of DBT and thiophene was studied by varying the mass of the adsorbents from 25 to 750 mg in fixed solution volume 25 mL, at room temperature (25 ºC), shaking speed 200 rpm and sulfur containing compound initial concentration (C_o) 250 mg/L. It has been observed that, the percentage removal of DBT increase while the adsorption capacity decrease with increase of ACU5 and CNTU5amount as shown in figure 4-56 (a & b). However, the thiophene removalefficiency increased with the increase the amount of ACU5 while there is no significant effect for CNTU5 on the adsorption efficiency of thiophene. High removal percentage of DBT about 98 % was found to be at adsorbent dosage of 200 mg for ACU5 and about 75 % for CNTU5. The maximum adsorption of DBT (99.5 % removal and 85 %) was found at 500 mg of ACU5 and CNTU5 was used respectively. Same trend of adsorption was observed when ACU5 and CNT5 were used to remove thiophen from model diesel with maximum removal efficiency only 26 % and 15 % respectively. The higher removal efficiency of DBT and thiophene using ACU5 compared to CNTU5 can be explained by the ACU5 higher surface area and larger micropores volume than those for CNTU5.

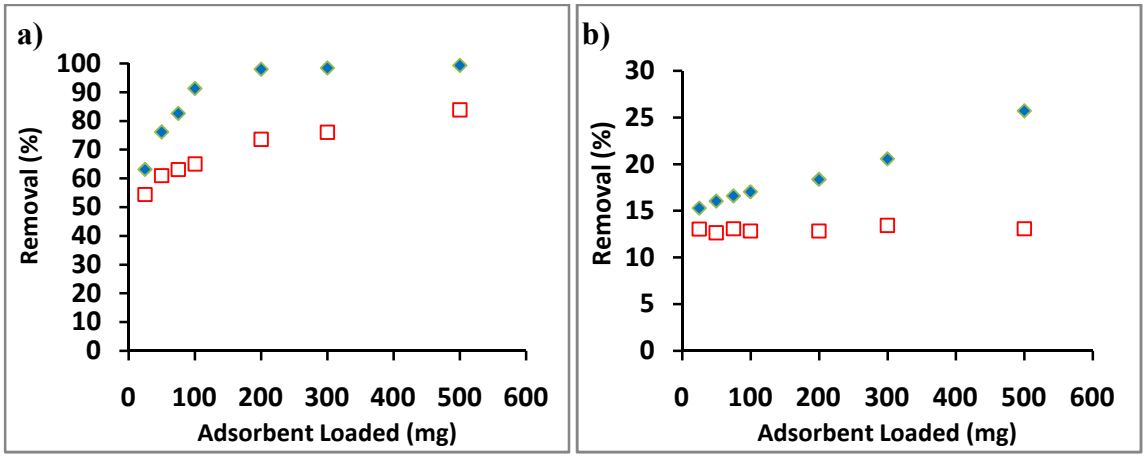

Figure 4-56: Effect of the adsorbents mass on the adsorption capacity and removal efficiency of a) dibenzothiophene (DBT) and b) thiophene, on AC and CNT modified with UO_3. The adsorption time is 2 hours at 25 ºC, the shaking speed 200 rpm and the initial sulfur compound concentration is 250 mg.

4.5.6 Selectivity of the adsorbents

The selectivity of ACU5 and CNTU5 for DBT adsorption from *n*-hexane has been studied relative to thiophene as model molecule for small aromatic sulfur containing compound, as well as relative to naphthalene which represents the availability of polyaromatic hydrocarbon (PAH) compounds with molecular structure close to DBT molecular structure. The stock solution for ternary mixture from these three compounds Thiophene, DBT and naphthalene in *n*-hexane was prepared with concentrations of 250 mg/L for both thiophene and DBT and 1000 mg/L for naphthalene to simulate the actual availability of PAH in real fuel. A 75 mg adsorbent was used in 25 mL of model fuel solution and the batch adsorption experiments were performed over a wide range of concentration ranging from 25 to 250 mg/L for both thiphene and DBT and from 100 to 1000 mg/L of naphthalene at 200 rpm shaking speed and 120 min adsorption time at room temperature. The described HPLC method was used to measure the concentrations of these three compounds simultaneously before and after the adsorption equilibrium was achieved.

As shown in table 4-29, the ACU5 and CNTU5 exhibit high adsorption capacities for DBT about 59 and 43 mg/g respectively in presence of thiophene and naphthalene competitor molecules. The removal efficiency of DBT using these adsorbents was around 7 times higher than the removal efficiency of naphthalene and 23 times than thiophene. However, the selectivity factor of DBT to naphthalene was 18 by ACU5 and 6 by CNTU5. Higher selectivity factors were shown when DBT was compared to thiphene. The selectivity factor of DBT to thiophene was 69 using ACU5 and about 14 using CNTU5. The selectivity of ACU5 and CNTU5 to DBT compared to thiophene and

naphthalene can be explained by three possible factors; 1) the size of DBT molecule is closer to the size of adsorbents pores which allowed them to be trapped into the adsorbent better than others, 2) the dipole moment of DBT is higher than those for thiophene and naphthalene which lead to stronger van der Waals and π-π interactions between the DBT and the adsorbents surface and 3) the high basicity of DBT compared to thiophene and naphthalene.

Table 4-29: Adsorption selectivity of ACU5 and CNTU5 for DBT.

Adsorbate	Adsorbent							
	ACU5				CNTU5			
	Q_{max}(mg/g)	K_d	$K_{DBT/Naph}$	$K_{DBT/Thio}$	Q_{max}(mg/g)	K_d	$K_{DBT/Naph}$	$K_{DBT/Thio}$
DBT	59.2	0.622	18.3	69.1	43.9	0.253	6.17	14.1
Thiophene	2.20	0.009			4.20	0.018		
Naphthalene	31.2	0.034			38.4	0.041		

4.5.7 Conclusion

Two different types of carbonaceous adsorbents namely AC and CNT were modified with 5% uranium in the form of $UO_3$and then used for removal of DBT and thiophene from *n*-hexane as model fuel. The $UO_3$was doped on the surface of AC and CNT using wetness impregnation technique. The raw and modified carbonaceous materials were characterized using TGA, SEM, EDX, TEM and XPS. The highest removal efficiency of DBT was achieved using ACU5 adsorbent with high selectivity to DBT. The adsorption capacities of DBT were 109mg/g and 64 mg/g on ACU5 and CNTU5 respectively. The selectivity study of DBT relative to thiophene and DBT relative to naphthalene was carried out. It has been found that, the selectivity factor of DBT to thiophenewas 69 and of DBT to naphthalene was 18on ACU5, while the selectivity of DBT to thiophene and DBT to naphthalene using CNTU5 was 14 and 6 respectively.

CHAPTER 5

5. Comparative Analysis

5.1 Comparative Analysis of the Prepared Adsorbents for DBT and Thiophene Removal

As discussed in previous chapters the experimental data for DBT and thiophene adsorption isotherms were fitted with Freundlich and Langmuir models. The squared correlation coefficient, n and Q_{max} are listed in table 5-1. Figure 5-1 shows that as a group the highest adsorption capacity was obtained using the AC based adsorbents, while the GO based adsorbents had the lowest adsorption capacity. That is attributedto the difference in surface area of these adsorbents which follow (as a group) the same trend.

Table 5-1: Comparison between the Freundlich and Langmuir parameters for all the prepared adsorbents.

Adsorbent	Freundlich				Langmuir			
	Thiophene		DBT		Thiophene		DBT	
	n	R^2	n	R^2	Q_{max}(mg/g)	R^2	Q_{max}(mg/g)	R^2
AC	0.83	0.9898	1.72	0.9747	---------	---------	41.70	0.9795
ACNI10	1.30	0.9897	1.69	0.9480	14.16	0.811	47.54	0.9850
ACNI1	1.02	0.9991	1.59	0.9948	-------	0.4975	52.84	0.9556
ACAL10	1.20	0.9987	1.29	0.9821	26.10	0.9414	70.20	0.8503
ACNI5	1.12	0.9989	1.29	0.9782	31.31	0.8208	73.61	0.9793
ACAL5	1.18	0.9971	1.26	0.9953	29.00	0.7401	84.50	0.9603
ACU5	1.18	0.9979	1.17	0.9913	21.62	0.8335	108.95	0.9374
CNT	0.45	0.9934	1.69	0.9968	---------	---------	23.50	0.9702
CNTNI10	1.12	0.9856	1.80	0.9880	-------	0.1792	28.11	0.9337
CNTAL10	1.32	0.9943	1.93	0.9982	16.50	0.8729	32.70	0.9395
CNTNI1	0.88	0.9908	1.45	0.9992	-------	0.4191	33.78	0.9542
CNTNI5	1.03	0.9986	1.39	0.9976	-------	0.1287	38.88	0.9616
CNTAL5	1.10	0.9901	1.55	0.9973	---------	---------	40.60	0.9450
CNTU5	0.91	0.9964	1.27	0.9961	-------	0.4159	63.77	0.9286
GO	0.75	0.9935	1.22	0.9912	---------	---------	23.10	0.9201
GOAL10	0.93	0.9692	1.49	0.9935	---------	---------	16.40	0.9571
GOAL5	1.08	0.9991	1.42	0.9562	---------	---------	29.30	0.5310

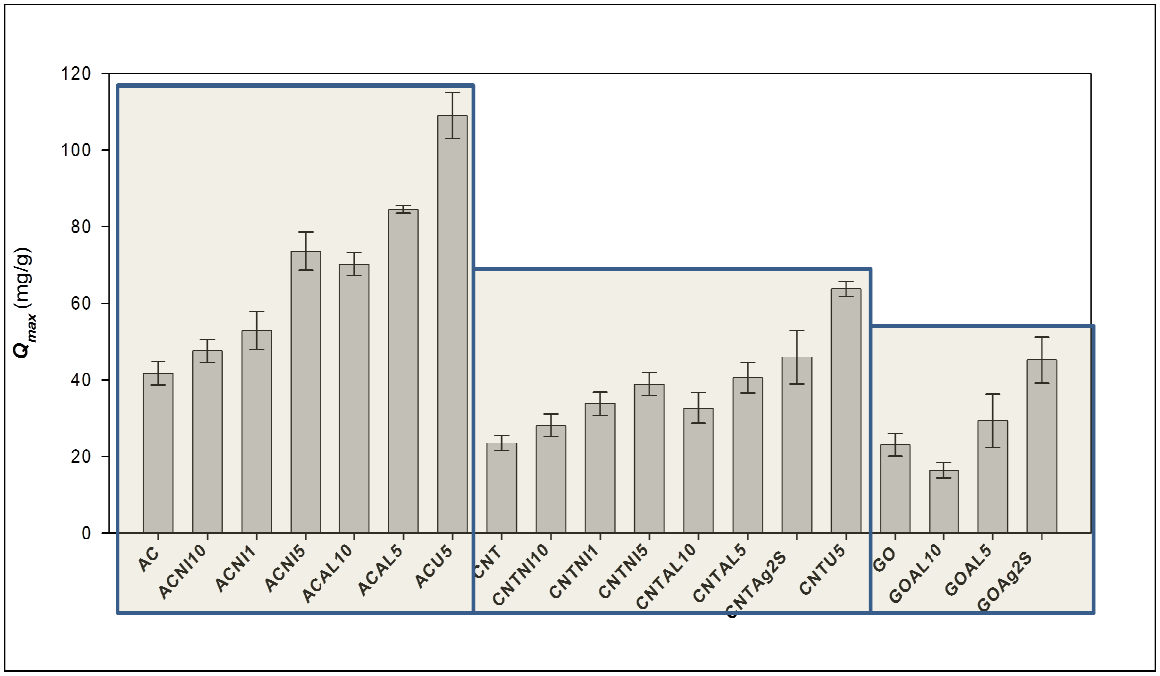

Figure 5-1: The histogram comparison between the adsorption capacity of the prepared adsorbents

As shown in table 5-2, the highest selectivity factor relative to thiophene and naphthalene was obtained by ACAL5 and the others follow the order CNTAL5>ACU5>ACNI5>CNTU5>AC>CNTNI5>CNT.

Table 5-2: Summary of selectivity factors for unmodified and modified AC and CNT with different metals oxide

	Selectivity Factor	
Adsorbent	$K_{DBT/Naph}$	$K_{DBT/Thio}$
AC	5.86	11.7
ACNI5	12.0	49.5
ACU5	18.3	69.1
ACAL5	25.1	255
CNT	1.71	5.89
CNTNI5	5.71	8.70
CNTU5	6.17	14.1
CNTAL5	6.49	127

The adsorbent adsorption capacity is highly affected with the experimental conditions such as nature of model fuel, operation temperature, sulfur compounds concentration, presence of other competitive compounds and adsorbent/model fuelratio,therefore summarizing a fully accurate comparison between the adsorption capacity of adsorbents is not possible. As summarized in table 5-3 at the same temperature (25 ºC), the adsorption capacities of the prepared adsorbents in this work is favorably comparable with other adsorbents reported in the literature used for adsorptive removal of DBT.

Table 5-3: Comparison of various carbon based adsorbents for DBT removal

Adsorbent	Sulfur Compound	Model Diesel	Adsorption Capacity	Reference
AC [1]	DBT	n-Octane	0.2748 (mmol/g)	[117]
AC-HNO_3 [2] 90 ºC	DBT	n-Octane	0.2887 (mmol/g)	
Cu-Al_2O_3	Thiophene	n-Pentane	1.79 (mg S / g)	[110]
Nanocrystalline NaY Zeolite	DBT	n-Nonane	1.70 (mg S/g)	[111]
ACFH[3]	DBT	n-Hexane	14.0 (mg S/ g)	[96]
ACFH-Cu(I) [4]	DBT	n-Hexane	19.0 (mg S/ g)	
D-MIP/TiO_2[5]	DBT	n-Octane	18.24(mg/g)	[133]
D-NIP/TiO_2[6]	DBT	n-Octane	6.15(mg/g)	
GPP [7]	DBT	n-Tetradecane	10.6 (mg S/ g)	[22]
GPH [8]	DBT	n-Tetradecane	5.50(mg S/ g)	
AC [1]	DBT	n Heptane	10.19 (mg/g)	[32]
ACWS [9]	DBT	n Heptane	47.1 (mg/g)	
Alumina	DBT	n-Hexane	21.02 (mg/ g)	[17]
GC[10]	DBT	Hexadecane	3.90(mg/g	[82]
Cu/GC15[11]	DBT	Hexadecane	5.70(mg/g)	
NiCeY[12]	DBT	n-Octane	22.2 mg/g	[134]
D-MIP/CMSs [13]	DBT	n-Hexane	105.0 (mg/g)	[118]
CMSs Without imprinting polymer[14]	DBT	n-Hexane	28.01 (mg/g)	
SMIP[15]	DBT	n-Octane	70.42 (mg/g)	[135]
Fe_3O_4@-SiO_2@MIPs[16]	DBT	n-Octane	63.29 (mg/g)	[136]
CAs[17]	DBT	n-Hexadecane	11.18 (mg S /g)	[137]
GAC 50% $ZnCl_2$[18]	DBT	n-Decane	42.56 (mg/g)	[19]
20%NiAlKIT-6 (15) [19]	DBT	n-Octane	22.04 (mg/g)	[138]
ACNI5	DBT	n-Hexane	73.61(mg/g)	This work
ACAL5	DBT	n-Hexane	84.50(mg/g)	This work
ACU5	DBT	n-Hexane	108.95(mg/g)	This work
CNTNI5	DBT	n-Hexane	38.88(mg/g)	This work
CNTAL5	DBT	n-Hexane	40.60(mg/g)	This work
CNT-Ag2S	DBT	n-Hexane	52.18 (mg/g)	This work
CNTU5	DBT	n-Hexane	63.77 (mg/g)	This work

GOAL5	DBT	n-Hexane	29.30 (mg/g)	This work
GO-Ag2S	DBT	n-Hexane	49.65 (mg/g)	This work

(1) Activated carbon
(2) Activated carbon modified with nitric acid at 90 °C
(3) Activated carbon fiber thermally treated
(4) Activated carbon fiber thermally treated and modified with copper (I) cation
(5) Titanium oxide particles modified with double-template molecularly imprinted polymer
(6) Titanium oxide particles modified with not imprinted polymer
(7) Graphene prepared using phosphoric acid
(8) Graphene oxide prepared using Hummers's method
(9) Activated carbon treated with steam at 900 °C then washed by H_2SO_4
(10) Graphite carbon.
(11) Granular carbon modified with copper
(12) Y zeolite type modified with nickel and cesium metals
(13) Carbon mictrosphere modified with double-template molecularly imprinted polymer
(14) Carbon mictrosphere modified with not imprinted polymer
(15) Single molecularly imprinted polymer
(16) Iron oxide coated with silicon oxide nanoparticles coated with molecularly imprinted polymer
(17) Carbon aerogels
(18) Granular activated carbon from dates' stones activated by 50% $ZnCl_2$
(19) Mesoporous silica contains aluminum and impregnated by 20 % nickel

CHAPTER 6

6. Conclusion and Recommendation

In this research three carbonaceous materials namely activated carbon, carbon nanotube and graphene oxide were impregnated successfully with different percentage loading of Al (5 % and 10 %) in the form of Al_2O_3, Ni (1, 5 and 10 %) in the form of nickel oxide, Ag 10 % in the form of silver sulfide or U 5 % in the form of uranium trioxide. The wetness impregnation technique was used to modify the carbon based adsorbents' surface. The modified and unmodified adsorbents were characterized using thermal gravimetric analysis (TGA), N_2 adsorption-desorption surface area analyzer, scanning electron microscope (SEM), energetic dispersive X-ray diffractogram (EDX), field emission electron microscope (FE-TEM),X-ray diffractometer (XRD)and X-ray photoelectron spectrometer (XPS) characterization techniques.

The investigation of adsorption capacities of the prepared adsorbents for DBT and thiophene from model fuelat constant temperature (25 ºC) shows that, the adsorption of both organosulfur compounds depends on their initial concentration, mass of adsorbent dosage, agitation speed and contact time. The effect of these factors on the DBT removal efficiency was more significant than onthe thiophene removal efficiency. The DBT and thiophene adsorption capacities on the modified and unmodified adsorbents increase with an increasing in their initial concentration from 25 to 250 mg/L. In contrary the adsorption capacities decrease and the removal efficiencies increase with an increasing

the amount of dosage from 50 to 1500 mg adsorbent at the specified conditions in this research. The DBT and thiopene removal efficiencies increase slightly with an increase in agitation speed from 50 to 200 rpm and then no significant change was observed at 250 rpm. The adsorption capacities increase with an increase in the contact time to reach equilibrium 120 minutes and almost no change was observed from 120 to 1560 minutes.

Among the three modified carbonaceous materials, as a group, the modified activated carbon adsorbents have the highest removal efficiency for DBT followed by modified carbon nanotube then modified graphene oxide. The adsorption isotherms fitted the Langmuir and Freundlich models. The highest adsorption capacity (Q_{max}) of DBT were 108.95mg/g using ACU5 and the other adsorbents followed the trend ACAL5 >ACNI5 >ACAL10 >CNTU5 >ACNI1 >ACNI10 >AC ≈ CNTAL5 ≈ CNTNI5> CNTNI1 ≈ CNTAL10 ≈ GOAL5 > CNT ≈ GO > GOAL10.

The adsorption rates for DBT and thiophene follow pseudo-second order kinetics involving relatively a fast sorption stage followed by a slow sorption stage.The selective removal by ACU5 ACAL5, CNTAL5, ACNI5 CNTNI5 and CNTU5 adsorbents of DBT relative to thiophene and naphthalene was evaluated. It has been found that, among these adsorbents ACAL5 has the highest selectivity for DBT relative to thiophene and relative to naphthalene to be 255 and 25 respectively. Moreover, it has been found the ACAL5, CNTAL5, ACNI5 and CNTNI5adsorbents are reusable for at least 5 times without a significant loss, not more than 10 %, in their adsorption capacity. The effect of the percentage of benzene in the model fuel on the adsorption capacity of ACNI5 and CNTNI5 are also evaluated. It was found that the adsorption capacities of ACNI5 and CNTNI5 for DBT decrease significantly in presence of 30 % of aromatic compounds.

It has been concluded that, doping the activated carbon, CNT and GO with a Lewis acid such as aluminum oxide, nickel oxide, silver sulfide or uranyl oxide improves the adsorbents' adsorption capacities, removal efficiencies and removal selectivity of DBT sulfur compound from model fuel,as a result of introducing additional adsorption sites. Those findings established new nano-composites adsorbents offer efficient complementary materials for selective removal of DBT as a representative organosulfur compound in model fuel.

The physical propertiesof adsorbents such asdiameter and volume of the adsorbents' porosity also affects on the adsorption of organosulfur compounds, therefore, in the future this significant factors will be investigated deeply. Other nano-composites and modified metal organic frame (MOF) based adsorbents will be prepared and investigated for selective removal of dibenzothiophene and 4,6-dimethyldibenzothiophene organosulfur compounds. The thermodynamic, kinetics and adsorption isotherms will be investigated at different concentration ranges.

References

[1] J. H. Kim, X. Ma, A. Zhou, and C. Song, "Ultra-deep desulfurization and denitrogenation of diesel fuel by selective adsorption over three different adsorbents: A study on adsorptive selectivity and mechanism," *Catalysis Today,* vol. 111, pp. 74-83, 2006.

[2] Commission E.E. DIRECTIVE 98/70/EC of the European Parliament and of theCouncil of 13 October 1998 relating to the quality of petrol and diesel fuels andamending Council Directive 93/12/EEC, 1998.

[3] Commission E.E. DIRECTIVE 2003/17/EC of the European Parliament and ofthe Council of 3 March 2003 amending Directive 98/70/EC relating to the qualityof petrol and diesel fuels, 2003.

[4] Commission E.E. Directive 2009/30/EC of the European Parliament and of theCouncil of 23 April 2009 amending Directive 98/70/EC, 2009.

[5] U.S. EPA, Tier 2 Act, 1998.

[6] U.S. EPA, Control of Air Pollution from New Motor Vehicles Amendment to theTier-2/Gasoline Sulfur Regulations, April 2001.

[7] H. Tao, T. Nakazato, and S. Sato, "Energy-efficient ultra-deep desulfurization of kerosene based on selective photooxidation and adsorption," *Fuel,* vol. 88, pp. 1961-1969, 2009.

[8] M. Seredych, C. T. Wu, P. Brender, C. O. Ania, C. Vix-Guterl, and T. J. Bandosz, "Role of phosphorus in carbon matrix in desulfurization of diesel fuel using adsorption process," *Fuel,* vol. 92, pp. 318-326, 2012.

[9] C. Song and X. Ma, "New design approaches to ultra-clean diesel fuels by deep desulfurization and deep dearomatization," *Applied Catalysis B: Environmental,* vol. 41, pp. 207-238, 2003.

[10] J. M. Campos-Martin, M. C. Capel-Sanchez, P. Perez-Presas, and J. L. G. Fierro, "Oxidative processes of desulfurization of liquid fuels," *Journal of Chemical Technology & Biotechnology,* vol. 85, pp. 879-890, 2010.

[11] W. Zhu, H. Li, X. Jiang, Y. Yan, J. Lu, and J. Xia, "Oxidative desulfurization offuels catalyzed by peroxotungsten and peroxomolybdenum complexes in ionicliquids," *Energy & Fuels*, vol. 21, pp. 2514-2516, 2007.

[12] M. Cortes-Jacome, M. Morales, C. Angeles Chavez, L. Ramirez-Verduzco, E.Lopez-Salinas, and J. Toledo-Antonio, "WO x/TiO2 Catalysts via TitaniaNanotubes for the Oxidation of Dibenzothiophene," *Chemistry of Materials*, vol.19, pp. 6605-6614, 2007.

[13] S. Matsuzawa, J. Tanaka, S. Sato, and T. Ibusuki, "Photocatalytic oxidation ofdibenzothiophenes in acetonitrile using TiO 2: effect of hydrogen peroxide andultrasound irradiation," *Journal of photochemistry and photobiology A: Chemistry*, vol. 149, pp. 183-189, 2002.

[14] Y. Shiraishi, H. Hara, T. Hirai, and I. Komasawa, "A deep desulfurization processfor light oil by photosensitized oxidation using a triplet photosensitizer andhydrogen peroxide in an oil/water two-phase liquid-liquid extraction system,"*Industrial & engineering chemistry research*, vol. 38, pp. 1589-1595, 1999.

[15] R. T. Yang, A. J. Hernández-Maldonado, and F. H. Yang, "Desulfurization of transportation fuels with zeolites under ambient conditions," *Science,* vol. 301, pp. 79-81, 2003.

[16] A. J. Hernández-Maldonado, G. Qi, and R. T. Yang, "Desulfurization of commercial fuels by π-complexation: Monolayer CuCl/γ-Al2O3," *Applied Catalysis B: Environmental,* vol. 61, pp. 212-218, 11/9/ 2005.

[17] A. Srivastav and V. C. Srivastava, "Adsorptive desulfurization by activated alumina," *Journal of hazardous materials,* vol. 170, pp. 1133-1140, 2009.

[18] J.-C. Hoguet, G. P. Karagiannakis, J. A. Valla, C. C. Agrafiotis, and A. G. Konstandopoulos, "Gas and liquid phase fuels desulphurization for hydrogen production via reforming processes," *international journal of hydrogen energy,* vol. 34, pp. 4953-4962, 2009.

[19] Y. A. Alhamed and H. S. Bamufleh, "Sulfur removal from model diesel fuel using granular activated carbon from dates' stones activated by ZnCl 2," *Fuel,* vol. 88, pp. 87-94, 2009.

[20] S. Kumagai, H. Ishizawa, and Y. Toida, "Influence of solvent type on dibenzothiophene adsorption onto activated carbon fiber and granular coconut-shell activated carbon," *Fuel,* vol. 89, pp. 365-371, 2010.

[21] Q. Wang, X. Liang, W. Qiao, C. Liu, X. Liu, L. Zhan*, et al.*, "Preparation of polystyrene-based activated carbon spheres with high surface area and their adsorption to dibenzothiophene," *Fuel Processing Technology,* vol. 90, pp. 381-387, 2009.

[22] H. S. Song, C. H. Ko, W. Ahn, B. J. Kim, E. Croiset, Z. Chen*, et al.*, "Selective dibenzothiophene adsorption on graphene prepared using different methods," *Industrial & Engineering Chemistry Research,* vol. 51, pp. 10259-10264, 2012.

[23] O. Mabayoje, M. Seredych, and T. J. Bandosz, "Enhanced reactive adsorption of hydrogen sulfide on the composites of graphene/graphite oxide with copper (hydr) oxychlorides," *ACS applied materials & interfaces,* vol. 4, pp. 3316-3324, 2012.

[24] S.-T. Yang, Y. Chang, H. Wang, G. Liu, S. Chen, Y. Wang, *et al.*, "Folding/aggregation of graphene oxide and its application in Cu 2+ removal," *Journal of colloid and interface science,* vol. 351, pp. 122-127, 2010.

[25] H. Chen, X. Zhou, H. Shang, C. Liu, J. Qiu, and F. Wei, "Study of dibenzothiophene adsorption over carbon nanotube supported CoMo HDS catalysts," *Journal of Natural Gas Chemistry,* vol. 13, pp. 209-217, 2004.

[26] L. Wang, D. Zhu, L. Duan, and W. Chen, "Adsorption of single-ringed N-and S-heterocyclic aromatics on carbon nanotubes," *Carbon,* vol. 48, pp. 3906-3915, 2010.

[27] C. Ania and T. Bandosz, "Metal-loaded polystyrene-based activated carbons as dibenzothiophene removal media via reactive adsorption," *Carbon,* vol. 44, pp. 2404-2412, 2006.

[28] A. Zhou, X. Ma, and C. Song, "Liquid-phase adsorption of multi-ring thiophenic sulfur compounds on carbon materials with different surface properties," *The Journal of Physical Chemistry B,* vol. 110, pp. 4699-4707, 2006.

[29] C. O. Ania and T. J. Bandosz, "Importance of structural and chemical heterogeneity of activated carbon surfaces for adsorption of dibenzothiophene," *Langmuir,* vol. 21, pp. 7752-7759, 2005.

[30] M. Seredych and T. J. Bandosz, "Template-derived mesoporous carbons with highly dispersed transition metals as media for the reactive adsorption of dibenzothiophene," *Langmuir,* vol. 23, pp. 6033-6041, 2007.

[31] G. Yu, S. Lu, H. Chen, and Z. Zhu, "Diesel fuel desulfurization with hydrogen peroxide promoted by formic acid and catalyzed by activated carbon," *Carbon,* vol. 43, pp. 2285-2294, 2005.

[32] Y. Yang, H. Lu, P. Ying, Z. Jiang, and C. Li, "Selective dibenzothiophene adsorption on modified activated carbons," *Carbon,* vol. 45, pp. 3042-3044, 2007.

[33] M. Seredych, J. Lison, U. Jans, and T. J. Bandosz, "Textural and chemical factors affecting adsorption capacity of activated carbon in highly efficient desulfurization of diesel fuel," *Carbon,* vol. 47, pp. 2491-2500, 2009.

[34] D. Crespo and R. T. Yang, "Adsorption of organic vapors on single-walled carbon nanotubes," *Industrial & engineering chemistry research,* vol. 45, pp. 5524-5530, 2006.

[35] M. Seredych and T. J. Bandosz, "Adsorption of dibenzothiophenes on activated carbons with copper and iron deposited on their surfaces," *Fuel Processing Technology,* vol. 91, pp. 693-701, 2010.

[36] H.-J. Jeon, C. H. Ko, S. H. Kim, and J.-N. Kim, "Removal of refractory sulfur compounds in diesel using activated carbon with controlled porosity," *Energy & Fuels,* vol. 23, pp. 2537-2543, 2009.

[37] M. Seredych and T. J. Bandosz, "Adsorption of dibenzothiophenes on nanoporous carbons: identification of specific adsorption sites governing capacity and selectivity†," *Energy & Fuels,* vol. 24, pp. 3352-3360, 2010.

[38] M. Seredych and T. J. Bandosz, "Investigation of the enhancing effects of sulfur and/or oxygen functional groups of nanoporous carbons on adsorption of dibenzothiophenes," *Carbon,* vol. 49, pp. 1216-1224, 2011.

[39] M. Seredych, M. Khine, and T. J. Bandosz, "Enhancement in dibenzothiophene reactive adsorption from liquid fuel via incorporation of sulfur heteroatoms into the nanoporous carbon matrix," *ChemSusChem,* vol. 4, pp. 139-147, 2011.

[40] M. Seredych and T. J. Bandosz, "Selective adsorption of dibenzothiophenes on activated carbons with Ag, Co, and Ni species deposited on their surfaces," *Energy & fuels,* vol. 23, pp. 3737-3744, 2009.

[41] Y. Hamerlinck, D. Mertens, and E. Vansant, "Activated carbon principles in separation technology," *Elsevier, New York,* 1994.

[42] C. L. Mantell, "Carbon and Graphite Handbook," 1968.

[43] D. Mohan and K. P. Singh, "Granular activated carbon," *Water Encyclopedia,* 2005.

[44] T. Otowa, Y. Nojima, and T. Miyazaki, "Development of KOH activated high surface area carbon and its application to drinking water purification," *Carbon,* vol. 35, pp. 1315-1319, 1997.

[45] J. S. Mattson and H. B. Mark, *Activated carbon: surface chemistry and adsorption from solution*: M. Dekker, 1971.

[46] Y. Sun, J.-P. Zhang, G. Yang, and Z.-H. Li, "Removal of Pollutantswith Activated Carbon Produced from K2CO3 Activation of Lignin From Reed Black Liquors," *Chemical and biochemical engineering quarterly,* vol. 20, pp. 429-435, 2006.

[47] IUPAC. Compendium of Chemical Terminology, 2nd ed. (the "Gold Book").Compiled by A. D. McNaught and A. Wilkinson. Blackwell ScientificPublications, Oxford (1997). XML on-line corrected version:http://goldbook.iupac.org (2006) created by M. Nic, J. Jirat, B. Kosata; updatescompiled by A. Jenkins. ISBN 0-9678550-9-8.doi:10.1351/goldbook. Last update:2014-02-24; version: 2.3.3. DOI of this term:doi:10.1351/goldbook.A00243.

[48] X. Wang, Q. Li, J. Xie, Z. Jin, J. Wang, Y. Li*, et al.*, "Fabrication of ultralong and electrically uniform single-walled carbon nanotubes on clean substrates," *Nano letters,* vol. 9, pp. 3137-3141, 2009.

[49] W. Meyer, "Coping with resistance to copper/silver disinfection," *Water Engineering & Management,* vol. 148, pp. 25-27, 2001.

[50] http://en.wikipedia.org/wiki/Carbon_nanotube. Last accessed on April 2015

[51] P. G. Collins and P. Avouris, "Nanotubes for electronics," *Scientific American,* vol. 283, pp. 62-69, 2000.

[52] S. Niyogi, M. Hamon, H. Hu, B. Zhao, P. Bhowmik, R. Sen*, et al.*, "Chemistry of single-walled carbon nanotubes," *Accounts of Chemical Research,* vol. 35, pp. 1105-1113, 2002.

[53] J. Hone, M. Whitney, C. Piskoti, and A. Zettl, "Thermal conductivity of single-walled carbon nanotubes," *Physical Review B,* vol. 59, p. R2514, 1999.

[54] T. Ebbesen and P. Ajayan, "Large-scale synthesis of carbon nanotubes," *Nature,* vol. 358, pp. 220-222, 1992.

[55] The Smalley Group at Rice University, http://www.ruf.rice.edu. Last accessed onMarch 2014

[56] C. Journet and P. Bernier, "Production of carbon nanotubes," *Applied physics A: Materials science & processing,* vol. 67, pp. 1-9, 1998.

[57] H. Dai, "Carbon nanotubes: opportunities and challenges," *Surface Science,* vol. 500, pp. 218-241, 2002.

[58] M. D. Stoller, S. Park, Y. Zhu, J. An, and R. S. Ruoff, "Graphene-based ultracapacitors," *Nano letters,* vol. 8, pp. 3498-3502, 2008.

[59] A. A. Balandin, S. Ghosh, W. Bao, I. Calizo, D. Teweldebrhan, F. Miao*, et al.*, "Superior thermal conductivity of single-layer graphene," *Nano letters,* vol. 8, pp. 902-907, 2008.

[60] K. S. Novoselov, A. K. Geim, S. Morozov, D. Jiang, Y. Zhang, S. Dubonos*, et al.*, "Electric field effect in atomically thin carbon films," *science,* vol. 306, pp. 666-669, 2004.

[61] C. Lee, X. Wei, J. W. Kysar, and J. Hone, "Measurement of the elastic properties and intrinsic strength of monolayer graphene," *science,* vol. 321, pp. 385-388, 2008.

[62] H. He and C. Gao, "Graphene nanosheets decorated with Pd, Pt, Au, and Ag nanoparticles: Synthesis, characterization, and catalysis applications," *Science China Chemistry,* vol. 54, pp. 397-404, 2011.

[63] G. Liu, C. Yu, C. Chen, W. Ma, H. Ji, and J. Zhao, "A new type of covalent-functional graphene donor-acceptor hybrid and its improved photoelectrochemical performance," *Science China Chemistry,* vol. 54, pp. 1622-1626, 2011.

[64] A. Bianco, H.-M. Cheng, T. Enoki, Y. Gogotsi, R. H. Hurt, N. Koratkar*, et al.*, "All in the graphene family–a recommended nomenclature for two-dimensional carbon materials," *Carbon,* vol. 65, pp. 1-6, 2013.

[65] Y.-P. Chang, C.-L. Ren, J.-C. Qu, and X.-G. Chen, "Preparation and characterization of Fe 3 O 4/graphene nanocomposite and investigation of its adsorption performance for aniline and p-chloroaniline," *Applied Surface Science,* vol. 261, pp. 504-509, 2012.

[66] Z. Khan, T. R. Chetia, A. K. Vardhaman, D. Barpuzary, C. V. Sastri, and M. Qureshi, "Visible light assisted photocatalytic hydrogen generation and organic dye degradation by CdS–metal oxide hybrids in presence of graphene oxide," *RSC Advances,* vol. 2, pp. 12122-12128, 2012.

[67] J. Li, S. Guo, Y. Zhai, and E. Wang, "High-sensitivity determination of lead and cadmium based on the Nafion-graphene composite film," *Analytica chimica acta,* vol. 649, pp. 196-201, 2009.

[68] D. Wang, L. Wang, X. Dong, Z. Shi, and J. Jin, "Chemically tailoring graphene oxides into fluorescent nanosheets for Fe 3+ ion detection," *Carbon,* vol. 50, pp. 2147-2154, 2012.

[69] S. M. Maliyekkal, T. Sreeprasad, D. Krishnan, S. Kouser, A. K. Mishra, U. V. Waghmare*, et al.*, "Graphene: a reusable substrate for unprecedented adsorption of pesticides," *Small,* vol. 9, pp. 273-283, 2013.

[70] X. Liu, H. Zhang, Y. Ma, X. Wu, L. Meng, Y. Guo*, et al.*, "Graphene-coated silica as a highly efficient sorbent for residual organophosphorus pesticides in water," *Journal of Materials Chemistry A,* vol. 1, pp. 1875-1884, 2013.

[71] J. Xu, L. Wang, and Y. Zhu, "Decontamination of bisphenol A from aqueous solution by graphene adsorption," *Langmuir,* vol. 28, pp. 8418-8425, 2012.

[72] H. Ma, J. Shen, M. Shi, X. Lu, Z. Li, Y. Long*, et al.*, "Significant enhanced performance for rhodamine B, phenol and Cr (VI) removal by Bi 2 WO 6 nancomposites via reduced graphene oxide modification," *Applied Catalysis B: Environmental,* vol. 121, pp. 198-205, 2012.

[73] H. Topsøe, B. S. Clausen, and F. E. Massoth, *Hydrotreating catalysis*: Springer, 1996.

[74] E. Furimsky and F. E. Massoth, "Deactivation of hydroprocessing catalysts," *Catalysis Today,* vol. 52, pp. 381-495, 1999.

[75] C. Song, "Keynote: new approaches to deep desulfurization for ultra-clean gasoline and diesel fuels: an overview, Am," *Chem. Soc., Div. Fuel Chem. Prepr,* vol. 47, p. 438, 2002.

[76] K. G. Knudsen, B. H. Cooper, and H. Topsøe, "Catalyst and process technologies for ultra low sulfur diesel," *Applied Catalysis A: General,* vol. 189, pp. 205-215, 1999.

[77] F. Bataille, J.-L. Lemberton, P. Michaud, G. Pérot, M. Vrinat, M. Lemaire*, et al.*, "Alkyldibenzothiophenes hydrodesulfurization-promoter effect, reactivity, and reaction mechanism," *Journal of catalysis,* vol. 191, pp. 409-422, 2000.

[78] E. Lecrenay, K. Sakanishi, and I. Mochida, "Catalytic hydrodesulfurization of gas oil and model sulfur compounds over commercial and laboratory-made CoMo and NiMo catalysts: Activity and reaction scheme," *Catalysis Today,* vol. 39, pp. 13-20, 1997.

[79] H. Rang, J. Kann, and V. Oja, "Advances in desulfurization research of liquid fuel," *Oil Shale,* vol. 23, pp. 164-176, 2006.

[80] H. Sheldon, "Desulfurization of a heavy hydrocarbon fraction," ed: Google Patents, 1970.

[81] S. Bonde, D. Chapados, W. Gore, G. Dolbear, and E. Skov, "NPRA Annunal Meeting 2000," AM-00-25.

[82] U. Arellano, J. Shen, J. Wang, M. Timko, L. Chen, J. V. Rodríguez*, et al.*, "Dibenzothiophene oxidation in a model diesel fuel using CuO/GC catalysts and H 2 O 2 in the presence of acetic acid under acidic condition," *Fuel,* 2014.

[83] J. Wang, Q. Guo, C. Zhang, and K. Li, "One-pot extractive and oxidative desulfurization of liquid fuels with molecular oxygen in ionic liquids," *RSC Advances,* vol. 4, pp. 59885-59889, 2014.

[84] I. Babich and J. Moulijn, "Science and technology of novel processes for deep desulfurization of oil refinery streams: a review☆," *Fuel,* vol. 82, pp. 607-631, 2003.

[85] P. Forte, "Process for the removal of sulfur from petroleum fractions," ed: Google Patents, 1996.

[86] I. Funakoshi and T. Aida, "Process for recovering organic sulfur compounds from fuel oil," ed: Google Patents, 1998.

[87] Y. Horii, H. Onuki, S. Doi, T. Mori, T. Takatori, H. Sato*, et al.*, "Desulfurization and denitration of light oil by extraction," ed: Google Patents, 1996.

[88] S. A. Dharaskar, K. L. Wasewar, M. N. Varma, D. Z. Shende, and C. K. Yoo, "Ionic Liquids:-The Novel Solvent for Removal of Dibenzothiophene from Liquid Fuel," *Procedia Engineering,* vol. 51, pp. 314-317, 2013.

[89] X. Lu, L. Yue, M. Hu, Q. Cao, L. Xu, Y. Guo*, et al.*, "Piperazinium-Based Ionic Liquids with Lactate Anion for Extractive Desulfurization of Fuels," *Energy & Fuels,* vol. 28, pp. 1774-1780, 2014.

[90] J. Wang, D. Zhao, and K. Li, "Extractive desulfurization of gasoline using ionic liquid based on CuCl," *Petroleum Science and Technology,* vol. 30, pp. 2417-2423, 2012.

[91] R. Javadli and A. de Klerk, "Desulfurization of heavy oil," *Applied Petrochemical Research,* vol. 1, pp. 3-19, 2012.

[92] R. L. Irvine and D. M. Varraveto, "Adsorption process for removal of nitrogen and sulphur," *PETROLEUM TECHNOLOGY QUARTERLY,* pp. 37-46, 1999.

[93] M. Tamura, A. Sasaki, T. Kato, and K. Sugawara, "Selective removal of organic sulfur in fuels."

[94] C. Yu, J. S. Qiu, Y. F. Sun, X. H. Li, G. Chen, and Z. B. Zhao, "Adsorption removal of thiophene and dibenzothiophene from oils with activated carbon as adsorbent: effect of surface chemistry," *Journal of Porous Materials,* vol. 15, pp. 151-157, 2008.

[95] J. Xiao, Z. Li, B. Liu, Q. Xia, and M. Yu, "Adsorption of benzothiophene and dibenzothiophene on ion-impregnated activated carbons and ion-exchanged Y zeolites," *Energy & Fuels,* vol. 22, pp. 3858-3863, 2008.

[96] E. S. Moosavi, S. A. Dastgheib, and R. Karimzadeh, "Adsorption of Thiophenic Compounds from Model Diesel Fuel Using Copper and Nickel Impregnated Activated Carbons," *Energies,* vol. 5, pp. 4233-4250, 2012.

[97] N. A. Khan, Z. Hasan, K. S. Min, S.-M. Paek, and S. H. Jhung, "Facile introduction of Cu+ on activated carbon at ambient conditions and adsorption of benzothiophene over Cu+/activated carbon," *Fuel Processing Technology,* vol. 116, pp. 265-270, 2013.

[98] W. S. Hummers Jr and R. E. Offeman, "Preparation of graphitic oxide," *Journal of the American Chemical Society,* vol. 80, pp. 1339-1339, 1958.

[99] C. Lastoskie, K. E. Gubbins, and N. Quirke, "Pore size distribution analysis of microporous carbons: a density functional theory approach," *The journal of physical chemistry,* vol. 97, pp. 4786-4796, 1993.

[100] M. Dubinin, "Porous structure and adsorption properties of active carbons," *Chemistry and physics of carbon,* vol. 2, pp. 51-120, 1966.

[101] B. C. Lippens and J. De Boer, "Studies on pore systems in catalysts: V. The t method," *Journal of Catalysis,* vol. 4, pp. 319-323, 1965.

[102] H. Freundlich, "Over the adsorption in solution," *J. Phys. Chem,* vol. 57, pp. 385-470, 1906.

[103] I. Langmuir, "THE CONSTITUTION AND FUNDAMENTAL PROPERTIES OF SOLIDS AND LIQUIDS. PART I. SOLIDS," *Journal of the American Chemical Society,* vol. 38, pp. 2221-2295, 1916.

[104] M. Temkin and V. Pyzhev, "Kinetics of ammonia synthesis on promoted iron catalysts," *Acta physiochim. URSS,* vol. 12, pp. 217-222, 1940.

[105] A. W. Adamson and A. P. Gast, "Physical chemistry of surfaces," 1967.

[106] L. Li, P. A. Quinlivan, and D. R. Knappe, "Effects of activated carbon surface chemistry and pore structure on the adsorption of organic contaminants from aqueous solution," *Carbon,* vol. 40, pp. 2085-2100, 2002.

[107] C. Song and X. Ma, "New design approaches to ultra-clean diesel fuels by deep desulfurization and deep dearomatization," *Applied Catalysis B: Environmental,* vol. 41, pp. 207-238, 2003.

[108] Y. Ho and G. McKay, "A comparison of chemisorption kinetic models applied to pollutant removal on various sorbents," *Process Safety and Environmental Protection,* vol. 76, pp. 332-340, 1998.

[109] S. Brunauer, L. S. Deming, W. E. Deming, and E. Teller, "On a theory of the van der Waals adsorption of gases," *Journal of the American Chemical Society,* vol. 62, pp. 1723-1732, 1940.

[110] X. Yang, L. E. Erickson, K. L. Hohn, P. Jeevanandam, and K. J. Klabunde, "Sol-gel Cu-Al2O3 adsorbents for selective adsorption of thiophene out of hydrocarbon," *Industrial & engineering chemistry research,* vol. 45, pp. 6169-6174, 2006.

[111] K. Tang, X. Hong, Y. Zhao, and Y. Wang, "Adsorption desulfurization on a nanocrystalline NaY zeolite synthesized using carbon nanotube templated growth," *Petroleum Science and Technology,* vol. 29, pp. 779-787, 2011.

[112] "<NIST XPS Database, Spectrum Search Menu.pdf>."

[113] K. A. A. Safieh, Y. S. Al-Degs, M. S. Sunjuk, A. I. Saleh, and M. A. Al-Ghouti, "Selective removal of dibenzothiophene from commercial diesel using manganese dioxide-modified activated carbon: a kinetic study," *Environmental technology,* vol. 36, pp. 98-105, 2015.

[114] W. Weber, "Asce, Jr JM and Morris, JC, Kinetic of Adsorption on carbon from solutions," in *Journal of Sanitary Engineering Division, Proceedings of the American Society of Civil Engineers*, 1963, pp. 31-59.

[115] S. Lagergren, "About the theory of so-called adsorption of soluble substances," *Kungliga Svenska Vetenskapsakademiens Handlingar,* vol. 24, pp. 1-39, 1898.

[116] D. G. Kinniburgh, "General purpose adsorption isotherms," *Environmental Science & Technology,* vol. 20, pp. 895-904, 1986.

[117] C. Yu, X. Fan, L. Yu, T. J. Bandosz, Z. Zhao, and J. Qiu, "Adsorptive removal of thiophenic compounds from oils by activated carbon modified with concentrated nitric acid," *Energy & Fuels,* vol. 27, pp. 1499-1505, 2013.

[118] W. Liu, X. Liu, Y. Yang, Y. Zhang, and B. Xu, "Selective removal of benzothiophene and dibenzothiophene from gasoline using double-template

molecularly imprinted polymers on the surface of carbon microspheres," *Fuel,* vol. 117, pp. 184-190, 2014.

[119] H. M. Raymond, "Classical and modern regression with applications," *PWS-KENT Publishing Compagny,* 1990.

[120] D. A. Ratkowsky and D. E. Giles, *Handbook of nonlinear regression models*: Marcel Dekker New York, 1990.

[121] S. J. Allen, Q. Gan, R. Matthews, and P. A. Johnson, "Comparison of optimised isotherm models for basic dye adsorption by kudzu," *Bioresource Technology,* vol. 88, pp. 143-152, 2003.

[122] Y.-S. Ho, "Isotherms for the sorption of lead onto peat: comparison of linear and non-linear methods," *Polish Journal of Environmental Studies,* vol. 15, pp. 81-86, 2006.

[123] B. Armagan and F. Toprak, "Optimum isotherm parameters for reactive azo dye onto pistachio nut shells: comparison of linear and non-linear methods," *Polish Journal of Environmental Studies,* vol. 22, 2013.

[124] M. A. Larrubia, A. d. Gutièrrez-Alejandre, J. Ramìrez, and G. Busca, "A FT-IR study of the adsorption of indole, carbazole, benzothiophene, dibenzothiophene and 4, 6-dibenzothiophene over solid adsorbents and catalysts," *Applied Catalysis A: General,* vol. 224, pp. 167-178, 2002.

[125] H. Shang, C. Liu, and F. Wei, "FT-IR study of carbon nanotube supported Co-Mo catalysts," *Journal of Natural Gas Chemistry,* vol. 13, pp. 95-100, 2004.

[126] W. Brockner, C. Ehrhardt, and M. Gjikaj, "Thermal decomposition of nickel nitrate hexahydrate, Ni (NO 3) 2· 6H 2 O, in comparison to Co (NO 3) 2· 6H 2 O and Ca (NO 3) 2· 4H 2 O," *Thermochimica Acta,* vol. 456, pp. 64-68, 2007.

[127] B. Cullity, "Elements of," *X-ray! Jiffraction,* 1978.

[128] J. F. Risher and S. W. Rhodes, "Toxicological profile for fuel oils," *Agency for Toxic Substances and Disease Registry, Atlanta, Ga,* 1995.

[129] N. D. Priest, "The distribution and behaviour of heavy metals in the skeleton and body: Studies with bone-seeking radionuclides," *Trace metals and fluoride in bones and teeth,* pp. 83-139, 1990.

[130] N. Priest, "Toxicity of depleted uranium," *The Lancet,* vol. 357, pp. 244-246, 2001.

[131] M. Betti, "Civil use of depleted uranium," *Journal of environmental radioactivity,* vol. 64, pp. 113-119, 2003.

[132] K. IWAMOTO, "Thermal Decomposition of Uranyl Nitrate Hexahydrate in the Presence of Graphite," *Journal of Nuclear Science and Technology,* vol. 1, pp. 113-119, 1964.

[133] P. Xu, W. Xu, X. Zhang, J. Pan, and Y. Yan, "Molecularly-imprinted material for dibenzothiophene recognition prepared by surface imprinting methods," *Adsorption Science & Technology,* vol. 27, pp. 975-987, 2009.

[134] J. Wang, F. Xu, W.-j. Xie, Z.-j. Mei, Q.-z. Zhang, J. Cai*, et al.*, "The enhanced adsorption of dibenzothiophene onto cerium/nickel-exchanged zeolite Y," *Journal of hazardous materials,* vol. 163, pp. 538-543, 2009.

[135] W. Yang, W. Zhou, W. Xu, H. Li, W. Huang, B. Jiang*, et al.*, "Synthesis and characterization of a surface molecular imprinted polymer as a new adsorbent for the removal of dibenzothiophene," *Journal of Chemical & Engineering Data,* vol. 57, pp. 1713-1720, 2012.

[136] H. Li, W. Xu, N. Wang, X. Ma, D. Niu, B. Jiang*, et al.*, "Synthesis of magnetic molecularly imprinted polymer particles for selective adsorption and separation of dibenzothiophene," *Microchimica Acta,* vol. 179, pp. 123-130, 2012.

[137] S. Haji and C. Erkey, "Removal of dibenzothiophene from model diesel by adsorption on carbon aerogels for fuel cell applications," *Industrial & engineering chemistry research,* vol. 42, pp. 6933-6937, 2003.

[138] F. Subhan, Z. Yan, P. Peng, M. Ikram, and S. Rehman, "The enhanced adsorption of sulfur compounds onto mesoporous Ni-AlKIT-6 sorbent, equilibrium and kinetic analysis," *Journal of hazardous materials,* vol. 270, pp. 82-91, 2014.

Vitae

Name	**Mazen Khaled Hamed Nazal**
Nationality	**Jordanian**
Date of Birth	**18/12/1981**
Email	mazen_nazzaL1981@hotmail.com, nazalmazen@gmail.com
Permanent Address	**Amman-Jordan**

Academic Background

PhD (Analytical Chemistry)
King Fahd University of Petroleum and Minerals (KFUPM), Dhahran-Saudi Arabia
November-2015

MSc. (Analytical Chemistry)
The University of Jordan (UJ), Amman-Jordan
June-2006

BSc. (Chemistry Science)
The University of Jordan (UJ), Amman-Jordan
June-2003

Representative training courses

GLP for Analytical Laboratories
By Newland GxP Consultancy Amman – Jordan
20th– 21thJuly, 2003

ISO/IEC 17025:2 005 Standard Field of Application and Requirements By Royal Scientific Society Amman-Jordan
11th– 12th June, 2008

PTI's course on **"Dissolution Testing, Bioequivalence and Bioavailability"** By Pharmaceutical Training International
Amman-Jordan 12th– 13th October, 2008

Representative Papers

Nazal, M.K., Albayyari, M.A., Khalili, F.I.**"Effect of high ionic strength on the extraction of uranium(VI) ions**" *Journal of Saudi Chemical Society.18, 1 (2014)*, 59–67

Mazen Khaled. **"Adsorption performance of multiwall carbon nanotubes and graphene oxide for removal of thiophene and dibenzothiophene from model diesel fuel"***Res Chem Intermed(2015)* DOI 10.1007/s11164-015-1986-5

Mazen Khaled Nazal, Ghassan A. Oweimreen, Mazen Khaled, Muataz A. Atieh, Isam H. Aljundi, Abdalla M. Abulkibash**"Adsorption Isotherms and Kinetics for Dibenzothiophene on Activated Carbon and Carbon Nanotube Doped with Nickel Oxide Nanoparticles"** *Bulliten of Materials Science*

Mazen K. Nazal, Mazen Khaled, Muataz A. Atieh, Isam H. Aljundi, Ghassan A.Oweimreen, Abdalla M. Abulkibash.**"The Nature and Kinetics of the Adsorption of Dibenzothiophene in Model Diesel Fuel on Carbonaceous Materials Loaded with Aluminum Oxide Particles"** *Arabian Journal of Chemistry*

Muhammad Sajid, ***Mazen Khaled Nazal***, Muhammad Mansha, Abdulnaser Alsharaa, Shehzada Muhammad Sajid Jillani**"Chemically modified electrodes for electrochemical detection of dopamine in presence of uric acid and ascorbic acid: A review"** *TrAC Trends in Analytical Chemistry (2015), http://dx.doi.org/doi: 10.1016/j.trac.2015.09.006*

Books:

Mazen K. Nazal and Fawwaz Khalili "**Extraction of U(VI) From High ionic strength Solution By (HDDPA)"** *(2014)LAMBERT Academic Publishing***ISBN:** *978-3-659-19327-9*

Conferences

247th American Chemical Society National Meeting & Exposition. **"Elechtrochemical-electron paramagnetic resonance (EC-EPR) new technique for Ketoconazole detection in urine and its quantitative assay in pharmaceutical product forms"*Mazen K. Nazal***, Abdel-Nasser M. Kawde and Morsy M. A. Dallas, TX *(2014)*

247th American Chemical Society National Meeting & Exposition. **"Mercury and other trace metals in saliva: Electroanalytical detection in dental amalgam"*Mazen K. Nazal*** and Abdel-Nasser M. Kawde. Dallas, TX *(2014)*

PPS2015, 2015 Europe/Africa Regional Conference of the Polymer Processing Society**"Investigation of Morphological properties and Proton-conductivity of Different Sulfonated Poly(ether ether ketone) (SPEEK) blends"** Al-Ahmed Amir, Sultan Abdullah, ***Nazal Mazen Khaled***, Adewole Jimoh K, Zaidi Javaid. Austria *(2015)*